PHYSICAL MODELING FOR SIDE-CHANNEL WEIRS

by

Ka-Leung Lee and E. R. Holley
Center for Research in Water Resources
The University of Texas at Austin
Austin, TX 78712 USA

CRWR Online Report 02-2
http://www.crwr.utexas.edu/online.shtml

prepared for

Harris Flood Control District
Suite 200
9900 Northwest Freeway
Houston, TX 77092 USA

April 15, 2002

TABLE OF CONTENTS

LIST OF FIGURES

LIST OF TABLES

ACKNOWLEDGMENTS

This project was supported by the Harris County Flood Control District. Mr. Steve Fitzgerald was very helpful with both the technical and administrative aspects of this project.

The project was conducted at the Center for Research in Water Resources of the University of Texas at Austin. Kevin Wei assisted with some of the experimental work. Part of the project work is reported by Burgin and Holley (2002). That report is a user's manual for the computational scheme that has been developed for watershed hydrology, channel and side-weir hydraulics, and filling and emptying of detention basins.

Red Valve Co., Inc., Pittsburgh, Pennsylvania, provided information on their Tideflex check valves as presented in Section 2.7.1.

PHYSICAL MODELING FOR SIDE-CHANNEL WEIRS

By Ka-Leung Lee and E. R. Holley
Center for Research in Water Resources
The University of Texas at Austin
Austin, TX 78712

1 - INTRODUCTION

1.1 - REGIONAL BASINS

As watersheds become urbanized, the additional impervious cover and land improvements produce an increase in the volume and speed of storm water runoff. In consequence, downstream flooding becomes more recurrent and more severe, motivating the affected property owners to demand that restrictions be placed on the further land development in the watershed. The conflict between upstream and downstream interests has led many jurisdictions to adopt regulations allowing new development only when it causes no increase in the maximum discharge downstream. Developers can satisfy the regulations by using detention basins to reduce peak flow rates. Onsite detention provides temporary storage for excess discharges near their source, serving to redistribute the excess runoff from a single development.

A more comprehensive solution employs one or more regional detention basins to consolidate the capacity of a number of separate, small detention facilities into fewer and larger facilities. Storm runoff is allowed to enter a receiving channel. If flow in the channel approaches that which will cause flooding, a portion of the flow is diverted into a regional detention basin for temporary storage. When the flow in the channel has decreased sufficiently on the falling limb of the hydrograph, the water stored in the regional detention basin is released back into the stream. A side-channel weir can be used as the structure that diverts excess discharges from the main channel into the regional detention basin.

This report presents a method to assist in designing side-channel weir and detention systems. To model the performance of a trial design, the method connects a hydrologic model, a channel hydraulics model, and a side-discharge hydraulics model into a recursive system that adjusts assumed diversions until they are matched by calculated diversions.

1.2 - OBJECTIVES

In a previous project conducted at the Center for Research in Water Resources (CRWR) and sponsored by the Harris County Flood Control District (HCFCD), experiments were conducted (Tynes, 1989) to determine the hydraulic characteristics of embankment-shaped side weirs, and a design and modeling method (Davis and Holley, 1988) was developed for side weirs. The previous method used manual iteration between HEC-1, HEC-2, and a new program, SIDEHYDR, which was developed specifically for the task of modeling flow beside and over side-discharge weirs.

The present project has built directly on the work done in the previous project. The objectives of the present project were as follows:

1. Develop a computer program to automatically perform the iterations between the programs HEC-1, HEC-2, and SIDEHYDR for the design of side-channel diversion weirs;
2. Add "pop-up" screens for input and for graphical display of the results of the iterations on the computer monitor;
3. Identify the source of computational oscillations in the computer program SIDEHYDR and change the program to remove the oscillations;
4. Prepare a user's manual for the entire computational package of programs, including an improved treatment of the potential pitfalls and error messages in the SIDEHYDR program;
5. Expand the SIDEHYDR program to calculate culvert drainage of water stored in the detention basin below the weir crest;
6. Modify the SIDEHYDR program to allow the choice of either side weirs or culverts for flow diversion;
7. Conduct hydraulic model experiments to evaluate the effects of channel side slopes on side weir hydraulics;
8. Modify the existing side weir physical model and conduct experiments to determine the size and hydraulic effects of the separation zone created in the main channel by the side weir diversion flow;
9. Reanalyze data from the previous project and use computations of water surface profiles along side weirs to evaluate the potential effects of channel slope and roughness on weir hydraulics;
10. Conduct experiments to evaluate the effects of channel flow on the hydraulics of culverts used for diversion and basin drainage at detention facilities,

11. Change the method used in the computational program for flow from the channel into the detention basin based on the results from Tasks 7 and 8,
12. Extend the work of Task 8 to include channels with 4H:1V side slopes.

Only subcritical channel flows are considered in the computational methods and experiments in this report.

Tasks 7 – 10 and 12 are all related to experimental work and are addressed in this report. The other tasks are related to the computational scheme and are addressed in a companion report (Burgin and Holley, 2002). The computational scheme presented in that report uses the empirical results given in this report.

2 - BACKGROUND

As the name implies, side-channel weirs (Fig. 2.1) are placed along the side of a channel parallel (or at a small angle relative to) the flow in the channel. The crest elevation, the crest length, and the length of the weir can be designed to control the operating characteristics of the weir.

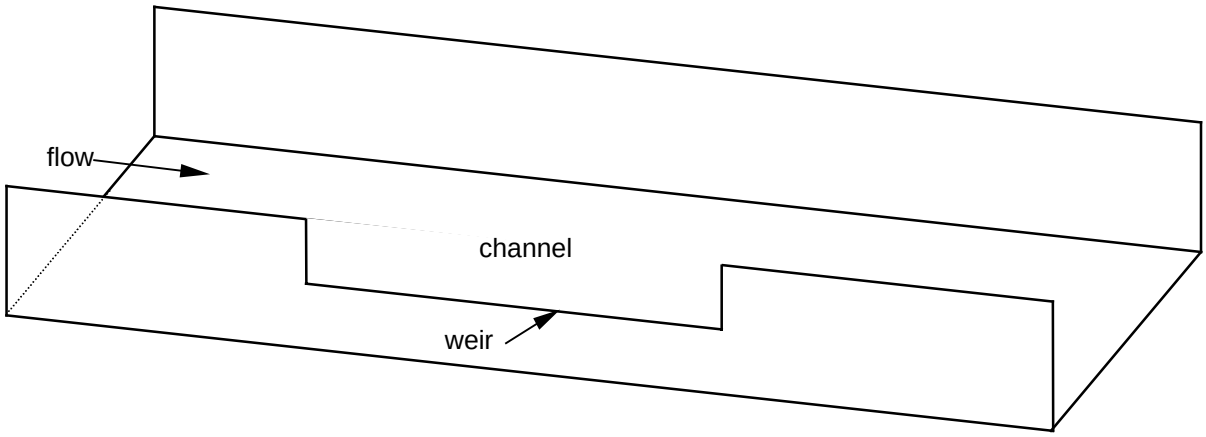

Fig. 2.1 - Schematic diagram of side-channel weir

2.1 - SIDE WEIR FLOW CONDITIONS

There are three general types of flow conditions that can exist with side weirs:

(a) During the rising and falling parts of the hydrograph when the water level in the channel is lower than the weir crest, gradually varied flow exists in the channel section where the weir is located.

(b) When the water level in the channel is above the weir crest and above the water level in the basin, forward flow takes place from the channel into the basin.

(c) If the basin fills to the point that the water level in the basin is above the weir crest, reverse flow from the basin back into the channel will occur when the water level in the channel fall below the water level in the basin during hydrograph recession.

Depending on the relative values of the heads on the weir from both the channel and the basin sides, the weir flow in both directions may have either free or submerged flow conditions. A brief summary is given first for no weir flow and for reverse flow from the basin into the river channel, and then a more detailed treatment is given for forward flow from the channel into the basin.

2.2 - NO WEIR FLOW

When there is no flow in either direction over the weir, HEC-2 could be used for computations as if the weir were not present. However, the overall computational scheme is based on using HEC-2 in the sections of the channel with no weir for diversion and using the program SIDEHYD, which is a revised version of SIDEHYDR from the previous project (Davis and Holley, 1988), for computations in the channel where the weir is located. Thus, when there is no flow over the weir, the depth at the downstream end of the weir is taken from the HEC-2 computations. Then SIDEHYD computes the water surface profile in the part of the channel where the weir is located. This computation is based on the differential momentum equation, which can be written for gradually varied flow (Yen and Wenzel, 1970) as

$$\frac{\partial y}{\partial x} = \frac{S_o - S_f}{1 - \beta\, Fr^2} \tag{2.1}$$

where y = flow depth in the channel, x = longitudinal distance which is positive in the flow direction, S_o = bed slope, S_f = friction slope, β = momentum correction factor, and Fr = channel Froude number which is defined as

$$Fr = \frac{U}{\sqrt{g\frac{A}{T}}} \tag{2.2}$$

where U = average channel velocity (Q/A), A = channel flow area and T = top width of flow. These computations in SIDEHYD give the water surface elevation at the upstream end of the weir. This elevation is put into the HEC-2 input file for restarting the HEC-2 calculations for the channel upstream of the weir.

2.3 - REVERSE FLOW

For reverse flow from the basin back into the channel, the weir behaves as a normal weir rather than as a side weir. The discharge equation for normal broad-crested weirs can be written as

$$Q_w = C_n C_s \frac{2}{3}\sqrt{\frac{2}{3}g}(\Delta x)h^{3/2} \tag{2.3}$$

where Q_w = weir discharge, C_n = discharge coefficient for a broad-crested weir, C_s = submergence correction factor, g = acceleration due to gravity, h = head on the weir, and Δx = increment of length along the weir crest. Eq. (2.3)assumes that the approach velocity is small, as it should be since the flow back over the weir is coming from the detention basin. The sign convention is

that reverse flow from the basin to the channel is positive (Eq. (2.3)) while forward flow from the channel to the basin is negative (Eq. (2.4), Eq. (2.7)). If the weir crest is inclined (e.g., parallel to the invert of an improved channel), then the head on the weir will decrease in the upstream direction since the water level in the detention basin will normally be horizontal.

For reverse flow with subcritical channel flow, both the head loss in the channel due to the disturbance caused by the flow coming over the weir and the increasing discharge in the downstream direction mean that the depth in the channel decreases in the downstream direction. As a result of this change of depth in the channel, C_S can vary along the length of a weir when submerged flow conditions exist.

2.4 - FORWARD FLOW

Flow over side weirs depends on the head on the weir, among other factors. The head depends on the water surface profile along the channel where the diversion is taking place. While the primary factor affecting the water surface profile is the diversion itself, the channel slope and roughness also have an effect on the water surface profile just as they do in a channel without a side weir. Depending on the flow conditions and the channel geometry, the flow over the side weir will cause the flow remaining in the channel to develop a lateral distribution of velocity that is asymmetrical and may cause the flow to separate from the side of the channel opposite the weir.

2.4.1 - Water Surface Profiles

Some of the possible longitudinal water surface profiles in a channel along a side weir for forward flow from the channel into the basin are illustrated in Fig. 2.2, which has been adapted from Henderson (1966). There are several things that are illustrated or implied in this figure that have a direct bearing on the flow diversion problem. One is that, for subcritical flow (Fig. 2.2a), the water surface elevation usually increases in the downstream direction. The second thing is that it is possible to have a hydraulic jump (Fig. 2.2c) in the channel because of the outflow. The possible occurrence of the jump depends on the hydraulics of the outflow and does not require supercritical flow in the channel upstream of the weir. Thus, in a channel with subcritical flow, it is possible for the outflow itself (even on a horizontal or very mild slope channel) to cause the flow in the channel to pass through critical depth at the upstream end of the weir giving supercritical flow, then a hydraulic jump, and finally subcritical flow again. Since the calculation of water surface profiles for subcritical flows depends on knowing a downstream boundary condition (depth), a third thing implied by the first two is that it is impossible to correctly calculate the depths and water surface profile in the channel upstream of a weir without first considering the

details of the flow over the weir and the type of profile which exists at the weirs. Only subcritical flow along the full length of the weir is considered in this design procedure.

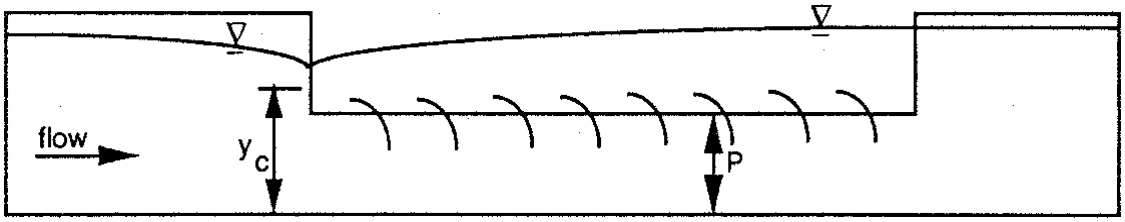

(a) Subcritical flow throughout

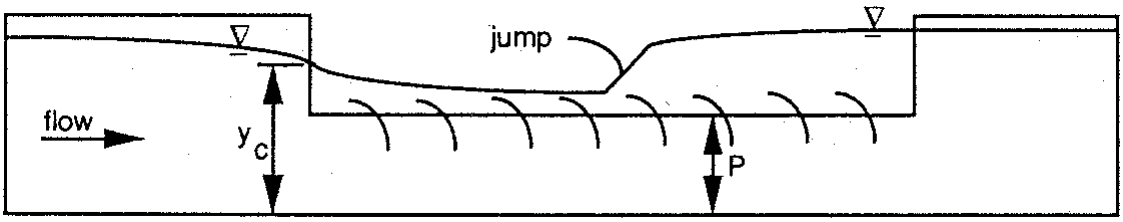

(b) Jump due to side discharge with subcritical flow upstream and downstream

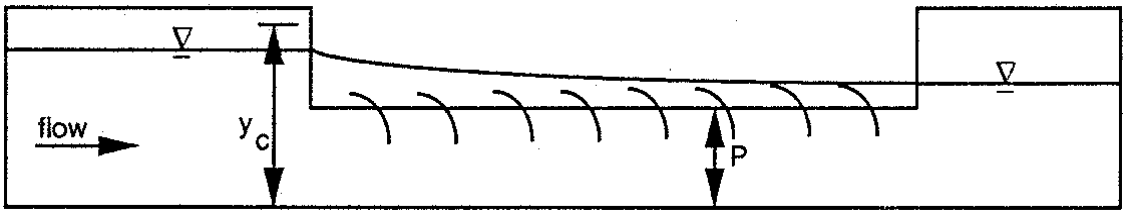

(c) Supercritical flow throughout

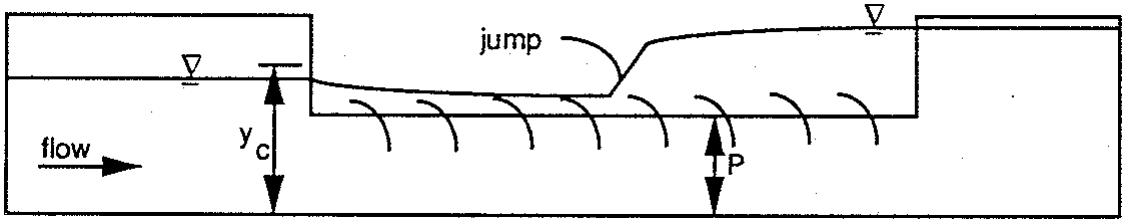

(d) Jump due to supercritical flow upstream and subcritical flow downstream

Fig. 2.2 - Water surface profiles in a channel beside a side-weir

2.4.2 - Previous Work of Others

The water that remains in the channel experiences the normal frictional head losses as the channel flow occurs along the weir, and these losses tend to reduce the total head in the flow direction. Hager (1987) discussed the fact that, when one-dimensional analysis is used, the hydraulic characteristics of side weir flow cause an additional head change that may be either positive or negative, depending on the flow conditions. This condition is also discussed by Idelchik (1986) in conjunction with flow bifurcations in ducts. However, it was found in this project

that using the kinetic energy correction factor (α) eliminated the need for including an additional head change in the energy equation (Section **6.8**).

Most of the previous work has considered only forward flow from the channel into the basin. The earliest studies of the hydraulic characteristics of side-channel weirs were concerned primarily with the analytical prediction of the effects of the weirs on the longitudinal water surface profile in the channel for the idealized case of a rectangular channel with a vertical weir plate and a constant discharge coefficient (Forchheimer, 1930; de Marchi, 1934; Ackers, 1957; Collinge, 1957; Frazer, 1957; Chow, 1959; Henderson, 1966; Bos, 1976). Some other studies on evaluation of the discharge over the side-channel weir are those of Mostafa and Chu (1974), Subramanya and Awasthy (1972), and Hager (1987).

Part of Hager's (1987) analysis was based on the side weir discharge per unit length of the weir (q_w) written as

$$q_w = -\frac{dQ}{dx} = C_1 \frac{2}{3}\sqrt{\frac{2}{3} g}\, h^{3/2} \tag{2.4}$$

where Q is the flow rate in the channel, C_1 is an empirical coefficient, and h is the head at any point along the weir. C_1 may be constant or variable along the weir. Hager wrote C_1 as $C_n\omega$ where C_n is a discharge coefficient for a normal weir of the same geometry as the side weir and ω is a lateral flow coefficient given by

$$\omega = \left(\frac{(Fw^2 + 2)(1 - C_3)}{Fw^2 + 2(1 - C_3)} \right)^{1/2} \tag{2.5}$$

where Fw is defined as

$$Fw = \frac{U}{\sqrt{gh}} \tag{2.6}$$

and is called a weir Froude number since it is based on the head on the weir rather than the flow depth. C_3 is a residual pressure coefficient that is related to the pressure distribution at the control section for the weir flow and is less than unity. Hager used a value of 2/3 for C_3 in Eq. (2.5). Apparently C_3 should depend on the particular type of weir under consideration. The effective discharge coefficient $C_n\omega$ is variable along the weir.

2.5 - PREVIOUS WORK AT CRWR ON HYDRAULIC COMPUTATIONS

2.5.1 - Purpose

Engineers designing side weir and detention basin facilities have to determine the side weir and basin dimensions necessary to reduce the channel flow depth and discharge to acceptable levels for given channel characteristics and a given storm. Although HEC-1 and HEC-2 contain some capabilities for modeling diversions, neither program is flexible enough to represent some of the essential hydraulic features of side weir flows. For example, experimental work indicates that side weir discharge coefficients vary with channel velocity and head on the weir as they change during the passage of the hydrograph, but HEC-1 and HEC-2 cannot represent these changes. Also, the programs cannot predict when submergence of side weirs occurs as the basin fills, nor can they model the flow of water from the basin back to the channel as the channel water level drops. Thus, a program originally called SIDEHYDR was developed in the previous project to model side weir hydraulic characteristics. SIDEHYD used in the modeling presented later in this report is a revision of SIDEHYDR.

SIDEHYDR represents side weir flow including the effects of channel flow characteristics, possible submergence as the basin fills, the discharge characteristics for an embankment-shaped weir, and possible reverse flow over the weir as the channel water level drops during the recession limb of the hydrograph. The channel flow and flow over a side weir interact in such a way that trial and error computations are normally required to determine the side discharge and all of the depths in the channel (at the weir and both upstream and downstream of the weir and in the basin). The side discharge depends on the depths in the channel, but the depths are controlled from downstream for subcritical flow and these depths depend on the discharge, which cannot be known until the side discharge is known. In addition, the depth at the downstream end of one weir can depend on other weirs downstream of it, and the discharge at the upstream end of a weir depends on other upstream weirs. Because of all of these interdependencies, it is necessary to iterate between HEC-1, HEC-2, and SIDEHYDR. In the previous project, these iterations were done manually. The procedure was to

(1) run HEC-1 with an assumed diversion hydrograph at the weir to obtain hydrographs in the channel,
(2) run HEC-2 for times throughout the hydrograph to obtain stage hydrographs at the weirs,
(3) run SIDEHYDR using the discharge hydrographs from HEC-1 and the stage hydrographs from HEC-2 and weir discharge characteristics from the experimental part of the project to calculate the weir diversion hydrograph and the stage hydrograph in the basin,
(4) run HEC-1 again using the calculated diversion hydrograph, and

(5) continue looping through these programs until the diversion hydrographs at the beginning and end of an iteration loop agreed within a specified tolerance. The manual iterations were extremely time consuming. Thus, part of the present project has been to automate the iteration process.

This section gives a summary of the general computational approach that is used for the hydraulic parts of the problem for various flow conditions. Only subcritical flow along the entire weir length (Fig. 2.2a) is considered. Thus, the computations to determine the weir discharge and the water surface profile along the weir (or the depth change between the downstream (sub-d) and upstream (sub-u) ends of the weir) begin with the downstream water level and the downstream head on the weir.

2.5.2 - Forward Weir Flow

2.5.2.1 - Method of Analysis in the Previous Project

In this section, the method of analysis used in the previous project is reviewed. All of Tynes' (1989) test data are listed in Appendix 1 of this report. The tests were conducted in a channel with a trapezoidal cross section with 2.5H:1V side slopes.

For side-channel weirs, the head and the discharge coefficient vary along the length of the weir crest. However, side weirs can be calibrated so that the total side discharge (Q_w) can be written in terms of a bulk discharge coefficient (C_e). For broad-crested weirs, this expression is

$$Q_w = -C_e C_s \frac{2}{3}\sqrt{\frac{2}{3}g}A_w h^{1/2} \tag{2.7}$$

where A_w = a representative flow area (e.g., Lh in Eq. (2.3) for normal weir flow) and C_e = bulk discharge coefficient. The sign convention is that flow into the channel is positive while flow out of the channel is negative. Thus, Eq. (2.3) is positive while Eq. (2.4) and Eq. (2.7) have a negative sign. In Eq. (2.7), some convention must also be established for defining h since the head varies along the length of the weir. Likewise, a convention is needed for defining A_w. In the previous project, h was taken at the downstream (sub-d) end of the part of the weir crest parallel to the channel invert and A_w was taken as h_d times the average length of the flow area over the weir (Fig. 2.3). Thus, Eq. (2.7) can then be written as

$$Q_w = -C_e C_s \frac{2}{3}\sqrt{\frac{2}{3}g}\left[L + h_d\ ES\right]h_d^{3/2} \tag{2.8}$$

where h = height of the water surface above the side weir crest, sub-d = downstream end of side weir crest, L = length of the weir crest parallel to the bed slope (Fig. 2.3), and ES = slope of the

ends of the side weir (e.g., ES = 6 for a 6H:1V slope). The subscript u, which will appear later, denotes the upstream end of the weir crest.

2.5.2.2 - Flow Asymmetry

For forward flow from the channel into the basin, the flow in the channel develops an asymmetrical velocity profile compared to the one that would exist with no diversion (Chapter **6**). Frequently, as part of the flow goes toward and over the weir into the detention basin, a separation zone forms in the channel on the side opposite to the weir. The flow going over the weir effectively pulls the flow that remains in the channel away from the opposite side of the channel. When separation occurs, the flow in the channel at the downstream end of the weir may be concentrated on the side of the channel next to the weir, as shown by the velocity profiles in Section 6.4. Thus, the true velocity head and true momentum flux cannot be obtained from the average velocity given by Q_d divided by the channel area. This condition needs to be taken into account in determining the actual depth in the channel at the downstream end of the weir from the depth indicated by HEC-2 calculations.

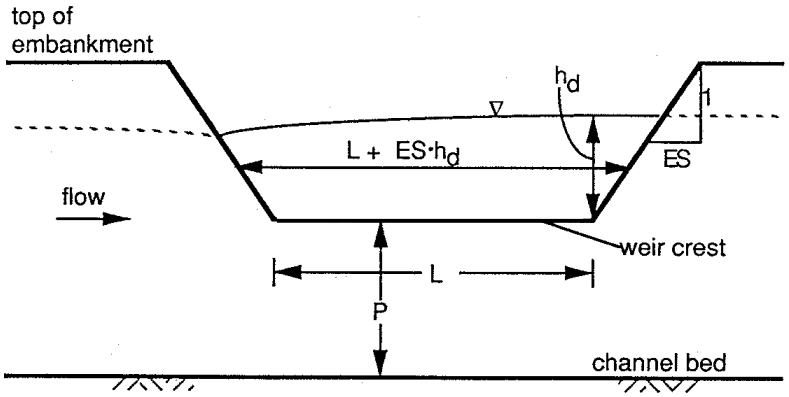

Fig. 2.3 - Definition sketch for side-channel weirs

As pointed out in the HEC-2 User's Manual (US Army Corps Of Engineers, 1984) in conjunction with the flow conditions downstream of bridges, some channel length is required for flow expansion to take place downstream of a separation zone. Nevertheless, it was assumed in the previous project that the channel length for this flow expansion is negligible. Thus, there were two cross sections essentially adjacent to each other at the downstream end of the weir. Cross section db corresponds to the conditions calculated by HEC-2 for the downstream end of the weir but is actually at the downstream end of the zone of flow expansion since HEC-2 inherently assumes that the flow fills the entire cross section. Cross section da corresponds to the

actual conditions at the downstream end of the weir including the flow separation. The designations da and db are used as subscripts.

2.5.2.3 - Downstream Depth

The energy equation can be used to relate the depths at cross section da and db since

$$y_{da} + \alpha_{da} \frac{U_{da}^2}{2g} - K_E \frac{(U_e - U_{db})^2}{2g} = y_{db} + \frac{U_{db}^2}{2g} \tag{2.9}$$

where $U_{da} = Q_d/A_{da}$ = the apparent velocity at cross section da, α = the kinetic energy correction factor, U_e = the effective velocity at cross section da, i.e., the average velocity in the part of the cross section in which flow is actually taking place, and K_E = expansion loss coefficient. This form for head loss term (Henderson, 1966) is more appropriate for this type of flow expansion than the form used in HEC-2. From Eq. (2.9),

$$y_{da} = y_{db} + \frac{U_{db}^2}{2g} - \alpha_{da} \frac{U_{da}^2}{2g} + K_E \frac{(U_e - U_{db})^2}{2g} \tag{2.10}$$

The velocity head at cross section da (the third term on the right-hand side of Eq. (2.10)) is always greater than at cross section db (the second term) for subcritical flow, and K_E is less than unity. The result is that y_{da} is less than y_{db} and that the flow asymmetry and resulting flow re-establishment at the downstream end of the weir suppress the head on the weir relative to y_{db}.

Although Eq. (2.10) may be helpful toward understanding why $y_{da} < y_{db}$, it is not very useful for calculating y_{da}; the K_E value in these equations is unknown and varies with the flow conditions. Thus, the depth at section da needs to be determined from the momentum equation. In the previous project, the boundary shear force and gravitational force within the flow expansion region were neglected as is common for this type of problem so the momentum equation (divided by the density) for a control volume between cross sections da and db gave

$$\left(g\bar{y}A + \beta \frac{Q^2}{A} \right)_{da} = \left(g\bar{y}A + \frac{Q^2}{A} \right)_{db} \tag{2.11}$$

where $\bar{y}$ = distance from the water surface to the centroid of the flow area (A) and β = momentum correction factor (which is assumed in the previous project to be unity at db). Using the value of β_{da} from Eq. (2.19) below, Eq. (2.11) was written as

$$g(\bar{y}A)_{da} + \frac{Q_u Q_d}{A_{da}} = g(\bar{y}A)_{db} + \frac{Q_d^2}{A_{db}} \tag{2.12}$$

This equation was used to calculate y_{da}, which is contained within $\bar{y}$ and A, from the specified conditions at section db. Since the weir discharge and therefore Q_u are unknown at the beginning of the computation, iterations must be done to determine y_{da} from y_{db}.

2.5.2.4 - Kinetic Energy and Momentum Correction Factors

The kinetic energy correction factor is defined as

$$\alpha = \frac{1}{A}\int_A \left(\frac{u^3}{U^3}\right) dA \tag{2.13}$$

where u = point velocity in the channel and U is the average velocity. The velocity distributions in the separation zone were not measured in the previous project. Evaluation of α and the velocity head in the previous project was based on visual observations of the flow conditions in the physical model studies. These observations indicated that the flow at the downstream end of the weir was confined to a fraction of the cross-sectional area approximately equivalent to one minus the fractional diversion over the weir. In the previous project, it was assumed that the flow velocity was uniform with a value u_e in an effective area (A_e), as shown in Fig. 2.4. It was assumed that the ratio of the effective flow area at the downstream end of the weir to the entire cross-sectional area was equal to Q_d/Q_u. Q_u and Q_d are the flow rates upstream and downstream of the diversion respectively, i.e. $Q_u - Q_d = Q_w$. Thus,

$$\frac{A_e}{A_{da}} = 1 - \frac{Q_w}{Q_u} = \frac{Q_d}{Q_u} \tag{2.14}$$

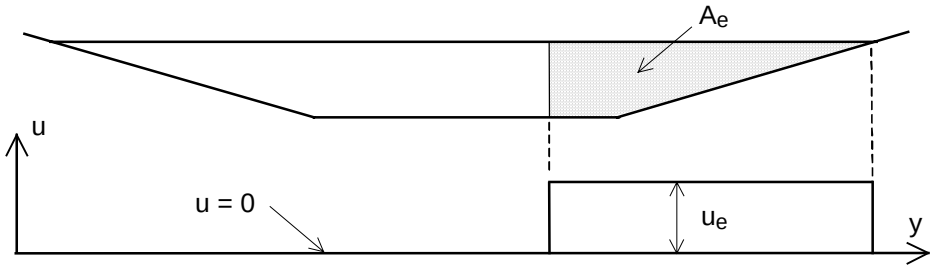

Fig. 2.4 - Assumed velocity distributions and effective flow area

It was assumed that v was zero in the separation zone and uniform in the effective flow area. Accordingly, in the effective flow area,

$$\frac{u}{U_{da}} = \frac{Q_u}{Q_d} \tag{2.15}$$

After substituting $U_{da} = Q_d/A_{da}$ and Eq. (2.15) into Eq. (2.13) and integrating over A_e (since v = 0 in the separation zone), the result can be written as

$$\alpha_{da} = \frac{Q_u^3}{Q_d^3}\frac{A_e}{A_{da}} \tag{2.16}$$

Substituting Eq. (2.14) yields

$$\alpha_{da} = \frac{Q_u^2}{Q_d^2} \tag{2.17}$$

Similarly, the momentum correction factor is

$$\beta = \frac{1}{A}\int_A \left(\frac{u^2}{U^2}\right) dA \tag{2.18}$$

Substitution of Eq. (2.14) for A_e with v = 0 in the separation zone gives

$$\beta = \frac{Q_u}{Q_d} \tag{2.19}$$

2.5.2.5 - Weir Discharge

The weir discharge was calculated from Eq. (2.8) with h_d coming from y_{da} minus the weir height (P). The bulk discharge coefficient (C_e) and submergence correction factor (C_s) were determined from physical model studies (Section 2.6).

2.5.2.6 - Upstream Depth

For the water which flows past the weir and remains in the channel and for the type of analysis used in the previous project, the hydraulic characteristics of side weir flow cause an additional head change (h_c) along the length of the weir, in addition to the frictional head loss (h_f). The energy equation can then be written as

$$H_u - h_f - h_c = H_d \tag{2.20}$$

where H = total head, sub-u = upstream end of the weir, sub-d = downstream end, h_f = frictional head loss along the length of the weir, and h_c = additional head change due to the hydraulic effects of the weir. Assuming that α_u is unity and using Eq. (2.17), Eq. (2.20) becomes

$$y_u + \frac{U_u^2}{2g} - h_f - h_c = y_{da} + \frac{Q_u^2}{Q_d^2}\frac{U_{da}^2}{2g} - S_o L \tag{2.21}$$

or

$$y_u + \frac{Q_u^2}{2gA_u^2} - h_f - h_c = y_{da} + \frac{Q_u^2}{2gA_{da}} - S_o L \tag{2.22}$$

The model results were used to evaluate h_c for forward flow over the weir (Section 2.6.2). With these results, y_u was calculated from Eq. (2.22). In principle, h_c for forward flow can be either positive or negative. For these studies, h_c was always negative for unsubmerged flow (Eq. (2.29)). Using h = y - P where P = weir height, Eq. (2.22) can be rearranged to give the upstream head on the weir as

$$h_u = h_d + h_f \frac{U_u^2}{2g}\left(1 - \frac{A_u^2}{A_d^2}\right) - S_w L + h_c \tag{2.23}$$

where A = cross-sectional area and S_w = longitudinal slope of the weir crest. The frictional head loss was estimated in English units as

$$h_f = \frac{n^2 L}{4.42}\left(\frac{Q_u^2}{A_u^2 R_{hu}^{4/3}} + \frac{Q_d^2}{A_d^2 R_{hd}^{4/3}}\right) \tag{2.24}$$

where n is Manning's n and R_h is the hydraulic radius.

2.5.3 - Reverse Weir Flow

2.5.3.1 - General Approach

For reverse flow, the water level in the basin was obtained from the accumulated volume of water in the basin and was used to determine the head on the weir for use in Eq. (2.3). Both the weir end slopes and the crest were divided into segments of length Δx, so that L in Eq. (2.3) was replaced by Δx. Also, h for each segment was taken as the water level in the basin minus the average weir height for that Δx accounting for the end slopes and for the fact that the weir crest is sloping parallel to the channel invert.

2.5.3.2 - Discharge Coefficients

C_n for a normal weir with a trapezoidal (embankment-shaped) cross-section was obtained from Bos (1985). He plotted the discharge coefficient as a function of h_w/W for a variety of

broad-crested normal weirs, where h_w is the head on the weir and W is the width of the weir crest. Bos' data can be represented by

$$C_n = 0.923 + 0.11\frac{h_w}{W} \tag{2.25}$$

2.5.3.3 - Submergence Correction Factor

The submergence correction factor for reverse flow was obtained by combining modular-limit criteria from Bos (1985) with the submergence correction factor given by DOT (1973). The first step is to determine whether submergence is important and, if so, the second step is to determine the value of the submergence correction factor (C_s).

The submergence of the weir is determined by comparing the tailwater head on the weir (h_t) to the headwater head (h_w). For reverse flow from the basin to the channel, h_w is in the basin and h_t is in the channel. When h_t/h_w exceeds a critical value called the modular limit (ML), submergence becomes an important factor. The modular limit increases as h_w increases. Bos (1985) gave the variation of ML as a function of h_w/P, where P = weir height, for broad-crested weirs which have downstream faces which are vertical or which have 4H:1V slopes. ML values for the previous study were obtained by linear interpolation to a 2.5H:1V downstream slope.

If the degree of submergence exceeds the modular limit so that the weir discharge is influenced by submergence, the submergence correction factor (C_s) must be computed. This calculation starts with C_s as a function of h_t/h_w (DOT, 1973). For other ML values, the C_s vs. h_t/h_w curve expanded and contracted.

2.5.3.4 - Channel Depths and Additional Head Change

The downstream depth in the channel was taken from the HEC-2 computations. The head loss (h_L) for reverse flow is due to the disturbance of the weir flow impinging on the channel flow. Thus, h_L was estimated from the head losses associated with channel flows intersecting at 90° (Idelchik, 1986):

$$h_c = \left[1.55\frac{Q_w}{Q_d} - \left(\frac{Q_w}{Q_d}\right)^2\right]\frac{U_d^2}{2g} \tag{2.26}$$

This head loss was assumed to be linearly distributed along the weir flow length so that Δh_L for each Δx could be determined. Then, the flow depth (y_{i+1}) at the upstream end of each Δx was found from the depth (y_i) at the downstream end of that Δx using the energy equation written as

$$\left(y + \frac{Q^2}{2gA^2} \right)_{i+1} - \Delta h_f - \Delta h_L = \left(y + \frac{Q^2}{2gA^2} \right)_i - S_o \Delta x \qquad (2.27)$$

where Δh_f is the friction loss in the channel for the Δx length. In this calculation, α for the channel flow was taken from Eq. (2.17).

2.6 - PREVIOUS EXPERIMENTAL WORK AT CRWR

2.6.1 - Introduction

The previous project for the Harris County Flood Control District (HCFCD) included a hydraulic model study to investigate the flow characteristics of embankment-shaped side-channel weirs. The model is described in Section 3.1. While the results of the model study were intended to be generally applicable, the model and the testing program were based on specific applications. The discharge coefficients (C_e), submergence correction factors, and the additional head changes (h_c) for both free and submerged flow conditions were determined in the physical model. The results of the previous hydraulic model studies for both forward and reverse flow are summarized by Tynes (1989) and in the following paragraphs.

2.6.2 - Results for Unsubmerged Forward Flow

In the previous project, 238 tests were conducted for unsubmerged flow. Two weir heights of 0.52 ft and 0.70 ft, two channel invert widths of 1.8 ft and 3.4 ft, and weir lengths of 2 ft, 5 ft, 10 ft, 15 ft, 20 ft and 23.91 ft were investigated. There were 16 sets of geometric conditions that were different combinations of the weir heights, invert widths and weir lengths. For each set of geometric conditions, three flow rates with at least five different diversions for each were investigated. The various sets of geometric conditions are listed in Appendix 2.

Using regression analysis, Tynes (1989) obtained the predictive equation for the bulk discharge coefficient as

$$C_e = \exp\left(0.126 - 0.0813\left[\log_e(Fw_d + 3)\right]^{5.15} - 0.0328\left[\log_e\left\{\frac{L}{B} + 3\right\}\right]^{2.20} \right) \qquad (2.28)$$

where V = mean flow velocity in the channel, L = crest length, and B = channel invert width, and the weir Froude number (Fw_d) at the downstream end of the weir is defined as

This expression has a standard error of 0.043, or equivalently, a coefficient of variation of 0.057, relative to the empirical values of C_e. The coefficient of determination (R^2) for Eq. (2.28) is 0.833. Tynes noted that C_e was primarily correlated with Fw_d and had an R^2 of 0.743 when using only Fw_d.

The relative additional head change was found to be

$$\frac{h_c}{h_d} = -0.0361\left(Fr_d \frac{L}{P}\right)^{0.81} \tag{2.29}$$

where P = height of the weir above the channel invert and Fr = channel Froude number defined as

$$Fr = \frac{U}{\sqrt{g\frac{A}{T}}} \tag{2.30}$$

where T is the top width of the flow cross section. R^2 for Eq. (2.29) is 0.751. The negative values of h_c indicate that the hydraulic effects of the weir actually cause an increase in the head in the downstream direction. Use of Eq. (2.29) in the calculation of h_u yielded a standard error of the upstream water surface elevation for the model results of about 0.005 feet. This is a very small standard error since the measurement accuracy was only 0.002 to 0.003 feet for the higher channel Froude numbers. A standard error of 0.005 ft in the model is equivalent to approximately 0.13 feet for prototype conditions.

The model parameters and testing conditions were obtained primarily by consideration of expected conditions in White Oak Bayou. Nevertheless, the results are not constrained to being applicable only for the cited prototype conditions. The results can be used for any geometrically similar channel and weir if they are used in terms of the dimensionless coefficients in Eq. (2.3) and Eq. (2.8). However, the empirical relations should be used only within the limits for dimensionless parameters that were investigated in the physical model. The ranges of values for which these relations are valid are

$$\begin{aligned} Fr_w &= 0.0 \text{ to } 1.5 \\ L/B &= 0.58 \text{ to } 13.3 \\ h_d/P &= 0.05 \text{ to } 0.85 \\ L/P &= 0.28 \text{ to } 46.0 \\ Fr_d &= 0.05 \text{ to } 0.71 \\ Q_w/Q_u &= 0.08 \text{ to } 0.53 \end{aligned} \tag{2.31}$$

2.6.3 - Results for Submerged Forward Flow

The effects of submergence on the side-weir bulk discharge coefficient and on h_c were investigated in the physical model. Thirty-five tests were conducted for submerged flow over the weir with a model weir height of 0.70 feet and model weir lengths of 5 ft, 10 ft and 15 feet. For

each weir length, model invert widths of 1.8 ft and 3.4 ft were investigated. The equation obtained for the submergence correction factor for C_e for forward flow was

$$\begin{aligned} C_s &= 1 && \text{for } \frac{h_t}{h_d} \le 0.5 \\ C_s &= \frac{C_{es}}{C_e} = 1 - 28.84\left(\frac{h_t}{h_d} - 0.5\right)^{4.85} && \text{for } 0.5 < \frac{h_t}{h_d} \le 1 \end{aligned} \tag{2.32}$$

where C_s = submergence correction factor for C_e, C_{es} = discharge coefficient for submerged conditions, and h_t = height of the tailwater in the detention basin above the downstream end of the side weir crest.

The submergence correction factor for h_c was given by

$$\begin{aligned} h_s &= 1 && \text{for } \frac{h_t}{h_d} \le 0.5 \\ h_s &= 1.326 - 0.651\frac{h_t}{h_d} && \text{for } 0.5 < \frac{h_t}{h_d} \le 0.93 \\ h_s &= 10.29\left(1 - \frac{h_t}{h_d}\right) && \text{for } 0.93 < \frac{h_t}{h_d} \le 1 \end{aligned} \tag{2.33}$$

where h_s = submergence correction factor such that h_c for submerged conditions comes from Eq. (2.29) times Eq. (2.33). Tynes (1989) did not give values of R^2 for Eq. (2.33).

2.6.4 - Unsubmerged Flow in Tapered Channels

Sixty-five tests were conducted with a model weir height of 0.70 ft and model weir lengths of 5 ft, 10 ft, 15 ft and 20 ft for tapered channels. The taper was a straight-line reduction of the channel width from a base width of 3.4 ft at the upstream end of the weir crest to 1.8 ft at the downstream end of the weir crest. The regression equation for the bulk discharge coefficient was found to be

$$C_e = 0.810 + 0.177\,Fw_d^3 + 1.77\,DW^3 \tag{2.34}$$

where DW is the change in channel width divided by the distance over which the change in width takes place. Eq. (2.34) has an R^2 of 0.993. Tynes (1989) noted that when considered independently of DW^3, the regression of C_e with Fw_d^3 had an R^2 of 0.991.

The regression equation for the additional head change is

$$\frac{h_c}{h_d} = -0.0402 - 0.0833\,Fw_d^2 + 0.152\,DW + 0.446\,F_d^3 \qquad (2.35)$$

Eq. (2.35) has an R^2 of 0.887.

Since it is assumed that the taper prevents the formation of a separation zone, the energy correction factor is no longer necessary and Eq. (2.23) becomes

$$h_u = h_d + h_f - \frac{U_u^2 - U_d^2}{2g} - S_w L + h_c \qquad (2.36)$$

The tests were not intended to provide a comprehensive study of side weirs in tapered channels. They provided only a preliminary indication of flow conditions for tapered channels.

2.6.5 - Results for Weirs Downstream of Bends

The main characteristics of water moving through a curved channel are the helical flow pattern that develops and superelevation of the water surface. As a channel curves, the water near the surface moves towards the outside of the curve, while the water near the bed flows towards the inside of the curve. This action, along with the forward motion down the channel, results in a helical flow pattern in the channel.

It was assumed that the superelevation would be negligible downstream of a bend. Ninety-five tests were done to investigate the influence of helical flow on side weir discharge coefficients. Deflector vanes were used to develop a helical motion similar to one that would exist in a channel bend. Two sets of vanes were used for different tests to simulate bends in either direction. The strength of the helical motion was equivalent to a bend with a radius of curvature relative to the channel width of approximately 3.

The weir discharge coefficients were determined from the experimental results in the same manner as for straight upstream flow. These coefficients were compared to the coefficients for straight flow in the channel. The average deviation of the values of C_e for the induced helical motion relative to the C_e values with straight channel flow was less than 1% for each deflector.

It should be noted that these tests simulate conditions for a straight weir downstream of a bend. If the weir itself is in a bend and is curved, the effects of the bend may be greater than the effects seen in these tests.

2.6.6 - Reverse Flow

Discharge coefficients for reverse flow were taken from the literature (Eq. (2.25)). Nine experiments were conducted to measure velocities in the channel during reverse flows. The addi-

tional head change was also determined for the experiments, but the results were too limited to develop a reliable empirical expression. Thus, h_c for reverse flow was estimated from Eq. (2.26).

2.7 - VALVES ON DRAINAGE CULVERTS

In the previous project, no provision was made in the model calculations to drain water that is stored in the basin below the height of the weir crest. As mentioned in Section 1.2, one of the objectives of this project was to include drainage culverts in the computational model. The culverts may have either flap gates or Tideflex valves on the downstream (channel) end. In order to develop the computational model, it was necessary to obtain the hydraulic characteristics (primarily the head loss characteristics) of these valves. These characteristics are summarized in this section.

2.7.1 - Tideflex Valves

2.7.1.1 - General

Tideflex check valves (Fig. 2.5) are manufactured by Red Valve Co., Inc., Pittsburgh, Pennsylvania, of reinforced rubber. The ones used by Harris County Flood Control District can be mounted on the downstream end of circular pipe culverts, as shown in the figure. Pressure in the culvert forces the downstream end of the valve to open with the amount of opening increasing as the flow increases. In addition to the normal catalog information on the hydraulic characteristics of the valves, the manufacturer supplied graphs of valve head loss vs. the flow rate (Q_{pipe}), total head loss vs. Q_{pipe}, jet (discharge) velocity vs. Q_{pipe}, and open downstream area (A_{valve}) vs. Q_{pipe} for 24 in., 36 in., 48 in., 60 in., 72 in., and 84 in. valves. This information was used as described below to develop the equations that were used in the computer simulation of flow in drainage culverts. A sample of the curves obtained from the manufacturer is shown in Fig. 2.6.

2.7.1.2 - Manufacturer's Information

The manufacturer's curves for the open area of the various sizes of valves were combined by scaling them relative to half of the inside culvert area, i.e., the scaling parameter was

$$A_{half} = \frac{A_{pipe}}{2} = \frac{\pi D_{pipe}^2}{8} \tag{2.37}$$

where A_{pipe} is the inside area of the culvert and D_{pipe} is the culvert ID. For each valve size, Q_{half} was defined as the flow when the open valve area (A_{valve}) is equal to A_{half}. The values read from the manufacturer's graphs are shown in Fig. 2.7. The best-fit line is given by

$$Q_{half} = 11.34 A_{half} \tag{2.38}$$

where Q_{half} is in cfs and A_{half} is in ft^2. These reference values for each pipe size were used to scale the flow area vs. Q curves, as shown in Fig. 2.8. The best analytical representation that could be found to represent the points in Fig. 2.8 was

$$\frac{A_{valve}}{A_{half}} = \left[0.9127 + 0.9277 \log\left(\frac{Q}{Q_{half}}\right) + \frac{0.09059}{\left(\frac{Q}{Q_{half}}\right)^{0.5967}} \right] \quad \text{for} \quad \frac{Q}{Q_{half}} > 0.036 \tag{2.39}$$

Since this equation is undefined at $Q/Q_{half} = 0$, it was used only for $Q/Q_{half} > 0.036$, which corresponds to the second smallest value read from the manufacturer's curves. For lower values, a linear interpolations was used, giving

$$\begin{aligned} \frac{A_{valve}}{A_{half}} &= \left[0.9127 + 0.9277 \log(0.036) + \frac{0.09059}{(0.036)^{0.5967}} \right] \left[\frac{Q/Q_{half}}{0.036} \right] \\ &= 6.44 \frac{Q}{Q_{half}} \quad \text{for} \quad \frac{Q}{Q_{half}} \le 0.036 \end{aligned} \tag{2.40}$$

The curves for Eq. (2.39) and Eq. (2.40) are shown in Fig. 2.8.

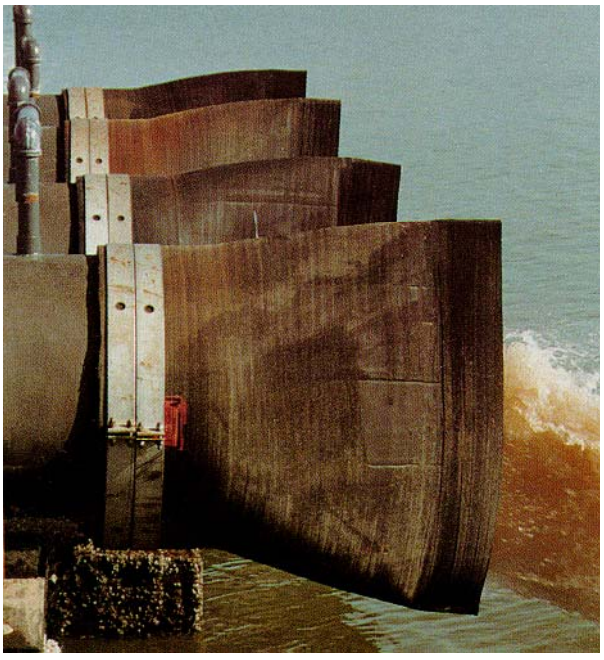

Fig. 2.5 - Tideflex valves (from Red Valve Co., Inc. catalog)

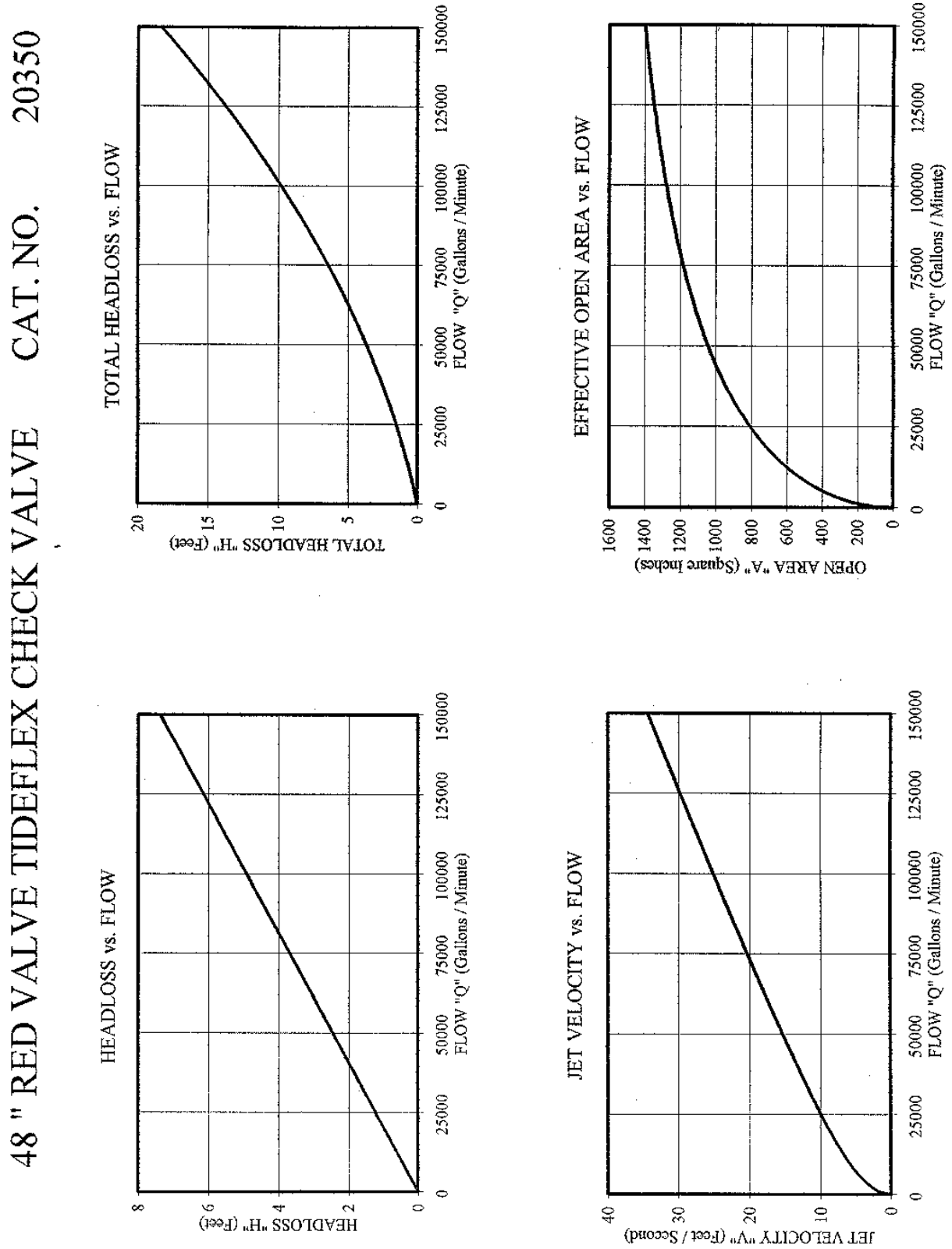

Fig. 2.6 - Sample of curves obtained from Red Valve Co., Inc. for Tideflex valves

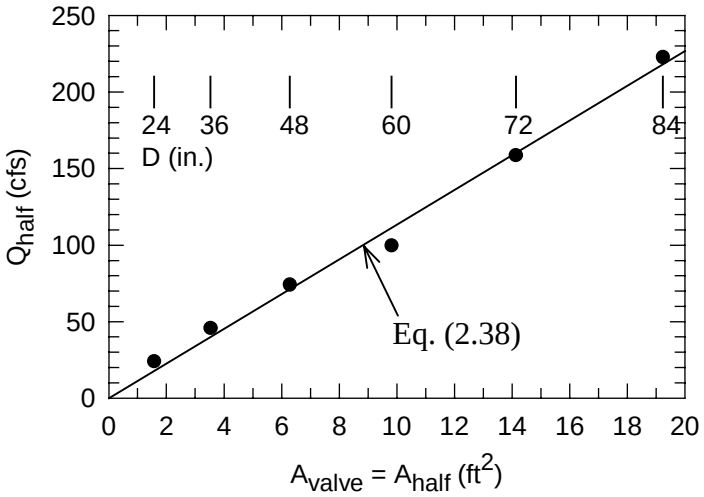

Fig. 2.7 - Q_{half} for Tideflex valves

As noted above, the manufacturer supplied both the head loss in the valve itself (H_L) and the "total head loss", which was defined as the head loss in the valve plus the velocity head in the pipe. However, the actual loss associated with a submerged valve is the loss in the valve plus exit loss or the velocity head of the jet leaving the valve (not the velocity head in the pipe), Thus, only the head loss in the valve was used in calculating a loss coefficient. The exit loss was included in the calculations separately. The head loss coefficient (K_L) was defined by

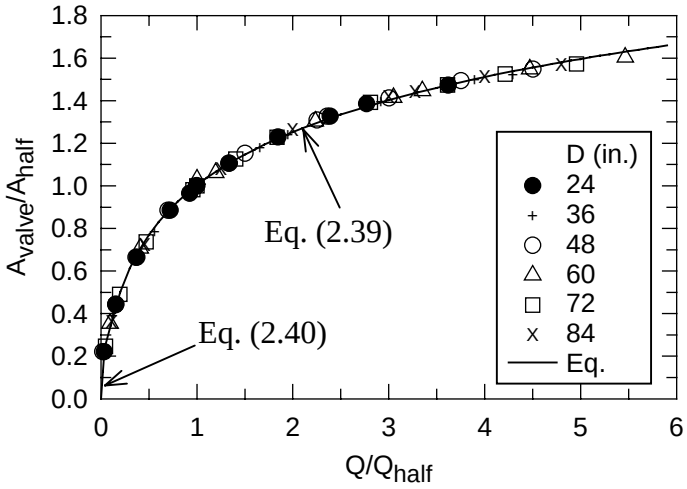

Fig. 2.8 - Scaled downstream areas for Tideflex valves

$$H_{L\,valve} = K_L \frac{\left(V_{valve} - V_{pipe}\right)^2}{2g} \tag{2.41}$$

where V_{valve} is the exit velocity from the valve and V_{pipe} is the velocity in the culvert. The head loss coefficients defined in this manner are shown in Fig. 2.9. The mean value of K_L is 1.0 with a standard deviation of 3%. There is a large amount of scatter for small values of Q/Q_{half}, but the velocities and therefore the head losses are small for these small flow rates.

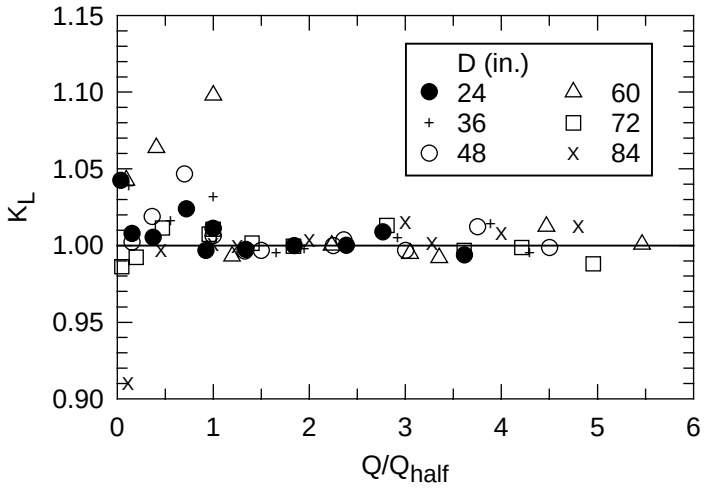

Fig. 2.9 - Head loss coefficients for Tideflex valves

2.7.1.3 - Calculation Method for Submerged Valves

This section summarizes the calculations used when the Tideflex valve is submerged. The valve is considered to be submerged when the tailwater is above the downstream soffit of the culvert pipe. In the calculations, the tailwater depth (TW) is measured from the downstream invert of the pipe (not the valve). As described by Burgin and Holley (2002), the culvert flow is calculated by trial and error based on assumed flows. The assumed flows are adjusted until the head required for the assumed flow matches the head available in the detention pond. For the assumed flow rate (Q), the calculation procedure is as follows, with all values being in feet and cfs:

1) Calculate the culvert cross sectional area in ft^2 from $A_{pipe} = \pi D^2/4$.
2) Calculate half of the culvert cross sectional area in ft^2 from $A_{half} = A_{pipe}/2$.
3) Calculate the flow rate in cfs corresponding to having an open area in the Tideflex valve equal to A_{half} from Eq. (2.38).
4) Calculate the open area (A_{valve}) of the Tideflex valve corresponding to the specified Q from Eq. (2.39) or Eq. (2.40).
5) Since the valve will flow full for submerged conditions, calculate the valve exit velocity head from

$$\frac{V_{valve}^2}{2g} = \left(\frac{Q}{A_{valve}} \right)^2 \frac{1}{2g} \tag{2.42}$$

where Q = assumed flow rate in the culvert.

6) Since the pipe will also flow full for submerged conditions, calculate the pipe velocity head from

$$\frac{V_{pipe}^2}{2g} = \left(\frac{Q}{A_{pipe}} \right)^2 \frac{1}{2g} \tag{2.43}$$

7) Since the valve loss coefficient based on the difference in the entrance and exit velocity heads (Eq. (2.41)) is 1.0, the sum (H_L) of the valve and exit head losses is

$$H_L = \left(\frac{V_{valve}^2}{2g} - \frac{V_{pipe}^2}{2g} \right) + \frac{V_{valve}^2}{2g} = 2\frac{V_{valve}^2}{2g} - \frac{V_{pipe}^2}{2g} \tag{2.44}$$

8) It is now possible to calculate the head at the end of the culvert (i.e., at the upstream end of the valve). Because of the way that the program for culvert flow does its calculations, the equivalent tailwater ($TW_{equivalent}$) at the downstream end of the culvert without the valve is needed. That is, a culvert with $TW_{equivalent}$ and with no valve would have the same flow as the culvert with the valve. $TW_{equivalent}$ to account for the valve and exit losses is

$$\begin{aligned} TW_{equivalent} &= TW_{actual} + H_L - \frac{V_{pipe}^2}{2g} \\ &= TW_{actual} + 2\left(\frac{V_{valve}^2}{2g} - \frac{V_{pipe}^2}{2g} \right) \end{aligned} \tag{2.45}$$

9) Calculate the headwater (HW) based on $TW_{equivalent}$ and the assumed flow rate (Q). HW is relative to the upstream invert of the culvert.

10) Store TW and the final Q and HW for each time step in the calculations. Only the values for the most recent time step are kept in storage. These values are needed for unsubmerged conditions discussed in the next section.

11) At the end of the calculations for a given time step, check to determine whether TW is below the downstream soffit. If so, the calculations then shift to those described in the next section.

2.7.1.4 - Calculation Method for Unsubmerged Valves

This section summarizes the calculations for unsubmerged conditions that are assumed to exist when the tailwater is below the downstream soffit. An approximate method of calculation is needed since information on the flow area of the valve and depth of flow in the valve outlet could not be obtained for unsubmerged conditions. Even when the valve outlet is not submerged, the head loss in the valve may cause the downstream end of the culvert to still be flowing full. At the end for the calculations for the assumed unsubmerged conditions, a check is made to determine if the downstream end of the culvert is full.

1) At the end of the first time step with the tailwater below the downstream soffit, a linear interpolation is used to determine Q_{soffit} and HW_{soffit} corresponding to having the TW at the downstream soffit.
2) For subsequent time steps, it is assumed that the water depth (y_{exit}) in the downstream valve opening decreases linearly in proportion to the decreasing headwater in the detention pond unless the tailwater is higher than the value indicated by this linear interpolation. Thus,

$$y_{exit} = \max\left(\frac{HW}{HW_{soffit}} D, TW\right) \tag{2.46}$$

where y_{exit} is measured from the pipe invert, not from the bottom of the valve. The depth in the valve opening ($y_{v_{exit}}$) is measured from the bottom of the valve, so

$$y_{v_{exit}} = y_{exit} + \frac{H - D}{2} \tag{2.47}$$

where H is the height of the downstream end of the valve (Fig. 2.10) and is given by H = 1.64D.

3) From Q_{soffit}, the valve open area (A_{soffit}) corresponding to having the tailwater at the soffit is obtained from Eq. (2.39) or Eq. (2.40).
4) For each subsequent tailwater which is below the downstream soffit, it is assumed that the valve open area decreases linearly, i.e.,

$$A_{valve} = A_{soffit} \frac{y_{v_{exit}}}{H} \tag{2.48}$$

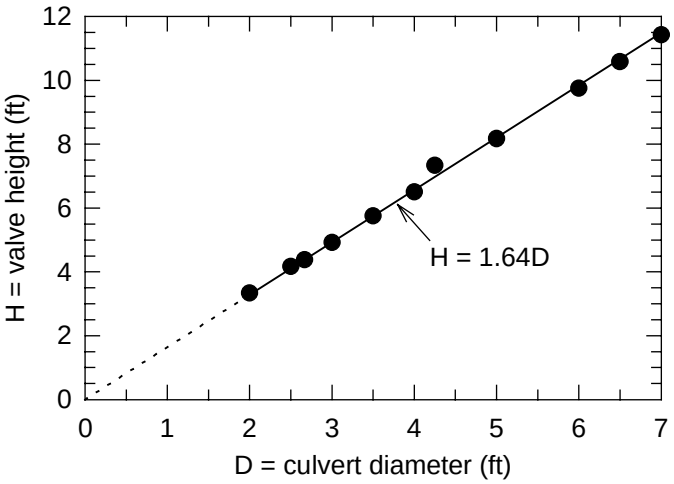

Fig. 2.10 - Height of Tideflex valves

5) It is further assumed that the open area of the valve is composed of two triangles with coincident bases and with heights equal to half of the valve height, as shown in Fig. 2.11. The base width of the two triangles is given by

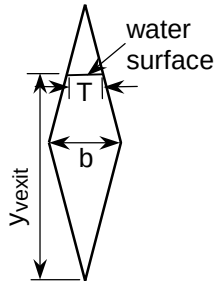

Fig. 2.11 - Assumed open shape of Tideflex valves

$$b = \frac{2A_{valve}}{H} \tag{2.49}$$

6) The surface width (T_{exit}) and the flow area in the valve opening (A_{exit}) are calculated from

$$\left.\begin{aligned} T_{exit} &= b\frac{H - y_{v_{exit}}}{H/2} \\ A_{exit} &= A_{valve} - T_{exit}\frac{H - y_{v_{exit}}}{2} \end{aligned}\right\} \quad \text{for } y_{v_{exit}} > \frac{H}{2}$$

$$\left.\begin{aligned} T_{exit} &= b\frac{y_{v_{exit}}}{H/2} \\ A_{exit} &= T_{exit}\frac{y_{v_{exit}}}{2} \end{aligned}\right\} \quad \text{for } y_{v_{exit}} \le \frac{H}{2} \tag{2.50}$$

7) The velocity head at the valve outlet is calculated from

$$\frac{V_{exit}^2}{2g} = \frac{(Q/A_{exit})^2}{2g} \tag{2.51}$$

8) Since $K_L = 1$, the head loss in the valve is

$$H_{L_{valve}} = \frac{V_{exit}^2}{2g} - \frac{(Q/A_{flow})^2}{2g} \tag{2.52}$$

where A_{flow} is the flow area corresponding to the flow depth (y_{pipe}) at the end of the culvert pipe.

9) $TW_{equivalent}$ is calculated from as follows: The energy equation between the end of the pipe and the valve exit is

$$\begin{aligned} y_{pipe} + \frac{(Q/A_{flow})^2}{2g} - \left(\frac{V_{exit}^2}{2g} - \frac{(Q/A_{flow})^2}{2g}\right) &= y_{exit} + \frac{V_{exit}^2}{2g} \\ y_{pipe} + 2\frac{(Q/A_{flow})^2}{2g} &= y_{exit} + 2\frac{V_{exit}^2}{2g} \end{aligned} \tag{2.53}$$

This equation is solved by trial and error to obtain y_{pipe}, which is $TW_{equivalent}$ if $y_{pipe} < D$.

10) If there is no solution of Eq. (2.53), then the downstream end of the culvert pipe is flowing full even though the valve is not submerged. For these conditions, $TW_{equivalent}$ is calculated from Eq. (2.43) and

$$TW_{equivalent} = y_{exit} + H_L - \frac{V_{pipe}^2}{2g}$$
$$= y_{exit} + 2\left(\frac{V_{valve}^2}{2g} - \frac{V_{pipe}^2}{2g}\right) \tag{2.54}$$

2.7.2 - Flap Gates

Nagler (1923) measured head losses due to flap gates. He concluded that the head loss caused by the gates is negligible for unsubmerged flow while for submerged conditions, the head loss coefficient (K_L) and the head loss (H_L) are

$$K_L = 8\exp\left(-\frac{1.15V_{pipe}}{\sqrt{D}}\right)$$
$$H_L = K_L\frac{V_{pipe}^2}{2g} \tag{2.55}$$

where V_{pipe} is in fps and D is in ft. Unfortunately, all of his tests were done for full pipe flow. However, his explanation for the negligible head loss for unsubmerged conditions was that the trajectory of the flow tends to fall rapidly after leaving the pipe so the flow does not impact very strongly on the gate. Thus, Nagler assumed that the head loss would be negligible also for unsubmerged flow with the pipe only partially full. Another unfortunate thing about his work is that he did not define how low the tailwater needs to be to met his definition of unsubmerged flow. Photographs in his paper imply that the tailwater was below the downstream invert of the culvert.

To account for the head loss for full pipe flow, $TW_{equivalent}$ was defined as the tailwater that would give the same flow conditions in the culvert without the flap gate and was taken as that actual tailwater plus H_L from Eq. (2.55). As the tailwater fails, the value of the head loss that exists when the tailwater just fills the culvert is saved. Then for tailwater levels between the downstream invert and soffit, the head loss due to the valve is assumed to vary like the square of the actual tailwater divided by the tailwater that just fills the culvert pipe.

3 - EXPERIMENTAL FACILITIES

For the experimental work reported in Sections 2.6 and Sections 6.4.3 - 6.4.7, the model was unchanged from the previous project (Section 3.1). However, channels may have flatter side slopes, and these flatter slopes can affect the hydraulics of weir flow by altering the velocity distribution in the channel and by effectively keeping the major part of the channel flow a greater distance from the weir crest. Thus, the model was modified to have 4H:1V side slopes for some of the experimental work in this project.

3.1 - PHYSICAL MODEL FOR PREVIOUS PROJECT

In the mid-1980, the Harris County Flood Control District (HCFCD) was planning to use regional detention facilities to alleviate flooding in the White Oak Bayou watershed in northwest Harris County, as well as in other parts of Harris County. Depths up to 25 feet and maximum flow rates of approximately 20,000 to 25,000 cfs were expected along White Oak Bayou. The plans were for the channel in the previous project to have a trapezoidal cross section with 2.5H:1V side slopes. This slope was also the slope of the front and back faces of the embankment-shaped weirs. Invert widths could vary from 45 to 80 feet, depending on the final design and location along the channel. These values were used in designing the model and in planning the testing program. Most of the geometric features of the model channel and weirs were specified by HCFCD. The model was operated according to the Froude similarity criteria with a length scale of 1:25 relative to the values for White Oak Bayou.

The weir crest would be used as an access road for maintenance; thus its crest width was planned to be 12 feet in the prototype. The horizontal distance from the berm between the channel and the detention basin to the weir crest was set at 50 feet in the prototype, and the height of the berm above the channel invert was designed to be 25 feet. Thus the slope of the weir ends varied depending on the height of the weir. The side of the weir that slopes into the channel was placed in line with the side embankment of the channel. All model tests were conducted with the weir placed along a straight section of the channel.

Plan and elevation drawings of the model weir are in Fig. 3.1. A photograph of the model and weir is in Fig. 3.2. The model was a 65-ft long trapezoidal channel with side slopes of 2.5H:1V, a longitudinal slope of 0.000385, and a Manning's n of 0.0125. In the previous project, channel base widths of 3.4 ft and 1.8 ft were used. The top of the berm separating the channel from the model detention basin was 1.2 feet wide, equivalent to 30 feet for a 1:25 model length scale, and was 1.0 foot (25 feet in the prototype) above the main channel invert. On the detention basin side, the berm had a slope of 3H:1V. The channel face of the weir was aligned

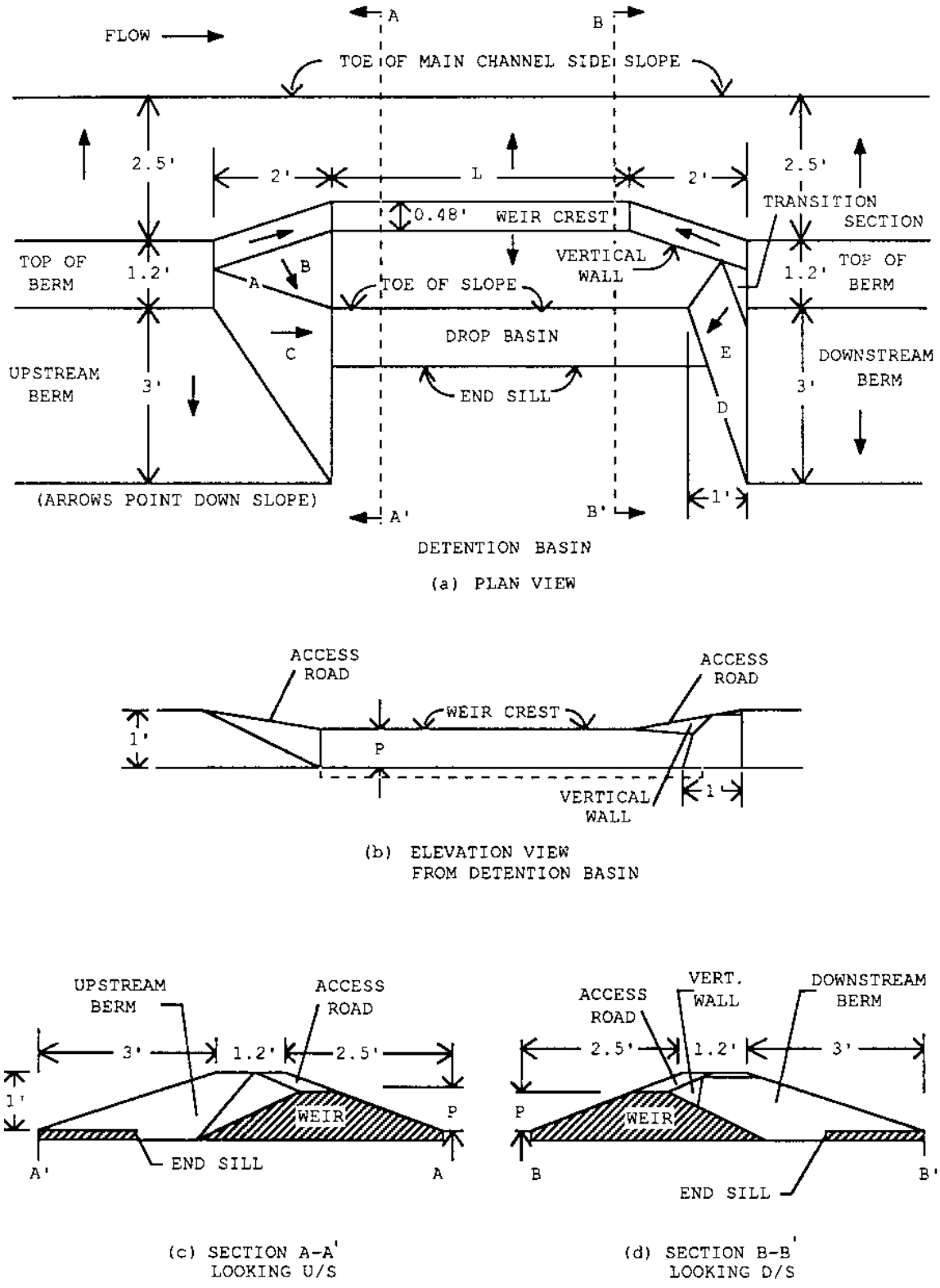

Fig. 3.1 - Plan and elevation views of the model weir

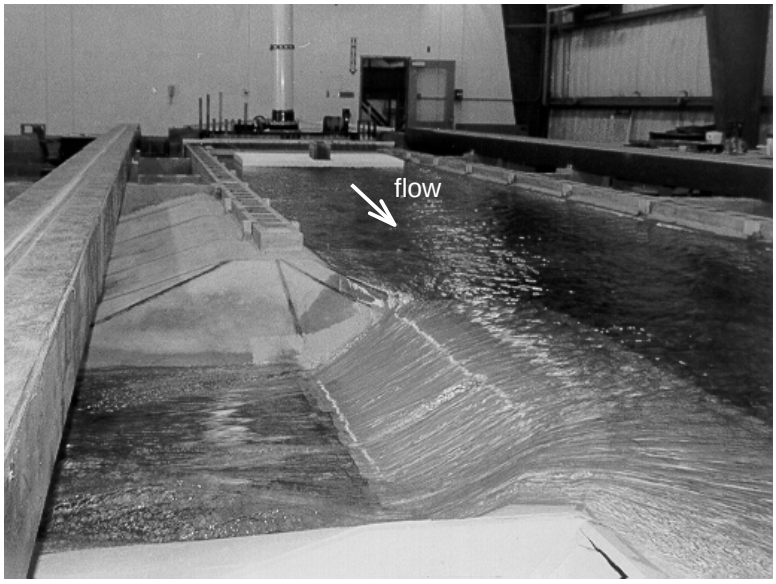

Fig. 3.2 - A photograph of the model and weir

with the side of the channel. The primary part of the crest was parallel to the channel invert and was 0.48 ft wide. The nearly horizontal part of the weir crest was separated longitudinally from the berm by a distance of 2.0 feet (50 feet in the prototype) at both the upstream and downstream ends of the weir. The access road sloped downward from the berm to the weir crest. The width of the access road was 0.48 feet (12.0 feet in the prototype), the same width as the weir crest. The slope of the inclined ends of the weir (the access road) varied according to the height of the weir crest above the channel invert. The face of the weir that sloped into the detention basin had a slope of 2H:1V. The slope of the end of the berm at the upstream end of the weir was also 2H:1V.

Initially the transition between the two ends (upstream and downstream) of the weir and the ends of the berm at the weir were identical. A sloping straight line connected the detention basin side of the top of the access road to the intersection of the base of the weir slope, the detention basin floor, and the end of the berm at the upstream end of the weir. The triangle formed by this sloping line, the detention basin side of the access road and the end of the face of the weir that sloped into the detention basin was planar and sloped as shown in the plan view for the upstream end (Fig. 3.1a). Another plane surface sloped from the top of the berm to the detention basin floor. The bottom of this surface was in line with the end of the weir, 2.0 feet (horizontal model dimension) from the top of the berm. The corner between this 2H:1V surface and the 3H:1V sloping face of the berm was a smooth quarter circle with a model radius of curvature of 0.5 feet.

This type of transition caused problems in the flow at the downstream end of the weir. The discharge over the weir per unit length of the weir is greater at the downstream end of the weir. Also, the flow goes across the weir at an angle because of residual longitudinal momentum associated with the flow in the channel. When the flow over the downstream part of the weir encountered the downstream surface that sloped from the top of the berm to the floor of the detention basin, it was forced back in the upstream direction. This condition caused severe aggregation of the flow in a relatively small area of the detention basin. There was concern by the investigators and the staff of HCFCD that the larger depths caused by this aggregation (compared to the more upstream region at the base of the weir) would cause difficulties with the stilling basin and energy dissipation. Because of these concerns, the downstream transition section between the berm and side weir was modified to be as shown in Fig. 3.1. A vertical wall was used on the detention basin side of the access road. A straight line was drawn from the base of the detention basin side of the weir (at a point 1.0 foot upstream of the top of the access road) to the base of the 3H:1V sloping side of the downstream berm. A plane surface was used for the end of the berm. Because this surface was downstream of the downstream end of the weir crest and was canted in the downstream direction, the aggregation of the flow at the downstream end of the weir was essentially eliminated.

Two-hundred-sixty-eight tests were conducted. The model results were used to develop empirical relations to predict the flow over the weir and the change in the water surface elevation along the length of the weir. Empirical relations were also developed to characterize the effect of submergence on these two parameters.

3.2 - MODIFICATION OF THE PHYSICAL MODEL TO 4H:1V SIDE SLOPES

After consideration of several alternatives, it was decided that the most feasible way of building the channel with 4H:1V side slopes was to build it in the existing channel that had 2.5H:1V side slopes. The same model length scale of 1:25 was used. In order to fit inside the existing channel, the new channel had an invert width of 1.8 ft and its invert was about two inches above that of the existing channel with 2.5H:1V side slopes.

Female plywood templates were put in the previous channel at intervals of four feet. The space between the templates was filled with concrete. The previous plywood side weir was removed. A new weir was made of concrete. However the transition from the downstream end of the weir crest to the channel side slope was made of plywood. The transition was similar to that in the previous model (Tynes, 1989.) The new weir was also embankment-shaped with 4H:1V slope on the front and back faces.

As mentioned by Tynes (1989), the vertical position of the measurement carriage, and therefore the point gauge, could vary as the carriage was moved. In the previous project, steel

washers were attached to the floor of the channel on each side of the channel. The washers served as elevation benchmarks to establish the vertical position of the measurement carriage. The same approach was used for the new channel. The washers were spaced at an interval of two feet upstream and downstream of the weir section, and at an interval of one foot along the weir section.

It was planned to keep the same longitudinal slopes of the new channel and weir crest as for the existing channel. However the new channel as built had a small hump along the weir section. The elevations of washers along the channel and the elevations of the weir crest are shown in Fig. 3.3. The weir crest had a slightly higher elevation on the side next to the channel than on the side next to the detention basin. The maximum difference was 0.023 ft. The elevation on the side of the channel was used when determining the weir height.

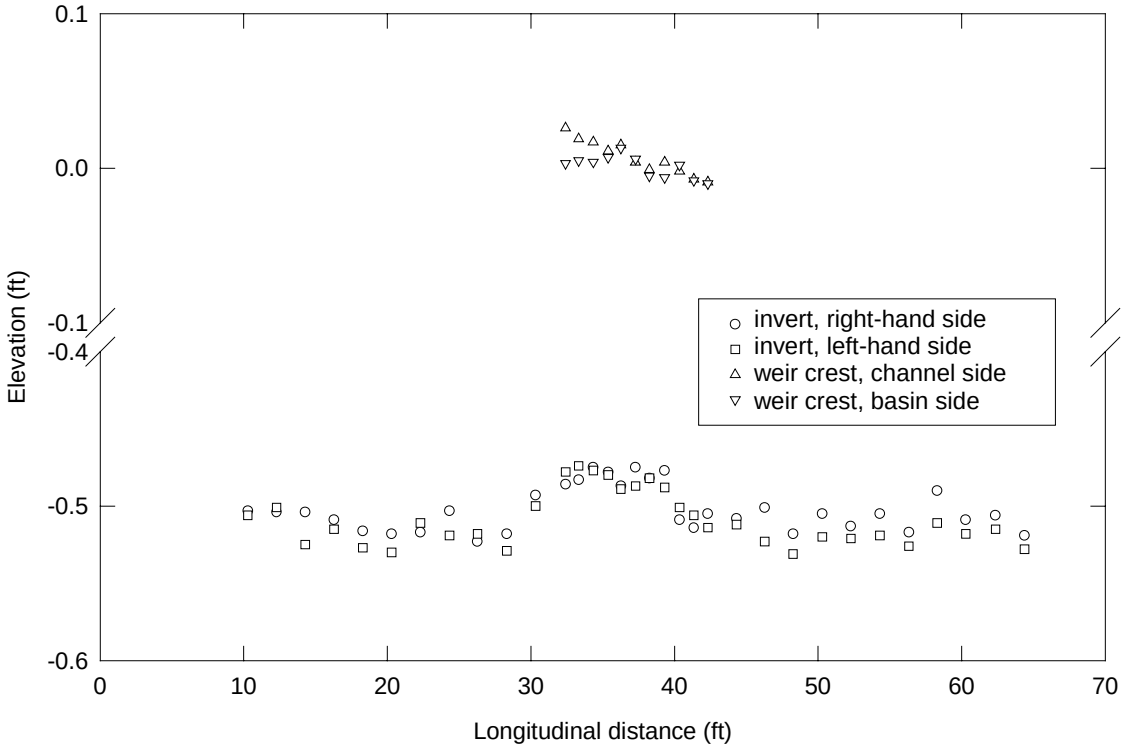

Fig. 3.3 - Longitudinal profiles of channel invert and weir crest (arbitrary datum)

Experiments were conducted to determine Manning's n for the new channel. The tests were conducted at discharges of 3.30 cfs and 4.41 cfs and depths of about half a foot at the downstream end of the channel. Only the part of the channel below the weir crest was used. Once the flow conditions stabilized, water surface elevations were measured along the entire length of the channel. The standard step method was used to determine the appropriate rough-

ness coefficient for the channel. Through trial and error, the value of n that generated the water surface profile most closely matching the one measured in the channel was determined. Manning's n for the new channel was found to be 0.0115. The n value for the previous channel was 0.0125.

3.3 - MEASUREMENT OF DISCHARGES

The flow into the model was pumped from a half-million gallon reservoir outside the laboratory. Two vertical turbine pumps, designated north and south, pumped from the reservoir into the two ends of an overhead 12-inch diameter steel pipe loop in the laboratory. The pumps could be operated separately or simultaneously. A Venturi meter in the north line of the system measured flow from the north pump into the model. Flow from the south pump was measured by a Model 220B propeller-type flow sensor connected to a Model 1000 digital flow monitor, both manufactured by Data Industrial Corporation of Mattapoisett, Massachusetts. Flow rates were determined by taking a time average using the total flow output from the flow monitor. Discharge over the side weir was measured with a V-notch weir in the return floor channel. Similar discharge measuring devices were used in the previous project and are described in Tynes (1989). However a new flow sensor and a new V-notch weir were installed for this project.

3.3.1 - Calibration of Venturi Meter

The Venturi meter was calibrated volumetrically in another project using part of the return floor channel as a volumetric tank (Hammons and Holley, 1995). The calibration was found to be

$$Q = 1.29\Delta h^{0.53} \tag{3.1}$$

where Q is the discharge in cfs and Δh is the difference in piezometric head between the entrance and throat of the Venturi meter in feet of water. This calibration was used in the present project for $Q < 0.6$ cfs. The root-mean-square of the deviations between the measured flow rates and those obtained from the regression line was 0.081 cfs and the maximum deviation was 7.4%.

Some of the side weir discharges in this set of experiments were smaller than the lowest flow rates in the calibrations to obtain Eq. (3.1). Therefore additional calibrations were done for the Venturi meter (and the V-notch weir discussed below) for low flows. The Venturi meter was calibrated volumetrically using the return floor channel as a volumetric tank. The low-flow calibration curve for the Venturi meter is shown in Fig. 3.4. The regression equation for the calibration data was found to be

$$Q = 1.310\ \Delta h^{0.550} \tag{3.2}$$

where Q is the discharge in cfs and Δh is the difference in piezometric head in feet of water between the entrance and throat of the Venturi meter. Eq. (3.2) is applicable for $Q \leq 0.6$ cfs and $\Delta h \leq 0.24$ ft. The root-mean-square of the deviations between the measured flow rates and those obtained from the regression line was 0.006 cfs and the maximum deviation was 3.0%.

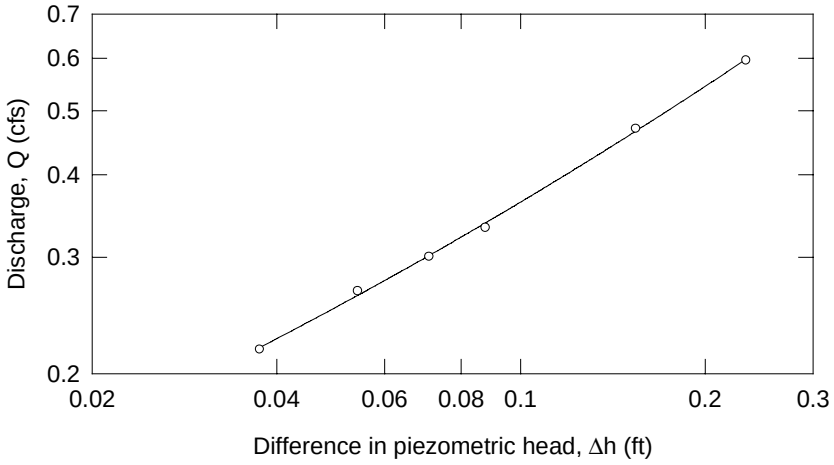

Fig. 3.4 - Low flow calibration of Venturi meter

3.3.2 - Calibration of V-Notch Weir

The V-notch weir was calibrated using discharges measured by the Venturi meter. The calibration curve is plotted in Fig. 3.5. The head-discharge relationship was found to be

$$\log(Q) = 0.381 + 2.685 \log(h) + 1.484 (\log(h))^2 \qquad (3.3)$$

where the logarithms are base 10, Q is in cfs and h is the head on the weir in feet (i.e., height of the water surface above the bottom of the V-notch of the weir). In the head-discharge relationship for a V-notch sharp-crested weir for idealized conditions, Q is proportional to $h^{2.5}$. Eq. (3.3) provided a better fit to the calibration data than the idealized relationship, and it was used in this project for $Q \geq 1$ cfs and $h \geq 0.7$ ft. The root-mean-square of the deviations between the measured flow rates and those obtained from the regression line was 0.025 cfs and the maximum deviation was 1.5%.

As with the Venturi meter, a separate calibration was needed for the V-notch weir for low flows. The low-flow calibration data for the V-notch weir are shown in Fig. 3.6. The head-discharge relationship was found by regression to be

$$Q = 2.236\, h^{2.240} \qquad (3.4)$$

where h is the head on the weir in feet (i.e., the height of the water surface above the bottom of the V-notch of the weir). Eq. (3.4) was used for $Q \leq 1$ cfs and $\Delta h \leq 0.7$ ft. The root-mean-square of the deviations between the measured flow rates and those obtained from the regression line was 0.008 cfs and the maximum deviation was 2.0%. This low-flow calibration for the Venturi meter was used to determine the discharge for calibrating the V-notch weir.

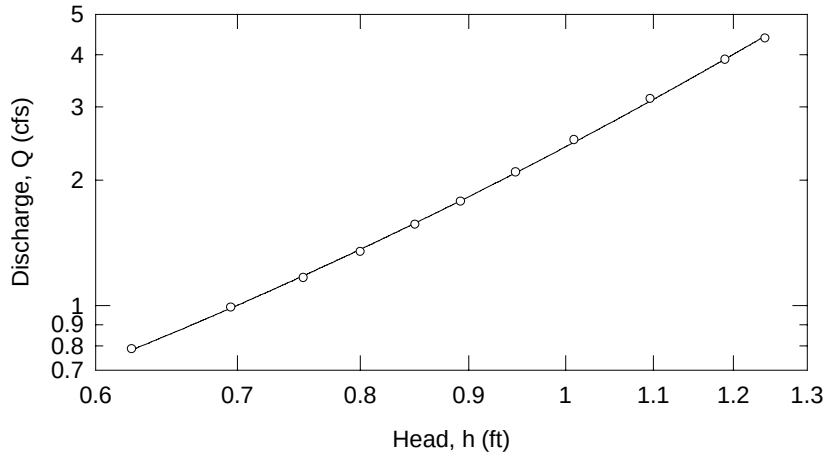

Fig. 3.5 - Calibration of V-notch weir

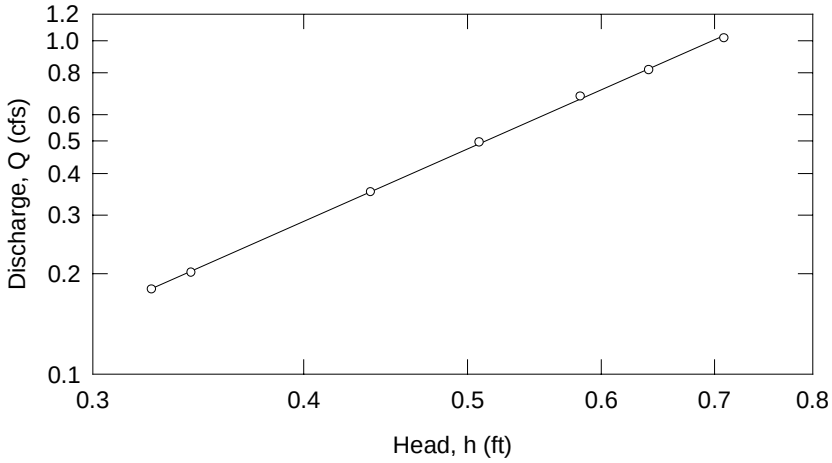

Fig. 3.6 - Low-flow calibration of V-notch weir

3.3.3 - Calibration of Flow Sensor

The flow sensor was calibrated using discharges measured by the V-notch weir. The calibration curve is plotted in Fig. 3.7. The fitted curve was forced to pass through the origin. The equation of the regression line is

$$Q_{sensor} = 0.997 Q_{V\text{-}notch} \tag{3.5}$$

where Q_{sensor} is the flow rate in cfs measured by the flow sensor and $Q_{V\text{-}notch}$ is the flow rate in cfs measured by the weir. The root-mean-square of the deviations between the measured Q_{sensor} and those obtained from the regression line was 0.090 cfs and the maximum deviation was 7.1%.

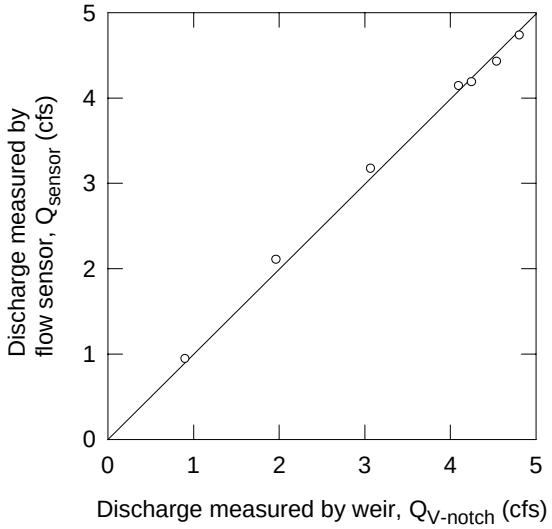

Fig. 3.7 - Calibration of flow sensor

3.4 - MEASUREMENT OF VELOCITIES

Velocities were measured by an acoustic Doppler velocimeter (ADV) manufactured by Sontek, Inc. of San Diego, California. An ADV Field probe with a 2-in. (5-cm) sensor was used. The instrument measures velocities in three orthogonal directions. A data acquisition program provided by the manufacturer was used to collect the velocity data. The sampling volume of the probe is about two inches below the tip of the probe and according to the manufacturer, the minimum distance to a flat boundary that still permits data collection is 0.16 in. to 0.24 in. Therefore the probe cannot measure velocities within the top two inches and the bottom 0.24 in of the flow depth.

A frame was built on the instrument carriage for mounting the ADV probe. The probe could be moved vertically as well as across the channel. The transverse position was determined by a scale on the instrument carriage and the vertical position was determined by the distance from boundary reported by the data acquisition program.

The accuracy of the distance from boundary reported by the data acquisition program was checked by comparing the reported distances with measurements using the point gauge. When the probe was above the invert of the channel, the differences between the distances from boundary that were reported by the data acquisition program and those measured with the point gauge

were less than 1%. When the probe was above the side slopes of the channel, the differences were about 5% to 6% for depths of about seven inches. When questioned about this situation, the manufacturer said that these discrepancies for distance measurements above a sloping surface are expected but that velocity measurements are not affected by the presence of a sloping surface.

Measurements were taken to determine the optimum sampling time. Two 4800-s measurements were made at 1 Hz. The measurements were taken at the downstream end of the weir. Record A came from the centerline and Record B was from 2.8 ft to the left of the centerline, which was near the region of reverse flow in the separation zone. The measurements were made near mid-depth. The total discharge was about 10 cfs and the side weir discharge was 3.84 cfs. The flow sensor was not operable during these measurements so the total discharge could not be determined exactly. Each record was divided into twenty-four 200-s segments, then twelve 400-s segments, then eight 600-s segments and finally six 800-s segments. The average longitudinal velocities for these different averaging times are shown in Fig. 3.8. The standard deviations of the velocities calculated using different averaging times are shown in Table 3.1.

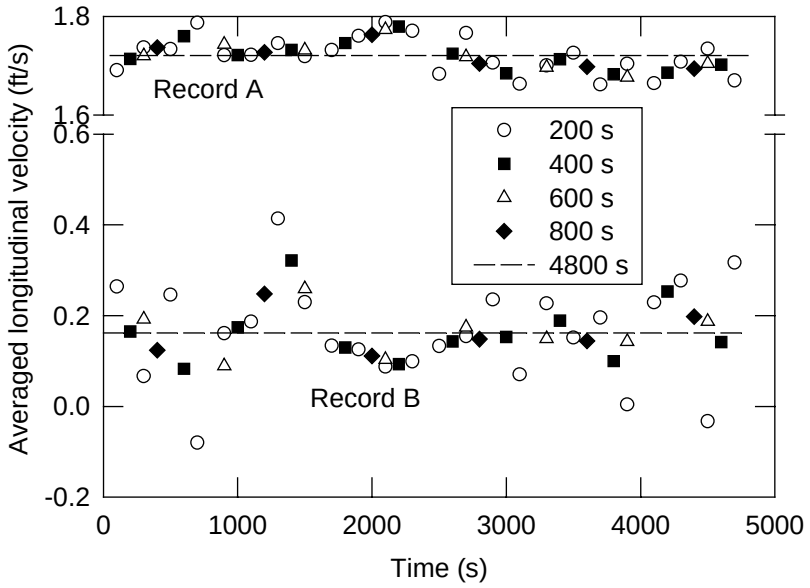

Fig. 3.8 - Effects of averaging time on longitudinal velocities

Table 3.1 - Effects of turbulent averaging time on velocities

Record	Average velocity of whole record (ft/s)	Standard deviation of average velocities (ft/s)			
		200 s	400 s	600 s	800 s
A	1.721	0.038	0.030	0.030	0.027
B	0.162	0.112	0.068	0.054	0.051

For Record A, there was acceptable accuracy even with the 200-s averaging time. However, near and in the separation zone, it would take an impracticably long sampling time to obtain a comparable accuracy. Based on a compromise between accuracy of the mean velocity and efficiency of measurement, a sampling time of 300 s was adopted even though a standard deviation on the order of 0.09 ft/s is indicated in Table 3.1 for measurements near a separation zone.

3.5 - MEASUREMENT OF WATER SURFACE ELEVATIONS

In the previous project, two carriages were moved longitudinally along the entire length of the channel on the railings parallel to the channel. One carriage was for instrumentation and the other was used by the personnel making measurements. A point gauge was mounted on the instrument carriage. The point gauge was used for determining flow depths. As mentioned by Tynes (1989), the vertical position of the point gauge could vary as the carriage was moved. Nevertheless, this variation did not create a problem in measuring flow depths since the flow depth was the difference between the water surface elevation and the bottom elevation measured at the same horizontal position.

The analysis in Section 6.8 required water surface elevations at different cross sections along the channel. Differences in water surface elevations on the order of a few thousandths of a foot needed to be determined reliably. Due to waves on the water surface and the variation in the vertical position of the point gauge when the carriage was moved, the required accuracy could not be achieved with the point gauge on the instrument carriage. Therefore a Pitot tube was used and the water surface elevations were measured with a point gauge in a stilling well connected to the static ports of the Pitot tube. The Pitot tube was mounted on the instrument carriage and the point gauge for the stilling well was mounted on one of the wooden beams supporting the railings. As the carriages were positioned at different locations along the channel, there was variation in the amount of the deflection of the wooden beam due to the weight of the carriages. As a result, the vertical position of the point gauge varied, thus changing the datum level of the measurement. Corrections were made for this variation. The maximum correction was only 0.002 ft.

4 - RE-EVALUATION OF SIDE WEIR DISCHARGE COEFFICIENTS

4.1 - DERIVATION OF EQUATION FOR CHANGES IN DEPTH

The calculation of the side weir discharge in the previous project did not take into account possible changes in channel slope and roughness. Therefore, strictly speaking, the discharge coefficients and other empirical parameters are applicable only for the particular channel slope, geometry, and roughness used in the model study. An improved method of analysis is needed to explicitly include the effect of channel slope, geometry, and roughness. Toward this end, a new analysis will be based Eq. (2.4) for the side weir discharge per unit length of the weir written as

$$q_w = -\frac{dQ}{dx} = C_1 \frac{2}{3}\sqrt{\frac{2}{3}g}\, h^{3/2} \tag{4.1}$$

where q_w is the weir discharge per unit length of weir crest, x is distance along the channel and is positive in the flow direction, dQ/dx is negative to indicate an outflow from the channel into the detention basin, C_1 is an empirical coefficient, and h is the head at any point along the weir.

This expression for the weir discharge will be incorporated into an equation for changes in the water depth for spatially varied flow (i.e., channel flow with distributed outflow along the weir length). The equation will be developed first for the general case of a tapered channel with a trapezoidal cross section. The equation for a prismatic channel is obtained when the terms related to tapering are dropped. This derivation is based on the momentum principle.

Fig. 4.1 shows the control volume for an incremental length along the channel and weir crest. The longitudinal axis parallel to the flow direction is the x-axis, which is positive in the downstream direction, Δx is the length of the control volume, η is the flow depth, U is the cross sectional average velocity in the channel, U_w is the velocity of the lateral flow, θ is the angle between the channel invert and the horizontal, ψ is the angle between the side slope and the horizontal, φ is the angle between the tapering wall and the longitudinal axis, ϕ is the angle between U_w and the longitudinal axis, B is the channel base width, and P is the weir height. All angles are positive as shown in Fig. 4.1.

The magnitudes of the momentum fluxes through sections 1 and 2 are $(\rho\beta AU^2)_1$ and $(\rho\beta AU^2)_2$ respectively, where ρ is the density of water and β is the momentum correction factor. The flux of x momentum in the lateral flow is

$$M_L = -\int_x^{x+\Delta x} \rho U_w \cos\phi \, dQ \tag{4.2}$$

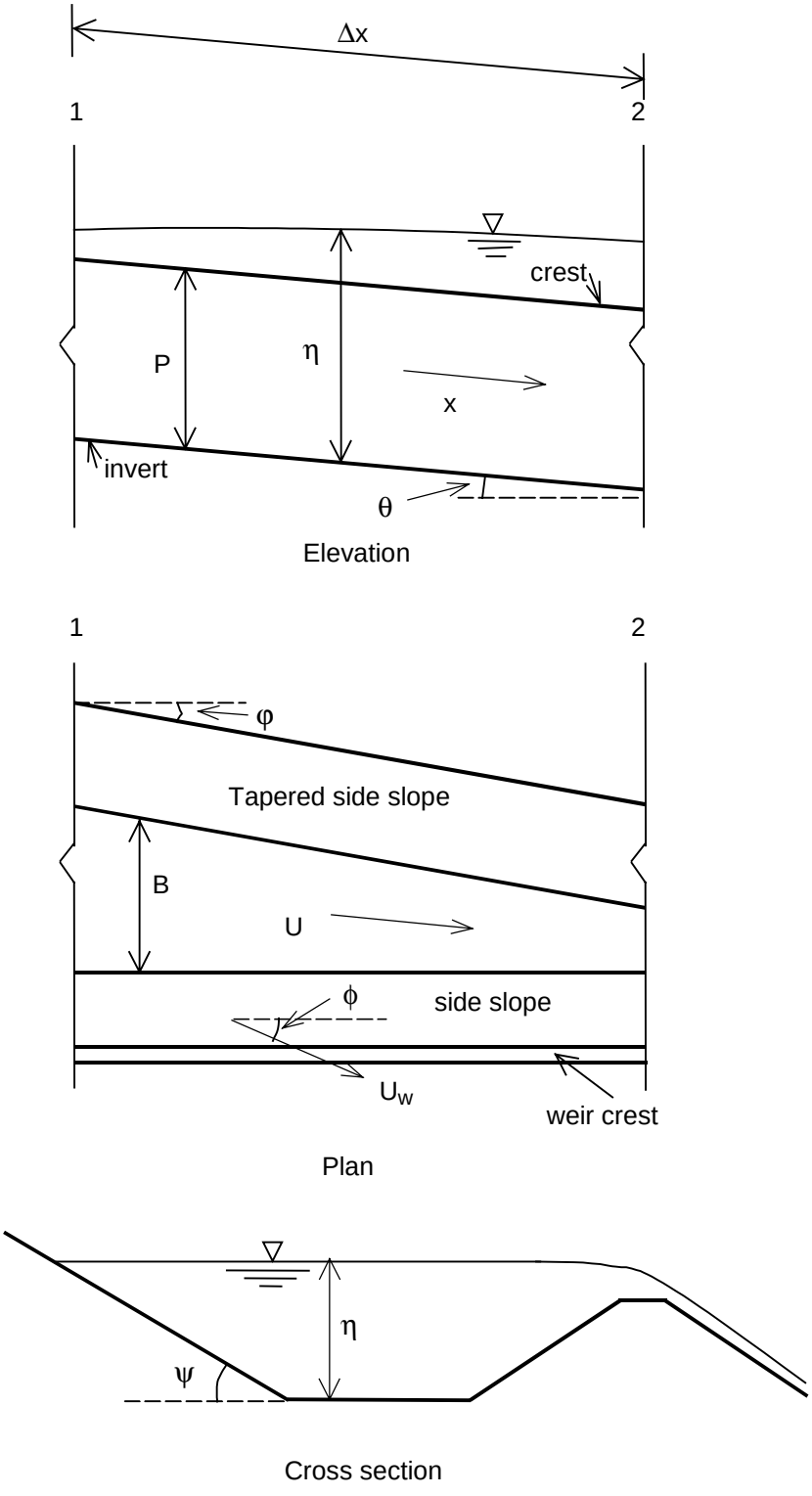

Fig. 4.1 - Definition sketch for channel with lateral flow

where dQ is the outflow in the incremental length Δx and is negative because Q in the channel decreases in the positive x direction when there is outflow over the weir. The minus sign in front of the integral in Eq. (4.1) makes M_L positive for outflow, as it should be to be consistent with the sign convention in the momentum equation. Hence the sum of x momentum fluxes for the length Δx is

$$\Sigma M = (\rho\beta AU^2)_2 - (\rho\beta AU^2)_1 - \int_x^{x+\Delta x} \rho U_w \cos\phi \, dQ \tag{4.3}$$

or

$$\Sigma M = \frac{d\left(\rho\beta AU^2\right)}{dx}\Delta x - \int_x^{x+\Delta x} \rho U_w \cos\phi \, dQ \tag{4.4}$$

The component of the fluid weight in the x-direction is

$$W_x = \int_x^{x+\Delta x} \rho g S_o A dx \tag{4.5}$$

where $S_o = \sin\theta = -dz_o/dx$ and z_o = elevation of the bottom of the channel. The pressure forces acting on sections 1 and 2 are $(K\rho gA\eta\cos\theta)_1$ and $-(K\rho gA\eta\cos\theta)_2$ respectively, where K is a pressure coefficient such that $K\eta$ is the distance from the water surface to the centroid of the flow area. The sum of the two pressure forces is

$$\Sigma F_p = -\left[(K\rho gA\eta\cos\theta)_2 - (K\rho gA\eta\cos\theta)_1\right] = -\frac{d}{dx}(K\rho gA\eta\cos\theta)\Delta x \tag{4.6}$$

The frictional force on the boundary is

$$F_\tau = -\int_x^{x+\Delta x} \tau_{ox} P dx \tag{4.7}$$

where P is the wetted perimeter and τ_{ox} is the x component of the boundary shear stress, which is assumed to be uniform laterally along the wetted perimeter. The x-component of the pressure force on the tapered side slope opposite to the weir is

$$F_{taper} = -\frac{\rho g \tan\varphi\cos\theta}{2}\int_x^{x+\Delta x} \eta^2 dx \tag{4.8}$$

Equating the sum of the momentum fluxes to the sum of the forces, both in the x-direction, gives

$$\frac{d\left(\rho\beta AU^2\right)}{dx}\Delta x - \int_x^{x+\Delta x}\rho U_w \cos\phi dQ = -\frac{d\left(K\rho gA\eta\cos\theta\right)}{dx}\Delta x - \frac{\rho g\tan\varphi\cos\theta}{2}\int_x^{x+\Delta x}\eta^2 dx - \int_x^{x+\Delta x}\tau_{ox}Pdx + \int_x^{x+\Delta x}\rho gS_o Adx \tag{4.9}$$

Dividing Eq. (4.9) by Δx and taking the limit as Δx tends to zero,

$$\frac{d\left(\rho\beta AU^2\right)}{dx} - \rho\frac{dQ}{dx}U_w\cos\phi = -\frac{d\left(K\rho gA\eta\cos\theta\right)}{dx} - \frac{\rho g\eta^2\tan\varphi\cos\theta}{2} - \tau_{ox}P + \rho gS_o A \tag{4.10}$$

Since Q = AU,

$$\frac{dQ}{dx} = A\frac{dU}{dx} + U\frac{dA}{dx} \tag{4.11}$$

For a trapezoidal channel,

$$A = \left(B + \frac{\eta}{\tan\psi}\right)\eta \tag{4.12}$$

where B = base width of trapezoidal cross section, and

$$K = \frac{3B + 2\dfrac{\eta}{\tan\psi}}{6\left(B + \dfrac{\eta}{\tan\psi}\right)} \tag{4.13}$$

Hence

$$\frac{dA}{dx} = \frac{\partial A}{\partial\eta}\frac{d\eta}{dx} + \frac{\partial A}{\partial B}\frac{dB}{dx} \tag{4.14}$$

or equivalently

$$\frac{dA}{dx} = T\frac{d\eta}{dx} - \eta\tan\varphi \tag{4.15}$$

since $dB/dx = -\tan\varphi$ and T (the surface width) = $\partial A/\partial\eta$. Moreover, from Eq. (4.12) and Eq. (4.13),

$$KA = \frac{\eta}{6}\left(3B + 2\frac{\eta}{\tan\psi}\right) \tag{4.16}$$

Using Eq. (4.11), Eq. (4.15), and Eq. (4.16), and assuming that $\cos\theta \approx 1$ and $d(\cos\theta)/dx = 0$, Eq. (4.10) can be expanded and written as

$$\frac{d\eta}{dx} = \frac{S_o - S_f + \frac{1}{gA}\frac{dQ}{dx}\left(U_w \cos\phi - 2\beta U\right) - \frac{U^2}{g}\left(\frac{d\beta}{dx} + \frac{\beta\eta\tan\varphi}{A}\right)}{1 - \frac{\beta T U^2}{gA}} \tag{4.17}$$

where S_f is the friction slope and dQ/dx is negative for outflow. This is the general equation for the change in flow depth in the channel along a side weir.

4.1.1 - Unsubmerged Flow in Prismatic Channels

For a prismatic channel, $\varphi = 0$ so that Eq. (4.17) becomes

$$\frac{d\eta}{dx} = \frac{S_o - S_f + \frac{1}{gA}\frac{dQ}{dx}\left(U_w \cos\phi - 2\beta U\right) - \frac{U^2}{g}\frac{d\beta}{dx}}{1 - \frac{\beta T U^2}{gA}} \tag{4.18}$$

Although Eq. (4.17) had been derived here for a trapezoidal channel, Eq. (4.18) is applicable for prismatic channels of any cross-sectional shape (Yen and Wenzel, 1970).

In many studies of side weir discharge, the velocity distribution in the channel is assumed to be uniform. Based on this assumption, $U_w \cos\phi = U$. However, in reality, the velocity distribution in the channel is highly nonuniform. (See Chapter 6.) El-Khashab and Smith (1976) observed that the flow over the weir originated from the high velocity flow in the channel. Their investigation concluded that for $Q_w/Q_u < 0.5$,

$$U_w \cos\phi = C_2\left(\frac{\eta}{P}\right)U \tag{4.19}$$

El-Khashab and Smith did not give the value of C_2, but it was estimated to be 0.85 from one of the figures in their article.

From the results of the study of flow asymmetry (Section 6.5), the values of β for the cross section at the downstream end of the weir for different values of Q_u and percentage diversions can be estimated. It is assumed that the velocity distribution at the upstream end of the

weir is the same as that without diversion. Furthermore, β is assumed to vary linearly between the upstream and downstream ends of the weir.

A computational scheme for the calculation of Q_w and h_u is as follows. Given Q_u, h_d, and values for C_1 and C_2, Eq. (4.1), Eq. (4.18), and Eq. (4.19) are used to obtain the water surface profile along the weir and the discharge over the weir. For the end slope (with a length of two feet in the model), the wedge of flow (which is generally shorter than two feet) at the downstream end of the weir is treated as flow over four small step weirs of equal lengths. The height of each step weir is taken as the height of the end slope at the middle of the step length. The water surface elevations for the step weirs are assumed to be the same as that at the downstream end of the weir crest. Eq. (4.1) is used to calculate the weir discharge over each step weir. A fourth-order Runge-Kutta method is used to integrate Eq. (4.1) and Eq. (4.18) along the weir crest. Details of the Runge-Kutta method are given in Press et al. (1989).

Observations in the model showed that frequently no discharge passed over the end slope at the upstream end of the weir. Moreover, even when there was a small amount of flow over the upstream end slope, it was very difficult to describe the flow mathematically. Therefore it is assumed in the computations that there is no flow over the end slope at the upstream end of the weir. Any resulting error should be negligible.

In the above procedure, C_1 may be constant or variable along the weir. Hager (1987) derived a lateral flow coefficient, ω, which was then multiplied by the weir discharge obtained for a normal weir to get the side weir discharge. The lateral flow coefficient is given by Eq. (2.5), which is

$$\omega = \left(\frac{\left(Fw^2 + 2\right)\left(1 - C_3\right)}{Fw^2 + 2\left(1 - C_3\right)} \right)^{1/2} \tag{4.20}$$

where C_3 is a residual pressure coefficient that is less than unity. Eq. (4.1) then becomes

$$q_w = C_1' \omega \frac{2}{3} \sqrt{\frac{2}{3} g}\, h^{3/2} \tag{4.21}$$

in which C_1' is a discharge coefficient for a normal weir of the same geometry. In this equation, the effective discharge coefficient $C_1' \omega$ is a variable along the weir. Hager used a value of 2/3 for C_3 in Eq. (4.20). Apparently C_3 should depend on the particular type of weir under consideration. Given C_3, the same computational scheme described earlier in this section can be used to obtain the water surface profile along the weir and the discharge over the weir.

4.1.2 - Submerged Flow in Prismatic Channels

The analysis procedure for submerged flow in prismatic channels is the same as in Section 4.1.1 except that C_1 has to be modified by a submergence correction factor (C_{1s}) which depends on the submergence ratio.

4.1.3 - Unsubmerged Flow in Tapered Channels

The primary purpose for tapering the channel is to eliminate the separation zone formed at the side of the channel opposite to the weir. Observations confirmed that separation zones were almost non-existent when the channel was tapered. Therefore, β should have the value for a symmetrical velocity distribution and $d\beta/dx = 0$ along the weir. Then Eq. (4.17) becomes

$$\frac{d\eta}{dx} = \frac{S_o - S_f + \frac{1}{gA}\frac{dQ}{dx}\left(U_w \cos\phi - 2\beta U\right) - \frac{\beta\eta U^2 \tan\varphi}{gA}}{1 - \frac{\beta T U^2}{gA}} \tag{4.22}$$

The computational scheme is similar to that in Section 4.1.1 except that Eq. (4.18) is replaced with Eq. (4.22).

4.2 - OPTIMIZATION AND REGRESSION ANALYSIS FOR CHANNEL WITH 2.5H:1V SIDE SLOPES

The computational scheme in Section 4.1 was coupled with the GRG2 nonlinear optimization code (Lasdon and Waren, 1994) to obtain values for the empirical coefficients. Then nonlinear regression analysis was performed to obtain predictive equations for the coefficients based on dimensionless hydraulic and geometric parameters.

4.2.1 - Unsubmerged Flow in Prismatic Channels with 2.5H:1V Side Slopes

4.2.1.1 - Constant Discharge Coefficient

For each of the 238 tests of the previous project (Tynes, 1989), the values of C_1 (Eq. (4.1)) and C_2 (Eq. (4.19)) were obtained by nonlinear optimization such that the calculated values of Q_w and h_u were equal to the measured values. Note that C_1 in Eq. (4.1) is constant along the length of the weir. It was found that C_2 was uncorrelated with any of the hydraulic and geometric parameters. Thus C_2 behaved essentially as a tuning parameter in the optimization. Therefore it was decided to try a few values of C_2 which were constant for all tests and to vary only C_1 so that the calculated values of Q_w were equal to the measured values. The calculated values of h_u were then different from the measured values. A root-mean-square error of h_u was calculated for a given value of C_2. For values of C_2 = 0.70, 0.75, 0.80, 0.85 0.90 and 1.00, the

root-mean-square error of h_u for C_2 = 0.85 was the smallest. This value of C_2 agreed with the result in El-Khashab and Smith (1976) and was adopted in subsequent calculations for both submerged and unsubmerged flow conditions in prismatic channels.

Regression analysis was performed using SigmaPlot 3.0 (Jandel Scientific). The predictive equation for C_1 is

$$C_1 = \exp\left\{-0.250 - 0.463\left[\ln\left(Fw_d + 1\right)\right]^{1.943} + 0.576\left[\ln\left(\frac{h_d}{P} + 1\right)\right]^{0.612}\right\} \qquad (4.23)$$

Adding one to both Fw_d and h_d/P makes the logarithmic values non-negative so that the power indices can be non-integers and still give real numbers. The t-statistics for the coefficients in Eq. (4.23) are shown in Table 4.1. All of the coefficients are significant at the 5% level. R^2 for Eq. (4.23) is 0.682 but R^2 for the calculated Q_w compared to measured values is much higher, as discussed in Section 4.3. The regression equation with only Fw_d and the regression equation with only h_d/P have R^2 of 0.456 and 0.463 respectively. The fit of Eq. (4.23) to the values of C_1 is not as good as the fit of Eq. (2.28) to the values of C_e. The correlation between C_1 and Fw_d is weaker than that between C_e and Fw_d. The fact that C_1 depends on h_d/P in Eq. (4.23) is consistent with the corresponding relationship for normal weir.

Table 4.1 - t-statistics for coefficients in Eq. (4.23)

Coefficient	t-statistic
-0.250	-2.36
-0.463	-8.59
1.943	5.30
0.576	9.03
0.612	2.39

4.2.1.2 - Variable Discharge Coefficient

The same experimental results analyzed in Section 4.2.1.1 were analyzed again using Eq. (4.20) and Eq. (4.21) for C_1 instead of Eq. (4.1). This approach effectively gives C_1 values that vary along the length of the weir. Since C_1' and ω appear in a product in Eq. (4.21), there are many pairs of C_1' and C_3 which give the same Q_w. Therefore an attempt to include both C_3 and C_1' as the parameters in the nonlinear optimization was unsuccessful. Furthermore, the root-mean-square error of h_u was found to be insensitive to C_3. Hence the procedure for determining C_2 in Section 4.2.1 could not be applied to C_3. In the absence of an independent investigation to estimate C_3, the value used by Hager was adopted, i.e. C_3 was assumed to be 2/3. With C_2 = 0.85, C_1' values for the 238 tests were obtained using the nonlinear optimization procedure.

C_1' was found to be poorly correlated with all the hydraulic and geometric parameters considered. The best regression equation is

$$C_1' = \exp\left[0.229 + 0.127 \ln\left(\frac{h_d}{P}\right)\right] \tag{4.24}$$

The t-statistics for the coefficients in Eq. (4.24) are shown in Table 4.2. Both coefficients are significant at the 5% level, but R^2 for Eq. (4.24) is only 0.337. Again R^2 for Q_w (calculated) vs. Q_w (measured) is much higher. Values are given in Section 4.3. It is noted that C_1' is uncorrelated with Fw_d. Apparently the lateral flow coefficient accounted for the variation of the discharge coefficient with the weir Froude number.

Table 4.2 - t-statistics for coefficients in Eq. (4.24)

Coefficient	t-statistic
0.229	14.13
0.127	10.84

4.2.2 - Submerged Flow in Prismatic Channels with 2.5H:1V Side Slopes

The values of C_{1s} were obtained for the 35 tests using the same procedure described in Section 4.2.1. Subscript s denotes submerged conditions. C_2 was taken to be 0.85, the same as that for the unsubmerged tests. The value of C_1 was calculated from Eq. (4.23) for each test. Various geometric and hydraulic parameters were correlated with the ratio C_{1s}/C_1. The best regression equation obtained for $h_t/h_d > 0.5$ is

$$\frac{C_{1s}}{C_1} = 1.00 - 19.5\left(\frac{h_t}{h_d} - 0.5\right)^{4.50} - 5.62\left[\ln\left(Fw_d + 1\right)\right]^{3.97} \tag{4.25}$$

For $h_t/h_d \le 0.5$, $C_{1s} = 1$. The t-statistics for the coefficients in Eq. (4.25) are shown in Table 4.3. R^2 for Eq. (4.25) is 0.965. All the coefficients are significant at the 5% level except -5.62. The term involving Fw_d is retained because of the improved correlation. However, Eq. (4.25) may give negative values of C_{1s}/C_1. When this situation happens, Eq. (4.26) below is used instead of Eq. (4.25) to determine C_{1s}/C_1.

The regression equation with h_t/h_d as the only parameter is

$$\frac{C_{1s}}{C_1} = 0.887 - 22.6\left(\frac{h_t}{h_d} - 0.5\right)^{4.76} \tag{4.26}$$

The t-statistics for the coefficients in Eq. (4.26) are shown in Table 4.4. R^2 for Eq. (4.26) is 0.799, which is substantially lower than that of Eq. (4.25). Although the coefficient -22.6 is not significant at the 5% level, the term involving h_t/h_d is needed because the plot of C_{1s}/C_1 vs. h_t/h_d shows a definite relationship between the two variables.

Table 4.3 - t-statistics for coefficients in Eq. (4.25)

Coefficient	t-statistic
1.00	24.24
-19.5	-2.82
4.50	8.95
-5.62	-1.35
3.97	3.79

4.2.3 - Unsubmerged Flow in Tapered Channels

The values of C_1 were obtained for the 65 tests for tapered channels using the same procedure described in Section 4.2.1. C_2 was adjusted to 0.70 to minimize the errors in h_u. The best regression equation for C_1 is

Table 4.4 - t-statistics for coefficients in Eq. (4.26)

Coefficient	t-statistic
0.887	13.7
-22.6	-1.15
4.76	3.83

$$C_1 = 1.101 + 0.105 \ln\left(\frac{h_d}{P}\right) \tag{4.27}$$

The t-statistics for the coefficients in Eq. (4.27) are shown in Table 4.5. Both coefficients are significant at the 5% level but R^2 for Eq. (4.27) is only 0.395. Again R^2 for Q_w (calculated) vs. Q_w (measured) is much higher. Values are given in Section 4.3.

Table 4.5 - t-statistics for coefficients in Eq. (4.27)

Coefficient	t-statistic
1.101	34.0
0.105	6.41

Recall that $U_w \cos\phi = C_2(\eta/P)U$ (Eq. (4.19)). A smaller value of C_2 for tapered channels seems to suggest that the longitudinal component of the velocity of side weir discharge is smaller

in tapered channels than in prismatic channels. This speculation can be evaluated only by detailed velocity measurements in the channel as well as in the region of the outflow.

4.3 - COMPARISON BETWEEN MEASURED AND CALCULATED VALUES FOR 2.5H:1V SIDE SLOPES

Based on empirical coefficients from regression equations in Section 2.6 and on the equations in Section 4.2, the various methods of calculating Q_w and h_u described in the previous sections are summarized in Table 4.6. Method A is the method used in the previous project (Tynes, 1989). Method B uses a C_1 that is constant along the weir but varies with the hydraulic conditions at the downstream end of the weir and also uses a variable head along the length of the weir; while Method C uses a C_1 that varies along the length of the weir based on ω and a variable head. In Method D, the average of the values of C_1' obtained from the 238 tests was used with a variable head along the weir.

For unsubmerged flow, the calculated flow depth at the upstream end of the weir using Method A was supercritical for Test A3B19N (identification code used by Tynes, 1989) and no solution could be obtained for h_u for Tests A1C20W and A5C18N. This condition presumably resulted from a critical or supercritical solution not being found. When Method B was used, supercritical flow depths were obtained in the computed water surface profile for Test A5C18N. The flow conditions calculated at the upstream end of the weir using Method C and Method D were subcritical for all of the 238 tests.

Table 4.6 - Methods of calculating Q_w and h_u

Method	Physical equations			Empirical equations			ω
	Unsub-merged	Sub-merged	Tapered	Unsub-merged	Sub-merged	Tapered	
A	Eq. (2.8), Eq. (2.23)	Eq. (2.8), Eq. (2.23)	Eq. (2.8), Eq. (2.36)	Eq. (2.28), Eq. (2.29)	Eq. (2.28), Eq. (2.29), Eq. (2.32), Eq. (2.33)	Eq. (2.34), Eq. (2.35)	not used
B	Eq. (2.4), Eq. (4.18)	Eq. (2.4), Eq. (4.18)	Eq. (2.4), Eq. (4.22)	Eq. (4.19), Eq. (4.23)	Eq. (4.19), Eq. (4.23), Eq. (4.25)	Eq. (4.19), Eq. (4.27)	not used
C	Eq. (4.18), Eq. (4.21)			Eq. (4.19), Eq. (4.24)			Eq. (4.20)
D	Eq. (4.18), Eq. (4.21)			Eq. (4.19), $C_1' = 1.063$			Eq. (4.20)

Note: Also see Table 4.11.

The calculated values of Q_w and h_u are plotted against the measured values in Fig. 4.2 to Fig. 4.17. The averages (avg), standard deviations (stdev) and root-mean-square values (rms) of the differences between measured and calculated values are shown in Table 4.7 to Table 4.10, in terms of both absolute values and relative values. (If the sum in the calculation of the standard deviation is divided by N instead of N - 1, then rms = $\sqrt{(\text{avg})^2 + (\text{stdev})^2}$).

From Table 4.7 to Table 4.10, the differences between stdev and rms of either ΔQ_w, where $\Delta Q_w = Q_{w(mea)} - Q_{w(cal)}$ as shown in Table 4.7 through Table 4.10, or $\Delta Q_w/Q_{w(mea)}$ were at most 2%, except for tapered channels using Method A. This result is illustrated in the figures by the fact that the points are scattered close to the 1:1 line. Similar observations were obtained for the upstream head on the weir. The differences between stdev and rms were generally larger for Δh_u, where $\Delta h_u = h_{u(mea)} - h_{u(cal)}$ as shown in Table 4.7 through Table 4.10, and for $\Delta h_u/h_{u(mea)}$ than for ΔQ_w and $\Delta Q_w/Q_{w(mea)}$. The largest difference was still only 8%, except for submerged flow using Method A and for tapered channels.

The root-mean-square values were used to compare the different methods of analysis. For meaningful comparison, the statistics had to be based on the same number of tests. Therefore, when comparing Methods A and B, Tests A1C20W, A3B19N and A5C18N were excluded and when comparing Methods B, C and D, Test A5C18N was excluded.

Method B gave smaller rms for the side weir discharge than Method A in terms of both ΔQ_w and $\Delta Q_w/Q_{w(mea)}$. For unsubmerged flow, the rms of $\Delta Q_w/Q_{w(mea)}$ was reduced only by 2% when Method B was used instead of Method A. However the reduction was 57% for submerged flow and 44% for tapered channels.

For unsubmerged flow, Method B gave smaller rms for Δh_u but larger rms for $\Delta h_u/h_{u(mea)}$ than Method A. For submerged flow, Method B gave smaller rms for both Δh_u and $\Delta h_u/h_{u(mea)}$ than Method A whereas for tapered channels, Method B gave larger rms than Method A for both Δh_u and $\Delta h_u/h_{u(mea)}$. Nevertheless, the differences between the rms for Δh_u using either method were only about 0.001 ft. Therefore, compared with Method A, Method B gave improved results or results of comparable accuracy.

Method B takes into consideration more details of the side weir hydraulics, specifically the water surface profile along the weir. Hence the head correction required in Method A (Eq. (2.29), Eq. (2.33), and Eq. (2.35)) is eliminated in Method B. Moreover, Method B explicitly accounts for the channel slope and roughness so that it is applicable for different slopes and roughnesses. However, the improvement for submerged flow is partly due to the use of two parameters in the regression equation instead of one (Eq. (4.25) vs. Eq. (2.33)). Table 4.11 summarizes the differences between Method A and Method B.

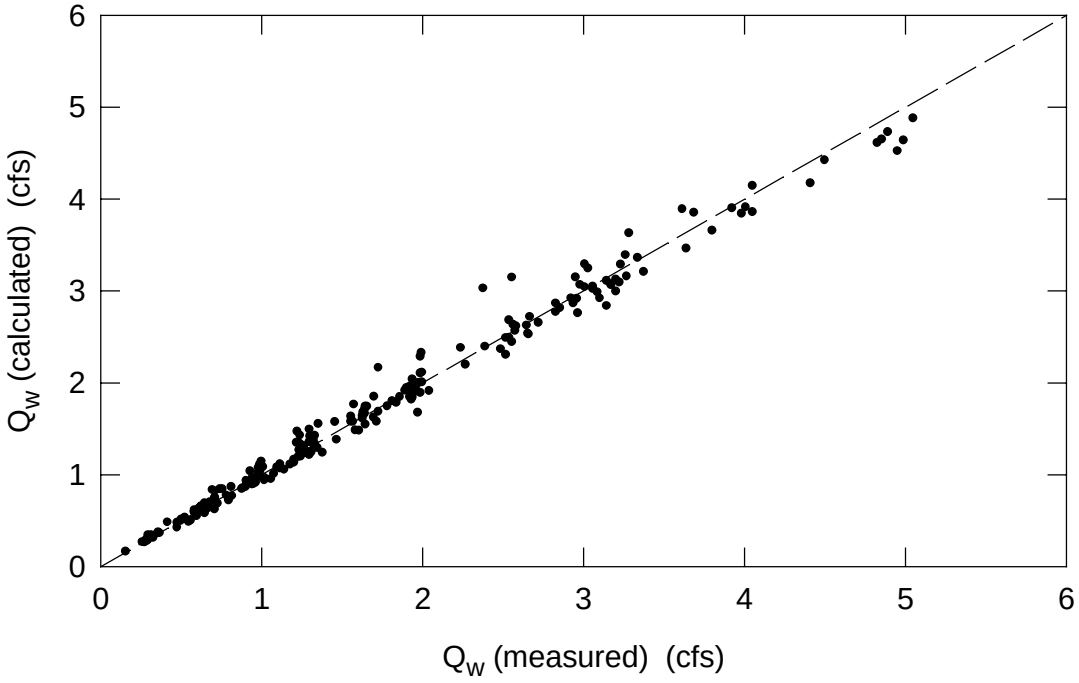

Fig. 4.2 - Comparison of measured and calculated model values of side-weir discharge for unsubmerged flow using Method A

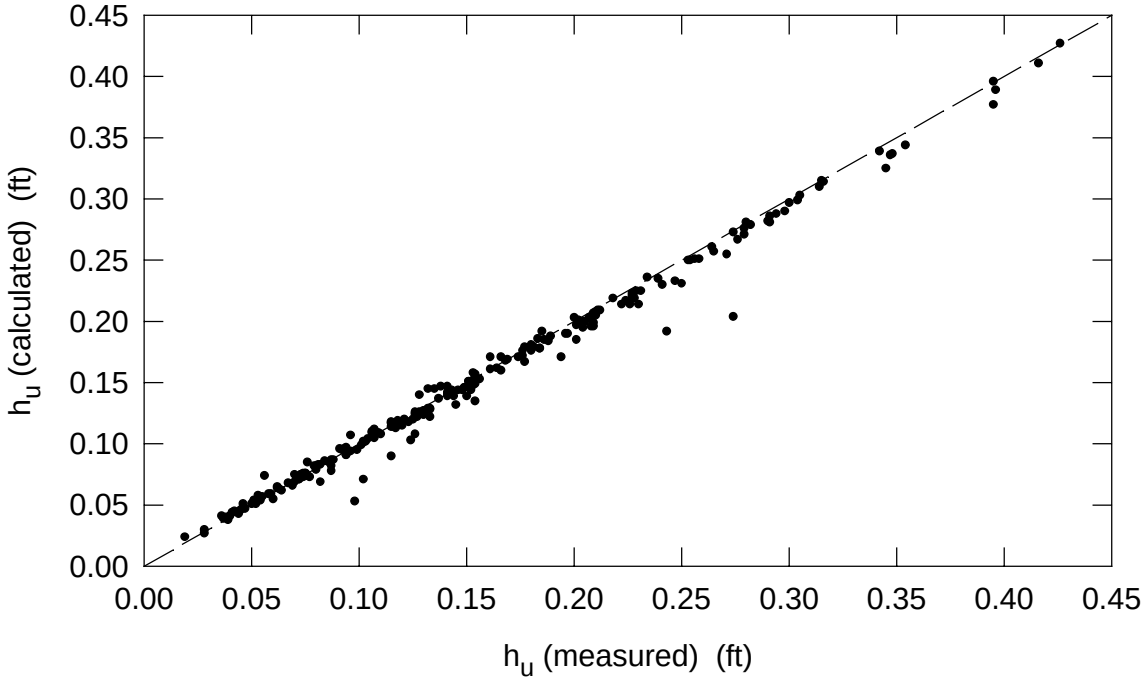

Fig. 4.3 - Comparison of measured and calculated model values of upstream head on the weir for unsubmerged flow using Method A

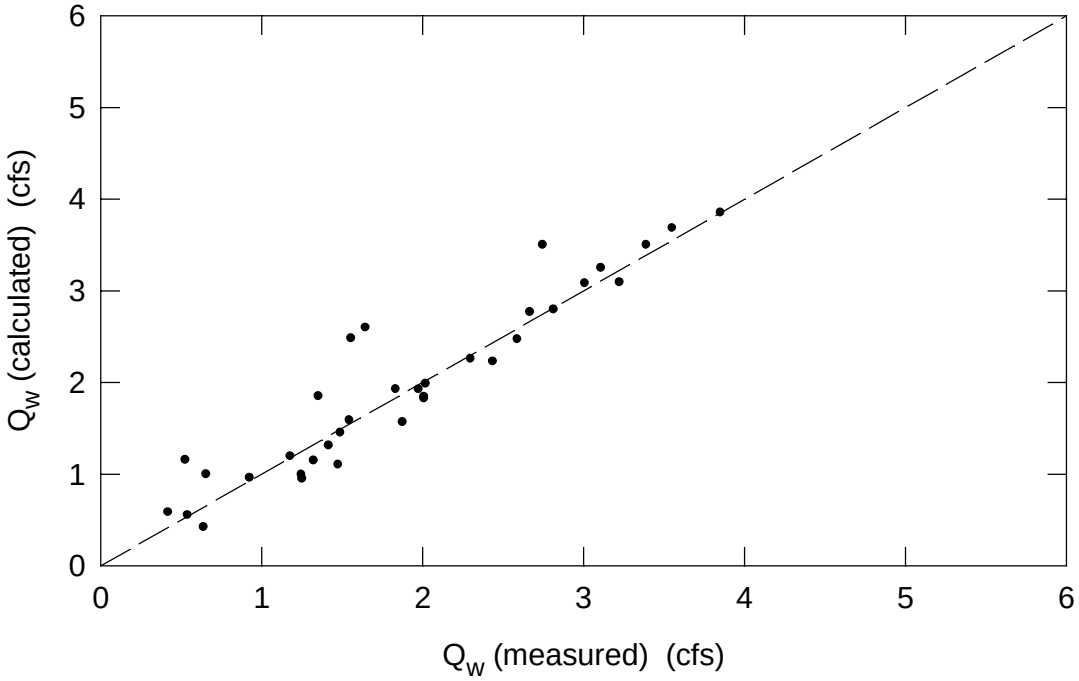

Fig. 4.4 - Comparison of measured and calculated model values of side-weir discharge for submerged flow using Method A

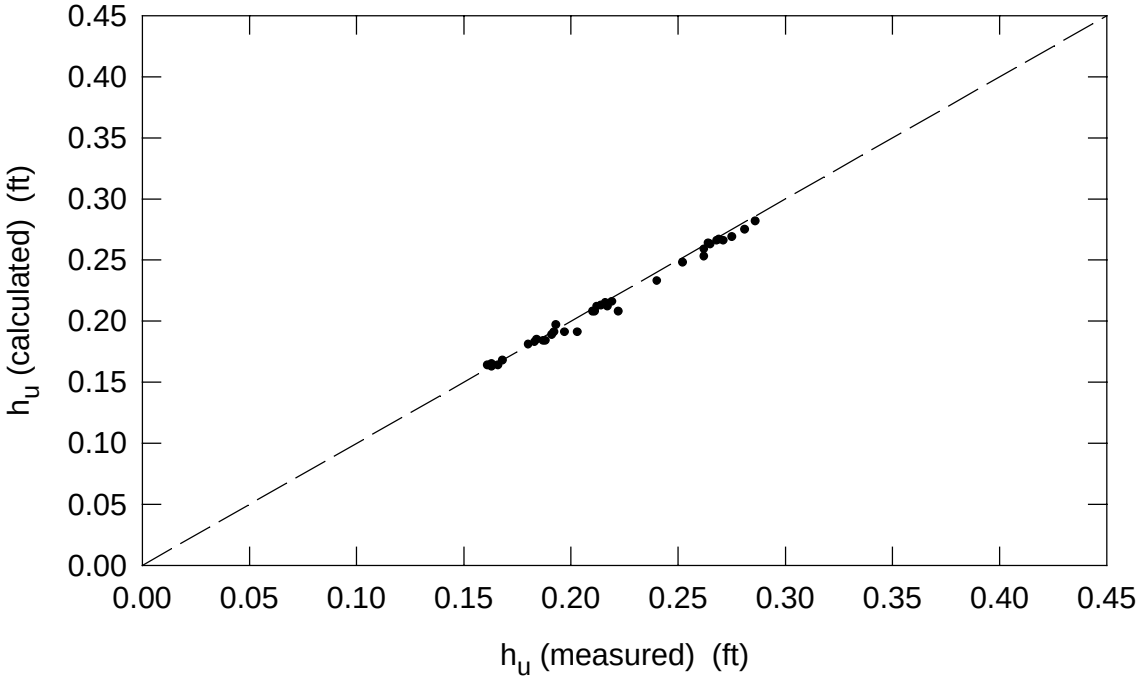

Fig. 4.5 - Comparison of measured and calculated model values of upstream head on the weir for submerged flow using Method **A**

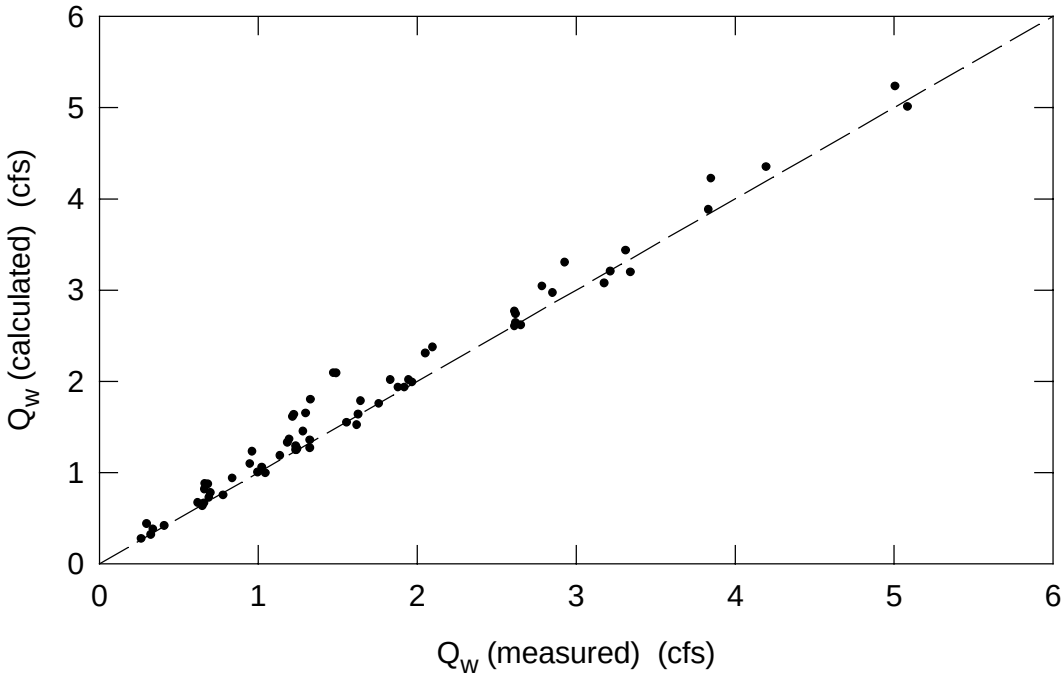

Fig. 4.6 - Comparison of measured and calculated model values of side weir discharge for tapered channels using Method A

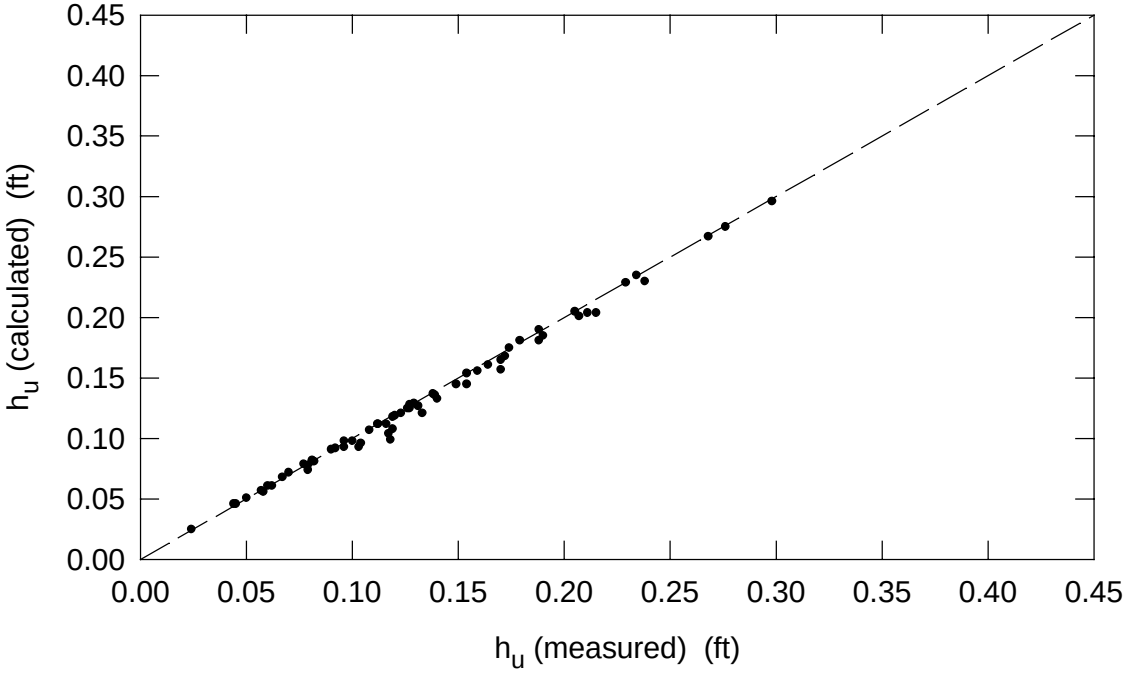

Fig. 4.7 - Comparison of measured and calculated model values of upstream head on the weir for tapered channels using Method A

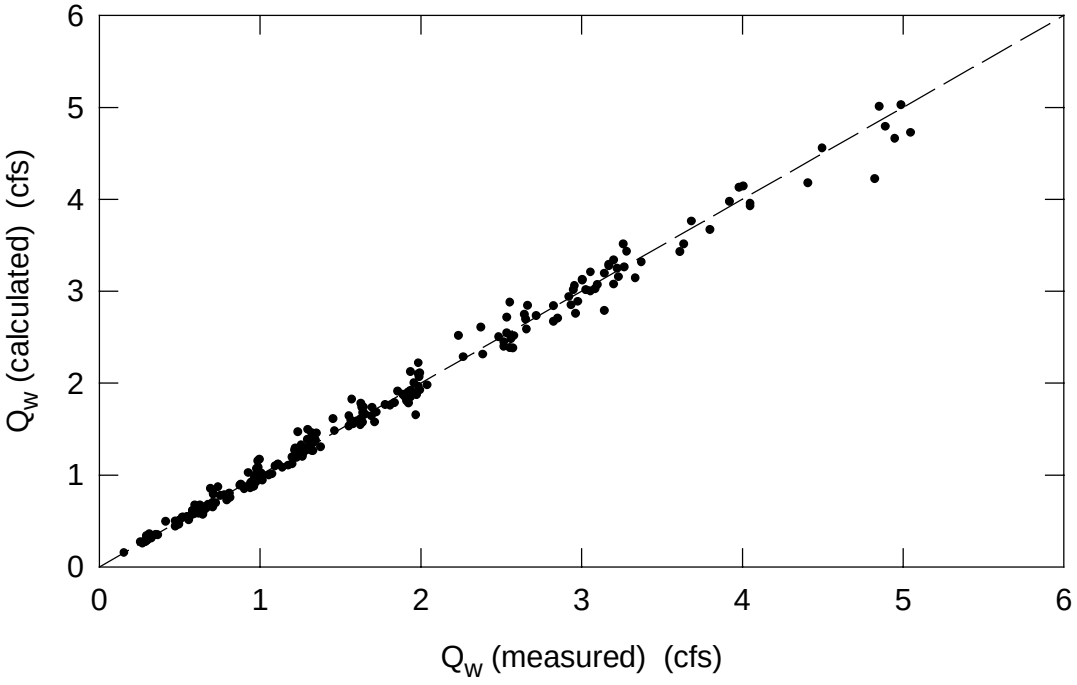

Fig. 4.8 - Comparison of measured and calculated model values of side weir discharge for unsubmerged flow using Method B

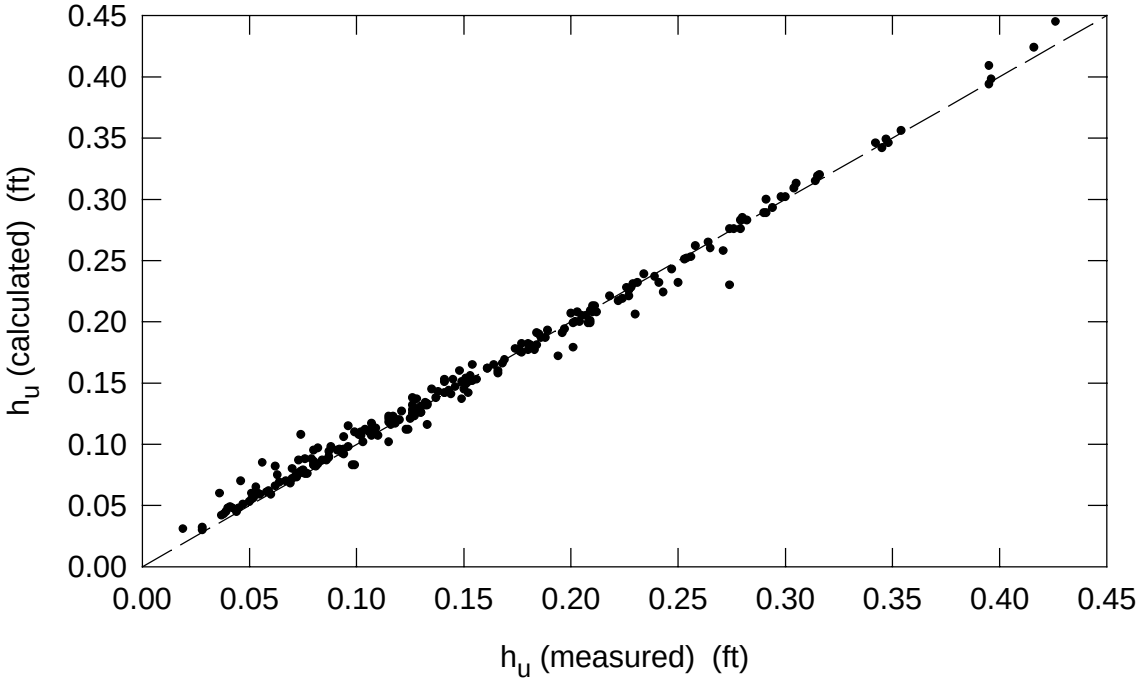

Fig. 4.9 - Comparison of measured and calculated model values of upstream head on the weir for unsubmerged flow using Method B

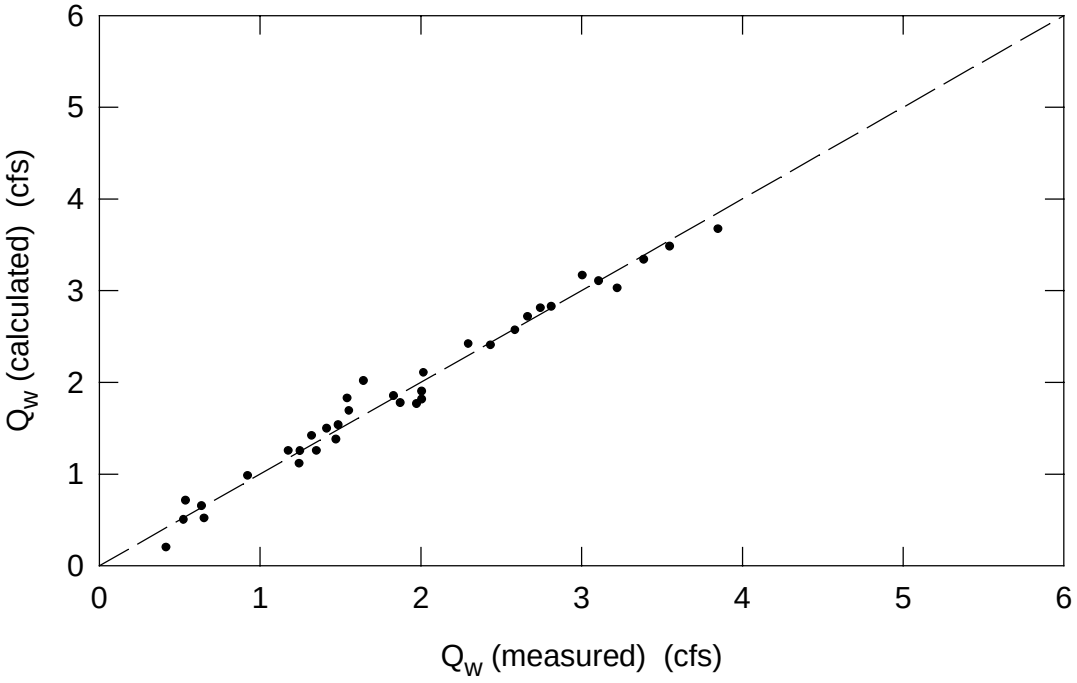

Fig. 4.10 - Comparison of measured and calculated model values of side weir discharge for submerged flow using Method B

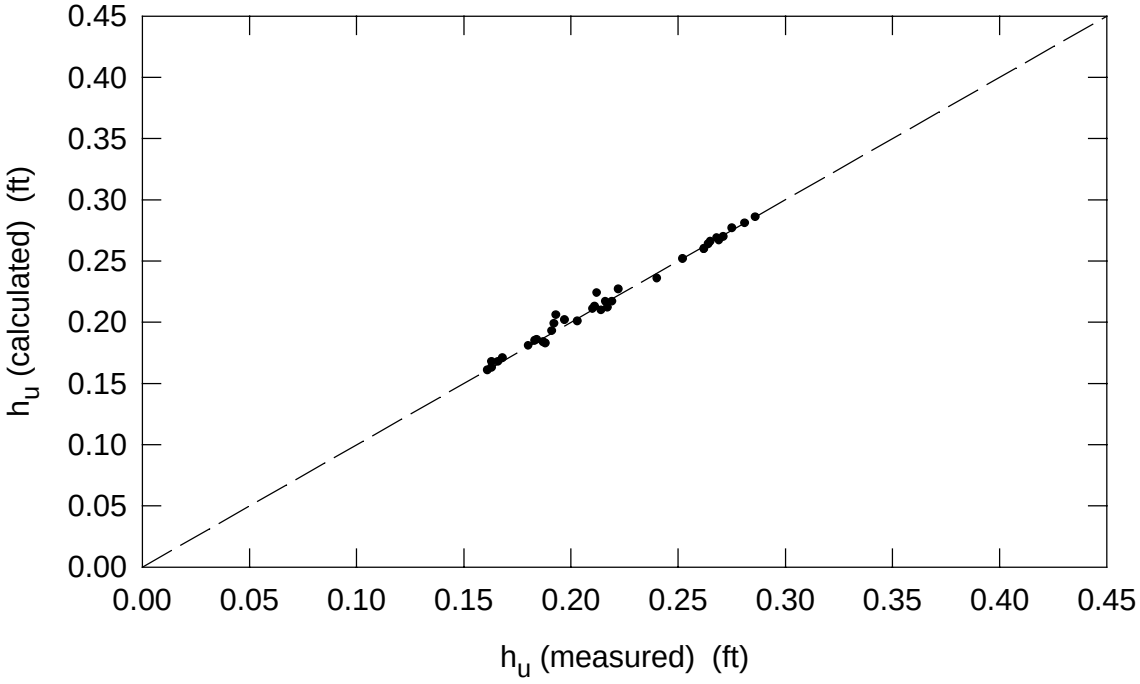

Fig. 4.11 - Comparison of measured and calculated model values of upstream head on the weir for submerged flow using Method B

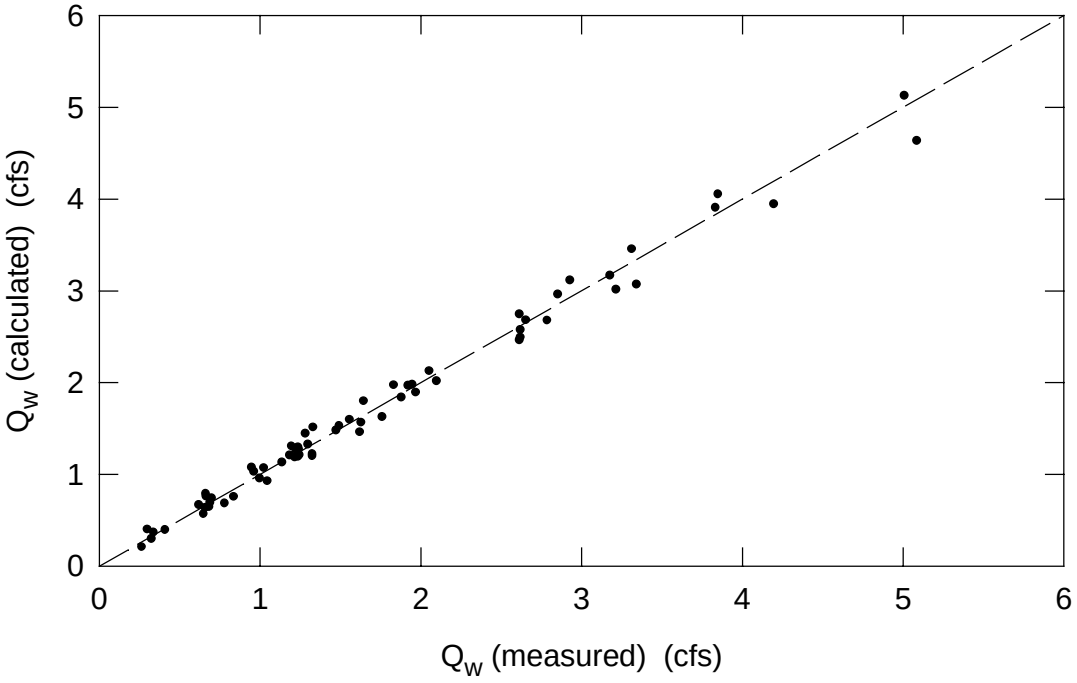

Fig. 4.12 - Comparison of measured and calculated model values of side weir discharge for tapered channels using Method B

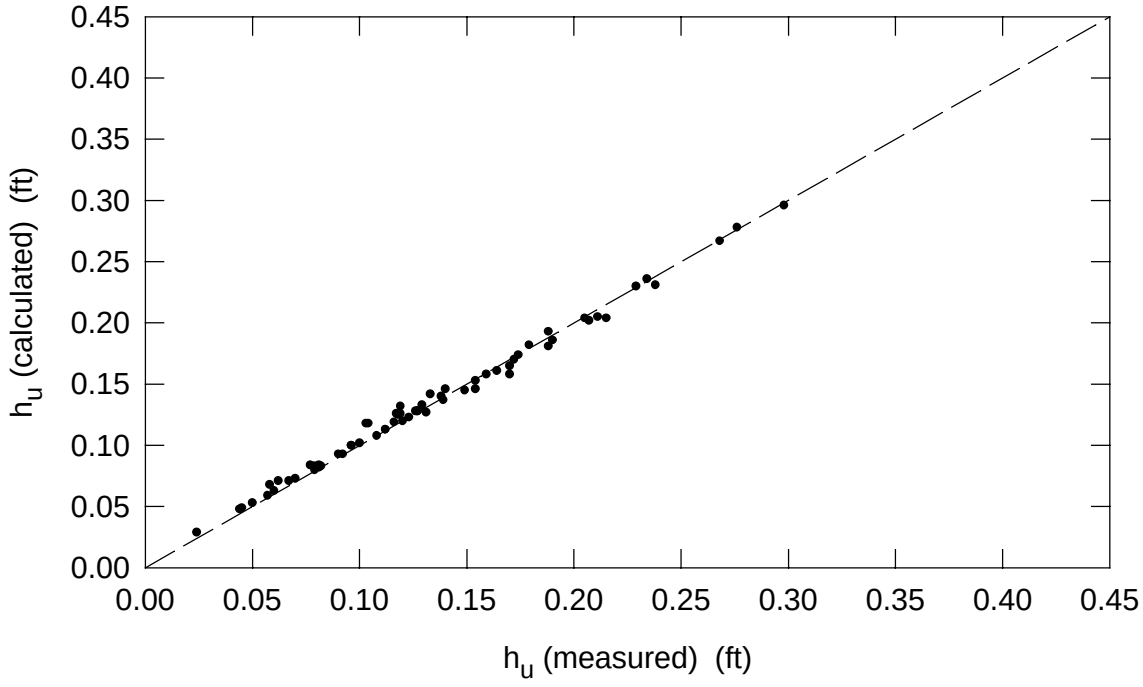

Fig. 4.13 - Comparison of measured and calculated model values of upstream head on the weir for tapered channels using Method B

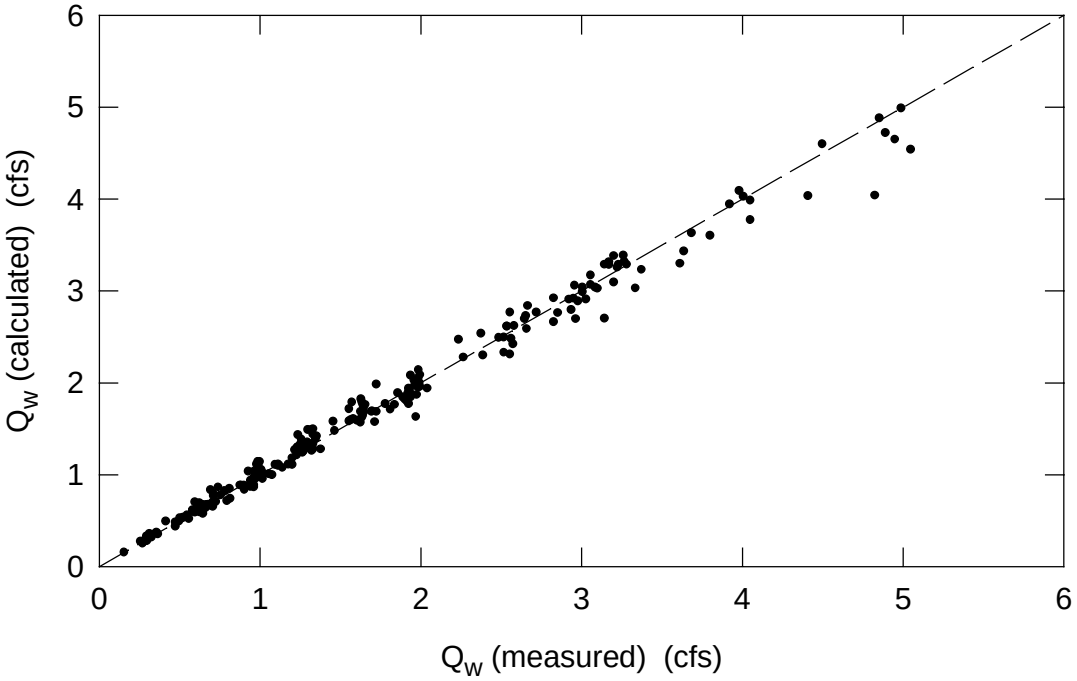

Fig. 4.14 - Comparison of measured and calculated model values of side weir discharge for unsubmerged flow using Method C

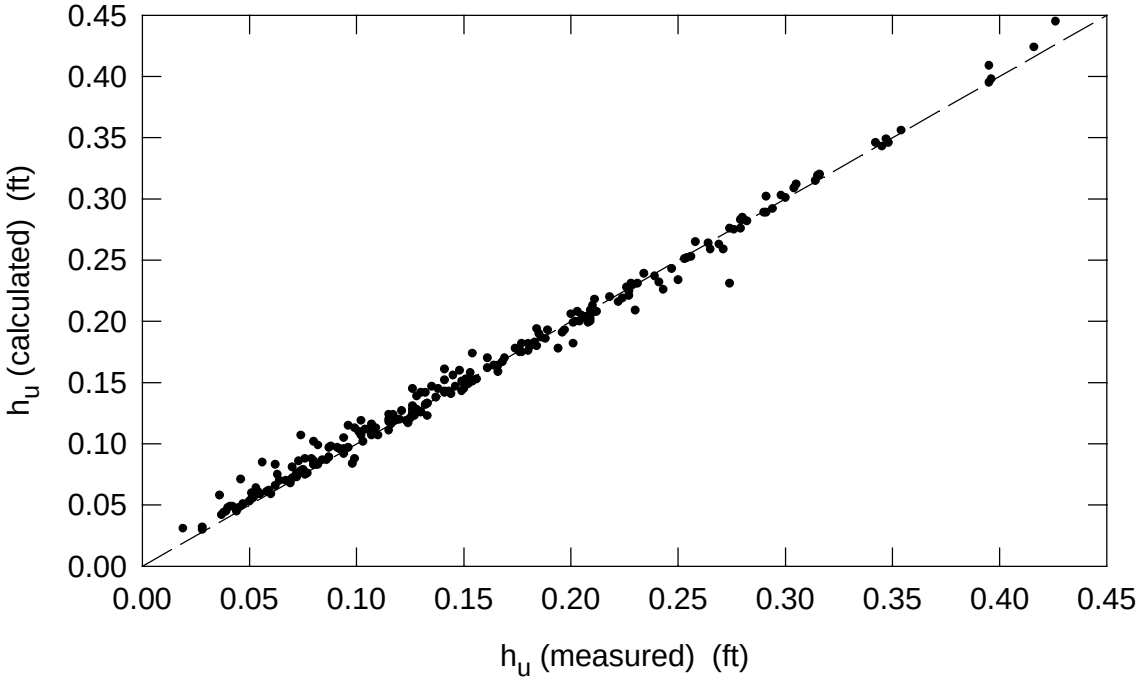

Fig. 4.15 - Comparison of measured and calculated model values of upstream head on the weir for unsubmerged flow using Method C

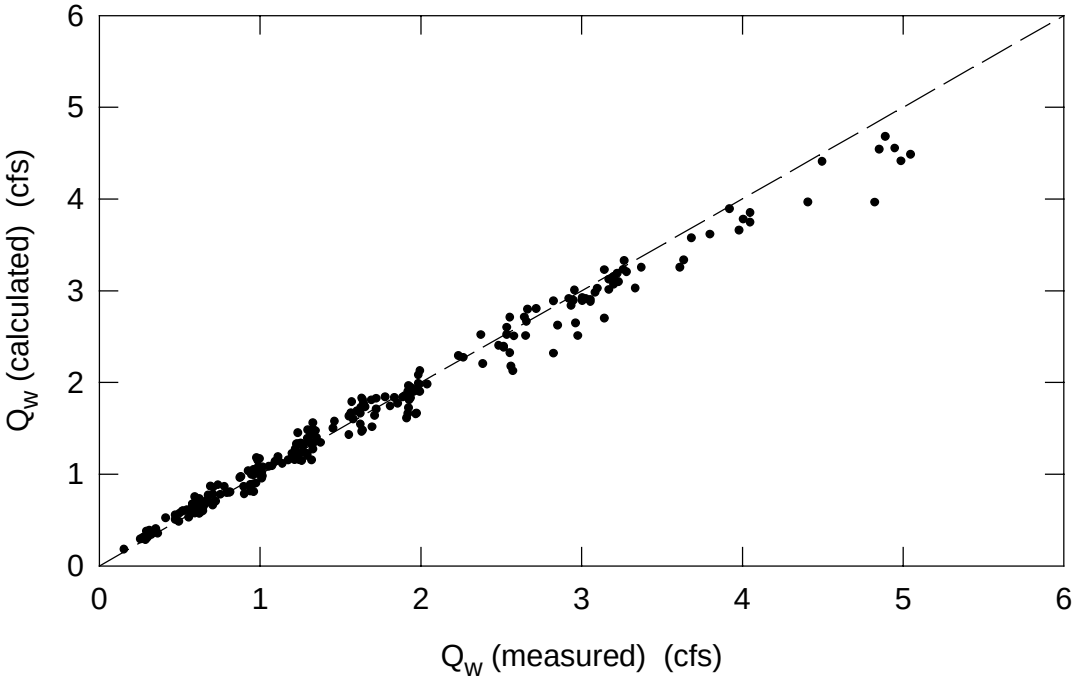

Fig. 4.16 - Comparison of measured and calculated model values of side weir discharge for unsubmerged flow using Method D

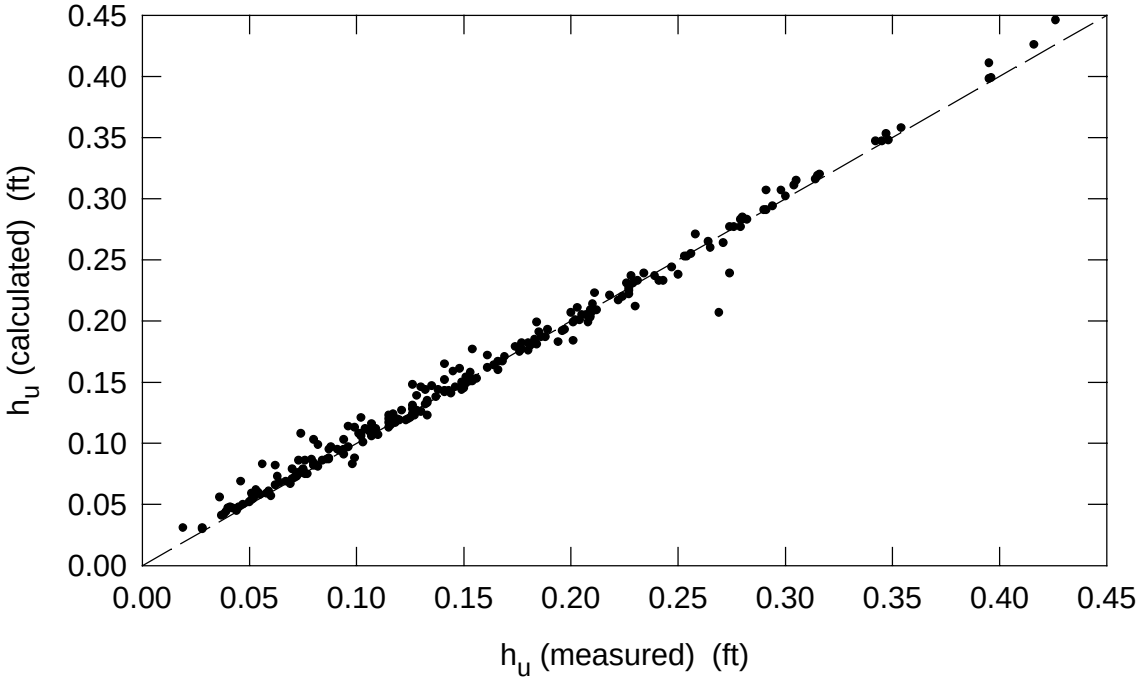

Fig. 4.17 - Comparison of measured and calculated model values of upstream head on the weir for unsubmerged flow using Method D

Table 4.7 - Statistics of differences between measured and calculated model values of Q_w and h_u (Method A)

	ΔQ_w (cfs)	$\Delta Q_w/Q_{w(mea)}$	Δh_u (ft)	$\Delta h_u/h_{u(mea)}$
Unsubmerged				
N = 238				
avg	-0.00474	-0.0112		
stdev	0.124	0.0680		
rms	0.123	0.0688		
Unsubmerged				
N = 235[(1)]				
avg	0.000983	-0.00819	0.00327	0.0123
stdev	0.112	0.0628	0.00877	0.0662
rms	0.112	0.0632	0.00934	0.0672
Submerged				
N = 35				
avg	-0.0737	-0.0751	0.00280	0.0118
stdev	0.328	0.298	0.00382	0.0177
rms	0.332	0.303	0.00469	0.0210
Tapered				
N = 65				
avg	-0.114	-0.0898	0.00280	0.0185
stdev	0.161	0.127	0.00452	0.0372
rms	0.197	0.155	0.00529	0.0413

Notes: $\Delta Q_w = Q_{w(mea)} - Q_{w(cal)}$, $\Delta h_u = h_{u(mea)} - h_{u(cal)}$, mea = measured, cal = calculated, N = number of tests.

[(1)] Tests A1C20W, A3B19N and A5C18N excluded

In the tests for tapered channels, large values of Q_u and small diversions were associated with small values of both h_d and h_u that were two to three times those of h_d. Under these conditions Fw_d was high and C_e was very large. As a result, C_e was found to be proportional to Fw_d^3. The relationship between C_e and Fw_d in Eq. (2.34) is an artifact of calculating Q_w in terms of h_d in Method A. In Method B, the variation of the head along the weir is considered directly in the computation. Fw_d does not enter into the regression equation of C_1 for tapered channels.

When Method B was used, the errors in the estimation of the side weir discharge averaged about 6%, 13% and 9% for unsubmerged flow, submerged flow and flow in tapered channels respectively. Even though the error is larger for submerged flows, the flows themselves are normally small because of the small head difference across the weir. The errors in the estimation of the upstream head on the weir at prototype scale were on average about 0.20 ft, 0.10 ft and

0.14 ft for unsubmerged flow, submerged flow and flow in tapered channels respectively for a 1:25 scale model.

Method B and Method C had comparable accuracy in predicting Q_w while Method D was less accurate. The rms values for ΔQ_w and $\Delta Q_w/Q_{w(mea)}$ from Method D were about 50% higher than those from Method B. Although Eq. (4.24) has a low R^2, using this equation to estimate C_1' is better than simply using the average value of C_1'. The root-mean-square values of Δh_u and $\Delta h_u/h_{u(mea)}$ obtained from Methods B, C, and D were all about 0.008 ft and 0.1 respectively at model scale. Therefore these three methods were comparable in accuracy in predicting h_u.

Table 4.8 - Statistics of differences between measured and calculated model values of Q_w and h_u (Method B)

	ΔQ_w (cfs)	$\Delta Q_w/Q_{w(mea)}$	Δh_u (ft)	$\Delta h_u/h_{u(mea)}$
Unsubmerged N = 237[(1)]				
avg	0.00173	-0.00361	-0.00165	-0.0338
stdev	0.106	0.0620	0.00807	0.101
rms	0.106	0.0619	0.00822	0.107
Unsubmerged N = 235[(2)]				
avg	0.00306	-0.00296	-0.00167	-0.0339
stdev	0.105	0.0618	0.00797	0.100
rms	0.105	0.0617	0.00813	0.106
Submerged N = 35				
avg	-0.00334	0.00181	-0.00100	-0.00554
stdev	0.136	0.132	0.00403	0.0200
rms	0.135	0.130	0.00410	0.0205
Tapered N = 65				
avg	-0.00017	-0.00840	-0.00154	-0.0265
stdev	0.120	0.0865	0.00531	0.0541
rms	0.119	0.0862	0.00549	0.0598

Notes: $\Delta Q_w = Q_{w(mea)} - Q_{w(cal)}$, $\Delta h_u = h_{u(mea)} - h_{u(cal)}$, mea = measured, cal = calculated, N = number of tests.

(1) Test A5C18N excluded.

(2) Tests A1C20W, A3B19N and A5C18N excluded.

Table 4.9 - Statistics of differences between measured and calculated model values of Q_w and h_u (Method C)

	ΔQ_w (cfs)	$\Delta Q_w/Q_{w(mea)}$	Δh_u (ft)	$\Delta h_u/h_{u(mea)}$
Unsubmerged N = 238				
avg	0.00250	-0.00936	-0.00233	-0.0390
stdev	0.120	0.0639	0.00799	0.100
rms	0.120	0.0644	0.00831	0.107
Unsubmerged N = 237[(1)]				
avg	0.00362	-0.00875	-0.00236	-0.0393
stdev	0.119	0.0633	0.00799	0.100
rms	0.119	0.0638	0.00831	0.107

Notes: $\Delta Q_w = Q_{w(mea)} - Q_{w(cal)}$, $\Delta h_u = h_{u(mea)} - h_{u(cal)}$, mea = measured, cal = calculated, N = number of tests.
[(1)] Test A5C18N excluded.

Table 4.10 - Statistics of differences between measured and calculated model values of Q_w and h_u (Method D)

	ΔQ_w (cfs)	$\Delta Q_w/Q_{w(mea)}$	Δh_u (ft)	$\Delta h_u/h_{u(mea)}$
Unsubmerged N = 238				
avg	0.0305	-0.0134	-0.00251	-0.0362
stdev	0.153	0.0913	0.00871	0.0959
rms	0.156	0.0921	0.00904	0.102
Unsubmerged N = 237[(1)]				
avg	0.0311	-0.0132	-0.00278	-0.0373
stdev	0.154	0.0915	0.00764	0.0946
rms	0.156	0.0922	0.00812	0.102

Notes: $\Delta Q_w = Q_{w(mea)} - Q_{w(cal)}$, $\Delta h_u = h_{u(mea)} - h_{u(cal)}$, mea = measured, cal = calculated, N = number of tests.
[(1)] Test A5C18N excluded.

Table 4.11 - Comparison between Method A and Method B

Method A	Method B
Bulk discharge equation	Discharge equation in terms of discharge per unit length
Discharge coefficient related to Fw_d and L/B	Discharge coefficient related to Fw_d and h_d/P
Q_w and h_u obtained from separate equations, h_u from energy equation but estimated Q_w required to calculate h_u	Q_w and h_u obtained from the same analysis based on momentum equation
α obtained from simplified assumption of velocity distribution in separation zone	β obtained from interpolation (in some cases extrapolation) of empirical results and assumed to vary linearly between upstream and downstream ends of weir
Details of hydraulics along weir not considered	Water surface profile along weir computed
h_c given by empirical equation	h_c not used
	Assumed $U_w \cos\phi = C_2(\eta/P)U$

Method C uses a simpler predictive equation for the discharge coefficient. However the derivation of the lateral flow coefficient does not seem to have a sound theoretical basis. The use of C_3 = 2/3 in the present calculation also lacks strong justification. Nevertheless, the lateral flow coefficient does seem to account for at least part of the variation of the discharge coefficient along the weir. The results should be regarded as preliminary and further study is needed.

The four methods of calculation were also compared using values of $R^2(Q_w)$ and $R^2(h_u)$ defined as

$$R^2(Q_w) = 1 - \frac{\sum_1^N \left(Q_{w(mea)} - Q_{w(cal)}\right)^2}{\sum_1^N \left(Q_{w(mea)} - \overline{Q}_{w(mea)}\right)^2} \tag{4.28}$$

and

$$R^2(h_u) = 1 - \frac{\sum_1^N \left(h_{u(mea)} - h_{u(cal)}\right)^2}{\sum_1^N \left(h_{u(mea)} - \overline{h}_{u(mea)}\right)^2} \tag{4.29}$$

where $\overline{Q}_{w(mea)}$ and $\overline{h}_{u(mea)}$ are the averages of $Q_{w(mea)}$ and $h_{u(mea)}$ respectively. $R^2(Q_w)$ and $R^2(h_u)$ are not coefficients of determination for regression equations; rather they are defined using the concept of the coefficient of determination. A value of $R^2(Q_w)$ close to unity indicates that there is good agreement between the values of $Q_{w(mea)}$ and $Q_{w(cal)}$ and similarly for h_u.

Although the values of R^2 for Eq. (4.23), Eq. (4.24), and Eq. (4.27) are low at 0.682, 0.337 and 0.395 respectively, the values of $R^2(Q_w)$ and $R^2(h_u)$ are all close to unity (Table 4.12). Method B gave higher values of $R^2(Q_w)$ than Method A for all flow conditions and higher values of $R^2(h_u)$ than Method A for both unsubmerged and submerged flows in prismatic channels. Both Methods A and B gave the same $R^2(h_u)$ for flow in tapered channels. Method B gave higher $R^2(Q_w)$ than both Method C and D and Methods B, C and D gave the same values of $R^2(h_u)$.

In view of the above comparison using rms, $R^2(Q_w)$ and $R^2(h_u)$, Method B is the best and is recommended for the calculation of side weir discharge and upstream head on the weir.

4.4 - EFFECTS OF CHANNEL SLOPE AND ROUGHNESS FOR 2.5H:1V SIDE SLOPES

Simulations for prototype conditions with unsubmerged flow were performed to evaluate the effects of slope and roughness on Q_w and h_u. The geometric conditions were selected from those used in the model study and are shown in Table 4.13 for a 1:25 model. From the model test data, the maximum and minimum Q_u for each geometric condition and the maximum and minimum h_d for each Q_u were selected and scaled to the prototype values.

Four values of Manning's n (0.0125, 0.02, 0.03 and 0.04), and four values of channel slope (0.000385, 0.0008, 0.0012 and 0.0016) were used in the simulation so that there were 16 combinations of different slopes and roughnesses. The model had a Manning's n of 0.0125 and a slope of 0.000385. Manning's n of 0.04 and slope of 0.0016 are probably maximum limits of prototype conditions in Harris County. Results of simulation of Q_w and h_u for different geometric and flow conditions using Methods A and B are presented in Appendix 3.

In Method A, the calculation of Q_w does not involve the slope and roughness. Therefore, only one value of Q_w was obtained for each particular geometry and flow. However, for calculation of h_u, Eq. (2.23) takes into account the roughness and slope. The largest differences between values of h_u calculated from Methods A and B are shown in Table 4.14 and the largest ratios between values of Q_w calculated from Methods A and B are shown in Table 4.15. The worst cases give a 75% difference in Q_w and a 1.5 ft difference in h_u. In general, larger slope and smaller roughness give larger values of $h_u(B) - h_u(A)$ but smaller values of $Q_w(B)/Q_w(A)$.

The following observations were obtained from the results of the simulation. For a particular slope, h_u increased as roughness was increased since higher head was required to overcome the increased frictional resistance. For a particular roughness, h_u decreased as the slope

was increased. In most cases, a major contribution to the decrease in h_u was the increase in the elevation of the upstream end of the weir crest relative to the downstream end. For flows with low velocities and thus negligible frictional loss, the decrease was entirely due to the change in elevation.

Table 4.12 - $R^2(Q_w)$ and $R^2(h_u)$ for comparison between measured and calculated values of Q_w and h_u

Method	Flow condition	Number of tests	$R^2(Q_w)$	$R^2(h_u)$
A	Unsubmerged	238	0.988	
	Unsubmerged	235[(2)]	0.990	0.988
	Submerged	35	0.868	0.985
	Tapered	65	0.969	0.992
B	Unsubmerged	237[(1)]	0.991	0.991
	Unsubmerged	235[(2)]	0.991	0.991
	Submerged	35	0.978	0.989
	Tapered	65	0.989	0.992
C	Unsubmerged	238	0.989	0.991
	Unsubmerged	237[(1)]	0.989	0.991
D	Unsubmerged	238	0.980	0.989
	Unsubmerged	237[(1)]	0.980	0.991

Notes: [(1)] Test A5C18N excluded.
[(2)] Tests A1C20W, A3B19N and A5C18N excluded.

Table 4.13 - Geometric conditions used in simulation

Weir length (ft)		Invert width (ft)		Weir height (ft)	
model	prototype	model	prototype	model	prototype
23.91	598	3.4	85	0.52	13.0
10.00	250	3.4	85	0.52	13.0
15.00	375	1.8	45	0.52	13.0
10.00	250	1.8	45	0.52	13.0
20.00	500	3.4	85	0.70	17.5
10.00	250	3.4	85	0.70	17.5
20.00	500	1.8	45	0.70	17.5
10.00	250	1.8	45	0.70	17.5

Table 4.14 - Largest differences between values of h_u calculated from Methods A and B

Parameter	Case 1	Case 2
L (ft)	500	250
B (ft)	45	85
P (ft)	17.5	13.0
Q_u (cfs)	30012	30022
h_d (ft)	3.00	3.55
n	0.04	0.02
S_o	0.000385	0.0012
Q_w(A) (cfs)	3977	3280
Q_w(B) (cfs)	6962	2856
Q_w(B)/Q_w(A)	1.75	0.87
h_u(A) (ft)	4.48	0.73
h_u(B) (ft)	3.92	2.20
h_u(B) - h_u(A) (ft)	-0.56	1.47

Table 4.15 - Largest ratios between values of Q_w calculated from Methods A and B

Parameter	Case 1	Case 3
L (ft)	500	598
B (ft)	45	85
P (ft)	17.5	13.0
Q_u (cfs)	30012	10156
h_d (ft)	3.00	0.97
n	0.04	0.0125
S_o	0.000385	0.0016
Q_w(A) (cfs)	3977	1082
Q_w(B) (cfs)	6962	430
Q_w(B)/Q_w(A)	1.75	0.40
h_u(A) (ft)	4.48	-0.36
h_u(B) (ft)	3.92	-0.10
h_u(B) - h_u(A) (ft)	-0.56	0.26

Since the side weir discharge is primarily a function of the head on the weir (Eq. (2.4)), the same trends of variation with roughness and slope were observed for the side weir discharge. That is, for a particular slope, Q_w increased as roughness was increased and for a particular roughness, Q_w decreased as the slope was increased.

In addition to the effects of the method of calculation (Table 4.14 and Table 4.15), the amount of variation of Q_w and h_u for different slopes and roughnesses depends on the geometric and flow conditions. For example, for L = 598 ft, B = 85 ft, P = 13 ft, Q_u = 30144 cfs and h_d =

4.85 ft, the difference between the maximum and minimum Q_w was about 7000 cfs and the difference between the maximum and minimum h_u was about 3 ft for the different S_o and n for which calculations were done.

All of these results indicate that it is definitely beneficial to use Method B to account for different channel roughnesses and slopes.

5 - DISCHARGE AND HEAD LOSS EXPERIMENTS FOR 4:1 SIDE SLOPES

5.1 - INTRODUCTION

The objective of the work reported in this section was to conduct hydraulic model experiments to evaluate the effects of channel side slope on weir hydraulics. The channel and weir were modified to have 4H:1V side slopes (Section 3.2). Slopes of 4H:1V are the expected extreme of flatter slopes, as contrasted to the previous experiments at the opposite extreme of steeper slopes at 2.5H:1V.

5.2 - MODEL RESULTS

Twenty-four tests were conducted for unsubmerged flow for the same general hydraulic conditions as some of the previous experiments with 2.5H:1V side slopes. The model height of the weir was 0.5 ft. Two weir lengths of 5 ft and 10 ft were investigated. There were 15 tests for the 10 ft weir and 9 tests for the 5 ft weir. Six of the 15 tests for the 10 ft weir were duplicate measurements that confirmed the reproducibility of the results. The test data are tabulated in Appendix 4. The results of these tests were compared with the previous results to determine the effect of side slope. The methods of analysis have been described in Sections 4.1 - 4.3.

5.2.1 - Analysis of Data using Method A

In Fig. 5.1, values of C_e obtained from experimental results (C_e (observed)) are plotted against values calculated from Eq. (2.28) (C_e (regression)); the conditions for each test (A1, A2, etc.) are given in Appendix 4. The data for the previous tests with 2.5H:1V side slopes, B = 1.8 ft and P = 0.52 ft are also shown in the figure. For this particular geometry, the figure shows a positive bias in the coefficients calculated from the regression equation, i.e., the values of C_e (regression) are all larger than the values of C_e (observed). The bias is observed in the data for the tests with 4H:1V side slopes as well as for the tests with 2.5H:1V side slopes. It is noted that the data for unsubmerged tests in the previous project (Tynes, 1989) as a whole do not show a bias.

The measured values of h_u are plotted against the values calculated using Method A in Fig. 5.2. The measured side weir discharges were used in this calculation. Due to the small hump in the channel invert, Eq. (2.23) was modified to be

$$h_u = h_d + P_d - P_u + h_f - \frac{U_u^2}{2g}\left(1 - \frac{A_u^2}{A_d^2}\right) - (EL_u - EL_d) + h_c \qquad (5.1)$$

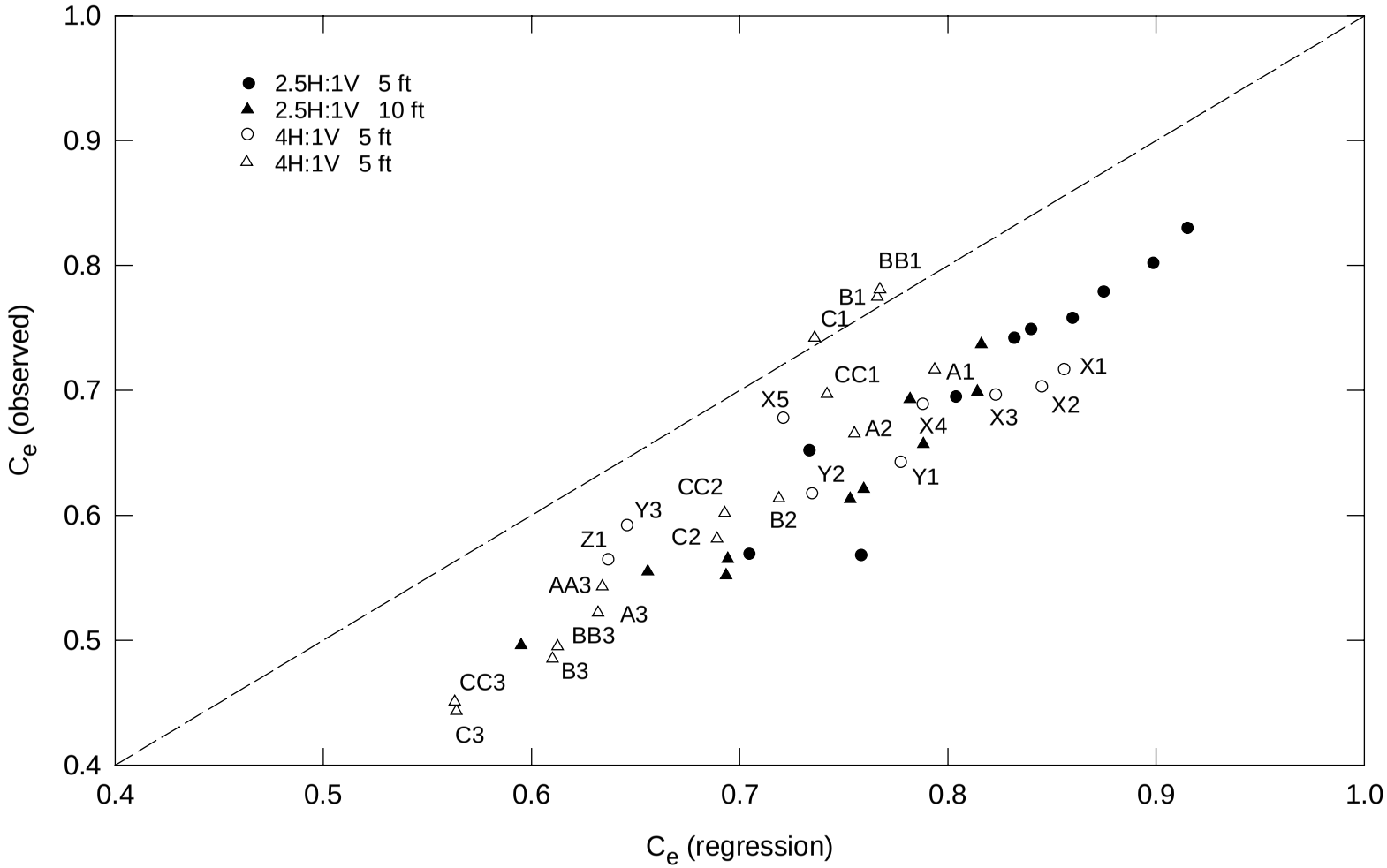

Fig. 5.1 - Observed and calculated C_e values

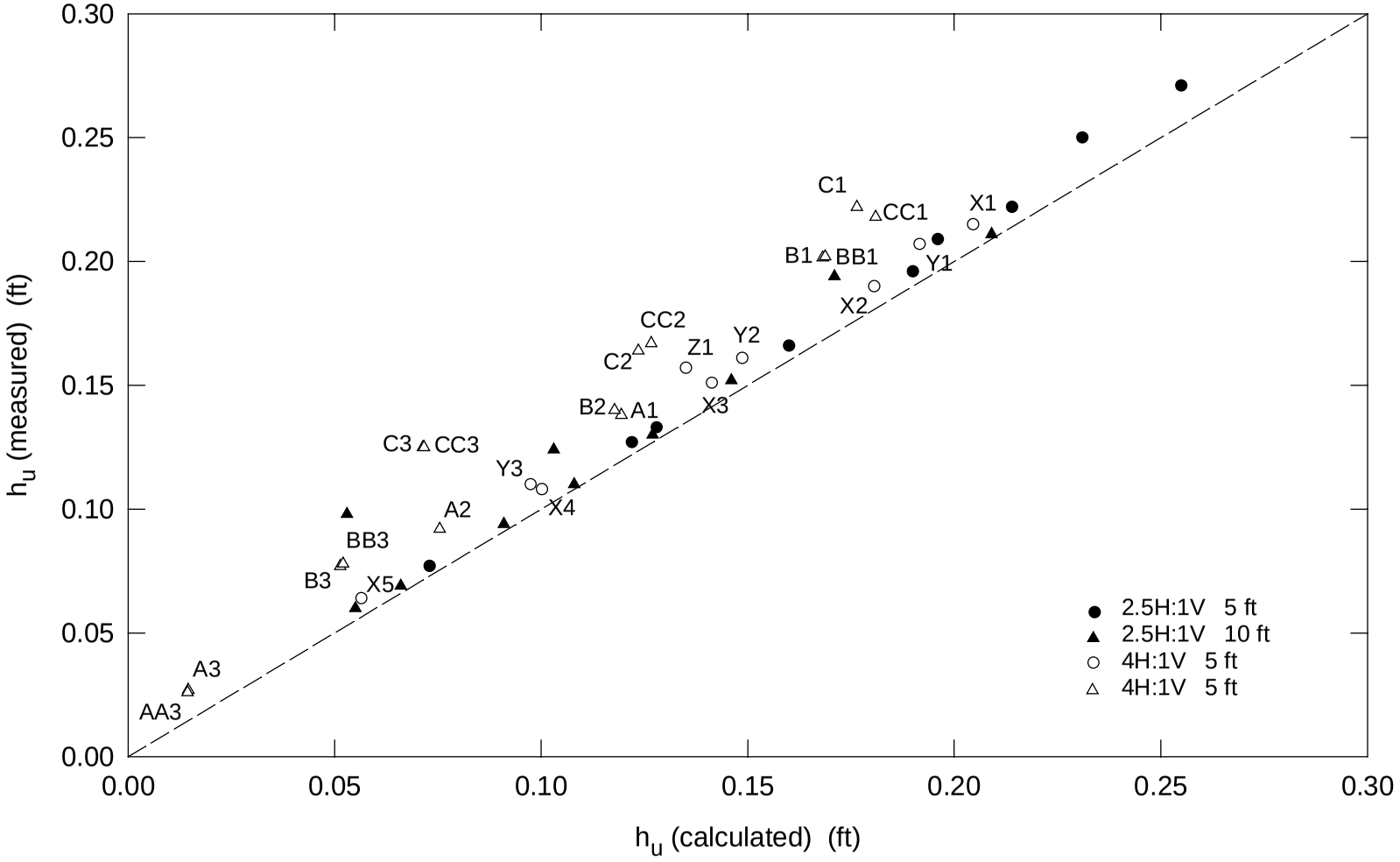

Fig. 5.2 - Measured and calculated h_u using Method A

where P_u and P_d are the weir heights at the upstream and downstream ends of the weir and EL_u and EL_d are the channel invert elevations at the upstream and downstream ends of the weir. The figure shows that there are larger discrepancies between measured and calculated values of h_u for the tests with 4H:1V side slopes than for the tests with 2.5H:1V side slopes.

Since the calculation of the side weir discharge by Method A does not take into account the longitudinal slope and roughness, it is more appropriate to analyze the data using Method B.

5.2.2 - Analysis of Data using Method B

In the analysis using Method B, the local invert slope and a local weir height were used for each of the computational step. Fig. 5.3 shows the comparison between values of C_1 obtained from numerical optimization with $C_2 = 0.85$ and values of C_1 calculated from Eq. (4.23). Super-critical flow depths were obtained in the computed water surface profiles for Tests B3, BB3, C2, CC2, C3 and CC3. Therefore, no results are presented for these tests. There is also a positive bias in the coefficients calculated from the regression equation for the tests with 2.5H:1V side slopes. However, the data points for the tests with 4H:1V side slopes exhibit a different pattern with about half of them above the 1:1 line. The values of h_u are shown in Fig. 5.4. While most of the points for the tests with 2.5H:1V side slopes lie close to the 1:1 line, the points for the tests with 4H:1V side slopes are all above the 1:1 line. In the analysis of the data of the previous project, C_2 was adjusted to minimize the discrepancies between the measured values of h_u and the values from the numerical optimization. Hence the larger discrepancies between the measured values of h_u and the values from the numerical optimization for the tests with 4H:1V side slopes suggested that $C_2 = 0.85$ was inappropriate for this set of data.

C_2 was changed to 1.10 and the results are shown in Fig. 5.5 and Fig. 5.6. Supercritical flow depths were obtained in the computed water surface profiles only for Tests C3 and CC3. For $C_2 = 1.10$, the values of h_u from the numerical optimization are in good agreement with the measured values for the tests with 4H:1V side slopes. Moreover, most of the points in the plot of C_1 (optimization) vs. C_1 (regression) are below the 1:1 line and follow a pattern similar to that for the tests with 2.5H:1V side slopes. Nevertheless, data points for a few tests (A3, AA3, B3, BB3 and X5) are still above the 1:1 line. These five tests had only about 10% diversion.

In Fig. 5.7 and Fig. 5.8, the measured values of Q_w and h_u are compared with the values calculated using discharge coefficients calculated from Eq. (4.23). Fig. 5.7 illustrates that even though the results for A3, AA3, B3, BB3 and X5 do not follow the general trend in Fig. 5.5, this behavior should not be of concern in terms of the estimated side weir discharge because the anomaly occurs only for low discharges. All the data points in Fig. 5.8 lie close to the 1:1 line indicating good agreement between measured and calculated values of h_u.

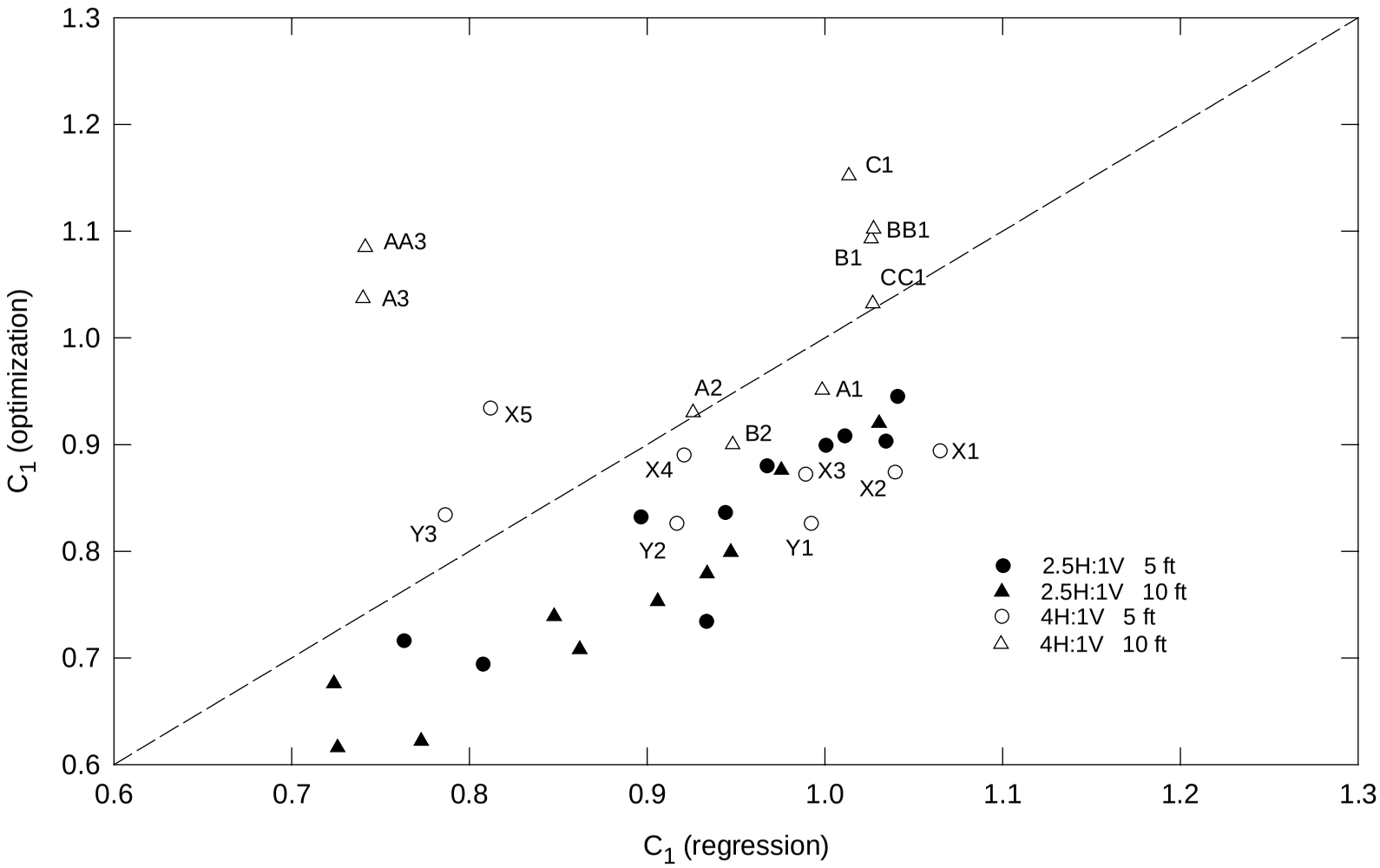

Fig. 5.3 - C_1 from regression equation and from optimization with $C_2 = 0.85$

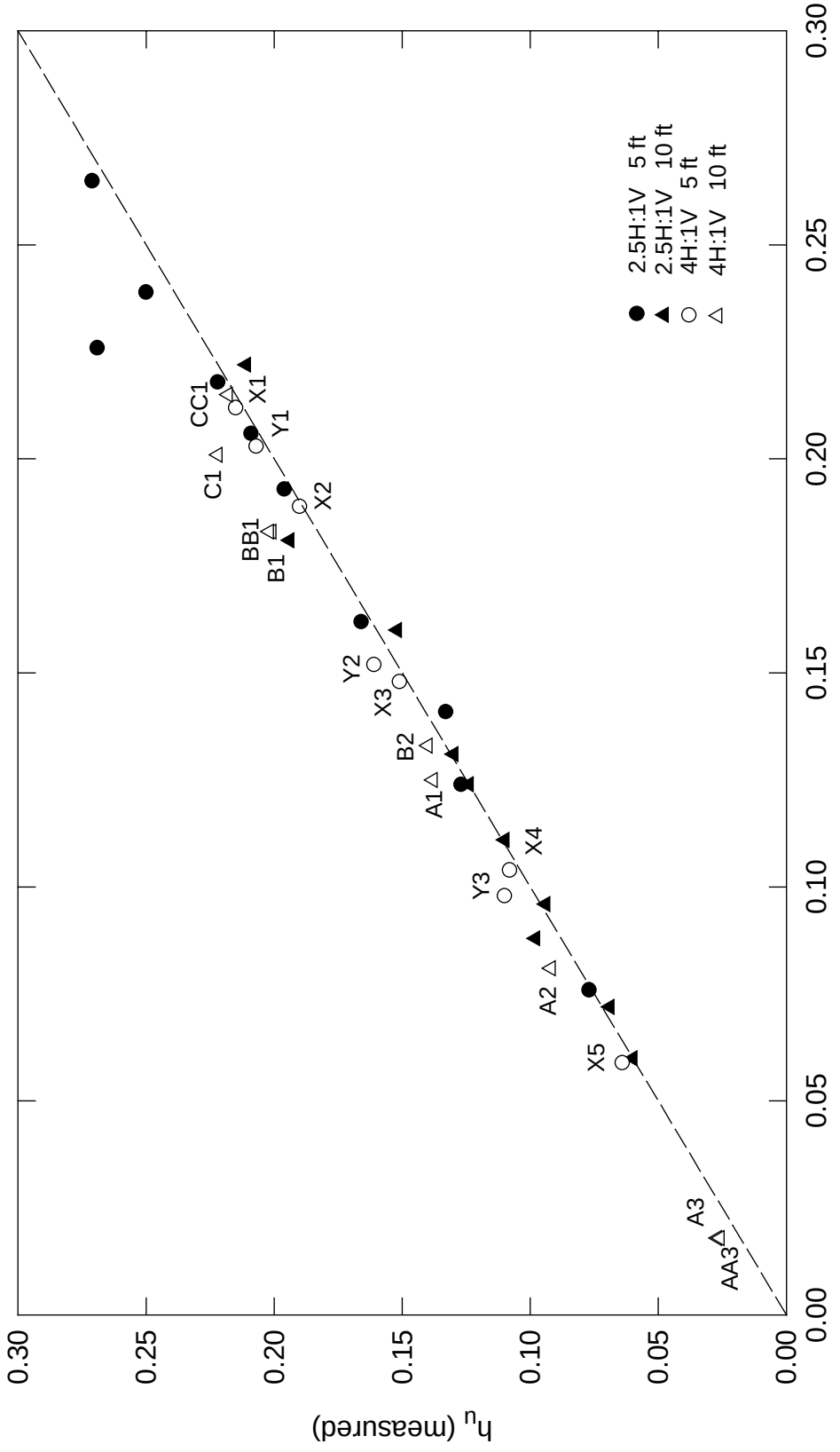

Fig. 5.4 - Measured and numerically optimized h_u with $C_2 = 0.85$

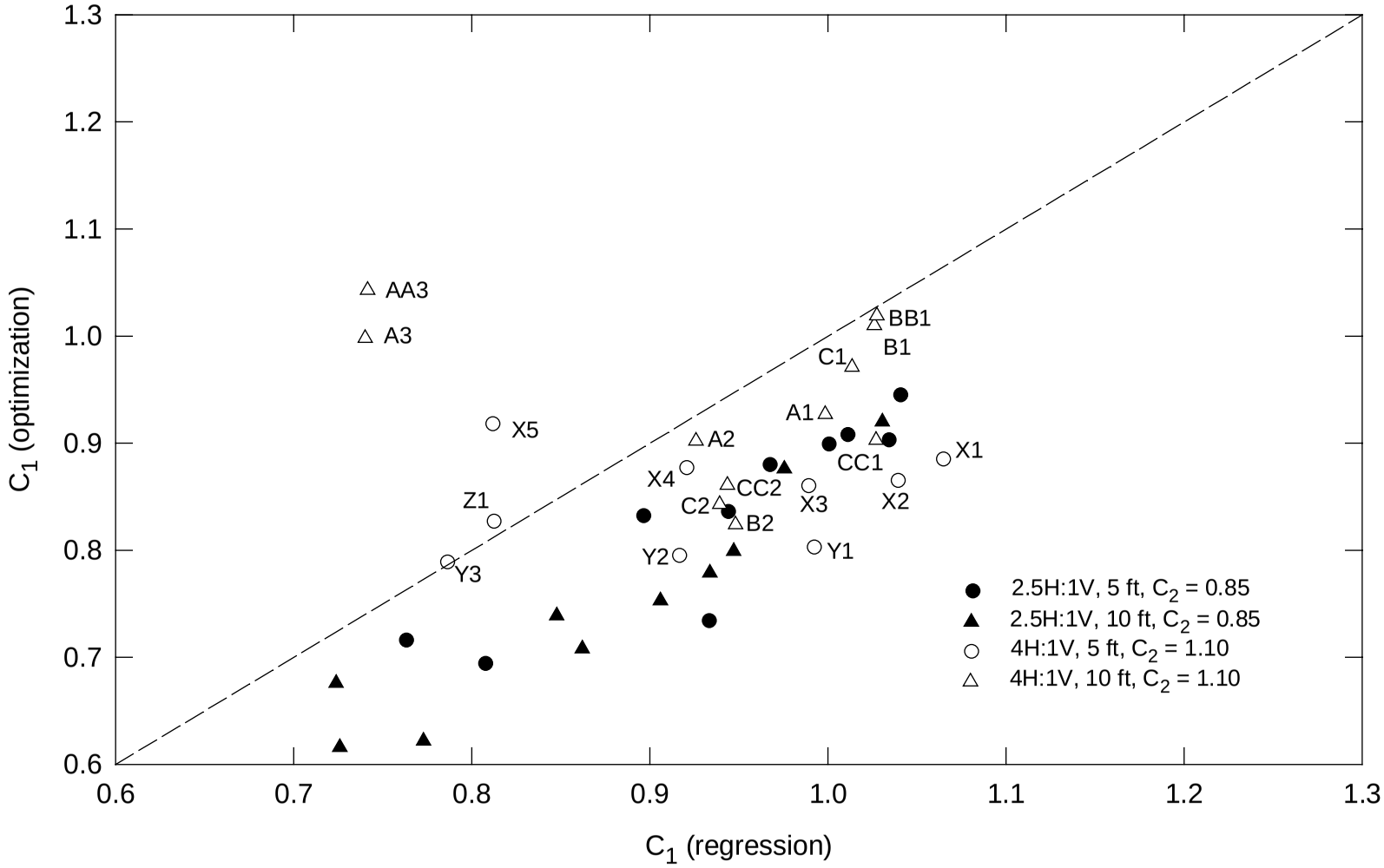

Fig. 5.5 - C_1 from regression equation and from optimization

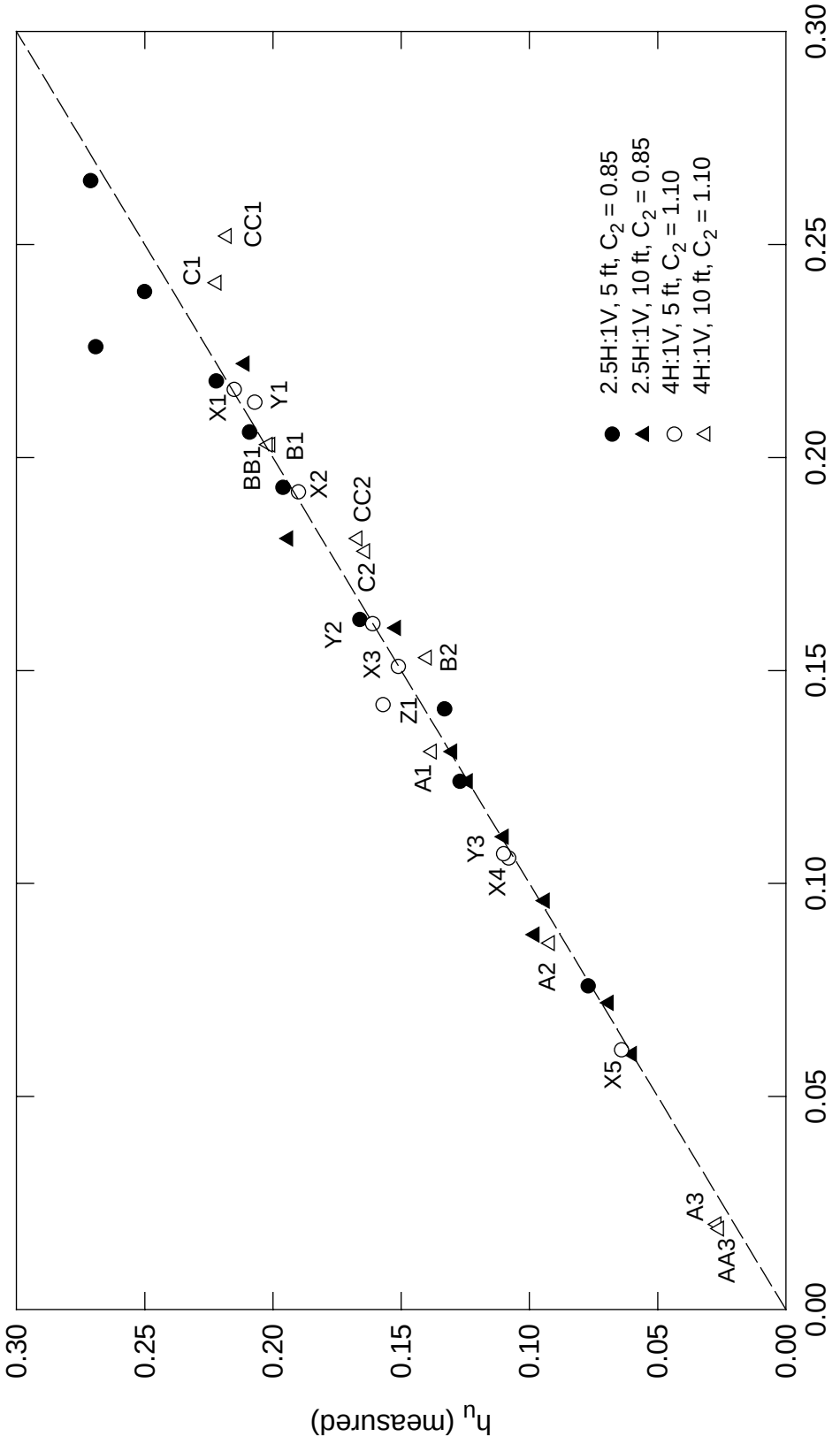

Fig. 5.6 - Values of h_u from regression equation and from optimization

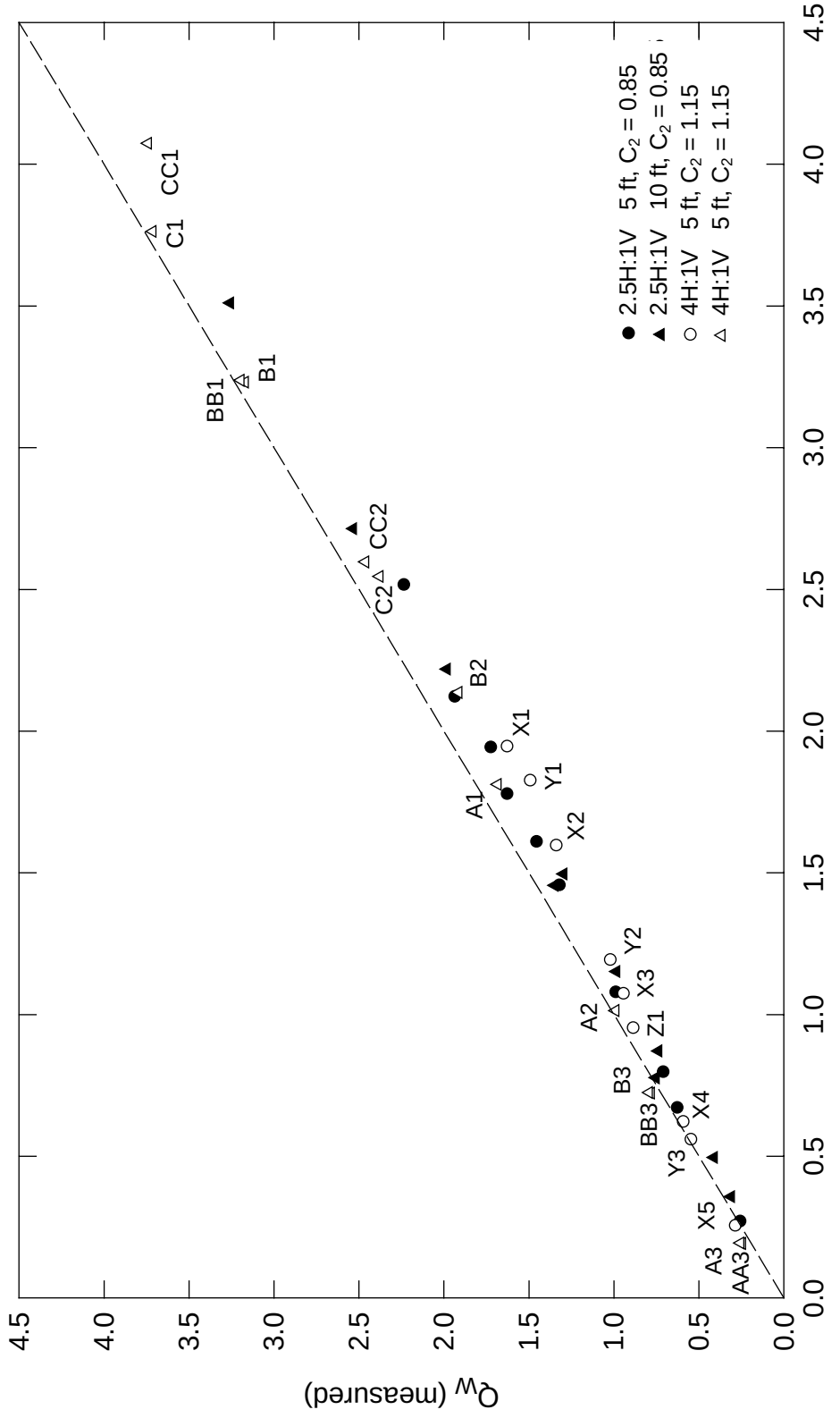

Fig. 5.7 - Measured and calculated Q_w using Method B

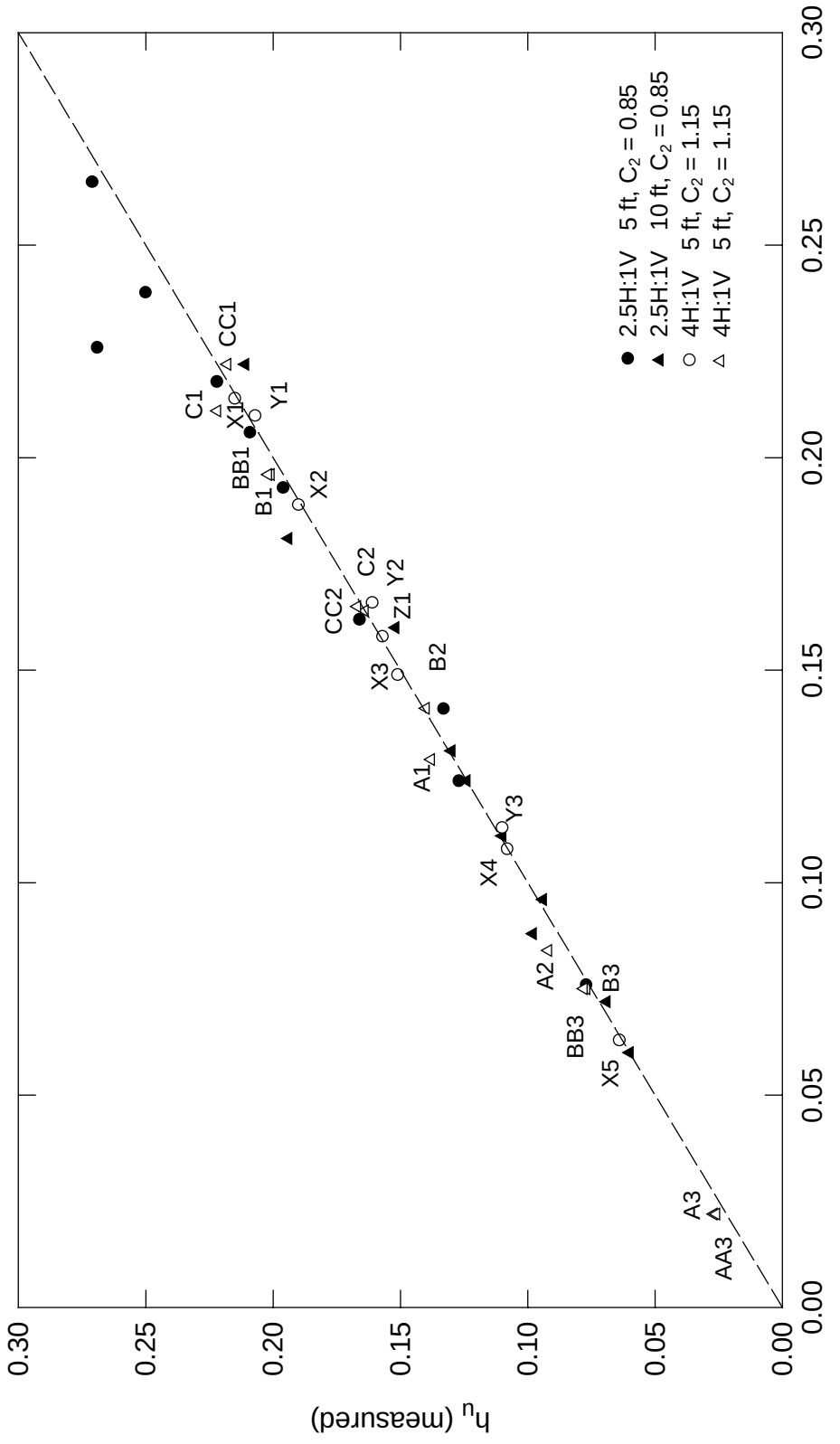

Fig. 5.8 - Measured and calculated h_u using Method B

Table 5.1 shows the root-mean-square values of ΔQ_w, $\Delta Q_w/Q_{w(mea)}$, Δh_u and $\Delta h_u/h_{u(mea)}$ for the data presented in Fig. 5.7 and Fig. 5.8. The accuracy of the prediction of Q_w for the tests with 2.5H:1V side slopes was similar to that for the tests with 4H:1V side slopes. The rms of Δh_u for the tests with 4H:1V side slopes was about half that of the tests with 2.5H:1V side slopes.

Table 5.1 - rms of ΔQ_w, $\Delta Q_w/Q_{w(mea)}$, Δh_u and $\Delta h_u/h_{u(mea)}$

	ΔQ_w (cfs)	$\Delta Q_w/Q_{w(mea)}$	Δh_u (ft)	$\Delta h_u/h_{u(mea)}$
2.5H:1V	0.155	0.119	0.00942	0.0590
4H:1V	0.172	0.130	0.00961	0.0839

The above discussion shows that the regression equation for discharge coefficient for channels with 2.5H:1V side slopes is applicable for channels with 4H:1V side slopes. However, C_2 should be increased to 1.1 for channels with 4H:1V side slopes. For slopes between 2.5H:1V and 4H:1V, linear interpolation may be used to estimate values for C_2.

6 - FLOW ASYMMETRY

6.1 - INTRODUCTION

6.1.1 - Background

Flow diversion at side-channel weirs causes an asymmetry in the velocity distribution for the flow that remains in the channel. For higher diversions and/or flatter channel side slopes, a separation zone is formed on the side of the channel opposite to the weir. Downstream of the weir, the velocity distribution gradually re-establishes itself to the conditions that would exist for the discharge downstream of the weir if there were no diversion. The asymmetry and possible separation zones are important because they can cause the momentum and kinetic energy correction factors (β and α, respectively) for the channel flow at the downstream end of the weir to be significantly greater than unity. For subcritical flows with downstream control, the result is that the head at the downstream end of the weir can be significantly lower than would be calculated if the flow were assumed to be symmetrical with β and α values near unity. When a separation zone is formed, it is also important for the traditional reasons such as sediment deposition.

Although there have been several papers on the hydraulics of side-channel weirs, most of them have addressed discharge coefficients for side weirs and/or the water surface profile in the channel along a side weir. Very few publications have addressed flow asymmetry and related considerations. Related literature is summarized in Section 6.1.2 below. Because of the sparsity of literature on flow asymmetry, the importance of this phenomenon was not recognized at the beginning of the previous project and experiments for the previous project were planned without making provisions for measurement of the effects of the separation zone. As a result, the effects of the separation zone could be included in the previous project only by estimating the size of the separation zone, not by directly measuring either its size or its effects on the channel and weir hydraulics. For some situations, that approximate analysis indicated that the flow asymmetry can cause a head decrease of one foot or more on the weir compared to the water level at the downstream end of the region of flow asymmetry. An effect with such a magnitude should be based on direct measurements, not on inferred or estimated characteristics of the separation zones, as was done previously.

6.1.2 - Related Literature

Subramanya and Awasthy (1972) conducted experiments in a rectangular channel with a side weir. They stated simply that a separation zone was observed on the side of the channel opposite the weir, but they did not give any quantitative information or further details. The velocity profiles in their Fig. 4 show no evidence of separation zones, so they apparently were not

present for all of the test conditions. They said that $\beta = 1.02$ and $\alpha = 1.04$ at the upstream end of the weir. They did not give any values for the downstream end and said that the values could be taken as unity without appreciable error.

El-Khashab and Smith (1976) presented a figure with velocity contours showing no separation zone in a rectangular channel for $Q_w/Q_u = 56\%$, where Q_w = weir discharge and Q_u = channel discharge at the upstream end of the weir. They stated that a separation zone existed for $Q_w/Q_u \geq 70\%$ for subcritical flow. They also stated that they used $\beta = 1$. More of their results are considered in Section 6.8 and Section 6.9.

Balmforth and Sarginson (1983) did experiments in a rectangular channel for the five flow types given by Frazer (1957). The flow types were identified by Balmforth and Sarginson as flows in a mild slope channel with (I) a low weir and no downstream throttle, (II) higher weirs and a downstream throttle, and (III) low weirs and a downstream throttle. Type IV and V were said to be similar to types I and III but for steep channels. The authors did not give their ranges of flow conditions and diversions. They said that β had only small deviations from 1.05, but they evaluated β for a tapered channel with a width that decreased in the flow direction beside the weir. This type of tapering can keep separation zones from forming, even in trapezoidal channels (Tynes, 1989).

For nearly prismatic, rectangular channels with small slopes, Hager (1981) gave β as

$$\beta = \sqrt{1 + \left(\frac{Q'B}{Q} \right)^2} \tag{6.1}$$

where $Q' = -dQ/dx$, x = longitudinal coordinate, and Q = discharge in the channel. This equation was for channels with side weirs and also with side and bottom orifices. It effectively gives not only β but also its variation along a side weir since both Q' and Q vary in a channel along a weir. Hager stated that the effects of β on the hydraulic calculations are limited to subcritical flows, and later Hager and Volkart (1986) concluded that the effects of β for rectangular channels are negligible in comparison to other effects and assumed $\beta = 1$. Hager and Volkart show velocity profiles which indicate asymmetry but no separation zone for $Q_w/Q_u = 50\%$.

Cheong (1992) used $\beta = 1$ for calculations for comparison with his experimental results for trapezoidal channels and for both subcritical and supercritical flows upstream of the side weir. (Note that Cheong's paper uses the symbol β for something other than the momentum correction factor.) Even though he had Q_w/Q_u values as high as almost 90%, he did not mention anything about separation zones.

6.1.3 - Objective

The objective of the experimental work and associated analysis presented in this chapter was to determine the effects of the flow asymmetry and separation zones on the channel hydraulics and the weir flow. The primary focus was on the asymmetry, β, and α, but limited information was also obtained on the length of the flow re-establishment region downstream of side weir.

6.2 - EQUATIONS FOR THE CHANNEL FLOW

Either the momentum equation or the energy equation can be used to calculate the change in stage in the channel due to flow asymmetry. The momentum equation was written for the prismatic channel used in the experiments described in this report as

$$+\gamma A_2(h_1 - h_2) - F_\tau = (\beta\rho QU)_2 - (\beta\rho QU)_1 \tag{6.2}$$

where ρ = fluid density, Q = flow rate, U = x component of cross sectional average velocity, γ = fluid specific weight, A = flow area, h = water surface elevation = piezometric head, F_τ = x component of shear force on the channel bed, x is horizontal (not parallel to the flow, so there is no weight component in the equation) and positive in the downstream direction, 1 and 2 are respectively the upstream and downstream cross sections (e.g., at the downstream end of the weir and the downstream end of the flow re-establishment region), and h_1 - h_2 is small. The term $\gamma A_2(h_1 - h_2)$ in Eq. (6.2) accounts for the pressure forces at cross sections 1 and 2 plus the x component of the pressure force on the channel bed and sides. In applying Eq. (6.2), it was assumed that the channel slope is small so that F_τ is essentially horizontal and so that it is not necessary to distinguish between the direction normal to the bed and vertical. Dividing Eq. (6.2) by γA_2 gives

$$\frac{A_1}{A_2}\frac{(\beta U^2)_1}{g} + h_1 - \frac{F_\tau}{\gamma A_2} = \frac{(\beta U^2)_2}{g} + h_2 \tag{6.3}$$

where g = gravitational acceleration. The momentum correction factor (β) is defined as

$$\beta = \frac{1}{A}\frac{\int_A \overline{u^2}\,dA}{U^2} \tag{6.4}$$

where u is the x component of the total point velocity and U is the cross sectional average velocity. The instantaneous value of u at a point can be written as

$$u = \bar{u} + u' \tag{6.5}$$

where $\bar{u}$ = time-averaged velocity and u' = turbulent fluctuation. An overbar on any quantity is used to indicate time averaging. Substitution of Eq. (6.5) into Eq. (6.4) gives

$$\beta = \frac{\langle \overline{u^2} \rangle}{U^2} = \underbrace{\frac{\langle \bar{u}^2 \rangle}{U^2}}_{\beta_1} + \underbrace{\frac{\langle \overline{u'^2} \rangle}{U^2}}_{\beta_2} \tag{6.6}$$

and the brackets indicate an average over the cross sectional area. Note that β and therefore the momentum flux include the turbulent flux. The components β_1 and β_2 in Eq. (6.6) are considered in Section 6.4.8. F_τ was calculated from

$$F_\tau = \frac{(\tau P)_1 + (\tau P)_2}{2} \Delta x \tag{6.7}$$

where Δx is the channel length for which F_τ is being calculated, P = wetted perimeter, and τ in English units is (Henderson, 1966)

$$\tau = \frac{\gamma n^2 U|U|}{2.21 R_h^{1/3}} \tag{6.8}$$

where R_h = hydraulic radius. Since F_τ was frequently the smallest term in Eq. (6.2), it was not necessary to include the effects of the flow asymmetry in calculating τ.

The energy equation can be written as

$$H_1 - h_f = H_2 \tag{6.9}$$

where h_f is the head loss due to boundary friction and H is the total head given by

$$H = h + \alpha \frac{U^2}{2g} \tag{6.10}$$

where α is the kinetic energy correction factor defined as

$$\alpha = \frac{1}{A} \frac{\int_A \overline{V^2 \vec{V}} \bullet d\vec{A}}{U^3} = \frac{1}{A} \frac{\int_A \overline{V^2 u} dA}{U^3} = \frac{\langle \overline{V^2 u} \rangle}{U^3} \tag{6.11}$$

where V is the magnitude of the point velocity vector ($\vec{V}$) and $\vec{A}$ is the area vector pointing downstream. Using Eq. (6.5), similar expressions for v and w, which are the y (transverse) and z (vertical) components of velocity, and $V^2 = u^2 + v^2 + w^2$, α in terms of the components of the velocity is

$$\alpha = \frac{\left\langle \bar{u}^3 \right\rangle}{U^3} + \frac{\left\langle 3\bar{u}\overline{u'^2} \right\rangle}{U^3} + \frac{\left\langle \bar{u}\overline{v'^2} \right\rangle}{U^3} + \frac{\left\langle \bar{u}\bar{v}^2 \right\rangle}{U^3} + \frac{\left\langle \bar{u}\bar{w}^2 \right\rangle}{U^3} + \frac{\left\langle \bar{u}\overline{w'^2} \right\rangle}{U^3} + \frac{\left\langle \overline{u'^3} \right\rangle}{U^3} + \frac{\left\langle 2\overline{\bar{v}u'v'} \right\rangle}{U^3} + \frac{\left\langle \overline{u'v'^2} \right\rangle}{U^3} + \frac{\left\langle 2\overline{\bar{w}u'w'} \right\rangle}{U^3} + \frac{\left\langle \overline{u'w'^2} \right\rangle}{U^3} \tag{6.12}$$

As with β, α includes the turbulent flux of kinetic energy. The experimental results showed that several of the terms in Eq. (6.12) contributed less than 1% to α so that α could be evaluated from

$$\alpha \approx \underbrace{\frac{\left\langle \bar{u}^3 \right\rangle}{U^3}}_{\alpha_1} + \underbrace{\frac{\left\langle 3\bar{u}\overline{u'^2} \right\rangle}{U^3}}_{\alpha_2} + \underbrace{\frac{\left\langle \bar{u}\overline{v'^2} \right\rangle}{U^3}}_{\alpha_3} + \underbrace{\frac{\left\langle \bar{u}\bar{v}^2 \right\rangle}{U^3}}_{\alpha_4} \tag{6.13}$$

The various components of α in Eq. (6.13) are considered in Section 6.4.8.

In English units, the head loss due to boundary friction was approximated as

$$h_f = \frac{n^2 \Delta x}{4.42}\left[\left(\frac{Q^2}{A^2 R_h^{4/3}}\right)_1 + \left(\frac{Q^2}{A^2 R_h^{4/3}}\right)_2\right] \tag{6.14}$$

Note that the only head loss in Eq. (6.9) is that due to boundary friction, i.e., there is no expansion loss. As will be discussed in Section 6.9, Eq. (6.9) does not need to include any other head loss terms for the region of flow re-establishment downstream of a side weir if appropriate values of α are used in defining the total head.

6.3 - FLOW CONDITIONS

The experiments for studying the flow asymmetry were organized into two types. In Type 1, velocities and water surface elevations were measured for at several cross sections in the region of flow re-establishment for various flow conditions (Cases A - D for 2.5H:1V side slopes and Case F and G for 4H:1V side slopes, Table 6.1). For Cases A, B, C, and F, there was diversion over the side weir. Since there was only about 27.2 ft of channel length downstream of the weir, the channel was not long enough for laterally symmetrical velocity distributions to be re-established for Cases A, B, and F. For Cases D and G, the side weir was blocked and the flow conditions at the downstream end of the weir for Cases A and F were recreated at the upstream end of the channel so that about 60 ft of flow length could be used for measurements. As shown in Fig. 6.22, this attempt to reproduce the separation zone at the upstream end of the channel was not successful for Case D because of the way in which the separation zone was created; the

problem was corrected for Case G. For Cases E and H, there was no separation zone and the weir was blocked in order to determine β and α for symmetrical velocity distributions. Measurements were made near the downstream end of the channel. For Cases A, B, and C, the first cross section (x = 0) was at the bottom of the downstream sloped access ramp. The analysis showed significant transverse velocities at this cross section. Therefore, for Case F the first cross section was 2 ft farther downstream; the transverse velocities were much smaller at this cross section. Also, for the Type 2 measurements (Table 6.2), measurements were made at the downstream end of the access ramp (x = 2 ft). Measurements showed that for a total discharge of 8.9 cfs with 54% and 26% diversion, there was only a 0.001 ft to 0.002 ft difference between the water surface elevations at the cross sections at x = 0 and x = 2 ft. The purpose of the tests in Type 2 was to get additional information on the flow asymmetry, β, and α at the downstream end of the weir.

Table 6.1 - Flow conditions for Type 1

Case	Channel side slope	Total discharge (cfs)	Diversion (%)	Remarks
A	2.5H:1V	8.9	54	Side weir diversion
B	2.5H:1V	3.0	54	Side weir diversion
C	2.5H:1V	8.9	25	Side weir diversion
D	2.5H:1V	4.1	N/A	Separation zone at the upstream end of the channel
E	2.5H:1V	4.1	N/A	No flow asymmetry
F	4H:1V	6.1	54	Side weir diversion
G	4H:1V	4.5	N/A	Separation zone at the upstream end of the channel
H	4H:1V	4.6	N/A	No flow asymmetry

6.4 - VELOCITY MEASUREMENTS

Velocities were measured using an acoustic Doppler velocimeter (Section 3.4). This section discusses the measured velocities and the β and α values (Appendix 5) that were obtained from those measurements. The downstream end of the weir is x = 0 for Cases A, B, C, and F while zero distance is at the downstream end of the flow straighteners for Cases D, E, and G. The components of the β and α values are discussed in Section 6.6.

Table 6.2 - Flow conditions for Type 2

Channel side slope	Total discharge (cfs)	Diversion (%)
2.5H:1V	8.9	54
2.5H:1V	8.9	40
2.5H:1V	8.9	25
2.5H:1V	6.0	55
2.5H:1V	6.1	39
2.5H:1V	3.0	54
2.5H:1V	3.0	40
2.5H:1V	3.0	25
4H:1V	9.0	54
4H:1V	9.0	40
4H:1V	9.0	25
4H:1V	6.0	54
4H:1V	6.0	40
4H:1V	6.0	25
4H:1V	3.0	54
4H:1V	3.0	40
4H:1V	3.0	25

6.4.1 - Measurement Procedures

The measurements were taken on seven verticals spaced at approximately 1.1 ft intervals. The middle vertical was at the centerline of the channel. The two outer verticals on each side were above the side slope. For smaller flow depths, the outermost vertical on each side was less than 3.3 ft from the centerline in order to maintain a sufficient distance between the sampling volume and the boundary. The other verticals were not moved for the smaller depths. Measurements were taken at three points on each of the middle three verticals. The top set of measurements was about 2.5 in. below the water surface. The bottom set of measurements was about 0.4 in. above the invert of the channel. The middle set of measurements was midway between the top and bottom measurements. Only one measurement was made on the outermost vertical on each side at about the same elevation as the top set of measurements on the middle three verticals. Two measurements were taken on the next-to-outermost vertical on each side at about the same elevations as the top and middle sets of measurements on the middle three verticals. Hence 15 points were measured in a cross section. The flow depth was measured at 0.4 ft to the right of the centerline. Water surface elevations were measured at the seven verticals for each cross section.

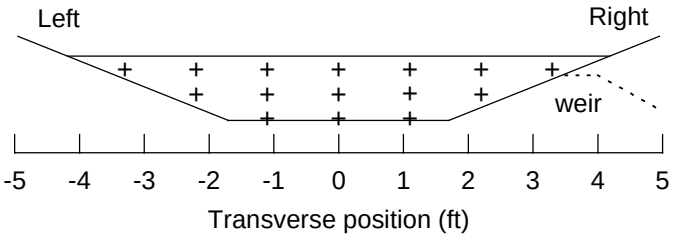

Fig. 6.1 - Typical locations of velocity measurements looking downstream

Due to the time-consuming nature of the measurements, several days were required to complete the measurements for a particular combination of total discharge and percentage diversion. The water surface elevations were measured in one day. The flow rate and percentage diversion quoted for each case in Table 6.1 referred to those during the day of the measurement of the water surface elevations. The flow rates on different days were within 2% of each other, thereby indicating that there was also good reproduction of the flow depths from day to day.

6.4.2 - Integrations

Numerical integrations of the measured velocities over the flow area had to be done to calculate β and α values (Eq. (6.4) and Eq. (6.11)). The velocities were also integrated to obtain the flow rate as a check against the flow rate from the flow meters. For all of the integration, each measured velocity was assumed to represent an area defined laterally and vertically by the midpoints between the measurements, the channel boundary, or the water surface. The area integrations were done first vertically then laterally using a trapezoidal rule in both directions. The integrands were assumed to be the same at the water surface as for the top measurement, while they were assumed to be zero at both the lateral boundary and the bottom boundary.

6.4.3 - Case A

Case A had Q_u = 8.9 cfs with 54% diversion for the channel with 2.5H:1V side slopes. Velocities were measured at x = 0, 4.3 ft, 10.2 ft, 17.3 ft and 22.3 ft.. Fig. 6.2 to Fig. 6.4 show the longitudinal velocity distributions for the cross sections at x = 0, 4.3 ft, and 22.3 ft. In Fig. 6.2, the presence of a separation zone is indicated by the upstream flow at the top on the left side of the channel and by the higher velocities on the right for the middle and bottom measurements; the weir is on the right side. At x = 4.3 ft, there was still a region of average upstream velocity but it had diminished in size (Fig. 6.3). Along the length of the weir, the flow on the right side of the channel next to the weir had a strong transverse velocity component due to the flow over the weir. Immediately downstream of the weir, the residual transverse velocity continued to pull the water to the right side of the channel. As a result, the velocity distribution was more skewed at x

= 4.3 ft than for x = 0. Fig. 6.4 shows that even at the end of the channel, the velocities were higher on the right than the left.

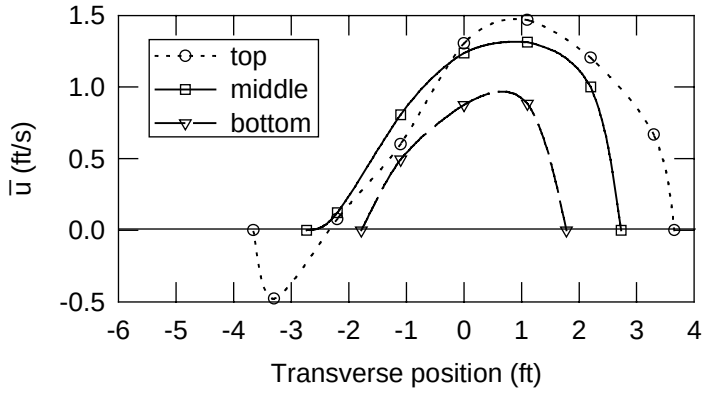

Fig. 6.2 - Longitudinal distributions of velocity at downstream end of weir crest (Case A)

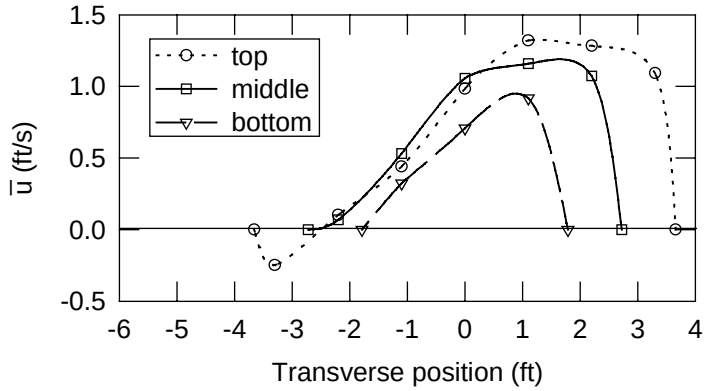

Fig. 6.3 - Longitudinal distributions of velocity 4.3 ft downstream from end of weir crest (Case A)

The β and α values for Case A are shown in Fig. 6.5. From both Fig. 6.4 and Fig. 6.5 it is evident that the channel was not long enough downstream of the weir for the velocities distributions to return to symmetry and for β and α to reach their asymptotic values for Case A.

6.4.4 - Case B

Case B had Q_u = 3.0 cfs with 54% diversion for the channel with 2.5H:1V side slopes. Velocities were measured at x = 0, 4.4 ft, 10.3 ft, 17.4 ft and 22.3 ft. The velocity distributions resembled those at the corresponding cross sections in Case A. The velocity measurements indicate that the relative velocity distributions depend primarily on the percent diversion without a strong dependence on the flow rate. This conclusion is also supported by the β and α values that are shown in Fig. 6.5 in comparison with the values for Case A. There are small differences in

the β and α values immediately downstream of the weir, but for x ≥ 10 ft, the values are much closer together.

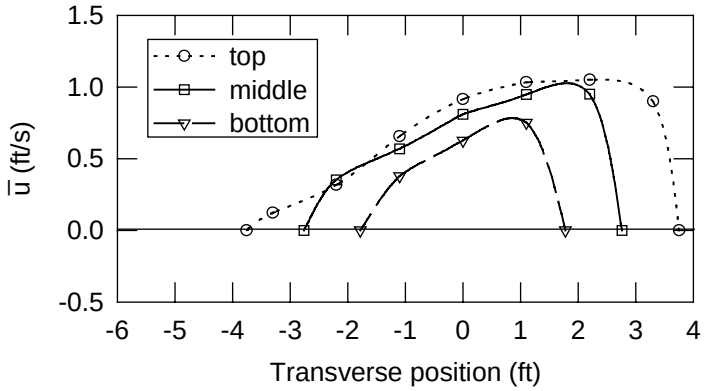

Fig. 6.4 - Longitudinal distributions of velocity 22.3 ft downstream from end of weir crest (Case A)

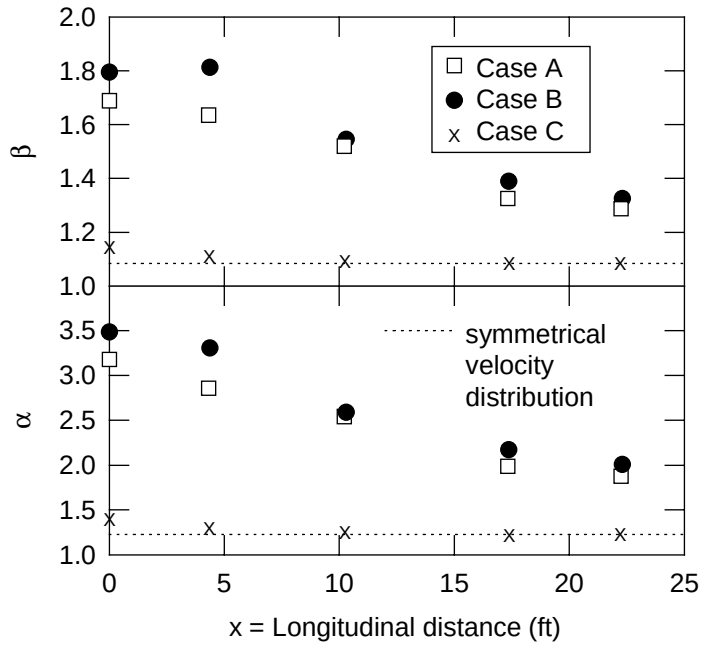

Fig. 6.5 - β and α values for Cases A - C

6.4.5 - Case C

Case C had Q_u = 8.9 cfs with 25% diversion for the channel with 2.5H:1V side slopes. Velocities were measured at x = 0, 4.4 ft, 10.2 ft, 17.4 ft and 22.2 ft. Fig. 6.6 shows the longitudinal velocity distributions at x = 4.4 ft. The velocities were higher on the left than on the right, in contrast to Cases A and B. This characteristic continued further downstream. The measured velocities were all positive, even at x = 0. The lateral flow over the weir was apparently not

strong enough to pull the bulk of the flow to the right side of the channel to create a separation zone. Dye tests showed that there were no separation zones for any diversions on the order of 30% or less for 2.5H:1V side slopes. For trapezoidal channels, specification of the conditions for initiation of a separation zone is somewhat subjective. Even very small diversions may cause a region of nearly zero or upstream velocity for a width of one to two inches in the model at the edge of the channel opposite to the weir. Also, upstream flow in a separation zone may be intermittent for low diversions. A separation zone was said to exist in the model when there was consistent upstream flow at the left most velocity measurement position (y = -3.3 ft).

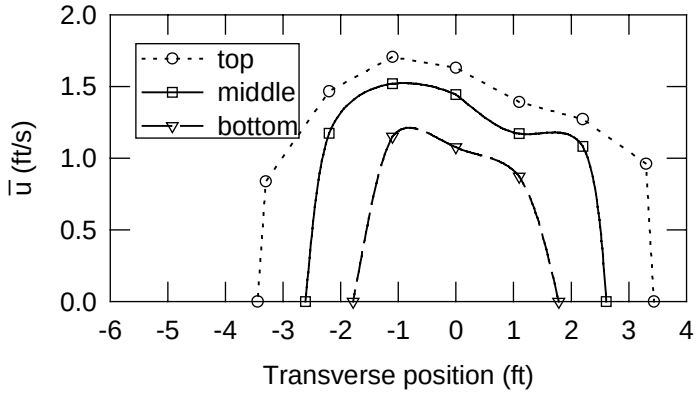

Fig. 6.6 - Longitudinal distributions of velocity 4.4 ft downstream from end of weir crest (Case C)

While there is no absolutely conclusive explanation for the change in the velocity distributions for Case C relative to Cases A and B, the following comments are offered as speculation. For several flow conditions, dye tests were done to determine the parts of the channel from which the flow over the weir was coming. Dye was injected into the flow at the upstream end of the weir. The injection tube was moved laterally until the dye streak at the downstream end of the weir was split about evenly with half going over the weir and half going downstream in the channel. This procedure was done for injections at the surface and at the bed. These dye tests indicated that the weir flow comes from farther away from the weir at the bottom of the channel than at the top for most diversions (Fig. 6.7). This behavior is reasonable because the flow has higher velocities near the surface than near the bed so the flow near the water surface has more downstream momentum and a resulting stronger tendency to continue down the channel rather than go over the weir. Applying this rationale to Case C, it is possible that the lower velocities on the side of the channel near the weir are a result of water being drawn from the lower regions of the approach flow to fill in the region vacated by water going over the weir. (Fig. 6.7 is for the channel after it had been modified to have 4H:1V side slopes. Earlier qualitative tests with the 2.5H:1V side slopes showed the same trends.)

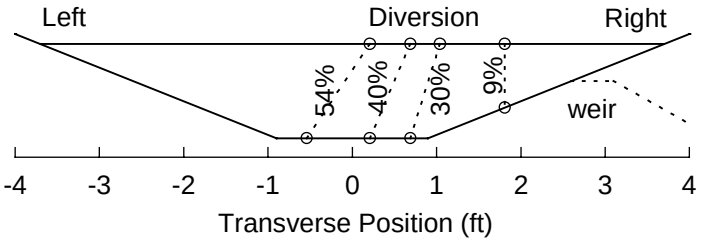

Fig. 6.7 - Left boundaries of regions from which weir flow comes

For Case C with Q_u = 8.9 cfs and 25% diversion, the β and α values are shown in Fig. 6.5. The values immediately downstream of the weir are only slightly greater than their asymptotic values, and they rapidly reach their asymptotic values.

6.4.6 - Case D

The channel downstream of the side weir was not long enough for the flow to completely re-establish itself for diversions on the order of 50%. To allow more channel length to study the re-establishment for a 54% diversion with a separation zone, the side weir was blocked and a separation zone was created at the upstream end of the channel after measurements had been made for separation zones created by outflow over the side weir. The discharge into the channel was adjusted to be the same as the flow rate downstream of the side weir for Q_u = 8.9 cfs with 54% diversion. For Case D, the left side of the channel cross section upstream of the flow straighteners at the head box was blocked to create a separation zone. The flow straighteners are thin vertical sheets 2 ft long and 2.4 in apart. Also, vertical wood strips were used to adjust the velocity distribution at the upstream end of the channel to be similar to that downstream of the side weir in the case with flow diversion. Even though the time-averaged velocities for the "forced" separation had reasonable agreement with the actual separation zone, analysis of the measurements (Section 6.7, Fig. 6.22) showed that there were significant differences in the turbulence for the two cases so that the forced separation zone did not accomplish the desired objective for Case D. The straighteners apparently had a significant effect on the turbulence created by the flow separation. Since this difference was not discovered until after the channel had been modified to have 4H:1V side slopes, it was not possible to repeat the measurements. For Case G (Section 6.4.9), blocking of part of the channel was done downstream of the flow straighteners. The agreement between the results for Cases F and G is much better than between Cases A and D (Section 6.7, Fig. 6.23) .

Case D had Q = 4.1 cfs with a forced separation zone at the upstream end of the channel with 2.5H:1V side slopes. This flow condition was similar to that downstream of the weir for Q_u = 8.9 cfs with a 54% diversion; the flow of 4.1 cfs is 46% of 8.9 cfs. Velocity measurements

were made at the cross sections 7.4 ft, 12.5 ft, 25.5 ft, 37.2 ft, 48.9 ft and 60.6 ft from the downstream end of the flow straighteners.

The values of β and α are shown in Fig. 6.8. Even with 60 ft of channel length, the β and α still do not reach their asymptotic values but they get much closer than for Cases A and B.

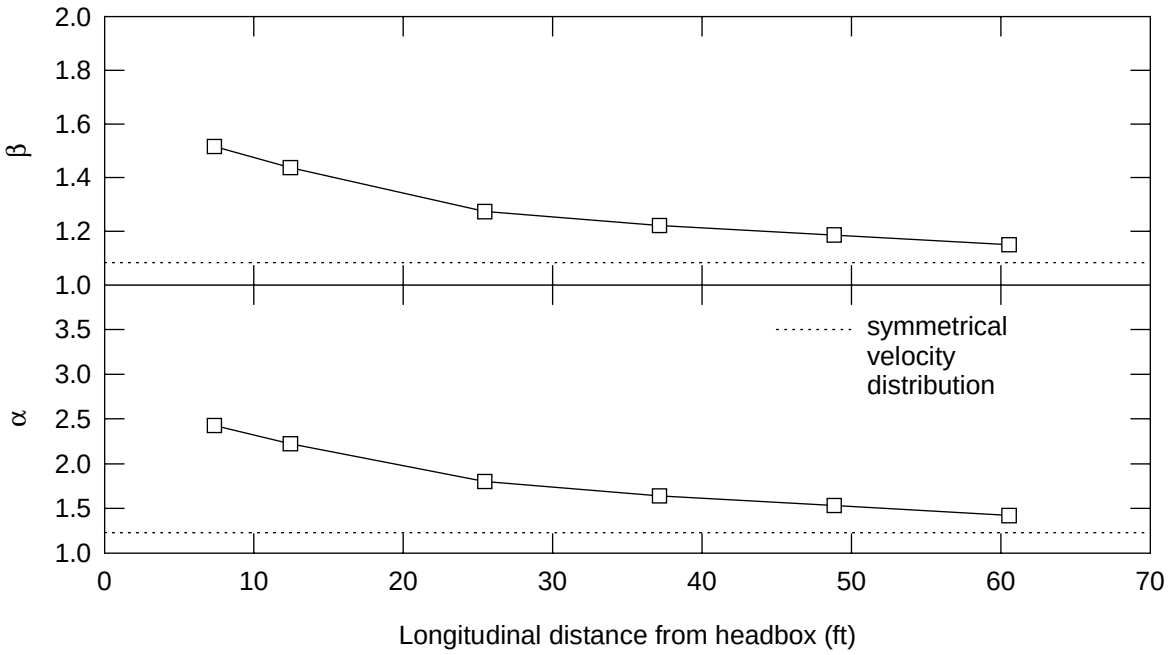

Fig. 6.8 - β and α values for Case D

6.4.7 - Case E

Case E had Q = 4.1 cfs with no separation zone in the channel with 2.5H:1V side slopes. With the side weir blocked with a thin metal sheet and with no flow modification at the headbox (other than the packed bed and flow straighteners to remove the large scale eddies generated in the headbox), velocity measurements were made at the cross section 60.6 ft from the downstream end of the flow straighteners to determine β and α values for established flow. These velocity distributions were essentially symmetrical about the channel centerline.

6.4.8 - Case F

Case F had Q_u = 6.1 cfs with 54% diversion for the channel with 4H:1V side slopes. Velocities were measured at x = 2.5 ft, 8.1 ft, 13.6 ft, and 19.2 ft.. Fig. 6.9 shows the longitudinal velocity distributions at x = 2.5 ft for two sets of measurements made on different days. For the top and middle measurements, the agreement is good. The bottom measurements are indicative of a problem in many of the measurements for the 4H:1V side slopes, namely that it was difficult to obtain good reproducibility of the bottom measurements. Because of the steep gradi-

ents of velocity near the bottom of the channel, small differences in the vertical position of the velocity probe could make a significant difference in the velocities. Nevertheless, it is difficult to believe that this potential problem is the source of the different velocities since the position of the probe relative to the boundary was measured with the acoustic probe itself. Except for this problem with the bottom set of measurements, the velocity distributions for the 4H:1V side slopes were very similar to those for the 2.5H:1V side slopes. Fortunately, the problem with the bottom set of measurements did not greatly affect the results for β and α. For the two sets of measurements in Fig. 6.9 the two β values were 1.99 and 1.91 (4% difference) and the two α values were 3.83 and 3.80 (less than 1% difference).

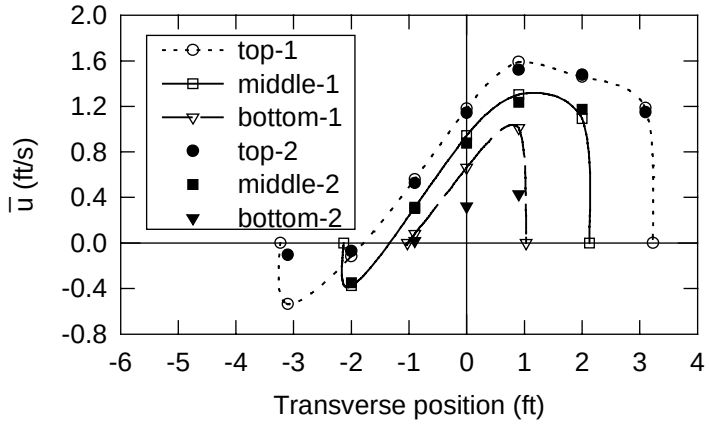

Fig. 6.9 - Longitudinal distributions of velocity 2.5 ft from downstream end of weir crest (Case F)

The β and α values are shown in Fig. 6.10. The values immediately downstream of the weir are a little larger than for Cases A and B (Fig. 6.5), and the values decrease more rapidly than for Cases A and B. The average values for Cases A and B are shown by the dashed lines in Fig. 6.10. The faster decrease is presumably a result of a greater influence of boundary shear with the flatter side slopes.

6.4.9 - Case G

Case G for the channel with 4H:1V side slopes is similar in purpose to Case D for 2.5H:1V side slopes in that a separation zone was created artificially at the upstream end of the channel to allow additional channel length for re-establishment of the flow. However, this time the flow was blocked on the downstream side of the flow straighteners. The flow rate was 4.5 cfs, which corresponds to the flow downstream of a weir with Q_u = 9.0 cfs and 50% diversion. The agreement between the results for Cases F and G is much better than between Cases A and D, as discussed in Section 6.7. Velocity measurements were made at 15 ft, 17.2 ft, 19.3 ft, 21.5

ft, 23.6 ft, 25.8 ft, 28 ft, 32.3 ft, 34.5 ft, 46.5 ft and 58.5 ft from the downstream end of the flow straighteners. The large number of measurements was due to the variation of β and α (Fig. 6.11) being somewhat irregular and the desire to try to determine the variation correctly.

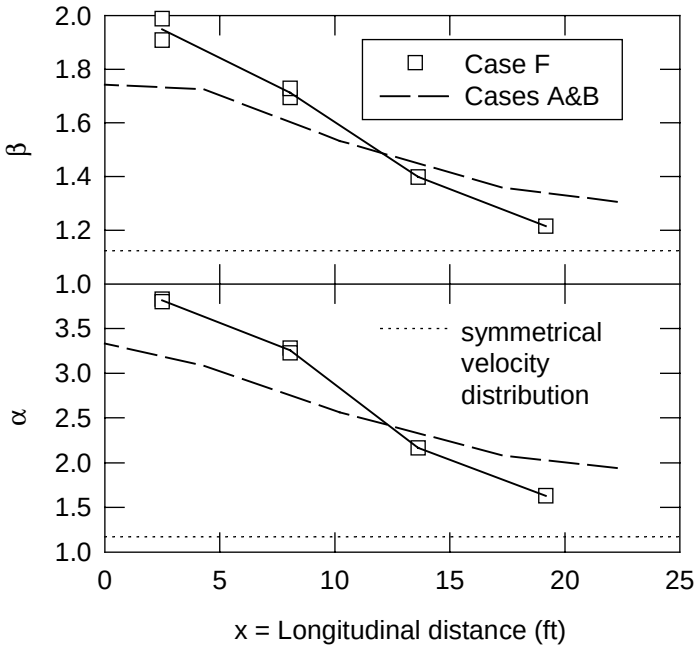

Fig. 6.10 - Variation of α and β (Case F)

Visual observation of the flow indicated that the flow immediately downstream of the obstruction blocking part of the channel to create the separation zone was not similar to the flow conditions at the downstream end of the weir. Thus, it was decided to start the measurements 15 ft downstream of the headbox. As the initial increases in β and α (Fig. 6.11) indicate, the asymmetry did not start to decrease until almost 20 ft downstream of the headbox.

6.4.10 - Case H

Case H had Q = 4.6 cfs with no separation zone in the channel with 4H:1V side slopes. With the side weir blocked with a thin metal sheet and with no flow modification at the headbox (other than the packed bed and flow straighteners to remove the large scale eddies generated in the headbox), velocity measurements were made at the cross section 62.5 ft from the downstream end of the flow straighteners to determine β and α values for established flow. These velocity distributions were essentially symmetrical about the channel centerline.

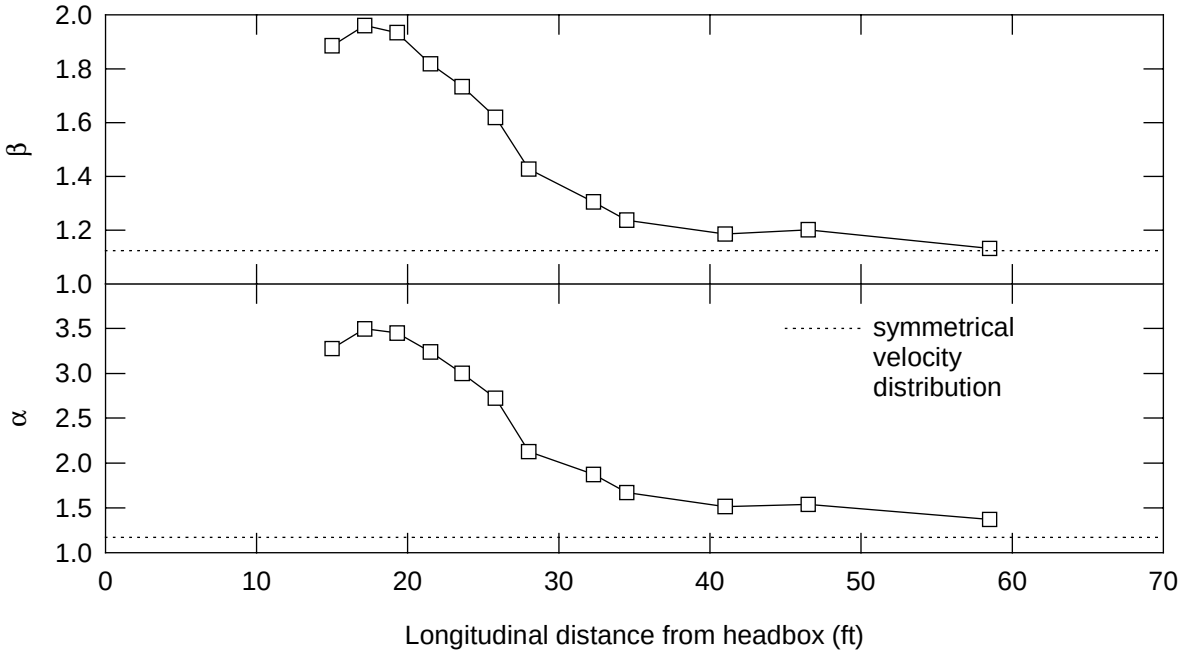

Fig. 6.11 - Variation of α and β (Case G)

6.5 - β AND α VALUES AT DOWNSTREAM END OF WEIR

The parameters β and α at the downstream end of the weir are important since at least one of them is needed to relate the head at the downstream end of the weir to the water level downstream of the flow re-establishment region. The importance of having reasonable values for β or α increases as the flow velocity increases. Eq. (6.3) shows that there is a linear relationship between $\beta U^2/g$ and water surface elevation (or flow depth). If U is 6 ft/s at the downstream end of the weir for prototype conditions, then assuming that β = 1 when the actual value is 1.75 will produce an error of 0.84 ft in the head on the weir while the error is only 0.05 ft when U = 1.5 ft/s. Eq. (6.10) shows a linear relationship between $\alpha U^2/2g$ and h for a given H so assuming α = 1 when the actual α = 3 for U = 6 ft/s gives an error of 1.12 ft in h while the error is only 0.07 ft when U = 1.5 ft/s.

In Fig. 6.12, measured β and α values at the end of the weir (Appendix 5.3) are plotted as functions of Q_w/Q_u for 2.5H:1V side slopes As mentioned earlier, the primary dependence of both β or α is on Q_w/Q_u, or equivalently Q_u/Q_d since $Q_u/Q_d = 1/(1 - Q_w/Q_u)$. The secondary variation (scatter about the curve) comes from the fact that both β and α decrease slightly as Q_u increases. Several attempts were made to find a suitable dimensionless parameter to represent this variation, but none could be found. The best relationships that could be found for 2.5H:1V side slopes using dimensionless parameters are

$$\beta = \begin{cases} 1.08 & \text{for } 1 \le \dfrac{Q_u}{Q_d} \le 1.25 \\ 0.991 - 0.301\dfrac{Q_u}{Q_d} + 0.298\left(\dfrac{Q_u}{Q_d}\right)^2 & \text{for } 1.25 < \dfrac{Q_u}{Q_d} < 2.2 \end{cases} \tag{6.15}$$

$$\alpha = \begin{cases} 1.23 & \text{for } 1 \le \dfrac{Q_u}{Q_d} \le 1.25 \\ 1.66 - 1.70\dfrac{Q_u}{Q_d} + 1.08\left(\dfrac{Q_u}{Q_d}\right)^2 & \text{for } 1.25 < \dfrac{Q_u}{Q_d} < 2.2 \end{cases} \tag{6.16}$$

where $Q_u/Q_d = 1/(1 - Q_w/Q_u)$. To obtain these relationships, polynomials were first fitted to the data points for flows with diversions. Then the intersections of the polynomials with the β and α values for undisturbed flow ($\beta = 1.08$ and $\alpha = 1.23$) were found. The values for undisturbed flow were assumed to apply below the intersections, both of which occurred at $Q_u/Q_d = 1.25$ or $Q_w/Q_u = 0.2$.

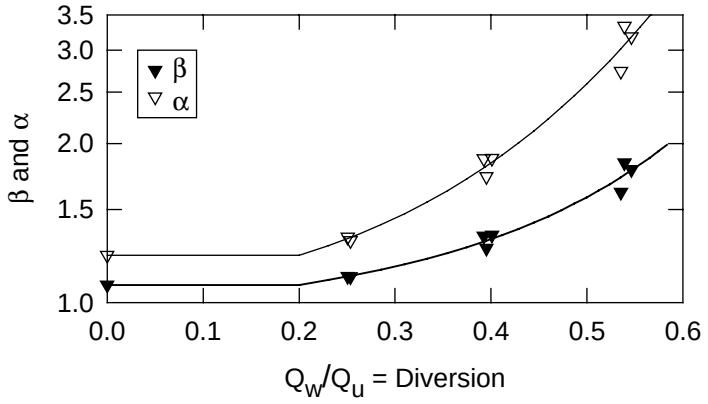

Fig. 6.12 - β and α values at end of weir for 2.5H:1V side slopes

The results for 4H:1V side slopes are given in Appendix 5.4. Curve fitting to the data points gave

$$\beta = \begin{cases} 1.12 & \text{for } 1 \le \dfrac{Q_u}{Q_d} \le 1.20 \\ -0.073 + 0.987\dfrac{Q_u}{Q_d} & \text{for } 1.20 < \dfrac{Q_u}{Q_d} < 2.2 \end{cases} \tag{6.17}$$

$$\alpha = \begin{cases} 1.17 & \text{for } 1 \le \dfrac{Q_u}{Q_d} \le 1.18 \\ -2.28 + 2.93\dfrac{Q_u}{Q_d} & \text{for } 1.18 < \dfrac{Q_u}{Q_d} < 2.2 \end{cases} \tag{6.18}$$

as the best fit equations.

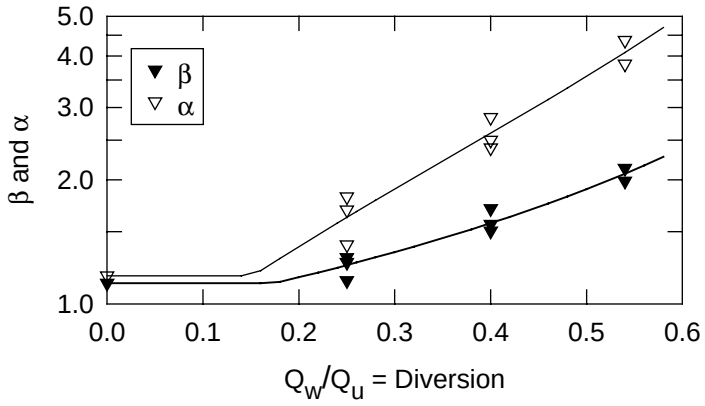

Fig. 6.13 - β and α values at end of weir for 4H:1V side slopes

In the absence of a detailed investigation, Tynes (1989) assumed that the velocity was zero in the separation zone and uniform in the effective flow area. The ratio of the effective flow area to the cross-sectional area was taken to be Q_d/Q_u. Accordingly, immediately downstream of the side weir,

$$\alpha = \left(\frac{Q_u}{Q_d}\right)^2 \quad \text{and} \quad \beta = \frac{Q_u}{Q_d} \tag{6.19}$$

The assumption by Tynes (1989) about the velocity distribution in the separation zone leads to overestimation of β and α. For example, depending on the flow rates, for 54% diversion, α is overestimated by 40% to 70% and β is overestimated by 20% to 30%.

6.6 - COMPONENTS OF β AND α

6.6.1 - Variation with Flow Distance

Appendix 5.1, Appendix 5.2, Fig. 6.15, Fig. 6.16, Fig. 6.17, Fig. 6.18 and Fig. 6.19 give the components of β and α (Eq. (6.4) and Eq. (6.13)) for the tests for which velocities were measured at different longitudinal distances in the channel. The components were evaluated to determine the relative significance of the various terms in the momentum and kinetic energy transport. The downstream end of the weir is x = 0 for Cases A, B, C, and F while zero distance is at the downstream end of the flow straighteners for Cases D, E, and G. The results for some of

the components of β and α were inaccurate for Case F, so there are some missing values in Appendix 5.2 and Fig. 6.18.

The longitudinal distances were normalized with respect to a transverse length scale (B_s) associated with the asymmetrical velocities at the end of the weir. To calculate B_s, it was assumed that all of the flow at the downstream end of the weir is in an effective area (A_e, Fig. 6.14) and that the velocity is zero in the remainder of the channel that has a width of B_s. The velocity (u_e) in the effective area was calculated so that $A_e u_e = Q$. Since Q also is equal to AU, $u_e/U = A/A_e$. Then, from Eq. (6.4) neglecting the turbulent transport of momentum,

$$\beta = \frac{1}{A}\frac{\int_A \bar{u}^2 dA}{U^2} = \frac{1}{A}\frac{\int_{A_e} u_e^2 dA}{U^2} = \frac{1}{A}\frac{\left(\frac{Q}{A_e}\right)^2 A}{\left(\frac{Q}{A}\right)^2} = \frac{A}{A_e} \qquad (6.20)$$

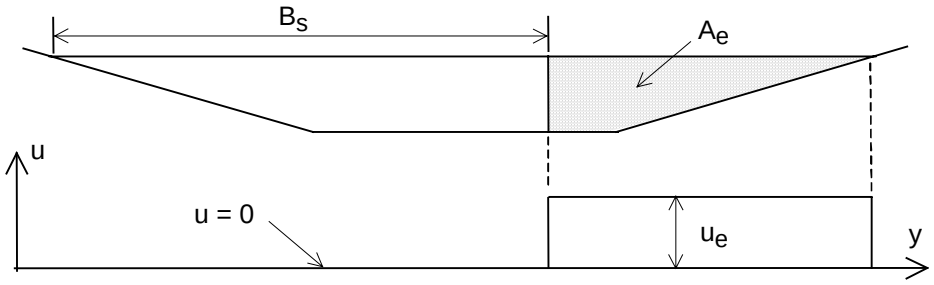

Fig. 6.14 - Assumed velocity distribution for calculating B_s

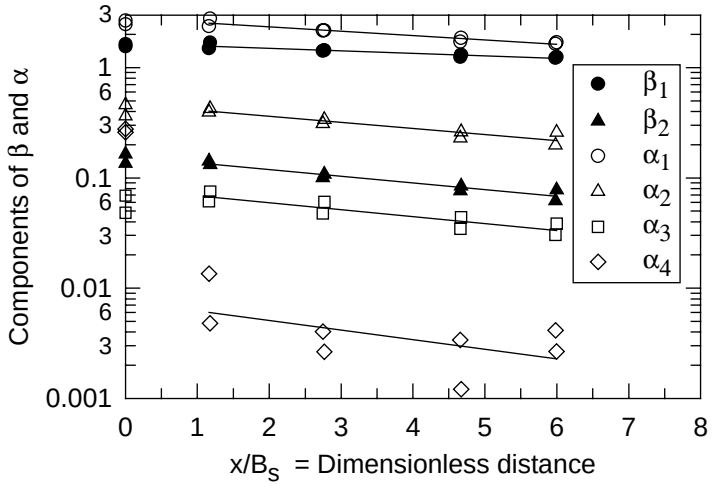

Fig. 6.15 - Components of β and α for 54% diversion (Cases A and B)

B_s was then calculated as the value needed to give A_e so that β in Eq. (6.20) is equal to the empirical β value at the downstream end of the weir. The results are shown in Appendix 5.1 and Appendix 5.2. Since Case D with the forced separation zone at the upstream end of the channel was supposed to represent the same flow conditions as Case A, B_s was also taken to be the same for Case D as for Case A. For the same reason, B_s for Case G is the same as for Case F. There were no B_s values for Cases E and H. The locations of the measurement cross sections for Cases A - C were essentially the same; the larger dimensionless distances for Case C are the result of the smaller B_s value, not larger x values.

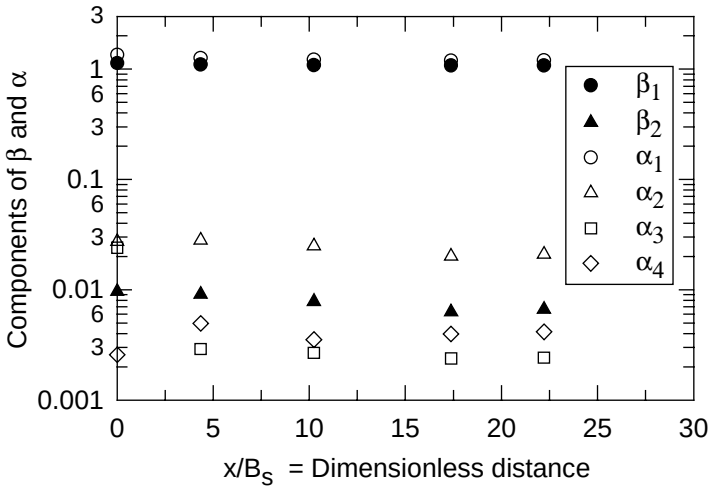

Fig. 6.16 - Components of β and α for 25% diversion (Case C)

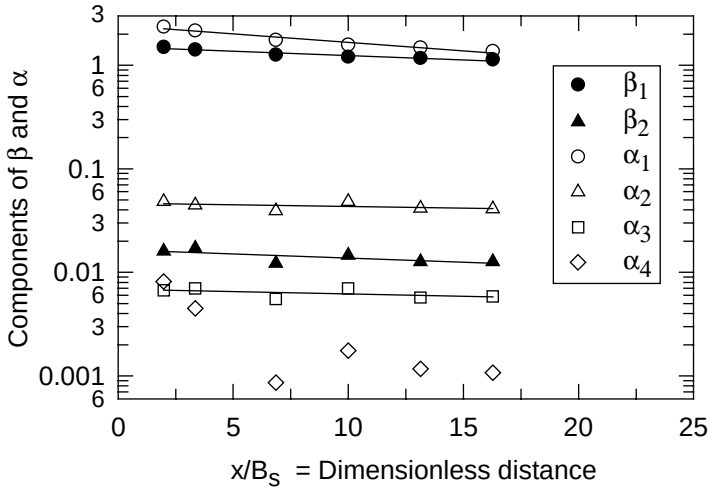

Fig. 6.17 - Components of β and α for forced separation zone (Case D)

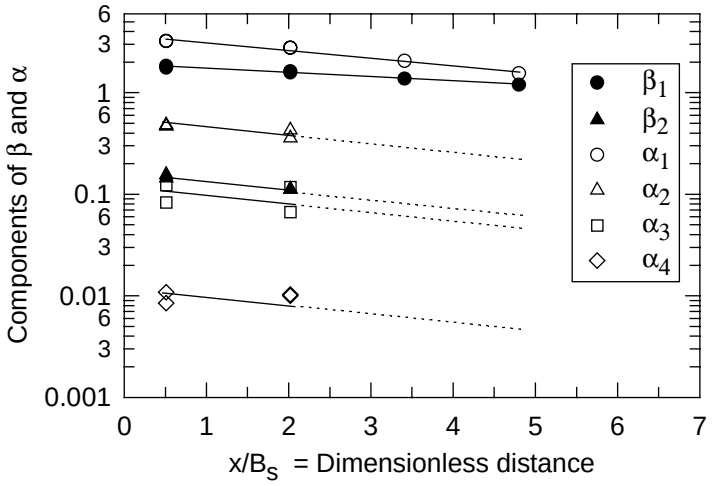

Fig. 6.18 - Components of β and α for forced separation zone (Case F)

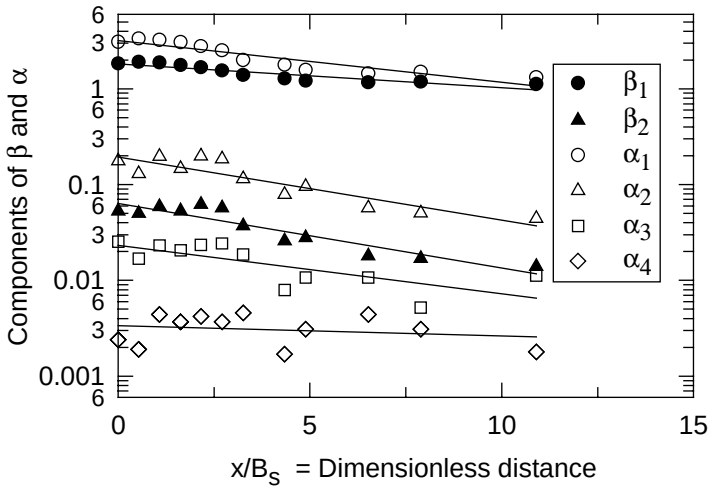

Fig. 6.19 - Components of β and α for forced separation zone (Case G)

Several trends are apparent from the measurements:

(1) Most of the measurements at the end of the weir for the 2.5H:1V side slopes (Fig. 6.15 and Fig. 6.16) do not fit the trends downstream from the weir. Thus, the trend lines are not extended to x = 0. The apparent reason is the relatively strong transverse time-averaged velocity component toward the weir at this cross section. One of the clearest indications of this behavior is that α_4, which includes the time-averaged transverse velocity ($\overline{v}^2$), is almost two orders of magnitude larger at the end of the weir for Cases A and B than would be indicated by extrapolating the trend of the other points back to the weir. At the end of the weir, most of the other components are a little smaller than would be indicated by extrapolation from the downstream points. The same type of problem does not exist for Case F since the first measurement cross section was at x = 2.5 ft, not x = 0.

(2) Downstream from the weir, β and α and each of their components decrease with increasing longitudinal distance as the flow asymmetry decreases.

(3) For Case C with the smaller diversion, the relative magnitudes of the turbulence terms are smaller than for Cases A, B, and F. There are no trend lines for Case C (Fig. 6.16) since the components for the first cross section were affected by the transverse velocities and since asymptotic conditions were reached upstream of the last two cross sections.

(4) The relative magnitudes of the turbulence terms are smaller for Case D with the forced separation zone for the channel with 2.5H:1V side slopes than for Cases A and B even though the time-averaged normalized longitudinal velocity distributions were nearly the same for all three cases. This comparison indicates that the manner in which the separation zone was created for Case D was not a good reproduction of the effects of the weir, as mentioned earlier. The same problem does not exist for Case G where the area was blocked downstream of the flow straighteners to create the separation zone.

(5) For Case E, the values of β and α were found to be 1.08 and 1.23. These values agree with the downstream values for Case C, so they were adopted as the values for undisturbed flow in the channel with 2.5H:1V side slopes. The corresponding values for the 4H:1V side slopes were $\beta = 1.12$ and $\alpha = 1.17$.

6.6.2 - Variation with Diversion

Appendix 5.3, Appendix 5.4, Fig. 6.20, and Fig. 6.21 give the components of β and α at the downstream end of the weir. All components for both β and α increase as the diversion increases, but β_2 and α_2 through α_4 increase at approximately the same rate and more rapidly than β_1 and α_1. Similar rates of increase might be expected for β_2, α_2, and α_3 since all of these terms have the mean of a squared turbulent velocity, but α_4 has about the same rate of increase with diversion even though it includes only time-averaged velocities and is the smallest of the terms. The relative importance of the turbulent transport increases as the diversion increases; β_2 varies from 1% to 10% of β while α_2 supplies 2% to 15% of α, α_3 supplies 0.2% to 2.4%, and α_4 supplies only 0.1% to 1.5%. All of the other terms that come from a complete expansion of $<\overline{V^2}u>$ (Eq. (6.12)) are less that 1% of α, even at the highest diversion rates.

6.7 - LENGTH FOR FLOW RE-ESTABLISHMENT

Downstream of a side weir, the velocity distribution gradually returns toward symmetry. At the beginning of the measurements and analysis, it was not clear how to best quantify the asymmetry of the velocity distributions. Thus, three parameters (in addition to β and α) were used and were calculated separately for the top, middle and bottom sets of measurements at each cross section. These parameters represented (a) the root-mean squared variation of differences

between the velocities on the right side of the channel and the velocities at the corresponding points on the left side, (b) the skewness of the velocity distributions, and (c) the area under the velocity distribution curve in the right half of the channel and that in the left half. None of these parameters proved to be significantly more informative than β and α, so β and α were used as the primary parameters to represent the amount of asymmetry in the velocity distributions.

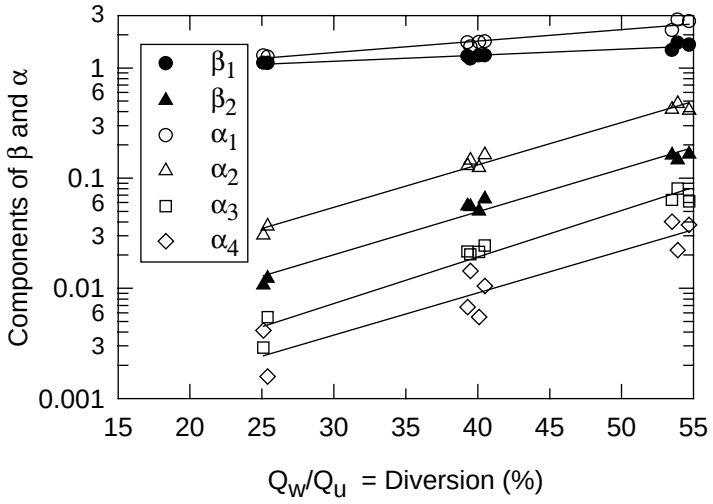

Fig. 6.20 - Variation of components of β and α near end of weir with diversion for 2.5H:1V side slopes

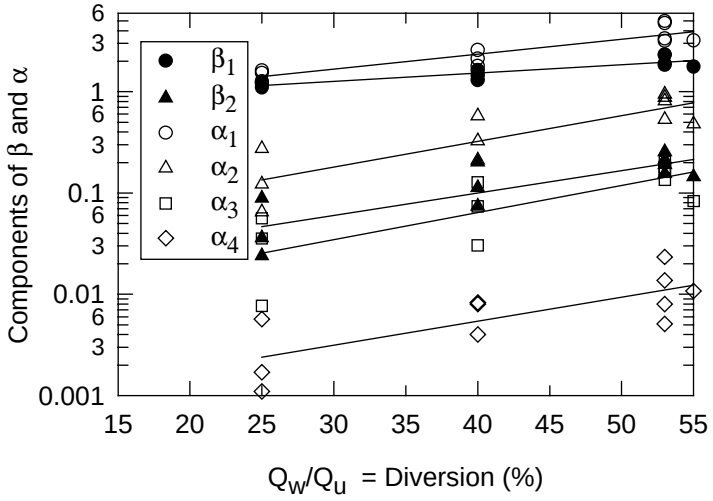

Fig. 6.21 - Variation of components of β and α near end of weir with diversion for 4H:1V side slopes

The variations of $\beta - \beta_o$, where β_o is the value for symmetrical velocity distributions, with distance were used to determine the flow length (L_s) required for the flow to return to symmetry.

For 2.5H:1V side slopes, β_o =1.08 while the value is 1.12 for 4H:1V side slopes. The variations of $\alpha - \alpha_o$ were also studied, but they gave slightly different results. It was decided to use β since it is used in the computer program rather than α. The variations of $\beta - \beta_o$ with distance for 2.5H:1V side slopes are given in Fig. 6.22 on a semi-logarithmic plot since decay processes frequently have an exponential decay as they approach their asymptotic values. For this figure, the results for Case D were treated as if the section at 12.5 ft from the flow straighteners were 4.3 ft downstream from the end of the weir crest. This matching is based on the fact that the measured velocities for these two cross sections were essentially the same.

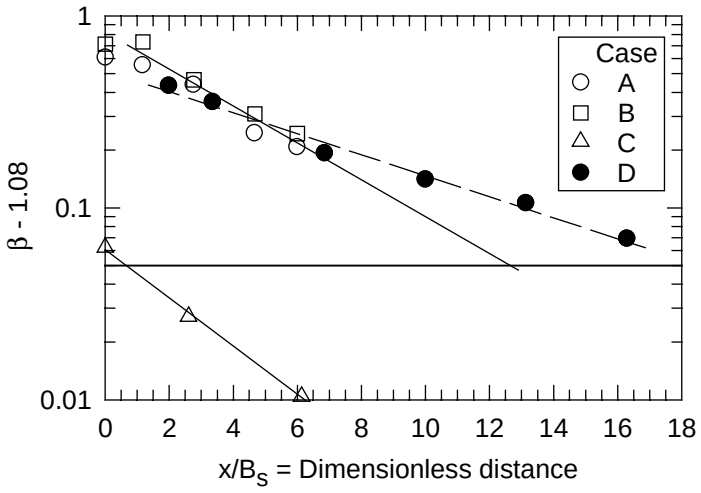

Fig. 6.22 - Exponential decay of excess β for 2.5H:1V side slopes

One of the prime objectives for Case D was to get a direct indication of the length required for the flow asymmetry to disappear. Since the turbulence for Case D was less intense than for Case A (Section 6.4.8), the asymmetry disappeared more slowly for Case D than for Case A. Nevertheless, Case D has data over a larger distance and indicates that there is indeed an exponential decay of $\beta - \beta_o$. Based on this type of behavior, the best fit line through the points for Cases A and B (except for x = 0, for reasons discussed earlier) is extrapolated to a value of 0.05 to represent the point at which β decays to within 5% of its asymptotic value. This process gives L_s/B_s = 12.5 for 54% diversion. For Case C, the last two points are not plotted since β had reached its asymptotic value upstream of these points. The best-fit line through the remaining points gives L_s/B_s = 0.6 for 25 % diversion. However, it must be recognized that these values of L_s come from extrapolation of the measurements, that different values of L_s would be obtained if different parameters other than β were used, and that the results for L_s are very limited. Thus, these values must be viewed as only an indication of the length of the flow re-establishment dis-

tance. Fortunately, as is illustrated in Section 6.9, it is normally not necessary to know L_s with high accuracy.

Similar results for 4H:1V side slopes are given in Fig. 6.23. For these measurements, the blocked area to create a separation zone was downstream of the flow straighteners. It can be seen that the trends for Cases F (with actual diversion) and G (with a forced separation zone) are essentially the same. For these measurements $L_s/B_s = 7.3$.

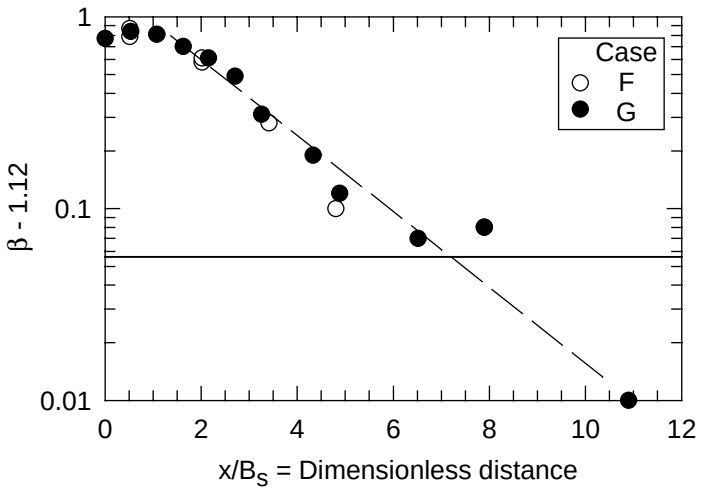

Fig. 6.23 - Exponential decay of excess β for 4H:1V side slopes

Assuming that L_s/B_s would be zero for no diversion and would remain small for diversions less than 30% since there is essentially no separation zone for those conditions, an estimated variation of L_s/B_s is given in Fig. 6.24. This figure, as well as a comparison of Fig. 6.22 and Fig. 6.23, shows that the flow conditions for 4H:1V side slopes return to symmetry more rapidly than for 2.5H:1V side slopes. These figures give the results in terms of dimensionless distances (x/B_s and L_s/B_s), but the same conclusion applies for actual distances (x and L_s). Because of the very limited data, Fig. 6.24 needs to be used with caution.

6.8 - MOMENTUM AND ENERGY BALANCES

The measurements allowed all terms in Eq. (6.3) except F_τ to be calculated, and F_τ could be found from Eq. (6.7) and Eq. (6.8). Thus, to investigate the accuracy of the measurements, the momentum equation (Eq. (6.3)) was written as

$$\frac{A_1}{A_2}\frac{\left(\beta U^2\right)_1}{g} + h_1 - \frac{F_\tau}{\gamma A_2} - \Delta h_M = \frac{\left(\beta U^2\right)_2}{g} + h_2 \qquad (6.21)$$

where Δh_M is a residual term to account for any inaccuracies in the measurements in balancing the momentum equation. The term Δh_M was evaluated from the measurements with cross sections 1 and 2 in Eq. (6.21) being successive measurement cross sections. The measurements also allowed determination of a residual term (Δh_E) for the energy equation written as

$$H_1 - h_f - \Delta h_E = H_2 \tag{6.22}$$

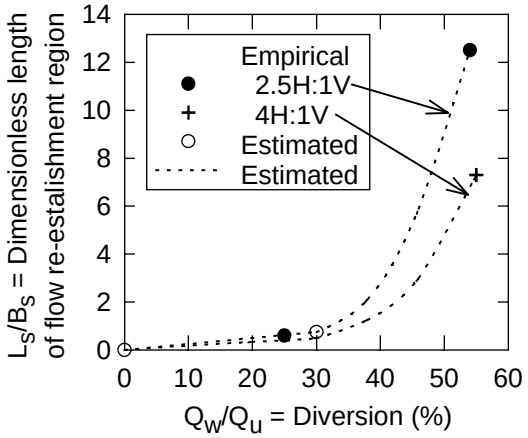

Fig. 6.24 - Length of flow re-establishment region

From the measurements, Δh_M (Eq. (6.21)) and Δh_E (Eq. (6.22)) were calculated for each pair of consecutive cross sections (Appendix 6.1 to Appendix 6.10). The rate at which momentum was transported across a section was calculated as $\rho\beta Q_d^2/A$, where Q_d is the measured flow rate, for all cross sections except x = 0. $\int_A \bar{u}dA$ was used in lieu of Q_d for the cross section at the downstream end of the weir crest because of the outflow over the downstream ramp. The velocity head was calculated as $\alpha Q_d^2/(2gA^2)$. In each case, Q_d during the water surface elevation measurements was used for the cross sections downstream from the side weir.

In the calculation of $\int_A \bar{u}dA$, a parabolic distribution was assumed for $\bar{u}$ below the bottom measurement point. Between the water surface and the top measurement point, $\bar{u}$ was assumed to be the same as that of the top measurement; $\bar{u}$ was assumed to vary linearly between the top and middle measurement points and between the middle and bottom measurement points. The vertical integration was done first using the assumed distribution of $\bar{u}$ and then laterally with $\bar{u}$ = 0 at the sides of the channel. For the cross section at the downstream end of the weir crest for Case A, the difference between $\int_A \bar{u}dA$ and Q_d was 8%. For all the other measurements, the differences were less than 6%. The discrepancies were considered acceptable given that velocities were measured only at 15 points in a cross section. There was lateral flow over the ramp at the downstream end of the side weir. The higher discrepancy for the cross section at the downstream end of the weir crest for Case A was probably due to the larger flow over the ramp.

As mentioned in Section 3.4, the distances from boundary reported by the data acquisition program were inaccurate for measurements above the side slopes. It was estimated that the errors in the calculation of $\int_A \bar{u} dA$, β and α due to the inaccuracy in the distance measurements were less than 1%.

The water surface elevations were measured at the same cross sections and the same seven transverse locations where velocities were measured. In the momentum and energy balances, the water surface elevation for each cross section was taken as the average of the measurements for that cross section. For the cross sections other than that at the downstream end of the weir crest, the differences between water surface elevations for the same cross section were at most 0.003 ft. For the section at the downstream end of the weir crest, there were larger differences because of the drawdown due to the flow over the weir crest. Therefore, for that section, the measurements at y = 1.1 ft, 2.2 ft, and 3.3 ft (i.e., the measurements on the weir side of the channel) were not included in the average for Case A, and the measurements at y = 3.3 ft were not included in the averages for Cases B and C; the drawdown at the weir was much smaller for Cases B and C than for Case A.

The largest values of Δh_M and Δh_E were between the cross section at the end of the weir and the next cross section since there was still a significant transverse velocity at the end of the weir. Excluding the values at the end of the weir, the residuals in balancing the equations are smaller. The residuals in Table 6.3 are rather small given that the measurement accuracy for water surface elevations was on the order of 0.001 ft to 0.002 ft and only 15 velocities were measured in each cross section. It was essential to include the turbulent fluxes of momentum and energy to obtain this good degree of closure for the momentum and energy equations. An indication of the magnitude of the turbulence flux terms is given in Section 6.4.8. The momentum and energy balances were not done for Case G; the excellent results for the other cases indicated that accurate measurement techniques were being used.

Table 6.3 - Summary of errors in balancing momentum and energy equations

	Δh_M (ft)		Δh_E (ft)	
	All cross sections	Exclude end of weir	All cross sections	Exclude end of weir
maximum	0.0009	0.0009	0.0023	0.0023
average	-0.0010	-0.0004	-0.0003	0.0001
minimum	-0.0077	-0.0016	-0.0045	-0.0015
standard deviation	0.0019	0.0006	0.0014	0.0009

The discussion above on the momentum and energy balances relates to the flow re-establishment region downstream of the weir. El-Khashab and Smith (1976) made detailed velocity and depth measurements in a rectangular channel in the region beside a side weir. The velocity and flow depth upstream of the weir were 3.9 ft/s and 0.85 ft. The diversion was 70%. (These values are only approximate since they had to be read from a graph or calculated from values read from a graph. Also, the 70% diversion is based on an estimated α of 3 at the downstream end of the weir.) They found a large imbalance in trying to close the energy equation for the section of the channel along the weir. The imbalance was approximately 0.8 in. between the upstream and downstream ends of the weir; this 0.8 in. was 16% of $\alpha U^2/2g$ at the upstream end of the weir and 1.7 times $\alpha U^2/2g$ at the downstream end of the weir. El-Khashab and Smith (1976) included the lateral and vertical velocities in their kinetic energy terms but not the turbulent transport of kinetic energy. If the estimated diversion is approximately correct, then there was little or no separation zone for this flow condition in their rectangular channel. For their channel, it is difficult to imagine that this 0.8 in. is head loss due only to flow asymmetry. Omitting the turbulence terms apparently accounted for at least part of the excess head loss.

6.9 - APPLICATION

To illustrate the importance of flow asymmetry and β, consider an improved trapezoidal channel with a bed slope of 0.0008, a base width of 85 ft, side slopes of 2.5H:1V, a Manning's n of 0.035, Q_u = 25,000 cfs, and a 50% diversion so that Q_d = 12,500 cfs. The flow depth (d_2) at the downstream end of the flow re-establishment region is the normal depth of 16.1 ft. From Eq. (6.15), β_1 = 1.58 at the downstream end of the weir. Eq. (6.2) or Eq. (6.3) with β_2 = 1.08 gives the depth (d_1) at the downstream end of the weir as 15.4 ft. The calculation of d_1 must be done by iteration or by using a solver since B_s (64.6 ft) depends on d_1 and β as described previously. From Fig. 6.24, $L_s/B_s \approx 9$ giving $L_s \approx 580$ ft. For this situation, the flow asymmetry at the end of the weir causes the flow depth and therefore the head on the downstream end of the weir to be 0.7 ft smaller than would be indicated by the downstream flow depth. Increasing or decreasing L_s by 50% gives essentially no change in d_1. Even though the change in L_s gives a significant change in F_τ, the change in L_s also gives a compensating change in the water surface elevations at the two cross sections (h in Eq. (6.3)). Thus, it is not necessary to know L_s with a high degree of accuracy. If the downstream controls give d_2 = 12.1 ft (half way between the critical and normal depths), then d_1 = 11.4 ft so that the depth at the downstream end of the weir is still 0.7 ft smaller than farther downstream.

The previous examples assume that Q_w is known. However, another level of iteration is required in most calculations since Q_w cannot be determined until the head on the weir is known. For river channels, the flow (Q_u) approaching a side weir is determined by the hydrology of the

watershed upstream of the weir but the flow depths are controlled from downstream for subcritical flows. Thus, iterative calculations are required to determine the flow depth (d_1) at downstream end of a weir and therefore to determine the flow (Q_w) over a weir since Q_w depends on the head which depends on the downstream depth which depends on the downstream flow (Q_d) which is equal to Q_u - Q_w. A typical computational approach would be to assume Q_w then use one-dimensional gradually varied flow calculations to obtain the water surface elevation at the downstream end of the flow re-establishment zone for $Q_d = Q_u - Q_w$ and thereby to obtain the right-hand side of Eq. (6.3) using β for established flow. From this depth, the head on the weir and then Q_w can be calculated. This process can be continued until the assumed and calculated values of Q_w agree. This is the type of calculation that is done in SIDEHYD (Burgin and Holley, 2002).

If the energy equation is used rather than the momentum equation, the approach is basically the same except that α, Eq. (6.9) and Eq. (6.10) are used rather than β and Eq. (6.3). It is important to recognize that the only head loss which is needed in Eq. (6.9) applied to the flow re-establishment region is the head loss due to the boundary shear stress, provided that appropriate α values are used. There is no additional head loss needed downstream of the weir to account for the flow asymmetry or even the separation zones, for those flows with separation zones. This condition is indicated by the excellent closure of the energy equation for the laboratory measurements when using only Eq. (6.9) with no additional head loss terms. If $\alpha = 1$ were assumed throughout the flow re-establishment region, then the energy equation might be written as

$$\left(h+\frac{U^2}{2g}\right)_1 - h_f - K_L\frac{U_2^2}{2g} = \left(h+\frac{U^2}{2g}\right)_2 \tag{6.23}$$

where K_L would appear to be a head loss coefficient. However, the laboratory measurements indicate that K_L would need to be negative to balance the energy equation so K_L could not actually be a head loss coefficient. Rather, it would be due to the fact that $U_1^2/2g$ is too small to account for the true velocity head, which is $\alpha U_1^2/2g$. These observations are consistent with those of Idelchik (1986) for other types of branching flows.

Some of the results presented here are dependent on the channel geometry. El-Khashab and Smith (1976) did experiments in a rectangular channel 1.51 ft wide with heights of 0.33 ft to 0.82 ft for thin plate weirs. They found that separation zones formed only for diversions of 70% or greater. The experimental work for this project was done in a trapezoidal channel with 2.5H:1V side slopes, and separation zones formed for diversions of about 30% and greater. Flow visualization was done in a trapezoidal channel with 4H:1V side slopes. For this channel, separation zones formed for diversions of 20% and greater. This type of trend seems reasonable since

flatter side slopes give larger regions of low velocity on the side opposite to the weir, thereby making it easier for a separation zone to form.

7 - DIVERSION CULVERTS

7.1 - INTRODUCTION

For some small diversions, it may be beneficial to use culverts for diversion rather than side weirs. Just as the discharge coefficients for side weirs depend on the channel flow characteristics as well as the normal weir parameters, it is to be expected that the flow through diversion culverts will also depend on the channel flow. Therefore the analysis of diversion for culverts needs to be modified to account for the effects of the channel flow.

The objective of these experiments was to evaluate the effects of channel flow on the hydraulics of culverts at diversion facilities.

7.2 - THE PHYSICAL MODEL

The diversion culvert model (Fig. 7.1) was built in the channel with 4H:1V side slopes. Part of the side weir was blocked leaving an opening 1.271 ft long for the culverts. The culvert model was made of 3/4 in. plywood with a base sitting on the weir crest of the side weir and with vertical walls at the upstream and downstream ends of the culverts. The vertical walls had a trapezoidal shape matching the 4H:1V side slopes of the embankment of the channel. Two vertical walls, 0.563 in. long, divided the culvert into three barrels 0.38 ft wide. The culvert model did not have a top so that the flow in the culvert could be observed more clearly. The invert of the culvert was about 0.55 ft from the invert of the channel. Manning's n for the plywood culvert model was assumed to be 0.0012 (Henderson, 1966). Some tests were done with flow in all three barrels. Tests were also done with only two barrels. For these tests, a false wall was installed parallel to the end wall and in line with one of the walls separating the barrels. An inclined cover in line with the sloped side of the channel was then placed over the opening between the two vertical walls so that the geometry for the two operating barrels was similar to that for the three barrels.

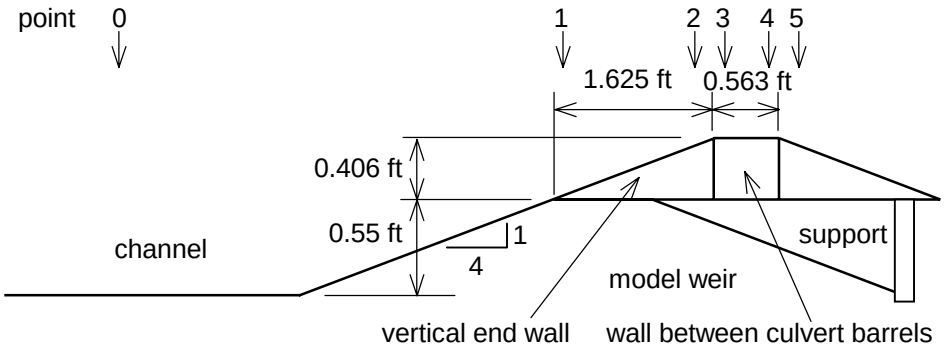

Fig. 7.1 - Schematic diagram of diversion culverts in model (not to scale)

Photographs of the model are shown in Fig. 7.2. For all flow conditions, large eddies developed upstream of the first and last barrel. Both eddies were caused by flow over the end walls; there was flow in the upstream direction, back into the culverts, over the downstream wall. The flow plunged over the walls, causing the eddies. The eddy on the most upstream barrel was frequently more pronounced than the one at the most downstream barrel since gravity added to the channel velocity as the flow plunged over the upstream wall while the gravity-induced flow and the channel flow were in opposite directions at the downstream wall.

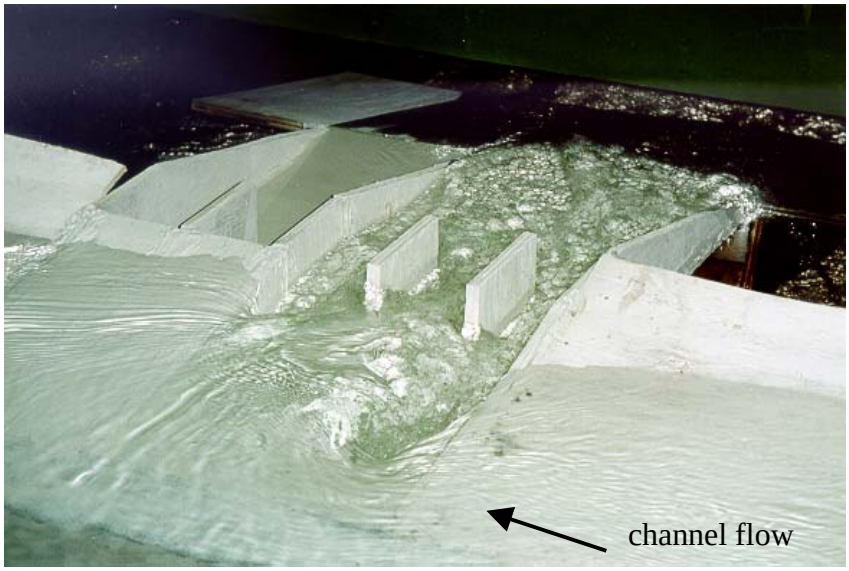

a) Higher channel velocity

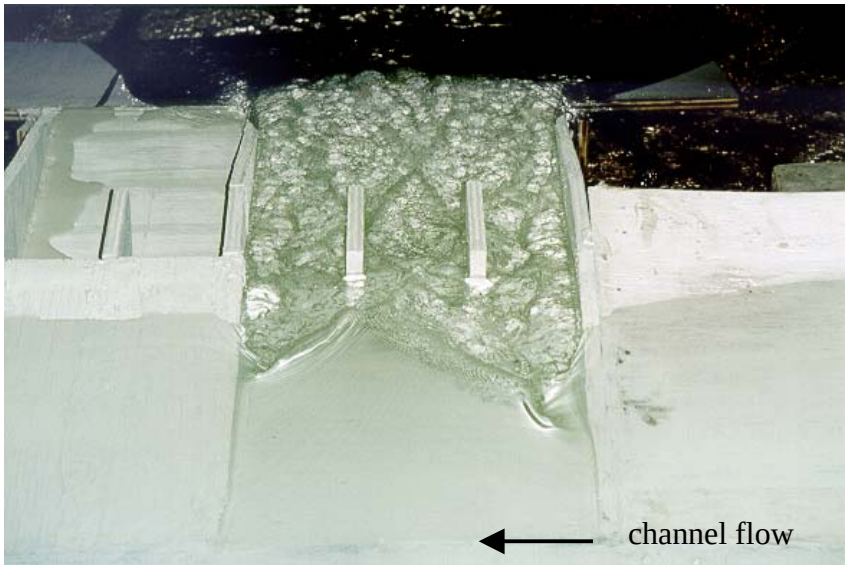

b) Lower channel velocity

Fig. 7.2 - Diversion culverts

7.3 - MODEL RESULTS

Experiments were conducted for four different upstream discharges. For each of four upstream discharge, different diversions were investigated. The total number of tests was 38. The results are given in Appendix 7. For most of the tests, there was free or unsubmerged flow at the downstream end of the culverts (cross section 4 in Fig. 7.1). A few tests were done with submerged conditions.

7.3.1 - Unsubmerged flow

Discharges and water levels were measured as described in Sections 3.3 and 3.5. In most cases, the water surface elevations upstream and downstream of the culvert were the same; the largest difference was only 0.002 ft.

Flow through the culvert was very complex. The simplified analysis of the flow was done as follows. Although there were multiple barrels, an average flow depth both upstream and downstream of the culvert barrels was used. Critical flow was assumed to exist at the downstream end of the barrels for unsubmerged flow conditions. Gradually varied flow calculations were performed from the downstream end of the barrels to the upstream end of the barrels. The entrance loss at the upstream end of the barrels, h_{entr}, was calculated as

$$h_{entr} = 0.3 \frac{\left(V_3^2 - V_2^2\right)}{2g} \tag{7.1}$$

where V_3 is the average velocity downstream of the entrance to the barrels and V_2 is the average velocity upstream of the entrance; Fig. 7.1 shows the numbering of the various cross sections in the flow. Hence

$$\eta_2 + \frac{V_2^2}{2g} - h_{entr} = \eta_3 + \frac{V_3^2}{2g} \tag{7.2}$$

where η_2 and η_3 are the average flow depths immediately downstream and upstream of the entrance. The total head immediately upstream of the barrels was related to the total head in the channel by

$$WS_o + \frac{V_o^2}{2g} - K_E \frac{V_2^2}{2g} = \eta_2 + z_2 + \frac{V_2^2}{2g} \tag{7.3}$$

where z_2 = invert elevation immediately upstream of the entrance of the barrels, WS_o = water surface elevation in the channel measured at the centerline, V_o = average velocity in the channel, and K_E = head loss coefficient for flow from the channel to cross section 2 just before the entrance into the barrels.

The velocity head in the channel was calculated using

- the average velocity in the channel upstream of the culvert
- the average velocity in the channel downstream of the culvert
- the mean of the average velocities in the channel upstream and downstream of the culvert, and
- no velocity head for the channel ($V_o = 0$ in Eq. (7.2)).

Different values of K_E were obtained using different methods. Including the velocity head in the channel gave better correlations than not including it. However the results for the three velocity heads were very similar. The downstream velocity head was preferred because the calculations proceed in the upstream direction for subcritical flows. K_E obtained using the downstream velocity for V_o was correlated with the upstream channel Froude number (F_u), downstream channel Froude number (F_d), upstream weir Froude number (Fw_u), downstream weir Froude number (Fw_d), and Q_w/NQ_u, where Q_w = discharge through the culverts, N = number of barrels, and Q_u = channel discharge upstream of the culverts. The correlations with the downstream Froude number and with Q_w/NQ_u were slightly better than the other correlations, but the channel Froude number does not include any parameters related to the flow through the culverts and the correlation with Q_w/NQ_u produced a more complicated predictive equation than the correlation with Fw_d. Thus, the correlation with the downstream weir Froude number is recommended. The results are shown by the symbols that are capital letters in Fig. 7.3. The regression equation for the data in Fig. 7.3a is

$$K_E = 0.248\frac{\eta_4}{\eta_c}10^{2.50Fw_d} \tag{7.4}$$

For unsubmerged flow, $\eta_4/\eta_c = 1$ since η_4, which is the depth at cross section 4, is equal to the critical depth (η_c) for flow in the culverts. The coefficient of determination (R^2) for Eq. (7.4) is 0.965 (versus 0.992 using the channel Froude number and 0.972 with Q_w/NQ_u in Fig. 7.3b). As stated above, the correlations with the weir Froude number is preferred since the correlation with Q_w/NQ_u, requires a more complicated equation, namely

$$K_E = \frac{\eta_4}{\eta_c}\left(1.020\left\{\frac{Q_w}{NQ_u}\right\}^{0.675}10^{0.504[\log(Q_w/NQ_u)]^2}\right) \tag{7.5}$$

7.3.2 - Submerged flow

For submerged outflow from the culverts, the loss coefficients for the flow from the channel to cross section 2 were larger than for unsubmerged flow. It was found that multiplying the

loss coefficients by η_c/η_4 caused them to follow the same general trend as for unsubmerged flow, as shown in Fig. 7.3. Thus, Eq. (7.4) can be used for both unsubmerged and submerged flows. For submerged conditions, the water level in the basin can be used to obtain η_4, which is assumed to be equal to η_5.

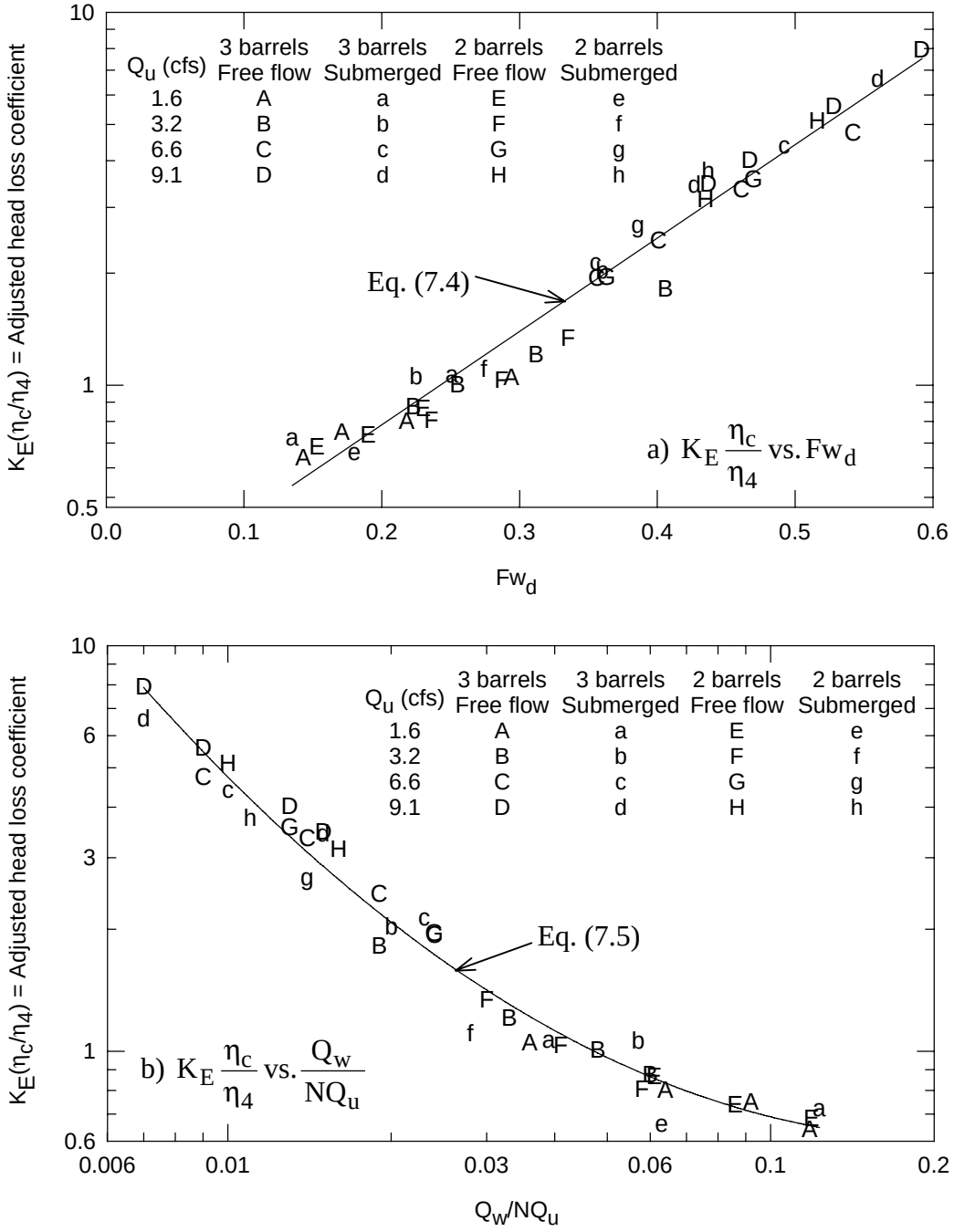

Fig. 7.3 - Adjusted loss coefficients for flow from point 0 to point 2

7.4 - CALCULATION PROCEDURE

The experimental results and the resulting correlations are valid for $0.007 < Q_w/NQ_u < 0.12$ for 2 or 3 barrels. For calculation of the flow through diversion culverts, it is assumed that the known information includes the culvert geometry, the flow conditions in the channel at the downstream end of the culverts, and the water level in the detention basin. For these conditions, the major steps in the calculation procedure for diversion culverts are as follows:

1) Assume a value of Q_w.
2) From Q_w and N, calculate the critical depth (η_c) in the culvert barrels.
3) Using Q_w/N, use gradually varied flow computations to get the water surface profile through the culvert barrel to obtain η_3, which is the depth in the barrels at the upstream end of the barrels. These calculations start with $\eta_4 = \eta_c$ if the water level in the basin is below η_c. Otherwise, η_4 comes from the water level in the basin.
4) Use Eq. (7.1) and Eq. (7.2) to calculate V_2 and η_2 just upstream of the culvert entrance.
5) Use Eq. (7.3) and Eq. (7.4) to calculate the water surface elevation (WS_o) in the channel.
6) If WS_o agrees with the know water level in the channel, then the assumed Q_w is correct. If not, assume another Q_w and repeat the previous steps until agreement is obtained.
7) Because Q_w/Q_u is small for diversion culverts, the water surface elevation in the channel at the upstream of the culverts can be assumed to be the same as at the downstream end.

When the stage in the channel first rises above the culvert invert, the headwater will be very small giving a very large Fw_d. The flow through the culverts will be very small giving a small Q_w/NQ_w. Using either Eq. (7.4) or Eq. (7.5), the calculated value of K_E can be extremely large. In the computer program for diversion culverts (Burgin and Holley, 2002), the value of K_E was taken as 10 if the calculated value was larger than 10. (See Fig. 7.3.) For these very small flows, any inaccuracy in the value of K_E does not have any practical significance.

8 - CONCLUSIONS

Side-channel weirs provide a viable means of flood control by diverting flow from channels into detention basins. The hydraulics of the weirs have been studied and improved methods have been developed for calculating the flow over side-channel weirs. Hydraulic information on flap gates and Tideflex valves for drainage culverts has been obtained and analyzed to provide relationships for calculating the culvert drainage from detention basins. The valves prevent flow from the channels into the detention basins but, to varying degrees, they also slow the drainage flow by restricting the flow area at the downstream end of the culverts.

This report addresses the experimental part of the project work. Another part of the project work is reported by Burgin and Holley (2002). That report is a user's manual for the computational scheme that has been developed for watershed hydrology, channel and side-weir hydraulics, and filling and emptying of detention basins. The computational scheme uses the results of the experimental work presented in this report.

An improved computational scheme was developed for the estimation of side weir discharge and upstream head on the weir. Of the four calculation methods tested in Chapter 4, Method B is recommended. In Method B, the side discharge per unit length of weir is calculated from a differential equation for changes in water surface elevation in the channel along the weir. This equation was derived from the momentum principle for spatially varied flow in prismatic and tapered channels with trapezoidal cross sections. The computational scheme involves the calculation of the water surface profile along the weir. The calculations explicitly account for channel roughness and slope since the results of simulations showed that the roughness and slope can have a significant effect on the side weir discharge and upstream head on the weir. The physical equations to be used for calculating the side discharge and the changes in flow depth in the channel for different situations are listed in Table 4.6 for the recommended Method B as well as for the other methods that were tested.

Regression equations were obtained for the empirical coefficients required in the computation; both previously published and new experimental results were used to develop the equations. Accuracy of the estimated values of side weir discharge and upstream head on the weir was generally good and was comparable to or better than that using the method of analysis in the previous project. The regression equations for the various empirical coefficients to be used in the calculations are also listed in Table 4.6.

The effects of channel side slope on weir hydraulics were investigated. Experiments were conducted in a channel with 4H:1V side slopes for unsubmerged conditions. The results were compared with those obtained in Chapter 4 for tests in a channel with 2.5H:1V side slopes. Using discharge coefficients (C_1) predicted by the regression equation obtained for tests in the

channel with 2.5H:1V side slopes, the agreement between measured and calculated values of the side weir discharge and upstream head on the weir for tests with 4H:1V side slopes was comparable to that for tests with 2.5H:1V side slopes. Therefore the same regression equation is applicable for side slopes of both 2.5H:1V and 4H:1V. However, the coefficient (C_2) in the relationship between the cross-sectional average velocity in the channel and the velocity of the lateral flow changes from 0.85 for 2.5H:1V side slopes to 1.10 for 4H:1V side slopes. For slopes between 2.5H:1V and 4H:1V, linear interpolation may be used to estimate values for C_2.

For channels with side weirs, flow over the weir creates an asymmetrical velocity distribution in the channel. For diversions of 30% or more of the approach flow in a trapezoidal channel with 2.5H:1V side slopes or 20% or more for 4H:1V side slopes, a separation zone is created on the side of the channel opposite to the weir. Downstream of the weir, there is a region of flow re-establishment as the asymmetry is eliminated. As a result of the asymmetry, the flow depth at the end of the weir is usually less than at the downstream end of the re-establishment region.

The flow depth at the end of the weir can be determined from the depth at the end of the flow re-establishment region using the momentum or energy equation with a momentum correction factor (β) or a kinetic energy correction factor (α) to account for the flow asymmetry. Section 6.5 gives the empirical β and α values for trapezoidal channels with 2.5H:1V and 4H:1V side slopes. Linear interpolation may be used to estimate β and α values for other side slopes between these two values.

The β and α values depend primarily on the ratio of the weir discharge (Q_w) to discharge (Q_u) upstream of the weir and increase as Q_w/Q_u increases, where $Q_u/Q_d = 1/(1 - Q_w/Q_u)$. The β and α values at the end of the weir are 1.6 and 2.6, respectively, for 50% diversion for a channel with 2.5H:1V side slopes and 1.9 and 3.6 for 50% diversion for a channel with 4H:1V side slopes. The β and α values in this report include the turbulent fluxes of momentum and kinetic energy. Including the turbulent fluxes was important in obtaining good closure of the momentum and energy balances for the measurements. The turbulent flux of momentum was as much as 10% of the total momentum flux, while the turbulent flux of kinetic energy was as much as 17% of the total. The type of results presented in this report depends on channel geometry.

The limited data obtained for the length of the flow re-establishment region were used to give an approximate relationship for this length. Fortunately, it is not necessary to know this length with high accuracy since it does not have a strong influence of the depth calculated at the downstream end of the weir.

Some experiments were done using culverts rather than weirs for diversion. The experiments were used as a basis for developing a method for calculating flow rates for diversion cul-

verts. This method is included in the computer programs (Burgin and Holley, 2002). Since the results are rather limited, this method for diversion culverts should be used with caution.

9 - REFERENCES

Ackers, P. (1957) "A Theoretical Consideration of Side Weirs as Stormwater Overflows," *Proceedings,* Institute of Civil Engineers, London, vol. 6, pp. 250, February.

Balmforth, D. J. and Sarginson, E. J. (1983) "An experimental investigation of the discharge capacity of side weirs," *Intern. Conf. on Hydraulic Aspects of Floods & Flood Control,* Paper No. F2, London, BHRA, Sept. 13-15.

Bos, M. G. (ed.) (1985), *Discharge Measurement Structures,* International Institute for Land Reclamation and Improvement, Wageningen, Netherlands, 464 pp.

Burgin, J. F. and Holley, E. R. (2002) *Side-Weir Analysis System,* Online Rept. 02-2, Center for Research in Water Resources, Univ. of Texas, Austin, TX (http://www.crwr.utexas.edu/online.shtml)

Cheong, H.-F. (1992) "Discharge coefficient of lateral diversion from trapezoidal channel," *J. Irr. and Drainage Engineering,* vol. 117, no. 4, pp. 461-475.

Chow, V. T. (1959) *Open Channel Hydraulics,* McGraw-Hill, New York, 680 p.

Collinge, V. K. (1957) 'The Discharge Capacity of Side Weirs," *Proceedings,* Institute of Civil Engineers, London, vol. 6, pp. 288-304.

Davis, J. E. and Holley, E. R. (1988) "Modeling side-weir diversions for flood control," *Hydraulic Engineering, Proc., National Conf.* ASCE, pp. 979-984.

de Marchi, G. (1934) "Essay on the performance of lateral weirs," (in Italian) *L'Energia Ellectrica,* Milan, vol. 11, no. 11, pp. 849, November.

DOT (Department of Transportation) (1973) "Hydraulics of Bridge Waterways," *Hydraulic Design Series,* No. 1, U.S. Dept. of Transportation/Federal Highway Administration.

El-Khashab, A. and Smith, K. V. H. (1976) "Experimental investigation of flow over side weirs," *J. Hydraulics Div., Proc. ASCE,* vol. 102, no. HY9, pp. 1255-1268.

Forchheimer, P. (1930) *Hydraulics,* Teubner Verlagsgevellschaft, Berlin, 3rd ed., pp. 406-409.

Frazer, W. (1957) "The behaviour of side weirs in prismatic rectangular channels," *Proc., Inst. of Civil Engineers,* Vol. 6, pp. 305-327.

Hager, W. H. (1981) *Die Hydraulik von Verteilkanälen (Hydraulics of distribution channels),* Doctoral Dissertation, parts I and II, Federal Institute of Technology (ETH), Zurich.

Hager, W. H. and P. U. Volkart (1986) "Distributions channels," *J. Hydraulic Engineering,* vol. 112, no. 10, pp. 935-952.

Hager, W. H. (1987) "Lateral outflow over side weirs," *J. Hydraulic Engineering*, vol. 113, no. 4, pp. 491-504.

Hammons, M. A. and Holley, E. R. (1995) *Hydraulics characteristics of flush depressed curb inlets and bridge deck drains.* Research Report #1409-1, Center for Transportation Research, The University of Texas at Austin, Austin, Texas, 168 pp.

Henderson, F. M. (1966) *Open Channel Flow*, Macmillan Publishing Co., Inc., New York, 522 p.

Idelchik, I. E. (1986) *Handbook of Hydraulic Resistance*, 2nd Ed., Hemisphere Publ., Washington, 640 p.

Lasdon, L. S. and Waren, A. D. (1994) *GRG2 User's Guide*. Dept. of Management and Information Sciences, Univ. of Texas, Austin, unpublished manuscript, 54 p.

Mostafa, M. G. and Chu, G. H. (1974) "Experimental and Mathematical Investigation of Flow Over Side Weirs in Open Channels," Report No. ERC-74-012-F, Engineering Research Center, Cal. State Univ., Long Beach Foundation, Report prepared for the Orange County Flood Control District. June.

Nagler, F. A. (1923) "Hydraulic tests of Calco automatic drainage gates," *The Transit*, vol. 28, no. 4, pp. 71-72, 90.

Press, Wh. H., Flannery, B. P., Teukolshy, S. A. and Vetterling, W. T. (1989) *Numerical Recipes. The Art of Scientific Computing (FORTRAN Version)*. Cambridge Univ. Press, Cambridge, 128 p.

Subramanya, K. and Awasthy, S. C. (1972) "Spatially varied flow over side-weirs," *J. Hydr. Div., Proc. ASCE*, vol. 98, no. HY1, pp. 1-10.

Tynes, K. A. (1989) *Hydraulics of Side-Channel Weirs for Regional Detention Basins*, M. S. Thesis, Dept. of Civil Engineering, University of Texas, Austin, 128 pp.

Yen, B. C. and Wenzel, H. G. (1970) "Dynamic equations for steady spatially varied flow," *J. Hydraulics Div., Proc. ASCE*, vol. 96, no. HY3, pp. 801-814.

U. S. Army Corps of Engineers (1984) *HEC-2 Water Surface Profiles Users Manual*, Hydrologic Engineering Center, U. S. Army Corps of Engineers, Davis, CA, 40 p. + appendices.

10 - APPENDICES

APPENDIX 1 - DATA FROM PREVIOUS PROJECT (TYNES, 1989)

Appendix 1.1 - Unsubmerged Flow Conditions

Test	L (ft)	B (ft)	P (ft)	Q_u (cfs)	Q_w (cfs)	h_u (ft)	h_d (ft)	C_e	Fw_d	F_d	h_c (ft)
A1A10W	23.91	3.40	0.52	3.250	0.293	0.019	0.039	0.978	0.293	0.512	-0.0156
A1A20W	23.91	3.40	0.52	3.243	0.813	0.040	0.061	0.611	0.225	0.724	-0.0149
A1A40W	23.91	3.40	0.52	3.232	1.199	0.054	0.076	0.443	0.180	0.766	-0.0150
A1A50W	23.91	3.40	0.52	3.237	1.713	0.072	0.092	0.292	0.129	0.820	-0.0125
A1B10W	23.91	3.40	0.52	6.516	0.595	0.036	0.062	1.474	0.547	0.517	-0.0313
A1B20W	23.91	3.40	0.52	6.493	1.199	0.046	0.089	1.037	0.453	0.603	-0.0389
A1B30W	23.91	3.40	0.52	6.471	1.810	0.062	0.111	0.780	0.375	0.651	-0.0409
A1B40W	23.91	3.40	0.52	6.527	2.554	0.082	0.130	0.591	0.304	0.723	-0.0386
A1B50W	23.91	3.40	0.52	6.535	3.142	0.099	0.140	0.468	0.247	0.795	-0.0302
A1C20W	23.91	3.40	0.52	9.566	2.374	0.080	0.161	0.904	0.507	0.485	-0.0570
A1C40W	23.91	3.40	0.52	9.614	3.612	0.102	0.180	0.688	0.403	0.623	-0.0539
A1C50W	23.91	3.40	0.52	9.646	4.823	0.126	0.194	0.519	0.313	0.742	-0.0474
A4A10W	10.00	3.40	0.52	3.287	0.281	0.041	0.054	0.818	0.285	0.711	-0.0102
A4A20W	10.00	3.40	0.52	3.205	0.666	0.075	0.087	0.502	0.216	0.814	-0.0084
A4A30W	10.00	3.40	0.52	3.199	0.961	0.096	0.108	0.383	0.182	0.842	-0.0087
A4A40W	10.00	3.40	0.52	3.188	1.307	0.117	0.129	0.282	0.144	0.871	-0.0083
A4A50W	10.00	3.40	0.52	3.205	1.580	0.133	0.143	0.225	0.120	0.897	-0.0064
A4B10W	10.00	3.40	0.52	6.497	0.669	0.073	0.100	1.054	0.485	0.660	-0.0216
A4B20W	10.00	3.40	0.52	6.472	1.328	0.117	0.145	0.705	0.379	0.738	-0.0220
A4B30W	10.00	3.40	0.52	6.428	1.984	0.152	0.176	0.520	0.302	0.815	-0.0187
A4B40W	10.00	3.40	0.52	6.417	2.484	0.177	0.199	0.414	0.253	0.842	-0.0169
A4B50W	10.00	3.40	0.52	6.414	3.170	0.203	0.230	0.300	0.193	0.855	-0.0210
A4C10W	10.00	3.40	0.52	9.607	0.926	0.074	0.142	1.238	0.665	0.532	-0.0427
A4C20W	10.00	3.40	0.52	9.586	1.984	0.145	0.200	0.797	0.487	0.667	-0.0355
A4C30W	10.00	3.40	0.52	9.613	3.005	0.184	0.241	0.586	0.384	0.753	-0.0386
A4C40W	10.00	3.40	0.52	9.573	4.005	0.228	0.274	0.437	0.300	0.818	-0.0328
A4C50W	10.00	3.40	0.52	9.590	4.852	0.258	0.300	0.340	0.241	0.858	-0.0305
A4D10W	10.00	3.40	0.52	1.560	0.154	0.028	0.036	0.488	0.141	0.720	-0.0045
A4D20W	10.00	3.40	0.52	1.548	0.351	0.050	0.058	0.312	0.112	0.796	-0.0044
A4D30W	10.00	3.40	0.52	1.555	0.500	0.062	0.072	0.239	0.095	0.816	-0.0063
A4D40W	10.00	3.40	0.52	1.575	0.622	0.074	0.084	0.195	0.083	0.802	-0.0063
A4D50W	10.00	3.40	0.52	1.583	0.779	0.086	0.093	0.153	0.068	0.859	-0.0033
A5A10W	5.00	3.40	0.52	3.191	0.324	0.075	0.084	0.601	0.258	0.810	-0.0080
A5A20W	5.00	3.40	0.52	3.194	0.636	0.115	0.127	0.398	0.204	0.829	-0.0105
A5A30W	5.00	3.40	0.52	3.180	0.964	0.151	0.161	0.286	0.161	0.860	-0.0085
A5A40W	5.00	3.40	0.52	3.195	1.256	0.177	0.189	0.219	0.132	0.865	-0.0103
A5A50W	5.00	3.40	0.52	3.197	1.552	0.200	0.213	0.167	0.105	0.879	-0.0112
A5B09W	5.00	3.40	0.52	6.446	0.557	0.104	0.122	0.929	0.466	0.774	-0.0145
A5B10W	5.00	3.40	0.52	6.546	0.724	0.126	0.144	0.808	0.434	0.773	-0.0177
A5B20W	5.00	3.40	0.52	6.534	1.240	0.174	0.193	0.586	0.356	0.825	-0.0170
A5B30W	5.00	3.40	0.52	6.542	1.929	0.227	0.241	0.416	0.274	0.891	-0.0122

Appendix 1.1 - Unsubmerged Flow Conditions (continued)

Test	L (ft)	B (ft)	P (ft)	Q_u (cfs)	Q_w (cfs)	h_u (ft)	h_d (ft)	C_e	Fw_d	F_d	h_c (ft)
A5B31W	5.00	3.40	0.52	6.347	1.957	0.231	0.247	0.389	0.259	0.868	-0.0145
A5B40W	5.00	3.40	0.52	6.527	2.652	0.276	0.288	0.296	0.208	0.910	-0.0105
A5B50W	5.00	3.40	0.52	6.586	3.170	0.304	0.319	0.235	0.171	0.915	-0.0131
A5B51W	5.00	3.40	0.52	6.431	3.199	0.305	0.322	0.220	0.161	0.909	-0.0147
A5C10W	5.00	3.40	0.52	9.547	0.899	0.154	0.175	1.061	0.624	0.701	-0.0232
A5C11W	5.00	3.40	0.52	9.639	1.011	0.148	0.185	0.968	0.574	0.721	-0.0206
A5C20W	5.00	3.40	0.52	9.695	1.857	0.226	0.255	0.673	0.453	0.781	-0.0235
A5C30W	5.00	3.40	0.52	9.679	3.055	0.298	0.327	0.444	0.326	0.846	-0.0241
A5C40W	5.00	3.40	0.52	9.603	3.980	0.347	0.369	0.332	0.254	0.896	-0.0188
A5C50W	5.00	3.40	0.52	9.599	4.987	0.395	0.406	0.245	0.193	0.952	-0.0097
A6A10W	2.00	3.40	0.52	3.317	0.300	0.126	0.131	0.452	0.234	0.819	-0.0042
A6A20W	2.00	3.40	0.52	3.322	0.614	0.188	0.190	0.300	0.180	0.879	-0.0013
A6A30W	2.00	3.40	0.52	3.305	0.975	0.234	0.242	0.208	0.137	0.905	-0.0071
A6A40W	2.00	3.40	0.52	3.287	1.244	0.274	0.279	0.159	0.110	0.890	-0.0042
A6A50W	2.00	3.40	0.52	3.192	1.638	0.315	0.320	0.105	0.077	0.907	-0.0042
A6B10W	2.00	3.40	0.52	6.575	0.622	0.189	0.200	0.630	0.386	0.813	-0.0090
A6B20W	2.00	3.40	0.52	6.499	1.260	0.279	0.289	0.394	0.276	0.844	-0.0085
A6B30W	2.00	3.40	0.52	6.355	1.919	0.342	0.351	0.273	0.205	0.892	-0.0077
A6B40W	2.00	3.40	0.52	6.455	2.573	0.396	0.400	0.207	0.162	0.931	-0.0031
A6C10W	2.00	3.40	0.52	9.552	0.940	0.247	0.254	0.733	0.491	0.799	-0.0054
A6C20W	2.00	3.40	0.52	9.578	1.973	0.354	0.364	0.450	0.342	0.856	-0.0080
A6C30W	2.00	3.40	0.52	9.611	2.826	0.416	0.430	0.334	0.267	0.889	-0.0116
A6D20W	2.00	3.40	0.52	1.636	0.356	0.137	0.140	0.182	0.097	0.867	-0.0022
A6D30W	2.00	3.40	0.52	1.625	0.495	0.161	0.164	0.142	0.080	0.918	-0.0022
A6D40W	2.00	3.40	0.52	1.620	0.580	0.180	0.184	0.118	0.070	0.879	-0.0032
A6D50W	2.00	3.40	0.52	1.741	0.810	0.218	0.222	0.090	0.057	0.879	-0.0032
A3A22N	15.00	1.80	0.52	3.271	0.692	0.067	0.091	0.759	0.356	0.532	-0.0261
A3A31N	15.00	1.80	0.52	3.281	0.996	0.081	0.108	0.593	0.300	0.590	-0.0272
A3A39N	15.00	1.80	0.52	3.268	1.236	0.093	0.122	0.480	0.256	0.607	-0.0280
A3A49N	15.00	1.80	0.52	3.247	1.571	0.107	0.137	0.361	0.202	0.646	-0.0279
A3B19N	15.00	1.80	0.52	6.307	1.219	0.099	0.142	1.064	0.603	0.475	-0.0491
A3B31N	15.00	1.80	0.52	6.314	1.990	0.115	0.177	0.750	0.464	0.552	-0.0549
A3B40N	15.00	1.80	0.52	6.336	2.554	0.130	0.207	0.569	0.374	0.556	-0.0623
A3B46N	15.00	1.80	0.52	6.328	3.005	0.141	0.210	0.493	0.326	0.640	-0.0573
A3B51N	15.00	1.80	0.52	6.331	3.281	0.154	0.221	0.431	0.291	0.645	-0.0560
A4A10N	10.00	1.80	0.52	3.199	0.312	0.060	0.068	1.008	0.412	0.555	-0.0107
A4A13N	10.00	1.80	0.52	3.232	0.413	0.069	0.082	0.866	0.385	0.552	-0.0142
A4A23N	10.00	1.80	0.52	3.206	0.739	0.094	0.111	0.608	0.308	0.621	-0.0162
A4A31N	10.00	1.80	0.52	3.217	0.986	0.110	0.129	0.490	0.265	0.657	-0.0174
A4A41N	10.00	1.80	0.52	3.227	1.298	0.130	0.148	0.379	0.217	0.699	-0.0160
A4B12N	10.00	1.80	0.52	6.411	0.754	0.098	0.130	1.234	0.669	0.496	-0.0322
A4B21N	10.00	1.80	0.52	6.391	1.350	0.124	0.174	0.863	0.527	0.565	-0.0393
A4B31N	10.00	1.80	0.52	6.390	1.984	0.152	0.211	0.634	0.417	0.613	-0.0448
A4B40N	10.00	1.80	0.52	6.404	2.535	0.194	0.228	0.517	0.350	0.693	-0.0293
A4B50N	10.00	1.80	0.52	6.377	3.259	0.211	0.257	0.371	0.262	0.737	-0.0371
A5A08N	5.00	1.80	0.52	3.185	0.256	0.077	0.083	0.910	0.409	0.652	-0.0092
A5A20N	5.00	1.80	0.52	3.187	0.627	0.127	0.135	0.552	0.305	0.742	-0.0093

Appendix 1.1 - Unsubmerged Flow Conditions (continued)

Test	L (ft)	B (ft)	P (ft)	Q_u (cfs)	Q_w (cfs)	h_u (ft)	h_d (ft)	C_e	Fw_d	F_d	h_c (ft)
A5A31N	5.00	1.80	0.52	3.187	0.989	0.166	0.174	0.383	0.235	0.779	-0.0085
A5A41N	5.00	1.80	0.52	3.205	1.320	0.196	0.204	0.284	0.186	0.802	-0.0080
A5A51N	5.00	1.80	0.52	3.191	1.628	0.222	0.227	0.213	0.145	0.830	-0.0050
A5B11N	5.00	1.80	0.52	6.457	0.709	0.133	0.172	1.011	0.617	0.569	-0.0336
A5B23N	5.00	1.80	0.52	6.457	1.454	0.209	0.236	0.657	0.453	0.695	-0.0262
A5B30N	5.00	1.80	0.52	6.439	1.935	0.250	0.268	0.521	0.376	0.749	-0.0193
A5B35N	5.00	1.80	0.52	6.392	2.235	0.271	0.290	0.443	0.329	0.758	-0.0196
A5C18N	5.00	1.80	0.52	9.568	1.723	0.269	0.295	0.822	0.613	0.568	-0.0267
A6A09N	2.00	1.80	0.52	3.204	0.289	0.130	0.131	0.632	0.344	0.789	-0.0023
A6A10N	2.00	1.80	0.52	3.263	0.364	0.141	0.148	0.578	0.332	0.806	-0.0059
A6A18N	2.00	1.80	0.52	3.262	0.595	0.186	0.193	0.423	0.270	0.829	-0.0059
A6A20N	2.00	1.80	0.52	3.197	0.644	0.201	0.205	0.377	0.245	0.806	-0.0043
A6A30N	2.00	1.80	0.52	3.284	0.940	0.239	0.243	0.299	0.208	0.866	-0.0032
A6A32N	2.00	1.80	0.52	3.189	1.007	0.254	0.258	0.258	0.183	0.832	-0.0040
A6A39N	2.00	1.80	0.52	3.177	1.236	0.282	0.287	0.206	0.152	0.839	-0.0048
A6A40N	2.00	1.80	0.52	3.287	1.294	0.280	0.289	0.213	0.158	0.867	-0.0078
A6A49N	2.00	1.80	0.52	3.202	1.552	0.314	0.317	0.158	0.120	0.875	-0.0028
A6A50N	2.00	1.80	0.52	3.283	1.633	0.316	0.321	0.158	0.121	0.899	-0.0041
A6B10N	2.00	1.80	0.52	6.407	0.633	0.204	0.216	0.813	0.539	0.722	-0.0125
A6B11N	2.00	1.80	0.52	6.576	0.706	0.210	0.230	0.789	0.538	0.719	-0.0133
A6B19N	2.00	1.80	0.52	6.418	1.215	0.290	0.302	0.524	0.393	0.750	-0.0119
A6B20N	2.00	1.80	0.52	6.498	1.320	0.291	0.301	0.530	0.398	0.820	-0.0077
A6B30N	2.00	1.80	0.52	6.490	1.913	0.348	0.355	0.391	0.310	0.871	-0.0055
A6B40N	2.00	1.80	0.52	6.482	2.560	0.395	0.412	0.282	0.235	0.875	-0.0140
A6B50N	2.00	1.80	0.52	6.433	2.977	0.426	0.442	0.228	0.194	0.887	-0.0134
A6C09N	2.00	1.80	0.52	9.615	0.902	0.243	0.271	0.982	0.708	0.681	-0.0193
A6C10N	2.00	1.80	0.52	9.626	0.961	0.274	0.274	0.979	0.711	0.711	-0.0020
A6C14N	2.00	1.80	0.52	9.639	1.294	0.291	0.332	0.758	0.587	0.669	-0.0275
A6C20N	2.00	1.80	0.52	9.615	1.697	0.345	0.364	0.657	0.526	0.736	-0.0118
C2A09W	20.00	3.40	0.70	3.201	0.296	0.028	0.038	0.683	0.180	0.639	-0.0051
C2A21W	20.00	3.40	0.70	3.213	0.677	0.047	0.061	0.451	0.149	0.713	-0.0084
C2A30W	20.00	3.40	0.70	3.189	0.961	0.059	0.073	0.355	0.127	0.770	-0.0081
C2A39W	20.00	3.40	0.70	3.217	1.227	0.070	0.084	0.290	0.111	0.794	-0.0079
C2A53W	20.00	3.40	0.70	3.192	1.693	0.087	0.101	0.193	0.080	0.826	-0.0075
C2B07W	20.00	3.40	0.70	6.347	0.472	0.039	0.052	1.150	0.353	0.634	-0.0154
C2B13W	20.00	3.40	0.70	6.343	0.794	0.052	0.069	0.915	0.320	0.694	-0.0176
C2B17W	20.00	3.40	0.70	6.338	1.074	0.064	0.083	0.772	0.294	0.708	-0.0184
C2B30W	20.00	3.40	0.70	6.325	1.935	0.094	0.116	0.515	0.228	0.764	-0.0191
C2B41W	20.00	3.40	0.70	6.351	2.658	0.115	0.139	0.381	0.182	0.794	-0.0199
C2B50W	20.00	3.40	0.70	6.327	3.199	0.132	0.153	0.300	0.150	0.824	-0.0165
C2C11W	20.00	3.40	0.70	9.525	1.055	0.063	0.089	1.187	0.467	0.625	-0.0334
C2C19W	20.00	3.40	0.70	9.537	1.836	0.088	0.123	0.866	0.394	0.662	-0.0368
C2C30W	20.00	3.40	0.70	9.552	2.935	0.115	0.158	0.620	0.314	0.719	-0.0403
C2C39W	20.00	3.40	0.70	9.569	3.798	0.141	0.180	0.489	0.261	0.760	-0.0356
C2C50W	20.00	3.40	0.70	9.545	4.890	0.169	0.207	0.353	0.200	0.787	-0.0334
C3B08W	15.00	3.40	0.70	6.498	0.522	0.051	0.068	0.994	0.346	0.617	-0.0177
C3B18W	15.00	3.40	0.70	6.497	1.112	0.079	0.102	0.689	0.288	0.705	-0.0214

Appendix 1.1 - Unsubmerged Flow Conditions (continued)

Test	L (ft)	B (ft)	P (ft)	Q_u (cfs)	Q_w (cfs)	h_u (ft)	h_d (ft)	C_e	Fw_d	F_d	h_c (ft)
C3B25W	15.00	3.40	0.70	6.486	1.566	0.102	0.124	0.550	0.251	0.734	-0.0197
C3B28W	15.00	3.40	0.70	6.463	1.779	0.109	0.131	0.504	0.235	0.766	-0.0194
C3B42W	15.00	3.40	0.70	6.418	2.718	0.146	0.166	0.334	0.173	0.808	-0.0165
C3B50W	15.00	3.40	0.70	6.338	3.266	0.164	0.183	0.257	0.138	0.833	-0.0151
C3C10W	15.00	3.40	0.70	9.610	0.947	0.056	0.099	1.131	0.467	0.629	-0.0423
C3C17W	15.00	3.40	0.70	9.629	1.643	0.096	0.140	0.819	0.393	0.638	-0.0412
C3C21W	15.00	3.40	0.70	9.611	1.995	0.121	0.155	0.724	0.363	0.661	-0.0326
C3C30W	15.00	3.40	0.70	9.637	2.921	0.141	0.184	0.559	0.302	0.739	-0.0386
C3C40W	15.00	3.40	0.70	9.611	3.921	0.181	0.215	0.418	0.240	0.775	-0.0301
C3C50W	15.00	3.40	0.70	9.611	4.948	0.209	0.232	0.321	0.190	0.867	-0.0201
C4A09W	10.00	3.40	0.70	3.270	0.269	0.044	0.050	0.600	0.181	0.754	-0.0350
C4A18W	10.00	3.40	0.70	3.254	0.580	0.072	0.081	0.398	0.150	0.773	-0.0061
C4A31W	10.00	3.40	0.70	3.269	0.979	0.107	0.115	0.274	0.122	0.755	-0.0052
C4A42W	10.00	3.40	0.70	3.262	1.328	0.128	0.136	0.202	0.096	0.786	-0.0047
C4A51W	10.00	3.40	0.70	3.272	1.638	0.144	0.149	0.160	0.079	0.839	-0.0017
C4B11W	10.00	3.40	0.70	6.368	0.663	0.080	0.092	0.781	0.312	0.725	-0.0115
C4B20W	10.00	3.40	0.70	6.358	1.269	0.120	0.132	0.543	0.254	0.788	-0.0106
C4B30W	10.00	3.40	0.70	6.369	1.924	0.154	0.167	0.399	0.206	0.822	-0.0109
C4B39W	10.00	3.40	0.70	6.391	2.535	0.184	0.196	0.305	0.169	0.837	-0.0096
C4B44W	10.00	3.40	0.70	6.377	2.826	0.197	0.208	0.267	0.152	0.848	-0.0085
C4B49W	10.00	3.40	0.70	6.365	3.142	0.210	0.222	0.230	0.134	0.848	-0.0092
C4C11W	10.00	3.40	0.70	9.591	1.011	0.102	0.124	0.958	0.437	0.693	-0.0224
C4C12W	10.00	3.40	0.70	9.526	1.175	0.107	0.133	0.887	0.417	0.721	-0.0251
C4C18W	10.00	3.40	0.70	9.593	1.723	0.150	0.166	0.709	0.366	0.743	-0.0163
C4C32W	10.00	3.40	0.70	9.589	3.084	0.208	0.225	0.459	0.269	0.814	-0.0155
C4C41W	10.00	3.40	0.70	9.587	4.048	0.241	0.258	0.347	0.214	0.854	-0.0148
C4C46W	10.00	3.40	0.70	9.580	4.497	0.256	0.278	0.298	0.190	0.838	-0.0189
C5A09W	5.00	3.40	0.70	3.204	0.281	0.072	0.076	0.459	0.169	0.789	-0.0029
C5A19W	5.00	3.40	0.70	3.210	0.611	0.116	0.120	0.301	0.136	0.821	-0.0027
C5A31W	5.00	3.40	0.70	3.209	0.979	0.153	0.158	0.211	0.107	0.834	-0.0035
C5A39W	5.00	3.40	0.70	3.203	1.252	0.176	0.182	0.166	0.089	0.841	-0.0045
C5A52W	5.00	3.40	0.70	3.213	1.653	0.209	0.213	0.117	0.067	0.848	-0.0024
C5B10W	5.00	3.40	0.70	6.408	0.649	0.119	0.127	0.641	0.296	0.795	-0.0083
C5B20W	5.00	3.40	0.70	6.377	1.265	0.176	0.184	0.430	0.233	0.834	-0.0076
C5B31W	5.00	3.40	0.70	6.392	1.962	0.227	0.235	0.305	0.182	0.850	-0.0072
C5B40W	5.00	3.40	0.70	6.382	2.580	0.264	0.273	0.229	0.145	0.859	-0.0079
C5B50W	5.00	3.40	0.70	6.420	3.229	0.300	0.308	0.172	0.114	0.868	-0.0068
C5C10W	5.00	3.40	0.70	9.599	0.940	0.149	0.162	0.805	0.413	0.768	-0.0143
C5C17W	5.00	3.40	0.70	9.591	1.624	0.205	0.219	0.582	0.338	0.795	-0.0142
C5C21W	5.00	3.40	0.70	9.601	1.995	0.229	0.245	0.505	0.307	0.803	-0.0156
C5C29W	5.00	3.40	0.70	9.575	2.851	0.279	0.291	0.383	0.248	0.848	-0.0117
C2A15N	20.00	1.80	0.70	3.258	0.472	0.038	0.054	0.765	0.252	0.598	-0.0105
C2A19N	20.00	1.80	0.70	3.246	0.595	0.042	0.060	0.683	0.236	0.643	-0.0122
C2A22N	20.00	1.80	0.70	3.262	0.709	0.052	0.070	0.597	0.222	0.606	-0.0120
C2A28N	20.00	1.80	0.70	3.239	0.882	0.058	0.075	0.527	0.202	0.679	-0.0108
C2A41N	20.00	1.80	0.70	3.248	1.294	0.073	0.092	0.382	0.161	0.729	-0.0123
C2A46N	20.00	1.80	0.70	3.230	1.463	0.080	0.099	0.328	0.143	0.736	-0.0122

Appendix 1.1 - Unsubmerged Flow Conditions (continued)

Test	L (ft)	B (ft)	P (ft)	Q_u (cfs)	Q_w (cfs)	h_u (ft)	h_d (ft)	C_e	Fw_d	F_d	h_c (ft)
C2A50N	20.00	1.80	0.70	3.239	1.604	0.084	0.103	0.295	0.131	0.760	-0.0121
C2B22N	20.00	1.80	0.70	6.327	1.376	0.070	0.104	0.889	0.396	0.642	-0.0275
C2B30N	20.00	1.80	0.70	6.340	1.935	0.091	0.129	0.677	0.332	0.649	-0.0297
C2B39N	20.00	1.80	0.70	6.386	2.516	0.106	0.144	0.548	0.281	0.712	-0.0292
C2B52N	20.00	1.80	0.70	6.333	3.372	0.128	0.172	0.365	0.202	0.724	-0.0335
C2C13N	20.00	1.80	0.70	9.604	1.231	0.082	0.120	1.357	0.644	0.461	-0.0321
C2C20N	20.00	1.80	0.70	9.593	1.899	0.087	0.146	1.078	0.556	0.526	-0.0404
C2C31N	20.00	1.80	0.70	9.470	3.027	0.123	0.187	0.741	0.424	0.571	-0.0435
C2C34N	20.00	1.80	0.70	9.613	3.334	0.133	0.190	0.713	0.411	0.613	-0.0392
C2C41N	20.00	1.80	0.70	9.594	4.048	0.132	0.211	0.576	0.347	0.632	-0.0519
C2C51N	20.00	1.80	0.70	9.570	5.046	0.161	0.228	0.439	0.272	0.698	-0.0455
C3A10N	15.00	1.80	0.70	3.256	0.300	0.037	0.049	0.861	0.271	0.585	-0.0081
C3A16N	15.00	1.80	0.70	3.243	0.517	0.051	0.065	0.668	0.240	0.655	-0.0096
C3A18N	15.00	1.80	0.70	3.257	0.580	0.055	0.070	0.626	0.233	0.656	-0.0105
C3A28N	15.00	1.80	0.70	3.245	0.875	0.071	0.086	0.484	0.198	0.722	-0.0102
C3A42N	15.00	1.80	0.70	3.219	1.345	0.092	0.110	0.323	0.148	0.759	-0.0127
C3A51N	15.00	1.80	0.70	3.245	1.643	0.107	0.122	0.257	0.123	0.790	-0.0097
C3B09N	15.00	1.80	0.70	6.402	0.546	0.053	0.074	1.321	0.504	0.567	-0.0190
C3B18N	15.00	1.80	0.70	6.373	1.112	0.076	0.110	0.908	0.414	0.628	-0.0272
C3B32N	15.00	1.80	0.70	6.386	2.039	0.118	0.149	0.599	0.312	0.718	-0.0243
C3B41N	15.00	1.80	0.70	6.365	2.645	0.138	0.177	0.448	0.251	0.711	-0.0304
C3B48N	15.00	1.80	0.70	6.383	3.099	0.153	0.187	0.378	0.216	0.764	-0.0263
C3C11N	15.00	1.80	0.70	9.641	1.093	0.087	0.125	1.345	0.650	0.506	-0.0286
C3C20N	15.00	1.80	0.70	9.668	1.968	0.101	0.152	1.046	0.549	0.672	-0.0339
C3C30N	15.00	1.80	0.70	9.659	2.949	0.149	0.209	0.703	0.421	0.610	-0.0406
C3C38N	15.00	1.80	0.70	9.659	3.684	0.166	0.231	0.573	0.358	0.650	-0.0443
C3C45N	15.00	1.80	0.70	9.680	4.407	0.183	0.239	0.491	0.310	0.736	-0.0387
C4A09N	10.00	1.80	0.70	3.168	0.271	0.045	0.054	0.794	0.262	0.675	-0.0062
C4A18N	10.00	1.80	0.70	3.174	0.580	0.075	0.086	0.529	0.216	0.705	-0.0078
C4A32N	10.00	1.80	0.70	3.174	1.018	0.103	0.113	0.364	0.168	0.807	-0.0066
C4A42N	10.00	1.80	0.70	3.181	1.328	0.126	0.137	0.272	0.137	0.777	-0.0074
C4A51N	10.00	1.80	0.70	3.182	1.633	0.143	0.155	0.207	0.109	0.786	-0.0083
C4B11N	10.00	1.80	0.70	6.406	0.706	0.080	0.100	1.049	0.459	0.678	-0.0165
C4B18N	10.00	1.80	0.70	6.388	1.139	0.106	0.131	0.796	0.392	0.716	-0.0199
C4B30N	10.00	1.80	0.70	6.418	1.919	0.151	0.176	0.543	0.303	0.754	-0.0197
C4B35N	10.00	1.80	0.70	6.310	2.265	0.168	0.193	0.452	0.262	0.767	-0.0197
C4B41N	10.00	1.80	0.70	6.367	2.665	0.185	0.217	0.375	0.228	0.746	-0.0256
C4B46N	10.00	1.80	0.70	6.387	2.956	0.202	0.225	0.336	0.208	0.780	-0.0180
C4B50N	10.00	1.80	0.70	6.393	3.221	0.212	0.232	0.303	0.189	0.809	-0.0154
C4C10N	10.00	1.80	0.70	9.597	1.015	0.094	0.137	1.259	0.632	0.594	-0.0272
C4C20N	10.00	1.80	0.70	9.592	1.889	0.135	0.193	0.861	0.500	0.639	-0.0373
C4C30N	10.00	1.80	0.70	9.594	2.963	0.201	0.230	0.638	0.397	0.754	-0.0211
C4C37N	10.00	1.80	0.70	9.590	3.636	0.230	0.258	0.516	0.336	0.767	-0.0206
C5A09N	5.00	1.80	0.70	3.250	0.291	0.076	0.080	0.643	0.255	0.753	-0.0033
C5A21N	5.00	1.80	0.70	3.269	0.663	0.125	0.128	0.408	0.200	0.801	-0.0020
C5A31N	5.00	1.80	0.70	3.243	0.982	0.156	0.161	0.297	0.161	0.811	-0.0037
C5A40N	5.00	1.80	0.70	3.256	1.265	0.180	0.184	0.235	0.134	0.834	-0.0027

Appendix 1.1 - Unsubmerged Flow Conditions (continued)

Test	L (ft)	B (ft)	P (ft)	Q_u (cfs)	Q_w (cfs)	h_u (ft)	h_d (ft)	C_e	Fw_d	F_d	h_c (ft)
C5A51N	5.00	1.80	0.70	3.245	1.624	0.207	0.211	0.170	0.103	0.847	-0.0026
C5B10N	5.00	1.80	0.70	6.421	0.644	0.116	0.130	0.895	0.441	0.759	-0.0134
C5B21N	5.00	1.80	0.70	6.421	1.328	0.181	0.196	0.570	0.334	0.786	-0.0137
C5B30N	5.00	1.80	0.70	6.411	1.935	0.227	0.238	0.423	0.268	0.820	-0.0100
C5B39N	5.00	1.80	0.70	6.406	2.516	0.265	0.274	0.323	0.216	0.832	-0.0081
C5B47N	5.00	1.80	0.70	6.438	3.055	0.294	0.304	0.254	0.177	0.840	-0.0088
C5C10N	5.00	1.80	0.70	9.634	0.961	0.153	0.177	1.057	0.594	0.676	-0.0200
C5C20N	5.00	1.80	0.70	9.614	1.924	0.224	0.247	0.703	0.451	0.764	-0.0196
C5C25N	5.00	1.80	0.70	9.624	2.386	0.253	0.280	0.588	0.397	0.760	-0.0225

Appendix 1.2 - Submerged Flow Conditions

Test	Compared to Test	L (ft)	B (ft)	P (ft)	Q_u (cfs)	Q_d (cfs)	h_u (ft)	h_d (ft)	h_b (ft)	Fw_d	C_{es}	h_{cs} (ft)
C3C21WS	C3C40W	15.0	3.40	0.70	7.152	1.486	0.192	0.212	0.202	0.421	0.300	-0.016
C3C26WS	C3C40W	15.0	3.40	0.70	7.686	2.006	0.197	0.217	0.204	0.414	0.391	-0.016
C3C32WS	C3C40W	15.0	3.40	0.70	8.310	2.665	0.191	0.216	0.192	0.413	0.523	-0.020
C3C35WS	C3C40W	15.0	3.40	0.70	8.696	3.106	0.183	0.211	0.176	0.417	0.633	-0.023
C3C37WS	C3C40W	15.0	3.40	0.70	9.016	3.387	0.184	0.214	0.173	0.415	0.675	-0.025
C3C38WS	C3C40W	15.0	3.40	0.70	9.193	3.548	0.180	0.211	0.155	0.421	0.723	-0.025
C3C40WS	C3C40W	15.0	3.40	0.70	9.430	3.848	0.187	0.215	0.152	0.410	0.761	-0.023
C3B32WS	C3B50W	15.0	3.40	0.70	4.566	1.473	0.163	0.178	0.170	0.264	0.393	-0.010
C3B45WS	C3B50W	15.0	3.40	0.70	5.437	2.434	0.168	0.185	0.165	0.249	0.610	-0.012
C3B30NS	C3B48N	15.0	1.80	0.70	4.724	1.414	0.166	0.185	0.174	0.384	0.355	-0.015
C3B38NS	C3B48N	15.0	1.80	0.70	5.290	2.017	0.163	0.185	0.165	0.380	0.506	-0.018
C3B46NS	C3B48N	15.0	1.80	0.70	6.073	2.812	0.161	0.188	0.145	0.373	0.688	-0.022
C3C10NS	C3C38N	15.0	1.80	0.70	6.641	0.652	0.212	0.230	0.223	0.577	0.116	-0.016
C3C21NS	C3C38N	15.0	1.80	0.70	7.683	1.643	0.203	0.231	0.207	0.580	0.290	-0.025
C3C31NS	C3C38N	15.0	1.80	0.70	8.703	2.745	0.188	0.229	0.182	0.576	0.491	-0.034
C4B28WS	C4B49W	10.0	3.40	0.70	4.499	1.248	0.216	0.224	0.216	0.230	0.332	-0.005
C4B36WS	C4B49W	10.0	3.40	0.70	5.169	1.873	0.211	0.222	0.207	0.235	0.505	-0.008
C4B44WS	C4B49W	10.0	3.40	0.70	5.828	2.586	0.210	0.222	0.191	0.231	0.698	-0.009
C4C19WS	C4C41W	10.0	3.40	0.70	6.833	1.320	0.252	0.261	0.252	0.342	0.273	-0.006
C4C36WS	C4C41W	10.0	3.40	0.70	9.164	3.221	0.240	0.256	0.218	0.375	0.688	-0.013
C4B33NS	C4B50N	10.0	1.80	0.70	4.746	1.542	0.219	0.233	0.217	0.305	0.384	-0.011
C4B42NS	C4B50N	10.0	1.80	0.70	5.420	2.295	0.217	0.230	0.202	0.300	0.584	-0.010
C4B49NS	C4B50N	10.0	1.80	0.70	6.148	3.005	0.214	0.233	0.162	0.299	0.749	-0.015
C4C07NS	C4C30N	10.0	1.80	0.70	7.128	0.524	0.222	0.233	0.221	0.628	0.131	-0.010
C4C19NS	C4C30N	10.0	1.80	0.70	8.220	1.552	0.193	0.232	0.190	0.636	0.390	-0.032
C5B15WS	C5B40W	5.0	3.40	0.70	4.430	0.636	0.264	0.268	0.263	0.233	0.219	-0.003
C5B25WS	C5B40W	5.0	3.40	0.70	5.050	1.244	0.265	0.271	0.258	0.231	0.420	-0.005
C5B34WS	C5B40W	5.0	3.40	0.70	5.806	2.006	0.268	0.275	0.245	0.228	0.659	-0.006
C5C12WS	C5C29W	5.0	3.40	0.70	7.704	0.923	0.286	0.292	0.280	0.385	0.273	-0.005
C5C23WS	C5C29W	5.0	3.40	0.70	8.685	1.973	0.281	0.290	0.259	0.383	0.590	-0.008
C5B12NS	C5B39N	5.0	1.80	0.70	4.471	0.537	0.269	0.273	0.266	0.328	0.179	-0.003
C5B23NS	C5B39N	5.0	1.80	0.70	5.084	1.175	0.271	0.278	0.261	0.320	0.379	-0.006
C5B32NS	C5B39N	5.0	1.80	0.70	5.712	1.830	0.262	0.272	0.235	0.324	0.613	-0.009
C5C05NS	C5C25N	5.0	1.80	0.70	7.676	0.415	0.275	0.278	0.270	0.594	0.134	-0.005
C5C16NS	C5C25N	5.0	1.80	0.70	8.610	1.350	0.262	0.275	0.236	0.600	0.444	-0.013

Appendix 1.3 - Tapered Channels

Test	L (ft)	ΔB' (ft)	P (ft)	Q_u (cfs)	Q_w (cfs)	h_u (ft)	h_d (ft)	F_d	Fw_d	C_e	h_c (ft)
C2A08T	20.0	0.080	0.70	3.205	0.263	0.024	0.024	0.288	1.289	1.137	-0.005
C2A20T	20.0	0.080	0.70	3.189	0.647	0.044	0.051	0.232	0.723	0.895	-0.005
C2A24T	20.0	0.080	0.70	3.194	0.779	0.050	0.058	0.216	0.635	0.886	-0.004
C2A32T	20.0	0.080	0.70	3.189	1.044	0.060	0.071	0.186	0.497	0.873	-0.004
C2A41T	20.0	0.080	0.70	3.172	1.324	0.070	0.084	0.155	0.384	0.857	-0.005
C2A51T	20.0	0.080	0.70	3.179	1.619	0.081	0.095	0.127	0.298	0.868	-0.003
C2B11T	20.0	0.080	0.70	6.339	0.683	0.058	0.032	0.542	2.111	1.912	-0.012
C2B13T	20.0	0.080	0.70	6.321	0.836	0.062	0.042	0.512	1.751	1.551	-0.011
C2B21T	20.0	0.080	0.70	6.445	1.324	0.077	0.073	0.442	1.165	1.061	-0.010
C2B28T	20.0	0.080	0.70	6.347	1.758	0.090	0.096	0.374	0.871	0.928	-0.008
C2B40T	20.0	0.080	0.70	6.327	2.612	0.112	0.132	0.278	0.562	0.845	-0.007
C2B51T	20.0	0.080	0.70	6.351	3.341	0.131	0.153	0.214	0.407	0.860	-0.001
C2C15T	20.0	0.080	0.70	9.694	1.473	0.103	0.035	0.782	2.916	3.602	-0.022
C2C16T	20.0	0.080	0.70	9.663	1.491	0.104	0.041	0.765	2.645	2.870	-0.021
C2C22T	20.0	0.080	0.70	9.601	2.096	0.116	0.090	0.621	1.488	1.221	-0.012
C2C29T	20.0	0.080	0.70	9.595	2.785	0.126	0.130	0.511	1.041	0.922	-0.011
C2C43T	20.0	0.080	0.70	9.573	4.195	0.154	0.182	0.358	0.633	0.825	-0.003
C2C53T	20.0	0.080	0.70	9.552	5.085	0.170	0.203	0.284	0.480	0.843	0.004
C3A10T	15.0	0.107	0.70	3.274	0.298	0.045	0.046	0.275	0.900	0.639	-0.006
C3A21T	15.0	0.107	0.70	3.285	0.661	0.067	0.074	0.226	0.592	0.687	-0.006
C3A30T	15.0	0.107	0.70	3.279	0.947	0.081	0.091	0.192	0.459	0.716	-0.006
C3A40T	15.0	0.107	0.70	3.271	1.281	0.096	0.110	0.157	0.343	0.723	-0.007
C3A52T	15.0	0.107	0.70	3.273	1.643	0.112	0.126	0.124	0.255	0.751	-0.005
C3B11T	15.0	0.107	0.70	6.411	0.663	0.079	0.053	0.522	1.597	1.146	-0.008
C3B19T	15.0	0.107	0.70	6.358	1.195	0.100	0.094	0.423	0.994	0.860	-0.007
C3B29T	15.0	0.107	0.70	6.316	1.830	0.123	0.131	0.336	0.682	0.788	-0.007
C3B41T	15.0	0.107	0.70	6.298	2.612	0.149	0.165	0.255	0.469	0.784	-0.004
C3B51T	15.0	0.107	0.70	6.298	3.311	0.170	0.191	0.195	0.338	0.790	-0.003
C3C12T	15.0	0.107	0.70	9.503	1.215	0.118	0.036	0.786	2.892	3.781	-0.011
C3C13T	15.0	0.107	0.70	9.496	1.223	0.117	0.044	0.769	2.569	2.807	-0.014
C3C14T	15.0	0.107	0.70	9.601	1.328	0.119	0.067	0.725	1.988	1.606	-0.020
C3C15T	15.0	0.107	0.70	9.485	1.298	0.119	0.053	0.743	2.275	2.245	-0.013
C3C21T	15.0	0.107	0.70	9.426	2.051	0.138	0.123	0.563	1.174	0.974	-0.011
C3C30T	15.0	0.107	0.70	9.567	2.928	0.164	0.175	0.449	0.806	0.801	-0.009
C3C39T	15.0	0.107	0.70	9.561	3.848	0.188	0.213	0.355	0.589	0.772	-0.006
C3C51T	15.0	0.107	0.70	9.559	5.006	0.215	0.248	0.263	0.410	0.788	0.000
C4A11T	10.0	0.160	0.70	3.180	0.337	0.057	0.056	0.255	0.762	0.794	-0.003
C4A20T	10.0	0.160	0.70	3.212	0.619	0.082	0.084	0.217	0.537	0.780	-0.002
C4A32T	10.0	0.160	0.70	3.197	1.022	0.108	0.114	0.169	0.365	0.799	-0.002
C4A39T	10.0	0.160	0.70	3.191	1.240	0.120	0.127	0.147	0.303	0.818	-0.002
C4A49T	10.0	0.160	0.70	3.191	1.556	0.139	0.146	0.118	0.229	0.823	0.000
C4B11T	10.0	0.160	0.70	6.430	0.698	0.096	0.074	0.492	1.290	1.070	-0.006
C4B20T	10.0	0.160	0.70	6.427	1.236	0.127	0.121	0.397	0.835	0.880	-0.005
C4B30T	10.0	0.160	0.70	6.427	1.919	0.159	0.164	0.312	0.576	0.844	-0.003
C4B41T	10.0	0.160	0.70	6.423	2.652	0.190	0.201	0.240	0.408	0.841	0.000
C4B49T	10.0	0.160	0.70	6.390	3.177	0.211	0.223	0.195	0.317	0.851	0.003
C4C10T	10.0	0.160	0.70	9.508	0.961	0.133	0.054	0.772	2.343	2.395	-0.010

Appendix 1.3 - Tapered Channels (continued)

Test	L (ft)	ΔB' (ft)	P (ft)	Q_u (cfs)	Q_w (cfs)	h_u (ft)	h_d (ft)	F_d	Fw_d	C_e	h_c (ft)
C4C12T	10.0	0.160	0.70	9.512	1.183	0.140	0.080	0.704	1.782	1.608	-0.008
C4C20T	10.0	0.160	0.70	9.539	1.946	0.172	0.151	0.542	1.034	0.976	-0.003
C4C29T	10.0	0.160	0.70	9.541	2.851	0.207	0.210	0.418	0.696	0.842	-0.001
C4C39T	10.0	0.160	0.70	9.547	3.831	0.238	0.254	0.325	0.503	0.829	0.001
C5A10T	5.0	0.320	0.70	3.149	0.324	0.079	0.075	0.247	0.640	0.929	-0.001
C5A13T	5.0	0.320	0.70	3.149	0.409	0.092	0.090	0.231	0.551	0.876	-0.002
C5A22T	5.0	0.320	0.70	3.142	0.689	0.127	0.128	0.188	0.384	0.833	-0.001
C5A31T	5.0	0.320	0.70	3.147	0.996	0.154	0.156	0.154	0.290	0.867	0.000
C5A39T	5.0	0.320	0.70	3.192	1.236	0.174	0.178	0.134	0.237	0.862	-0.001
C5A51T	5.0	0.320	0.70	3.196	1.628	0.205	0.209	0.100	0.166	0.863	0.001
C5B10T	5.0	0.320	0.70	6.442	0.658	0.129	0.109	0.464	1.018	1.034	-0.006
C5B20T	5.0	0.320	0.70	6.462	1.244	0.179	0.174	0.360	0.645	0.901	-0.004
C5B31T	5.0	0.320	0.70	6.433	1.968	0.229	0.232	0.271	0.432	0.871	-0.001
C5B41T	5.0	0.320	0.70	6.453	2.619	0.268	0.274	0.213	0.318	0.866	0.002
C5B50T	5.0	0.320	0.70	6.439	3.214	0.298	0.306	0.168	0.241	0.874	0.003
C5C12T	5.0	0.320	0.70	9.531	1.135	0.188	0.146	0.617	1.191	1.103	-0.007
C5C20T	5.0	0.320	0.70	9.496	1.878	0.234	0.219	0.475	0.775	0.919	-0.003
C5C27T	5.0	0.320	0.70	9.516	2.619	0.276	0.275	0.382	0.570	0.861	0.000

APPENDIX 2 - WEIR AND CHANNEL GEOMETRIES INVESTIGATED IN PREVIOUS PROJECT FOR UNSUBMERGED FLOW

Weir height P (ft)	Weir length L (ft)	Channel invert width B (ft)	Number of tests
0.52	23.91	3.4	12
0.52	15.00	1.8	9
0.52	10.00	3.4	20
0.52	10.00	1.8	10
0.52	5.00	3.4	19
0.52	5.00	1.8	10
0.52	2.00	3.4	16
0.52	2.00	1.8	21
0.70	20.00	3.4	16
0.70	20.00	1.8	17
0.70	15.00	3.4	12
0.70	15.00	1.8	16
0.70	10.00	3.4	17
0.70	10.00	1.8	16
0.70	5.00	3.4	14
0.70	5.00	1.8	13

APPENDIX 3 - RESULTS OF SIMULATION OF SIDE WEIR FLOW FOR DIFFERENT SLOPES AND ROUGHNESS

The results for Method A begin on page 140 while the results for Method B begin on p. 151. For Method A, there is no way to specify different channel slopes when calculating Q_w. Therefore, all calculated values of Q_w are the same for each case.

Notes for the tables:

All results are for prismatic channels.

(1) in the table means supercritical condition at upstream end.

(2) in the table means $Q_w > Q_u$ and iteration stopped.

(3) in the table means negative flow depth and iteration stopped.

(4) in the table means $Q_w > 0.6Q_u$ in final solution.

"Max. diff." is the largest difference between the values in the row or column.

Appendix 3.1 - Results of simulation using Method A

Input geometry data: L = 598 ft B = 85 ft P = 13.0 ft Input flow conditions: Q_u = 10156 cfs h_d = 0.97 ft

Calculated Q_w (cfs)

	Slope				
Manning's n	0.000385	0.0008	0.0012	0.0016	Max. diff.
0.0125	1082	1082	1082	1082	0
0.02	1082	1082	1082	1082	0
0.03	1082	1082	1082	1082	0
0.04	1082	1082	1082	1082	0
Max. diff.	0	0	0	0	

Calculated h_u (ft)

	Slope				
Manning's n	0.000385	0.0008	0.0012	0.0016	Max. diff.
0.0125	0.47	0.19	-0.09	-0.36	0.83
0.02	0.58	0.31	0.04	-0.23	0.81
0.03	0.80	0.53	0.28	0.03	0.77
0.04	1.08	0.83	0.59	0.35	0.73
Max. diff.	0.61	0.64	0.68	0.71	

Input geometry data: L = 598 ft B = 85 ft P = 13.0 ft Input flow conditions: Q_u = 10116 cfs h_d = 2.30 ft

Calculated Q_w (cfs)

	Slope				
Manning's n	0.000385	0.0008	0.0012	0.0016	Max. diff.
0.0125	4905	4905	4905	4905	0
0.02	4905	4905	4905	4905	0
0.03	4905	4905	4905	4905	0
0.04	4905	4905	4905	4905	0
Max. diff.	0	0	0	0	

Calculated h_u (ft)

	Slope				
Manning's n	0.000385	0.0008	0.0012	0.0016	Max. diff.
0.0125	1.67	1.40	1.14	0.87	0.80
0.02	1.73	1.46	1.20	0.94	0.79
0.03	1.84	1.58	1.33	1.08	0.76
0.04	1.99	1.74	1.50	1.26	0.73
Max. diff.	0.32	0.34	0.36	0.39	

Input geometry data: L = 598 ft B = 85 ft P = 13.0 ft Input flow conditions: Q_u = 29894 cfs h_d = 4.03 ft

Calculated Q_w (cfs)

	Slope				
Manning's n	0.000385	0.0008	0.0012	0.0016	Max. diff.
0.0125	9829	9829	9829	9829	0
0.02	9829	9829	9829	9829	0
0.03	9829	9829	9829	9829	0
0.04	9829	9829	9829	9829	0
Max. diff.	0	0	0	0	

Calculated h_u (ft)

	Slope				
Manning's n	0.000385	0.0008	0.0012	0.0016	Max. diff.
0.0125	(1)	(1)	(1)	(1)	
0.02	1.06	(1)	(1)	(1)	
0.03	2.92	2.54	2.15	1.76	1.16
0.04	4.20	3.91	3.63	3.35	0.85
Max. diff.	3.14	1.37	1.48	1.59	

(See notes on p. 139.)

Appendix 3.1 - Results of simulation using Method A (continued)

Input geometry data: L = 598 ft B = 85 ft P = 13.0 ft Input flow conditions: Q_u = 30144 cfs h_d = 4.85 ft

Calculated Q_w (cfs)

	Slope				
Manning's n	0.000385	0.0008	0.0012	0.0016	Max. diff.
0.0125	14305	14305	14305	14305	0
0.02	14305	14305	14305	14305	0
0.03	14305	14305	14305	14305	0
0.04	14305	14305	14305	14305	0
Max. diff.	0	0	0	0	

Calculated h_u (ft)

	Slope				
Manning's n	0.000385	0.0008	0.0012	0.0016	Max. diff.
0.0125	0.97	(1)	(1)	(1)	
0.02	2.36	1.78	1.08	(1)	1.28
0.03	3.54	3.18	2.82	2.44	1.10
0.04	4.55	4.26	3.98	3.70	0.85
Max. diff.	3.58	2.48	2.90	1.26	

Input geometry data: L = 250 ft B = 85 ft P = 13.0 ft Input flow conditions: Q_u = 30022 cfs h_d = 3.55 ft

Calculated Q_w (cfs)

	Slope				
Manning's n	0.000385	0.0008	0.0012	0.0016	Max. diff.
0.0125	3280	3280	3280	3280	0
0.02	3280	3280	3280	3280	0
0.03	3280	3280	3280	3280	0
0.04	3280	3280	3280	3280	0
Max. diff.	0	0	0	0	

Calculated h_u (ft)

	Slope				
Manning's n	0.000385	0.0008	0.0012	0.0016	Max. diff.
0.0125	(1)	(1)	(1)	(1)	
0.02	1.71	1.31	0.73	(1)	0.98
0.03	2.82	2.61	2.40	2.18	0.64
0.04	3.76	3.60	3.45	3.29	0.47
Max. diff.	2.05	2.29	2.72	1.11	

Input geometry data: L = 250 ft B = 85 ft P = 13.0 ft Input flow conditions: Q_u = 29969 cfs h_d = 7.50 ft

Calculated Q_w (cfs)

	Slope				
Manning's n	0.000385	0.0008	0.0012	0.0016	Max. diff.
0.0125	14482	14482	14482	14482	0
0.02	14482	14482	14482	14482	0
0.03	14482	14482	14482	14482	0
0.04	14482	14482	14482	14482	0
Max. diff.	0	0	0	0	

Calculated h_u (ft)

	Slope				
Manning's n	0.000385	0.0008	0.0012	0.0016	Max. diff.
0.0125	6.09	5.94	5.79	5.65	0.44
0.02	6.19	6.04	5.90	5.76	0.43
0.03	6.39	6.25	6.11	5.97	0.42
0.04	6.64	6.50	6.38	6.25	0.39
Max. diff.	0.55	0.56	0.59	0.60	

(See notes on p. 139.)

Appendix 3.1 - Results of simulation using Method A (continued)

Input geometry data: L = 250 ft B = 85 ft P = 13.0 ft Input flow conditions: Q_u = 4875 cfs h_d = 0.90 ft

Calculated Q_w (cfs)

	Slope				
Manning's n	0.000385	0.0008	0.0012	0.0016	Max. diff.
0.0125	523	523	523	523	0
0.02	523	523	523	523	0
0.03	523	523	523	523	0
0.04	523	523	523	523	0
Max. diff.	0	0	0	0	

Calculated h_u (ft)

	Slope				
Manning's n	0.000385	0.0008	0.0012	0.0016	Max. diff.
0.0125	0.73	0.63	0.52	0.42	0.31
0.02	0.74	0.64	0.53	0.43	0.31
0.03	0.76	0.66	0.55	0.45	0.31
0.04	0.79	0.68	0.58	0.48	0.31
Max. diff.	0.06	0.05	0.06	0.06	

Input geometry data: L = 250 ft B = 85 ft P = 13.0 ft Input flow conditions: Q_u = 4947 cfs h_d = 2.33 ft

Calculated Q_w (cfs)

	Slope				
Manning's n	0.000385	0.0008	0.0012	0.0016	Max. diff.
0.0125	2431	2431	2431	2431	0
0.02	2431	2431	2431	2431	0
0.03	2431	2431	2431	2431	0
0.04	2431	2431	2431	2431	0
Max. diff.	0	0	0	0	

Calculated h_u (ft)

	Slope				
Manning's n	0.000385	0.0008	0.0012	0.0016	Max. diff.
0.0125	2.12	2.02	1.92	1.81	0.31
0.02	2.13	2.02	1.92	1.82	0.31
0.03	2.14	2.03	1.93	1.83	0.31
0.04	2.15	2.05	1.95	1.84	0.31
Max. diff.	0.03	0.03	0.03	0.03	

Input geometry data: L = 375 ft B = 45 ft P = 13.0 ft Input flow conditions: Q_u = 10222 cfs h_d = 2.27 ft

Calculated Q_w (cfs)

	Slope				
Manning's n	0.000385	0.0008	0.0012	0.0016	Max. diff.
0.0125	2657	2657	2657	2657	0
0.02	2657	2657	2657	2657	0
0.03	2657	2657	2657	2657	0
0.04	2657	2657	2657	2657	0
Max. diff.	0	0	0	0	

Calculated h_u (ft)

	Slope				
Manning's n	0.000385	0.0008	0.0012	0.0016	Max. diff.
0.0125	1.54	1.34	1.15	0.95	0.59
0.02	1.68	1.49	1.30	1.11	0.57
0.03	1.94	1.75	1.58	1.40	0.54
0.04	2.26	2.09	1.92	1.76	0.50
Max. diff.	0.72	0.75	0.77	0.81	

(See notes on p. 139.)

Appendix 3.1 - Results of simulation using Method A (continued)

Input geometry data: L = 375 ft B = 45 ft P = 13.0 ft Input flow conditions: Q_u = 10147 cfs h_d = 3.43 ft

Calculated Q_w (cfs)

	Slope				
Manning's n	0.000385	0.0008	0.0012	0.0016	Max. diff.
0.0125	5595	5595	5595	5595	0
0.02	5595	5595	5595	5595	0
0.03	5595	5595	5595	5595	0
0.04	5595	5595	5595	5595	0
Max. diff.	0	0	0	0	

Calculated h_u (ft)

	Slope				
Manning's n	0.000385	0.0008	0.0012	0.0016	Max. diff.
0.0125	2.77	2.58	2.40	2.22	0.55
0.02	2.84	2.66	2.48	2.31	0.53
0.03	2.99	2.81	2.64	2.47	0.52
0.04	3.17	3.01	2.84	2.68	0.49
Max. diff.	0.40	0.43	0.44	0.46	

Input geometry data: L = 375 ft B = 45 ft P = 13.0 ft Input flow conditions: Q_u = 19709 cfs h_d = 3.55 ft

Calculated Q_w (cfs)

	Slope				
Manning's n	0.000385	0.0008	0.0012	0.0016	Max. diff.
0.0125	4720	4720	4720	4720	0
0.02	4720	4720	4720	4720	0
0.03	4720	4720	4720	4720	0
0.04	4720	4720	4720	4720	0
Max. diff.	0	0	0	0	

Calculated h_u (ft)

	Slope				
Manning's n	0.000385	0.0008	0.0012	0.0016	Max. diff.
0.0125	(1)	(1)	(1)	(1)	
0.02	1.19	(1)	(1)	(1)	
0.03	2.92	2.64	2.36	2.06	0.86
0.04	4.05	3.85	3.65	3.44	0.61
Max. diff.	2.86	1.21	1.29	1.38	

Input geometry data: L = 375 ft B = 45 ft P = 13.0 ft Input flow conditions: Q_u = 19784 cfs h_d = 5.53 ft

Calculated Q_w (cfs)

	Slope				
Manning's n	0.000385	0.0008	0.0012	0.0016	Max. diff.
0.0125	11534	11534	11534	11534	0
0.02	11534	11534	11534	11534	0
0.03	11534	11534	11534	11534	0
0.04	11534	11534	11534	11534	0
Max. diff.	0	0	0	0	

Calculated h_u (ft)

	Slope				
Manning's n	0.000385	0.0008	0.0012	0.0016	Max. diff.
0.0125	3.80	3.49	3.17	2.82	0.98
0.02	4.11	3.84	3.57	3.28	0.83
0.03	4.61	4.38	4.16	3.93	0.68
0.04	5.15	4.96	4.77	4.57	0.58
Max. diff.	1.35	1.47	1.60	1.75	

(See notes on p. 139.)

Appendix 3.1 - Results of simulation using Method A (continued)

Input geometry data: L = 250 ft B = 45 ft P = 13.0 ft Input flow conditions: Q_u = 9997 cfs h_d = 1.70 ft

Calculated Q_w (cfs)

	Slope				
Manning's n	0.000385	0.0008	0.0012	0.0016	Max. diff.
0.0125	1080	1080	1080	1080	0
0.02	1080	1080	1080	1080	0
0.03	1080	1080	1080	1080	0
0.04	1080	1080	1080	1080	0
Max. diff.	0	0	0	0	

Calculated h_u (ft)

	Slope				
Manning's n	0.000385	0.0008	0.0012	0.0016	Max. diff.
0.0125	1.23	1.09	0.96	0.83	0.40
0.02	1.34	1.21	1.08	0.95	0.39
0.03	1.56	1.43	1.31	1.19	0.37
0.04	1.84	1.72	1.60	1.49	0.35
Max. diff.	0.61	0.63	0.64	0.66	

Input geometry data: L = 250 ft B = 45 ft P = 13.0 ft Input flow conditions: Q_u = 10084 cfs h_d = 3.70 ft

Calculated Q_w (cfs)

	Slope				
Manning's n	0.000385	0.0008	0.0012	0.0016	Max. diff.
0.0125	4465	4465	4465	4465	0
0.02	4465	4465	4465	4465	0
0.03	4465	4465	4465	4465	0
0.04	4465	4465	4465	4465	0
Max. diff.	0	0	0	0	

Calculated h_u (ft)

	Slope				
Manning's n	0.000385	0.0008	0.0012	0.0016	Max. diff.
0.0125	3.15	3.03	2.91	2.79	0.36
0.02	3.20	3.07	2.96	2.84	0.36
0.03	3.29	3.17	3.06	2.94	0.35
0.04	3.42	3.30	3.19	3.08	0.34
Max. diff.	0.27	0.27	0.28	0.29	

Input geometry data: L = 250 ft B = 45 ft P = 13.0 ft Input flow conditions: Q_u = 20034 cfs h_d = 3.25 ft

Calculated Q_w (cfs)

	Slope				
Manning's n	0.000385	0.0008	0.0012	0.0016	Max. diff.
0.0125	2666	2666	2666	2666	0
0.02	2666	2666	2666	2666	0
0.03	2666	2666	2666	2666	0
0.04	2666	2666	2666	2666	0
Max. diff.	0	0	0	0	

Calculated h_u (ft)

	Slope				
Manning's n	0.000385	0.0008	0.0012	0.0016	Max. diff.
0.0125	(1)	(1)	(1)	(1)	
0.02	(1)	(1)	(1)	(1)	
0.03	2.82	2.60	2.37	2.13	0.69
0.04	3.88	3.72	3.57	3.41	0.47
Max. diff.	1.06	1.12	1.20	1.28	

(See notes on p. 139.)

Appendix 3.1 - Results of simulation using Method A (continued)

Input geometry data: L = 250 ft B = 45 ft P = 13.0 ft Input flow conditions: Q_u = 19928 cfs h_d = 6.42 ft

Calculated Q_w (cfs)

	Slope				
Manning's n	0.000385	0.0008	0.0012	0.0016	Max. diff.
0.0125	10657	10657	10657	10657	0
0.02	10657	10657	10657	10657	0
0.03	10657	10657	10657	10657	0
0.04	10657	10657	10657	10657	0
Max. diff.	0	0	0	0	

Calculated h_u (ft)

	Slope				
Manning's n	0.000385	0.0008	0.0012	0.0016	Max. diff.
0.0125	5.12	4.95	4.79	4.62	0.50
0.02	5.26	5.10	4.94	4.79	0.47
0.03	5.52	5.37	5.23	5.08	0.44
0.04	5.84	5.70	5.57	5.44	0.40
Max. diff.	0.72	0.75	0.78	0.82	

Input geometry data: L = 500 ft B = 85 ft P = 17.5 ft Input flow conditions: Q_u = 10003 cfs h_d = 0.95 ft

Calculated Q_w (cfs)

	Slope				
Manning's n	0.000385	0.0008	0.0012	0.0016	Max. diff.
0.0125	998	998	998	998	0
0.02	998	998	998	998	0
0.03	998	998	998	998	0
0.04	998	998	998	998	0
Max. diff.	0	0	0	0	

Calculated h_u (ft)

	Slope				
Manning's n	0.000385	0.0008	0.0012	0.0016	Max. diff.
0.0125	0.64	0.42	0.21	0.00	0.64
0.02	0.66	0.45	0.24	0.03	0.63
0.03	0.72	0.51	0.30	0.10	0.62
0.04	0.81	0.60	0.39	0.19	0.62
Max. diff.	0.17	0.18	0.18	0.19	

Input geometry data: L = 500 ft B = 85 ft P = 17.5 ft Input flow conditions: Q_u = 9975 cfs h_d = 2.53 ft

Calculated Q_w (cfs)

	Slope				
Manning's n	0.000385	0.0008	0.0012	0.0016	Max. diff.
0.0125	5068	5068	5068	5068	0
0.02	5068	5068	5068	5068	0
0.03	5068	5068	5068	5068	0
0.04	5068	5068	5068	5068	0
Max. diff.	0	0	0	0	

Calculated h_u (ft)

	Slope				
Manning's n	0.000385	0.0008	0.0012	0.0016	Max. diff.
0.0125	2.15	1.93	1.73	1.52	0.63
0.02	2.16	1.95	1.74	1.54	0.62
0.03	2.19	1.98	1.77	1.57	0.62
0.04	2.23	2.02	1.82	1.62	0.61
Max. diff.	0.08	0.09	0.09	0.10	

(See notes on p. 139.)

Appendix 3.1 - Results of simulation using Method A (continued)

Input geometry data: L = 500 ft B = 85 ft P = 17.5 ft Input flow conditions: Q_u = 29766 cfs h_d = 2.23 ft

Calculated Q_w (cfs)

	Slope				
Manning's n	0.000385	0.0008	0.0012	0.0016	Max. diff.
0.0125	2964	2964	2964	2964	0
0.02	2964	2964	2964	2964	0
0.03	2964	2964	2964	2964	0
0.04	2964	2964	2964	2964	0
Max. diff.	0	0	0	0	

Calculated h_u (ft)

	Slope				
Manning's n	0.000385	0.0008	0.0012	0.0016	Max. diff.
0.0125	1.21	0.90	0.60	0.29	0.92
0.02	1.50	1.21	0.93	0.64	0.86
0.03	2.03	1.77	1.52	1.26	0.77
0.04	2.67	2.43	2.20	1.97	0.70
Max. diff.	1.46	1.53	1.60	1.68	

Input geometry data: L = 500 ft B = 85 ft P = 17.5 ft Input flow conditions: Q_u = 29828 cfs h_d = 5.17 ft

Calculated Q_w (cfs)

	Slope				
Manning's n	0.000385	0.0008	0.0012	0.0016	Max. diff.
0.0125	14738	14738	14738	14738	0
0.02	14738	14738	14738	14738	0
0.03	14738	14738	14738	14738	0
0.04	14738	14738	14738	14738	0
Max. diff.	0	0	0	0	

Calculated h_u (ft)

	Slope				
Manning's n	0.000385	0.0008	0.0012	0.0016	Max. diff.
0.0125	4.05	3.80	3.54	3.29	0.76
0.02	4.16	3.91	3.66	3.42	0.74
0.03	4.37	4.13	3.90	3.66	0.71
0.04	4.65	4.42	4.19	3.97	0.68
Max. diff.	0.60	0.62	0.65	0.68	

Input geometry data: L = 250 ft B = 85 ft P = 17.5 ft Input flow conditions: Q_u = 10219 cfs h_d = 1.25 ft

Calculated Q_w (cfs)

	Slope				
Manning's n	0.000385	0.0008	0.0012	0.0016	Max. diff.
0.0125	842	842	842	842	0
0.02	842	842	842	842	0
0.03	842	842	842	842	0
0.04	842	842	842	842	0
Max. diff.	0	0	0	0	

Calculated h_u (ft)

	Slope				
Manning's n	0.000385	0.0008	0.0012	0.0016	Max. diff.
0.0125	1.06	0.95	0.85	0.74	0.32
0.02	1.07	0.97	0.86	0.76	0.31
0.03	1.10	1.00	0.89	0.79	0.31
0.04	1.14	1.04	0.93	0.83	0.31
Max. diff.	0.08	0.09	0.08	0.09	

(See notes on p. 139.)

Appendix 3.1 - Results of simulation using Method A (continued)

Input geometry data: L = 250 ft B = 85 ft P = 17.5 ft Input flow conditions: Q_u = 10225 cfs h_d = 3.72 ft

Calculated Q_w (cfs)

	Slope				
Manning's n	0.000385	0.0008	0.0012	0.0016	Max. diff.
0.0125	5215	5215	5215	5215	0
0.02	5215	5215	5215	5215	0
0.03	5215	5215	5215	5215	0
0.04	5215	5215	5215	5215	0
Max. diff.	0	0	0	0	

Calculated h_u (ft)

	Slope				
Manning's n	0.000385	0.0008	0.0012	0.0016	Max. diff.
0.0125	3.48	3.37	3.27	3.17	0.31
0.02	3.49	3.38	3.28	3.18	0.31
0.03	3.50	3.39	3.29	3.19	0.31
0.04	3.52	3.41	3.31	3.21	0.31
Max. diff.	0.04	0.04	0.04	0.04	

Input geometry data: L = 250 ft B = 85 ft P = 17.5 ft Input flow conditions: Q_u = 29972 cfs h_d = 3.10 ft

Calculated Q_w (cfs)

	Slope				
Manning's n	0.000385	0.0008	0.0012	0.0016	Max. diff.
0.0125	3023	3023	3023	3023	0
0.02	3023	3023	3023	3023	0
0.03	3023	3023	3023	3023	0
0.04	3023	3023	3023	3023	0
Max. diff.	0	0	0	0	

Calculated h_u (ft)

	Slope				
Manning's n	0.000385	0.0008	0.0012	0.0016	Max. diff.
0.0125	2.39	2.25	2.11	1.97	0.42
0.02	2.50	2.37	2.23	2.10	0.40
0.03	2.73	2.60	2.47	2.34	0.39
0.04	3.03	2.90	2.78	2.65	0.38
Max. diff.	0.64	0.65	0.67	0.68	

Input geometry data: L = 250 ft B = 85 ft P = 17.5 ft Input flow conditions: Q_u = 29938 cfs h_d = 6.95 ft

Calculated Q_w (cfs)

	Slope				
Manning's n	0.000385	0.0008	0.0012	0.0016	Max. diff.
0.0125	13816	13816	13816	13816	0
0.02	13816	13816	13816	13816	0
0.03	13816	13816	13816	13816	0
0.04	13816	13816	13816	13816	0
Max. diff.	0	0	0	0	

Calculated h_u (ft)

	Slope				
Manning's n	0.000385	0.0008	0.0012	0.0016	Max. diff.
0.0125	6.21	6.09	5.97	5.85	0.36
0.02	6.25	6.13	6.01	5.89	0.36
0.03	6.32	6.20	6.09	5.97	0.35
0.04	6.43	6.31	6.20	6.08	0.35
Max. diff.	0.22	0.22	0.23	0.23	

(See notes on p. 139.)

Appendix 3.1 - Results of simulation using Method A (continued)

Input geometry data: L = 500 ft B = 45 ft P = 17.5 ft Input flow conditions: Q_u = 10181 cfs h_d = 1.35 ft

Calculated Q_w (cfs)

	Slope				
Manning's n	0.000385	0.0008	0.0012	0.0016	Max. diff.
0.0125	1499	1499	1499	1499	0
0.02	1499	1499	1499	1499	0
0.03	1499	1499	1499	1499	0
0.04	1499	1499	1499	1499	0
Max. diff.	0	0	0	0	

Calculated h_u (ft)

	Slope				
Manning's n	0.000385	0.0008	0.0012	0.0016	Max. diff.
0.0125	0.92	0.69	0.47	0.25	0.67
0.02	0.99	0.76	0.55	0.33	0.66
0.03	1.13	0.91	0.69	0.48	0.65
0.04	1.31	1.10	0.89	0.68	0.63
Max. diff.	0.39	0.41	0.42	0.43	

Input geometry data: L = 500 ft B = 45 ft P = 17.5 ft Input flow conditions: Q_u = 10122 cfs h_d = 2.57 ft

Calculated Q_w (cfs)

	Slope				
Manning's n	0.000385	0.0008	0.0012	0.0016	Max. diff.
0.0125	4604	4604	4604	4604	0
0.02	4604	4604	4604	4604	0
0.03	4604	4604	4604	4604	0
0.04	4604	4604	4604	4604	0
Max. diff.	0	0	0	0	

Calculated h_u (ft)

	Slope				
Manning's n	0.000385	0.0008	0.0012	0.0016	Max. diff.
0.0125	2.09	1.86	1.65	1.43	0.66
0.02	2.13	1.90	1.69	1.48	0.65
0.03	2.21	1.99	1.78	1.57	0.64
0.04	2.31	2.10	1.89	1.69	0.62
Max. diff.	0.22	0.24	0.24	0.26	

Input geometry data: L = 500 ft B = 45 ft P = 17.5 ft Input flow conditions: Q_u = 30012 cfs h_d = 3.00 ft

Calculated Q_w (cfs)

	Slope				
Manning's n	0.000385	0.0008	0.0012	0.0016	Max. diff.
0.0125	3977	3977	3977	3977	0
0.02	3977	3977	3977	3977	0
0.03	3977	3977	3977	3977	0
0.04	3977	3977	3977	3977	0
Max. diff.	0	0	0	0	

Calculated h_u (ft)

	Slope				
Manning's n	0.000385	0.0008	0.0012	0.0016	Max. diff.
0.0125	(1)	(1)	(1)	(1)	
0.02	1.46	0.85	0.00	(1)	1.46
0.03	3.10	2.76	2.43	2.08	1.02
0.04	4.48	4.22	3.96	3.70	0.78
Max. diff.	3.02	3.37	3.96	1.62	

(See notes on p. 139.)

Appendix 3.1 - Results of simulation using Method A (continued)

Input geometry data: L = 500 ft B = 45 ft P = 17.5 ft Input flow conditions: Q_u = 29906 cfs h_d = 5.70 ft

Calculated Q_w (cfs)

	Slope				
Manning's n	0.000385	0.0008	0.0012	0.0016	Max. diff.
0.0125	15172	15172	15172	15172	0
0.02	15172	15172	15172	15172	0
0.03	15172	15172	15172	15172	0
0.04	15172	15172	15172	15172	0
Max. diff.	0	0	0	0	

Calculated h_u (ft)

	Slope				
Manning's n	0.000385	0.0008	0.0012	0.0016	Max. diff.
0.0125	3.78	3.40	3.01	2.59	1.19
0.02	4.13	3.79	3.45	3.09	1.04
0.03	4.72	4.42	4.14	3.84	0.88
0.04	5.37	5.11	4.86	4.61	0.76
Max. diff.	1.59	1.71	1.85	2.02	

Input geometry data: L = 250 ft B = 45 ft P = 17.5 ft Input flow conditions: Q_u = 9900 cfs h_d = 1.35 ft

Calculated Q_w (cfs)

	Slope				
Manning's n	0.000385	0.0008	0.0012	0.0016	Max. diff.
0.0125	835	835	835	835	0
0.02	835	835	835	835	0
0.03	835	835	835	835	0
0.04	835	835	835	835	0
Max. diff.	0	0	0	0	

Calculated h_u (ft)

	Slope				
Manning's n	0.000385	0.0008	0.0012	0.0016	Max. diff.
0.0125	1.11	1.00	0.89	0.78	0.33
0.02	1.15	1.03	0.93	0.82	0.33
0.03	1.22	1.10	1.00	0.89	0.33
0.04	1.31	1.20	1.09	0.99	0.32
Max. diff.	0.20	0.20	0.20	0.21	

Input geometry data: L = 250 ft B = 45 ft P = 17.5 ft Input flow conditions: Q_u = 9944 cfs h_d = 3.88 ft

Calculated Q_w (cfs)

	Slope				
Manning's n	0.000385	0.0008	0.0012	0.0016	Max. diff.
0.0125	5175	5175	5175	5175	0
0.02	5175	5175	5175	5175	0
0.03	5175	5175	5175	5175	0
0.04	5175	5175	5175	5175	0
Max. diff.	0	0	0	0	

Calculated h_u (ft)

	Slope				
Manning's n	0.000385	0.0008	0.0012	0.0016	Max. diff.
0.0125	3.57	3.46	3.36	3.25	0.32
0.02	3.59	3.48	3.37	3.27	0.32
0.03	3.61	3.51	3.40	3.30	0.31
0.04	3.65	3.54	3.44	3.34	0.31
Max. diff.	0.08	0.08	0.08	0.09	

(See notes on p. 139.)

Appendix 3.1 - Results of simulation using Method A (continued)

Input geometry data: L = 250 ft B = 45 ft P = 17.5 ft Input flow conditions: Q_u = 29991 cfs h_d = 3.43 ft

Calculated Q_w (cfs)

	Slope				
Manning's n	0.000385	0.0008	0.0012	0.0016	Max. diff.
0.0125	2925	2925	2925	2925	0
0.02	2925	2925	2925	2925	0
0.03	2925	2925	2925	2925	0
0.04	2925	2925	2925	2925	0
Max. diff.	0	0	0	0	

Calculated h_u (ft)

	Slope				
Manning's n	0.000385	0.0008	0.0012	0.0016	Max. diff.
0.0125	1.76	1.43	1.05	0.52	1.24
0.02	2.31	2.06	1.80	1.52	0.79
0.03	3.11	2.92	2.74	2.54	0.57
0.04	3.94	3.79	3.63	3.48	0.46
Max. diff.	2.18	2.36	2.58	2.96	

Input geometry data: L = 250 ft B = 45 ft P = 17.5 ft Input flow conditions: Q_u = 29969 cfs h_d = 6.45 ft

Calculated Q_w (cfs)

	Slope				
Manning's n	0.000385	0.0008	0.0012	0.0016	Max. diff.
0.0125	10778	10778	10778	10778	0
0.02	10778	10778	10778	10778	0
0.03	10778	10778	10778	10778	0
0.04	10778	10778	10778	10778	0
Max. diff.	0	0	0	0	

Calculated h_u (ft)

	Slope				
Manning's n	0.000385	0.0008	0.0012	0.0016	Max. diff.
0.0125	5.14	4.98	4.82	4.66	0.48
0.02	5.28	5.13	4.97	4.82	0.46
0.03	5.55	5.40	5.26	5.11	0.44
0.04	5.89	5.75	5.62	5.48	0.41
Max. diff.	0.75	0.77	0.80	0.82	

(See notes on p. 139.)

Appendix 3.2 - Results of simulation using Method B

Input geometry data: L = 598 ft B = 85 ft P = 13.0 ft Input flow conditions: Q_u = 10156 cfs h_d = 0.97 ft

Calculated Q_w (cfs)

	Slope				
Manning's n	0.000385	0.0008	0.0012	0.0016	Max. diff.
0.0125	951	739	564	430	521
0.02	1039	821	637	485	554
0.03	1216	991	795	622	594
0.04	1461	1226	1020	832	629
Max. diff.	510	487	456	402	

Calculated h_u (ft)

	Slope				
Manning's n	0.000385	0.0008	0.0012	0.0016	Max. diff.
0.0125	0.66	0.41	0.16	-0.10	0.76
0.02	0.76	0.51	0.28	0.03	0.73
0.03	0.95	0.72	0.49	0.27	0.68
0.04	1.18	0.97	0.76	0.55	0.63
Max. diff.	0.52	0.56	0.60	0.65	

Input geometry data: L = 598 ft B = 85 ft P = 13.0 ft Input flow conditions: Q_u = 10116 cfs h_d = 2.30 ft

Calculated Q_w (cfs)

	Slope				
Manning's n	0.000385	0.0008	0.0012	0.0016	Max. diff.
0.0125	4801	4348	3924	3523	1278
0.02	4875	4429	4010	3612	1263
0.03	5019	4587	4179	3787	1232
0.04	5203	4789	4399	4018	1185
Max. diff.	402	441	475	495	

Calculated h_u (ft)

	Slope				
Manning's n	0.000385	0.0008	0.0012	0.0016	Max. diff.
0.0125	1.81	1.55	1.29	1.03	0.78
0.02	1.87	1.61	1.35	1.10	0.77
0.03	1.97	1.72	1.48	1.24	0.73
0.04	2.10	1.87	1.64	1.41	0.69
Max. diff.	0.29	0.32	0.35	0.38	

Input geometry data: L = 598 ft B = 85 ft P = 13.0 ft Input flow conditions: Q_u = 29894 cfs h_d = 4.03 ft

Calculated Q_w (cfs)

	Slope				
Manning's n	0.000385	0.0008	0.0012	0.0016	Max. diff.
0.0125	6407	(2)	(3)	(3)	
0.02	8104	7287	6478	5642	2462
0.03	10257	9598	8987	8382	1875
0.04	12380	11819	11266	10715	1665
Max. diff.	5973	4532	4788	5073	

Calculated h_u (ft)

	Slope				
Manning's n	0.000385	0.0008	0.0012	0.0016	Max. diff.
0.0125	1.39	(2)	(3)	(3)	
0.02	2.29	1.97	1.65	1.32	0.97
0.03	3.28	3.05	2.84	2.63	0.65
0.04	4.20	4.02	3.83	3.64	0.56
Max. diff.	2.81	2.05	2.18	2.32	

(See notes on p. 139.)

Appendix 3.2 - Results of simulation using Method B (continued)

Input geometry data: L = 598 ft B = 85 ft P = 13.0 ft Input flow conditions: Q_u = 30144 cfs h_d = 4.85 ft

Calculated Q_w (cfs)

	Slope				
Manning's n	0.000385	0.0008	0.0012	0.0016	Max. diff.
0.0125	10338	9104	(3)	(2)	1234
0.02	11947	10916	9875	8950	2997
0.03	14069	13247	12401	11675	2394
0.04	15895	15268	14656	14034	1861
Max. diff.	5557	6164	4781	5084	

Calculated h_u (ft)

	Slope				
Manning's n	0.000385	0.0008	0.0012	0.0016	Max. diff.
0.0125	1.95	1.45	(3)	(2)	0.50
0.02	2.79	2.39	1.96	1.66	1.13
0.03	3.85	3.52	3.16	2.93	0.92
0.04	4.69	4.48	4.27	4.04	0.65
Max. diff.	2.74	3.03	2.31	2.38	

Input geometry data: L = 250 ft B = 85 ft P = 13.0 ft Input flow conditions: Q_u = 30022 cfs h_d = 3.55 ft

Calculated Q_w (cfs)

	Slope				
Manning's n	0.000385	0.0008	0.0012	0.0016	Max. diff.
0.0125	2845	2661	2469	2243	602
0.02	3174	3014	2856	2692	482
0.03	3721	3583	3449	3314	407
0.04	4368	4238	4112	3986	382
Max. diff.	1523	1577	1643	1743	

Calculated h_u (ft)

	Slope				
Manning's n	0.000385	0.0008	0.0012	0.0016	Max. diff.
0.0125	2.13	1.83	1.46	0.85	1.28
0.02	2.63	2.42	2.20	1.96	0.67
0.03	3.33	3.18	3.03	2.87	0.46
0.04	4.05	3.92	3.79	3.66	0.39
Max. diff.	1.92	2.09	2.33	2.81	

Input geometry data: L = 250 ft B = 85 ft P = 13.0 ft Input flow conditions: Q_u = 29969 cfs h_d = 7.50 ft

Calculated Q_w (cfs)

	Slope				
Manning's n	0.000385	0.0008	0.0012	0.0016	Max. diff.
0.0125	15596	15380	15170	14960	636
0.02	15699	15487	15280	15073	626
0.03	15903	15696	15496	15295	608
0.04	16170	15971	15778	15586	584
Max. diff.	574	591	608	626	

Calculated h_u (ft)

	Slope				
Manning's n	0.000385	0.0008	0.0012	0.0016	Max. diff.
0.0125	6.51	6.37	6.23	6.09	0.42
0.02	6.59	6.46	6.32	6.19	0.40
0.03	6.75	6.63	6.50	6.37	0.38
0.04	6.96	6.84	6.73	6.61	0.35
Max. diff.	0.45	0.47	0.50	0.52	

(See notes on p. 139.)

Appendix 3.2 - Results of simulation using Method B (continued)

Input geometry data: L = 250 ft B = 85 ft P = 13.0 ft Input flow conditions: Q_u = 4875 cfs h_d = 0.90 ft

Calculated Q_w (cfs)

	Slope				
Manning's n	0.000385	0.0008	0.0012	0.0016	Max. diff.
0.0125	481	437	397	358	123
0.02	485	441	400	362	123
0.03	493	449	408	370	123
0.04	504	460	419	380	124
Max. diff.	23	23	22	22	

Calculated h_u (ft)

	Slope				
Manning's n	0.000385	0.0008	0.0012	0.0016	Max. diff.
0.0125	0.78	0.67	0.57	0.47	0.31
0.02	0.79	0.68	0.58	0.48	0.31
0.03	0.81	0.70	0.60	0.51	0.30
0.04	0.83	0.73	0.63	0.53	0.30
Max. diff.	0.05	0.06	0.06	0.06	

Input geometry data: L = 250 ft B = 85 ft P = 13.0 ft Input flow conditions: Q_u = 4947 cfs h_d = 2.33 ft

Calculated Q_w (cfs)

	Slope				
Manning's n	0.000385	0.0008	0.0012	0.0016	Max. diff.
0.0125	2451	2367	2287	2208	243
0.02	2454	2370	2290	2211	243
0.03	2460	2376	2296	2218	242
0.04	2469	2385	2305	2227	242
Max. diff.	18	18	18	19	

Calculated h_u (ft)

	Slope				
Manning's n	0.000385	0.0008	0.0012	0.0016	Max. diff.
0.0125	2.17	2.07	1.96	1.86	0.31
0.02	2.18	2.07	1.97	1.87	0.31
0.03	2.19	2.08	1.98	1.88	0.31
0.04	2.20	2.09	1.99	1.89	0.31
Max. diff.	0.03	0.02	0.03	0.03	

Input geometry data: L = 375 ft B = 45 ft P = 13.0 ft Input flow conditions: Q_u = 10222 cfs h_d = 2.27 ft

Calculated Q_w (cfs)

	Slope				
Manning's n	0.000385	0.0008	0.0012	0.0016	Max. diff.
0.0125	2604	2422	2251	2085	519
0.02	2715	2535	2367	2203	512
0.03	2927	2753	2590	2430	497
0.04	3201	3029	2871	2717	484
Max. diff.	597	607	620	632	

Calculated h_u (ft)

	Slope				
Manning's n	0.000385	0.0008	0.0012	0.0016	Max. diff.
0.0125	1.64	1.47	1.30	1.13	0.51
0.02	1.75	1.59	1.43	1.27	0.48
0.03	1.97	1.82	1.67	1.52	0.45
0.04	2.23	2.09	1.96	1.83	0.40
Max. diff.	0.59	0.62	0.66	0.70	

(See notes on p. 139.)

Appendix 3.2 - Results of simulation using Method B (continued)

Input geometry data: L = 375 ft B = 45 ft P = 13.0 ft Input flow conditions: Q_u = 10147 cfs h_d = 3.43 ft

Calculated Q_w (cfs)

	Slope				
Manning's n	0.000385	0.0008	0.0012	0.0016	Max. diff.
0.0125	5708	5479	5261	5042	666
0.02	5776	5550	5336	5122	654
0.03	5910	5688	5481	5276	634
0.04	6085	5869	5667	5471	614
Max. diff.	377	390	406	429	

Calculated h_u (ft)

	Slope				
Manning's n	0.000385	0.0008	0.0012	0.0016	Max. diff.
0.0125	2.77	2.62	2.45	2.28	0.49
0.02	2.82	2.69	2.53	2.36	0.46
0.03	2.93	2.81	2.67	2.52	0.41
0.04	3.07	2.95	2.84	2.71	0.36
Max. diff.	0.30	0.33	0.39	0.43	

Input geometry data: L = 375 ft B = 45 ft P = 13.0 ft Input flow conditions: Q_u = 19709 cfs h_d = 3.55 ft

Calculated Q_w (cfs)

	Slope				
Manning's n	0.000385	0.0008	0.0012	0.0016	Max. diff.
0.0125	(2)	(3)	(3)	(3)	
0.02	3969	3578	3167	(3)	802
0.03	5199	4925	4661	4394	805
0.04	6342	6083	5863	5646	696
Max. diff.	2373	2505	2696	1252	

Calculated h_u (ft)

	Slope				
Manning's n	0.000385	0.0008	0.0012	0.0016	Max. diff.
0.0125	(2)	(3)	(3)	(3)	
0.02	1.99	1.71	1.43	(3)	0.56
0.03	2.97	2.80	2.64	2.47	0.50
0.04	3.79	3.63	3.50	3.38	0.41
Max. diff.	1.80	1.92	2.07	0.91	

Input geometry data: L = 375 ft B = 45 ft P = 13.0 ft Input flow conditions: Q_u = 19784 cfs h_d = 5.53 ft

Calculated Q_w (cfs)

	Slope				
Manning's n	0.000385	0.0008	0.0012	0.0016	Max. diff.
0.0125	10427	10025	9610	9156	1271
0.02	10785	10424	10061	9680	1105
0.03	11387	11069	10766	10453	934
0.04	(4)	11796	11513	11237	559
Max. diff.	960	1771	1903	2081	

Calculated h_u (ft)

	Slope				
Manning's n	0.000385	0.0008	0.0012	0.0016	Max. diff.
0.0125	3.91	3.66	3.39	3.08	0.83
0.02	4.17	3.97	3.75	3.51	0.66
0.03	4.49	4.39	4.27	4.10	0.39
0.04	(4)	4.74	4.65	4.57	0.17
Max. diff.	0.58	1.08	1.26	1.49	

(See notes on p. 139.)

Appendix 3.2 - Results of simulation using Method B (continued)

Input geometry data: L = 250 ft B = 45 ft P = 13.0 ft Input flow conditions: Q_u = 9997 cfs h_d = 1.70 ft

Calculated Q_w (cfs)

	Slope				
Manning's n	0.000385	0.0008	0.0012	0.0016	Max. diff.
0.0125	1064	999	939	880	184
0.02	1116	1051	990	931	185
0.03	1219	1155	1094	1035	184
0.04	1360	1294	1233	1174	186
Max. diff.	296	295	294	294	

Calculated h_u (ft)

	Slope				
Manning's n	0.000385	0.0008	0.0012	0.0016	Max. diff.
0.0125	1.34	1.22	1.11	0.99	0.35
0.02	1.44	1.33	1.21	1.10	0.34
0.03	1.63	1.52	1.42	1.31	0.32
0.04	1.87	1.77	1.67	1.57	0.30
Max. diff.	0.53	0.55	0.56	0.58	

Input geometry data: L = 250 ft B = 45 ft P = 13.0 ft Input flow conditions: Q_u = 10084 cfs h_d = 3.70 ft

Calculated Q_w (cfs)

	Slope				
Manning's n	0.000385	0.0008	0.0012	0.0016	Max. diff.
0.0125	4728	4608	4492	4376	352
0.02	4764	4645	4530	4416	348
0.03	4835	4718	4606	4494	341
0.04	4929	4816	4707	4598	331
Max. diff.	201	208	215	222	

Calculated h_u (ft)

	Slope				
Manning's n	0.000385	0.0008	0.0012	0.0016	Max. diff.
0.0125	3.21	3.09	2.97	2.84	0.37
0.02	3.25	3.13	3.02	2.90	0.35
0.03	3.34	3.22	3.11	3.00	0.34
0.04	3.46	3.34	3.24	3.13	0.33
Max. diff.	0.25	0.25	0.27	0.29	

Input geometry data: L = 250 ft B = 45 ft P = 13.0 ft Input flow conditions: Q_u = 20034 cfs h_d = 3.25 ft

Calculated Q_w (cfs)

	Slope				
Manning's n	0.000385	0.0008	0.0012	0.0016	Max. diff.
0.0125	(3)	(3)	(3)	(3)	
0.02	2343	2155	1940	(2)	403
0.03	3087	2942	2800	2654	433
0.04	3797	3678	3563	3448	349
Max. diff.	1454	1523	1623	794	

Calculated h_u (ft)

	Slope				
Manning's n	0.000385	0.0008	0.0012	0.0016	Max. diff.
0.0125	(3)	(3)	(3)	(3)	
0.02	1.93	1.66	1.19	(2)	0.74
0.03	2.96	2.80	2.64	2.46	0.50
0.04	3.77	3.65	3.54	3.42	0.35
Max. diff.	1.84	1.99	2.35	0.96	

(See notes on p. 139.)

Appendix 3.2 - Results of simulation using Method B (continued)

Input geometry data: L = 250 ft B = 45 ft P = 13.0 ft Input flow conditions: Q_u = 19928 cfs h_d = 6.42 ft

Calculated Q_w (cfs)

	Slope				
Manning's n	0.000385	0.0008	0.0012	0.0016	Max. diff.
0.0125	10959	10768	10582	10394	565
0.02	11082	10898	10718	10536	546
0.03	11319	11143	10974	10803	516
0.04	11624	11455	11293	11133	491
Max. diff.	665	687	711	739	

Calculated h_u (ft)

	Slope				
Manning's n	0.000385	0.0008	0.0012	0.0016	Max. diff.
0.0125	5.31	5.17	5.04	4.89	0.42
0.02	5.41	5.30	5.17	5.03	0.38
0.03	5.58	5.49	5.40	5.29	0.29
0.04	5.81	5.72	5.64	5.56	0.25
Max. diff.	0.50	0.55	0.60	0.67	

Input geometry data: L = 500 ft B = 85 ft P = 17.5 ft Input flow conditions: Q_u = 10003 cfs h_d = 0.95 ft

Calculated Q_w (cfs)

	Slope				
Manning's n	0.000385	0.0008	0.0012	0.0016	Max. diff.
0.0125	887	729	593	476	411
0.02	909	750	612	492	417
0.03	954	793	652	527	427
0.04	1017	853	708	578	439
Max. diff.	130	124	115	102	

Calculated h_u (ft)

	Slope				
Manning's n	0.000385	0.0008	0.0012	0.0016	Max. diff.
0.0125	0.72	0.51	0.31	0.10	0.62
0.02	0.74	0.54	0.34	0.14	0.60
0.03	0.80	0.60	0.40	0.20	0.60
0.04	0.88	0.68	0.49	0.29	0.59
Max. diff.	0.16	0.17	0.18	0.19	

Input geometry data: L = 500 ft B = 85 ft P = 17.5 ft Input flow conditions: Q_u = 9975 cfs h_d = 2.53 ft

Calculated Q_w (cfs)

	Slope				
Manning's n	0.000385	0.0008	0.0012	0.0016	Max. diff.
0.0125	5099	4768	4456	4152	947
0.02	5117	4786	4475	4172	945
0.03	5152	4823	4515	4213	939
0.04	5199	4875	4569	4270	929
Max. diff.	100	107	113	118	

Calculated h_u (ft)

	Slope				
Manning's n	0.000385	0.0008	0.0012	0.0016	Max. diff.
0.0125	2.21	2.00	1.79	1.59	0.62
0.02	2.22	2.01	1.81	1.60	0.62
0.03	2.25	2.04	1.84	1.64	0.61
0.04	2.29	2.09	1.89	1.69	0.60
Max. diff.	0.08	0.09	0.10	0.10	

(See notes on p. 139.)

Appendix 3.2 - Results of simulation using Method B (continued)

Input geometry data: L = 500 ft B = 85 ft P = 17.5 ft Input flow conditions: Q_u = 29766 cfs h_d = 2.23 ft

Calculated Q_w (cfs)

	Slope				
Manning's n	0.000385	0.0008	0.0012	0.0016	Max. diff.
0.0125	2785	2503	2243	1995	790
0.02	3050	2768	2505	2253	797
0.03	3567	3286	3023	2768	799
0.04	4254	3966	3699	3445	809
Max. diff.	1469	1463	1456	1450	

Calculated h_u (ft)

	Slope				
Manning's n	0.000385	0.0008	0.0012	0.0016	Max. diff.
0.0125	1.59	1.34	1.09	0.84	0.75
0.02	1.83	1.59	1.36	1.12	0.71
0.03	2.25	2.04	1.83	1.62	0.63
0.04	2.76	2.57	2.38	2.19	0.57
Max. diff.	1.17	1.23	1.29	1.35	

Input geometry data: L = 500 ft B = 85 ft P = 17.5 ft Input flow conditions: Q_u = 29828 cfs h_d = 5.17 ft

Calculated Q_w (cfs)

	Slope				
Manning's n	0.000385	0.0008	0.0012	0.0016	Max. diff.
0.0125	14698	14130	13581	13032	1666
0.02	14885	14327	13789	13251	1634
0.03	15246	14708	14191	13674	1572
0.04	15712	15198	14705	14213	1499
Max. diff.	1014	1068	1124	1181	

Calculated h_u (ft)

	Slope				
Manning's n	0.000385	0.0008	0.0012	0.0016	Max. diff.
0.0125	4.08	3.83	3.59	3.33	0.75
0.02	4.18	3.94	3.70	3.46	0.72
0.03	4.37	4.15	3.93	3.70	0.67
0.04	4.62	4.41	4.21	4.00	0.62
Max. diff.	0.54	0.58	0.62	0.67	

Input geometry data: L = 250 ft B = 85 ft P = 17.5 ft Input flow conditions: Q_u = 10219 cfs h_d = 1.25 ft

Calculated Q_w (cfs)

	Slope				
Manning's n	0.000385	0.0008	0.0012	0.0016	Max. diff.
0.0125	787	736	687	641	146
0.02	794	742	694	647	147
0.03	808	756	708	661	147
0.04	828	776	727	679	149
Max. diff.	41	40	40	38	

Calculated h_u (ft)

	Slope				
Manning's n	0.000385	0.0008	0.0012	0.0016	Max. diff.
0.0125	1.11	1.01	0.91	0.80	0.31
0.02	1.13	1.02	0.92	0.82	0.31
0.03	1.16	1.05	0.95	0.85	0.31
0.04	1.20	1.09	0.99	0.89	0.31
Max. diff.	0.09	0.08	0.08	0.09	

(See notes on p. 139.)

Appendix 3.2 - Results of simulation using Method B (continued)

Input geometry data: L = 250 ft B = 85 ft P = 17.5 ft Input flow conditions: Q_u = 10225 cfs h_d = 3.72 ft

Calculated Q_w (cfs)

	Slope				
Manning's n	0.000385	0.0008	0.0012	0.0016	Max. diff.
0.0125	5243	5133	5028	4923	320
0.02	5248	5138	5033	4928	320
0.03	5257	5148	5043	4939	318
0.04	5271	5161	5057	4953	318
Max. diff.	28	28	29	30	

Calculated h_u (ft)

	Slope				
Manning's n	0.000385	0.0008	0.0012	0.0016	Max. diff.
0.0125	3.53	3.43	3.33	3.22	0.31
0.02	3.54	3.43	3.33	3.23	0.31
0.03	3.55	3.45	3.34	3.24	0.31
0.04	3.57	3.46	3.36	3.26	0.31
Max. diff.	0.04	0.03	0.03	0.04	

Input geometry data: L = 250 ft B = 85 ft P = 17.5 ft Input flow conditions: Q_u = 29972 cfs h_d = 3.10 ft

Calculated Q_w (cfs)

	Slope				
Manning's n	0.000385	0.0008	0.0012	0.0016	Max. diff.
0.0125	2921	2823	2729	2637	284
0.02	2998	2900	2807	2715	283
0.03	3154	3056	2963	2872	282
0.04	3364	3268	3175	3084	280
Max. diff.	443	445	446	447	

Calculated h_u (ft)

	Slope				
Manning's n	0.000385	0.0008	0.0012	0.0016	Max. diff.
0.0125	2.60	2.47	2.35	2.22	0.38
0.02	2.70	2.58	2.46	2.33	0.37
0.03	2.91	2.79	2.67	2.55	0.36
0.04	3.17	3.06	2.95	2.84	0.33
Max. diff.	0.57	0.59	0.60	0.62	

Input geometry data: L = 250 ft B = 85 ft P = 17.5 ft Input flow conditions: Q_u = 29938 cfs h_d = 6.95 ft

Calculated Q_w (cfs)

	Slope				
Manning's n	0.000385	0.0008	0.0012	0.0016	Max. diff.
0.0125	14199	14019	13846	13673	526
0.02	14243	14064	13892	13720	523
0.03	14331	14154	13984	13813	518
0.04	14453	14278	14109	13941	512
Max. diff.	254	259	263	268	

Calculated h_u (ft)

	Slope				
Manning's n	0.000385	0.0008	0.0012	0.0016	Max. diff.
0.0125	6.29	6.17	6.06	5.94	0.35
0.02	6.33	6.21	6.10	5.98	0.35
0.03	6.40	6.29	6.17	6.06	0.34
0.04	6.50	6.39	6.28	6.16	0.34
Max. diff.	0.21	0.22	0.22	0.22	

(See notes on p. 139.)

Appendix 3.2 - Results of simulation using Method B (continued)

Input geometry data: L = 500 ft B = 45 ft P = 17.5 ft Input flow conditions: Q_u = 10181 cfs h_d = 1.35 ft

Calculated Q_w (cfs)

	Slope				
Manning's n	0.000385	0.0008	0.0012	0.0016	Max. diff.
0.0125	1493	1291	1116	955	538
0.02	1552	1349	1171	1007	545
0.03	1672	1468	1283	1115	557
0.04	1835	1629	1442	1266	569
Max. diff.	342	338	326	311	

Calculated h_u (ft)

	Slope				
Manning's n	0.000385	0.0008	0.0012	0.0016	Max. diff.
0.0125	1.01	0.80	0.60	0.39	0.62
0.02	1.07	0.86	0.67	0.47	0.60
0.03	1.20	1.00	0.80	0.61	0.59
0.04	1.36	1.17	0.98	0.80	0.56
Max. diff.	0.35	0.37	0.38	0.41	

Input geometry data: L = 500 ft B = 45 ft P = 17.5 ft Input flow conditions: Q_u = 10122 cfs h_d = 2.57 ft

Calculated Q_w (cfs)

	Slope				
Manning's n	0.000385	0.0008	0.0012	0.0016	Max. diff.
0.0125	4907	4573	4255	3948	959
0.02	4952	4622	4307	4002	950
0.03	5042	4717	4409	4108	934
0.04	5160	4844	4545	4249	911
Max. diff.	253	271	290	301	

Calculated h_u (ft)

	Slope				
Manning's n	0.000385	0.0008	0.0012	0.0016	Max. diff.
0.0125	2.13	1.91	1.69	1.48	0.65
0.02	2.16	1.95	1.73	1.52	0.64
0.03	2.24	2.03	1.82	1.61	0.63
0.04	2.33	2.13	1.94	1.73	0.60
Max. diff.	0.20	0.22	0.25	0.25	

Input geometry data: L = 500 ft B = 45 ft P = 17.5 ft Input flow conditions: Q_u = 30012 cfs h_d = 3.00 ft

Calculated Q_w (cfs)

	Slope				
Manning's n	0.000385	0.0008	0.0012	0.0016	Max. diff.
0.0125	2902	2386	(2)	(3)	516
0.02	3866	3446	3043	2635	1231
0.03	5412	5033	4670	4309	1103
0.04	6962	6631	6315	6003	959
Max. diff.	4060	4245	3272	3368	

Calculated h_u (ft)

	Slope				
Manning's n	0.000385	0.0008	0.0012	0.0016	Max. diff.
0.0125	1.14	0.66	(2)	(3)	0.48
0.02	1.96	1.67	1.38	1.07	0.89
0.03	3.02	2.80	2.58	2.37	0.65
0.04	3.92	3.75	3.59	3.43	0.49
Max. diff.	2.78	3.09	2.21	2.36	

Appendix 3.2 - Results of simulation using Method B (continued)

Input geometry data: L = 500 ft B = 45 ft P = 17.5 ft Input flow conditions: Q_u = 29906 cfs h_d = 5.70 ft

Calculated Q_w (cfs)

	Slope				
Manning's n	0.000385	0.0008	0.0012	0.0016	Max. diff.
0.0125	13613	12799	12011	11239	2374
0.02	14273	13566	12841	12106	2167
0.03	15337	14746	14163	13559	1778
0.04	16472	15965	15473	14974	1498
Max. diff.	2859	3166	3462	3735	

Calculated h_u (ft)

	Slope				
Manning's n	0.000385	0.0008	0.0012	0.0016	Max. diff.
0.0125	3.38	2.94	2.53	2.14	1.24
0.02	3.78	3.44	3.06	2.68	1.10
0.03	4.38	4.12	3.86	3.58	0.80
0.04	4.95	4.77	4.58	4.38	0.57
Max. diff.	1.57	1.83	2.05	2.24	

Input geometry data: L = 250 ft B = 45 ft P = 17.5 ft Input flow conditions: Q_u = 9900 cfs h_d = 1.35 ft

Calculated Q_w (cfs)

	Slope				
Manning's n	0.000385	0.0008	0.0012	0.0016	Max. diff.
0.0125	825	772	723	675	150
0.02	840	787	738	690	150
0.03	872	818	769	720	152
0.04	916	862	812	763	153
Max. diff.	91	90	89	88	

Calculated h_u (ft)

	Slope				
Manning's n	0.000385	0.0008	0.0012	0.0016	Max. diff.
0.0125	1.17	1.06	0.96	0.85	0.32
0.02	1.20	1.09	0.99	0.89	0.31
0.03	1.27	1.16	1.06	0.96	0.31
0.04	1.35	1.25	1.15	1.05	0.30
Max. diff.	0.18	0.19	0.19	0.20	

Input geometry data: L = 250 ft B = 45 ft P = 17.5 ft Input flow conditions: Q_u = 9944 cfs h_d = 3.88 ft

Calculated Q_w (cfs)

	Slope				
Manning's n	0.000385	0.0008	0.0012	0.0016	Max. diff.
0.0125	5427	5315	5208	5102	325
0.02	5437	5326	5219	5113	324
0.03	5457	5346	5240	5134	323
0.04	5485	5375	5270	5165	320
Max. diff.	58	60	62	63	

Calculated h_u (ft)

	Slope				
Manning's n	0.000385	0.0008	0.0012	0.0016	Max. diff.
0.0125	3.59	3.49	3.38	3.28	0.31
0.02	3.61	3.50	3.40	3.29	0.32
0.03	3.63	3.53	3.42	3.32	0.31
0.04	3.66	3.56	3.46	3.36	0.30
Max. diff.	0.07	0.07	0.08	0.08	

(See notes on p. 139.)

Appendix 3.2 - Results of simulation using Method B (continued)

Input geometry data: L = 250 ft B = 45 ft P = 17.5 ft Input flow conditions: Q_u = 29991 cfs h_d = 3.43 ft

Calculated Q_w (cfs)

	Slope				
Manning's n	0.000385	0.0008	0.0012	0.0016	Max. diff.
0.0125	2596	2448	2302	2152	444
0.02	2859	2722	2588	2453	406
0.03	3325	3201	3081	2961	364
0.04	3881	3763	3653	3544	337
Max. diff.	1285	1315	1351	1392	

Calculated h_u (ft)

	Slope				
Manning's n	0.000385	0.0008	0.0012	0.0016	Max. diff.
0.0125	2.13	1.90	1.65	1.37	0.76
0.02	2.54	2.35	2.16	1.95	0.59
0.03	3.18	3.03	2.88	2.73	0.45
0.04	3.84	3.71	3.59	3.47	0.37
Max. diff.	1.71	1.81	1.94	2.10	

Input geometry data: L = 250 ft B = 45 ft P = 17.5 ft Input flow conditions: Q_u = 29969 cfs h_d = 6.45 ft

Calculated Q_w (cfs)

	Slope				
Manning's n	0.000385	0.0008	0.0012	0.0016	Max. diff.
0.0125	10689	10481	10280	10077	612
0.02	10846	10643	10447	10250	596
0.03	11150	10956	10768	10580	570
0.04	11541	11356	11178	11000	541
Max. diff.	852	875	898	923	

Calculated h_u (ft)

	Slope				
Manning's n	0.000385	0.0008	0.0012	0.0016	Max. diff.
0.0125	4.92	4.76	4.60	4.43	0.49
0.02	5.06	4.91	4.75	4.60	0.46
0.03	5.33	5.19	5.05	4.91	0.42
0.04	5.67	5.54	5.41	5.28	0.39
Max. diff.	0.75	0.78	0.81	0.85	

(See notes on p. 139.)

APPENDIX 4 - SUMMARY OF MODEL DATA FOR 4H:1V SIDE SLOPES

Test	L (ft)	B (ft)	P_u (ft)	P_d (ft)	Q_u (cfs)	Q_w (cfs)	h_u (ft)	h_d (ft)	Fw_d	F_d	C_e
A1	10	1.8	0.513	0.506	3.208	1.685	0.138	0.168	0.216	0.137	0.717
A2	10	1.8	0.513	0.506	3.208	0.992	0.092	0.126	0.403	0.226	0.666
A3	10	1.8	0.513	0.506	3.208	0.246	0.027	0.060	0.928	0.377	0.522
B1	10	1.8	0.513	0.506	6.608	3.172	0.201	0.237	0.351	0.253	0.775
B2	10	1.8	0.513	0.506	6.608	1.915	0.140	0.201	0.566	0.383	0.614
B3	10	1.8	0.513	0.506	6.608	0.783	0.077	0.133	1.016	0.583	0.485
C1	10	1.8	0.513	0.506	9.165	3.714	0.222	0.268	0.490	0.369	0.742
C2	10	1.8	0.513	0.506	9.165	2.379	0.164	0.237	0.694	0.499	0.581
C3	10	1.8	0.513	0.506	9.165	0.983	0.125	0.162	1.201	0.748	0.443
AA3	10	1.8	0.513	0.506	3.200	0.256	0.026	0.060	0.922	0.375	0.543
BB1	10	1.8	0.513	0.506	6.570	3.196	0.202	0.237	0.345	0.248	0.781
BB3	10	1.8	0.513	0.506	6.570	0.794	0.078	0.132	1.010	0.579	0.495
CC1	10	1.8	0.513	0.506	9.094	3.742	0.218	0.278	0.462	0.352	0.697
CC2	10	1.8	0.513	0.506	9.094	2.463	0.167	0.237	0.678	0.488	0.602
CC3	10	1.8	0.513	0.506	9.094	0.980	0.125	0.160	1.204	0.746	0.451
X1	5	1.8	0.513	0.490	3.184	1.627	0.215	0.236	0.165	0.120	0.717
X2	5	1.8	0.513	0.490	3.184	1.339	0.190	0.213	0.217	0.152	0.703
X3	5	1.8	0.513	0.490	3.184	0.943	0.151	0.174	0.320	0.207	0.696
X4	5	1.8	0.513	0.490	3.184	0.591	0.108	0.132	0.472	0.273	0.689
X5	5	1.8	0.513	0.490	3.184	0.286	0.064	0.085	0.743	0.357	0.678
Y1	5	1.8	0.513	0.490	6.428	1.491	0.207	0.239	0.518	0.377	0.643
Y2	5	1.8	0.513	0.490	6.428	1.021	0.161	0.196	0.690	0.467	0.617
Y3	5	1.8	0.513	0.490	6.428	0.546	0.110	0.138	1.030	0.608	0.592
Z1	5	1.8	0.513	0.490	8.989	0.886	0.157	0.190	1.066	0.713	0.565

APPENDIX 5 - COMPONENTS OF β AND α

Appendix 5.1 - Variation of components of β and α with distance for 2.5H:1V side slopes

Case Q_u (cfs) Diver-sion (%) B_s (ft)	$\frac{x}{B_s}$	β	$\beta_1 = \frac{\langle \overline{u}^2 \rangle}{U^2}$	$\beta_2 = \frac{\langle \overline{u'^2} \rangle}{U^2}$	α	$\alpha_1 = \frac{\langle \overline{u}^3 \rangle}{U^3}$	$\alpha_2 = \frac{\langle 3\overline{u}\overline{u'^2} \rangle}{U^3}$	$\alpha_3 = \frac{\langle \overline{u}\overline{v'^2} \rangle}{U^3}$	$\alpha_4 = \frac{\langle \overline{u}\,\overline{v}^2 \rangle}{U^3}$
A	0.00	1.689	1.554	0.135	3.180	2.466	0.365	0.0483	0.2782
8.9	1.16	1.636	1.494	0.142	2.859	2.376	0.395	0.0612	0.0135
54	2.75	1.520	1.420	0.100	2.541	2.165	0.311	0.0477	0.0040
3.72	4.66	1.326	1.250	0.076	1.986	1.711	0.230	0.0346	0.0034
	5.98	1.287	1.225	0.062	1.876	1.640	0.198	0.0305	0.0041
B	0.00	1.794	1.630	0.165	3.483	2.669	0.461	0.0689	0.2593
3.0	1.18	1.813	1.681	0.132	3.309	2.779	0.426	0.0750	0.0048
54	2.77	1.545	1.437	0.108	2.588	2.171	0.338	0.0605	0.0026
3.72	4.67	1.388	1.304	0.084	2.166	1.855	0.262	0.0438	0.0012
	6.00	1.324	1.246	0.078	2.006	1.694	0.260	0.0385	0.0027
C	0.00	1.142	1.133	0.010	1.396	1.341	0.0273	0.0026	0.0241
8.9	2.60	1.107	1.098	0.009	1.295	1.258	0.0281	0.0029	0.0050
25	6.13	1.091	1.083	0.008	1.245	1.213	0.0249	0.0027	0.0035
1.67	10.41	1.082	1.075	0.006	1.219	1.191	0.0202	0.0024	0.0040
	13.30	1.084	1.077	0.007	1.227	1.199	0.0210	0.0024	0.0041
D	1.98	1.516	1.500	0.016	2.428	2.361	0.0481	0.0067	0.0081
4.1	3.35	1.437	1.420	0.017	2.225	2.166	0.0448	0.0070	0.0045
N/A	6.84	1.273	1.261	0.012	1.802	1.754	0.0394	0.0056	0.0009
3.72	9.99	1.221	1.206	0.015	1.639	1.579	0.0482	0.0070	0.0018
	13.13	1.186	1.174	0.013	1.531	1.481	0.0417	0.0057	0.0012
	16.28	1.149	1.137	0.013	1.421	1.372	0.0409	0.0059	0.0011
E	N/A	1.083	1.077	0.006	1.229	1.203	0.0200	0.0034	0.0014

Appendix 5.2 - Variation of components of β and α with distance for 4H:1V side slopes

Case Q_u (cfs) Diver-sion (%) B_s (ft)	$\frac{x}{B_s}$	β	$\beta_1 = \frac{\langle \overline{u}^2 \rangle}{U^2}$	$\beta_2 = \frac{\langle \overline{u'^2} \rangle}{U^2}$	α	$\alpha_1 = \frac{\langle \overline{u}^3 \rangle}{U^3}$	$\alpha_2 = \frac{\langle 3\overline{u}\overline{u'^2} \rangle}{U^3}$	$\alpha_3 = \frac{\langle \overline{u}\overline{v'^2} \rangle}{U^3}$	$\alpha_4 = \frac{\langle \overline{u}\,\overline{v}^2 \rangle}{U^3}$
F	0.51	1.989	1.833	0.156	3.828	3.164	0.532	0.168	0.0080
6.1	0.51	1.908	1.763	0.145	3.800	3.211	0.481	0.083	0.0108
54	2.02	1.695	1.584	0.112	3.283	2.755	0.431	0.118	0.0105
3.99	2.02	1.728	1.617	0.112	3.226	2.784	0.354	0.0669	0.103
	3.41	1.398	1.377		2.166	2.063			
	4.80	1.215	1.198		1.630	1.554			
G	0.00	1.885	1.832	0.053	3.276	3.094	0.177	0.0253	0.0024
4.5	0.54	1.960	1.910	0.050	3.497	3.346	0.130	0.0169	0.0019
N/A	1.08	1.934	1.876	0.059	3.450	3.236	0.197	0.0232	0.0044
3.99	1.63	1.818	1.765	0.053	3.240	3.065	0.147	0.0206	0.0037
	2.16	1.733	1.672	0.062	3.000	2.785	0.198	0.0236	0.0042
	2.71	1.612	1.555	0.057	2.724	2.521	0.185	0.0243	0.0037
	3.26	1.427	1.390	0.037	2.128	1.995	0.115	0.0186	0.0046
	4.34	1.305	1.280	0.026	1.874	1.783	0.0785	0.0079	0.0017
	4.89	1.236	1.209	0.028	1.671	1.565	0.0953	0.0107	0.0031
	6.52	1.185	1.167	0.018	1.516	1.444	0.0571	0.0107	0.0044
	7.89	1.201	1.184	0.017	1.536	1.495	0.0505	0.0052	0.0031
	10.90	1.132	1.118	0.014	1.371	1.317	0.0443	0.0112	0.0018
H	N/A	1.123	1.115	0.008	1.172	1.153	0.0133	0.0022	0.0035

Appendix 5.3 - Components of β and α just downstream of weir for 2.5H:1V side slopes

Case Q_u (cfs) Diver-sion (%) B_s (ft)	$\frac{x}{B_s}$	β	$\beta_1 = \frac{\langle \overline{u}^2 \rangle}{U^2}$	$\beta_2 = \frac{\langle \overline{u'^2} \rangle}{U^2}$	α	$\alpha_1 = \frac{\langle \overline{u}^3 \rangle}{U^3}$	$\alpha_2 = \frac{\langle 3\overline{u}\overline{u'^2} \rangle}{U^3}$	$\alpha_3 = \frac{\langle \overline{u}\overline{v'^2} \rangle}{U^3}$	$\alpha_4 = \frac{\langle \overline{u}\,\overline{v}^2 \rangle}{U^3}$
25	8.91	1.122	1.111	0.011	1.330	1.292	0.030	0.0029	0.0041
25	3.01	1.119	1.106	0.012	1.310	1.265	0.037	0.0055	0.0016
39	6.13	1.336	1.281	0.056	1.871	1.710	0.129	0.0216	0.0067
40	8.92	1.268	1.213	0.055	1.732	1.554	0.145	0.0204	0.0144
40	3.01	1.341	1.291	0.050	1.874	1.717	0.124	0.0215	0.0055
54	8.91	1.617	1.455	0.162	2.737	2.195	0.421	0.0633	0.0403
54	3.01	1.839	1.692	0.147	3.333	2.740	0.475	0.0803	0.0222
55	5.97	1.785	1.620	0.165	3.184	2.657	0.413	0.0615	0.0376

Appendix 5.4 - Components of β and α just downstream of weir for 4H:1V side slopes

Diver-sion (%)	Q_u (cfs)	β	$\beta_1 = \frac{\langle \overline{u}^2 \rangle}{U^2}$	$\beta_2 = \frac{\langle \overline{u'^2} \rangle}{U^2}$	α	$\alpha_1 = \frac{\langle \overline{u}^3 \rangle}{U^3}$	$\alpha_2 = \frac{\langle 3\overline{u}\overline{u'^2} \rangle}{U^3}$	$\alpha_3 = \frac{\langle \overline{u}\overline{v'^2} \rangle}{U^3}$	$\alpha_4 = \frac{\langle \overline{u}\,\overline{v}^2 \rangle}{U^3}$
25	3.0	1.262	1.238	0.024	1.692	1.618	0.0652	0.0077	0.0017
25	6.0	1.140	1.104	0.036	1.394	1.267	0.122	0.0355	0.0011
25	9.0	1.297	1.208	0.089	1.823	1.538	0.275	0.0562	0.0057
40	3.0	1.704	1.631	0.074	2.837	2.581	0.211	0.0304	0.0040
40	6.0	1.504	1.301	0.203	2.393	1.794	0.576	0.1278	0.0080
40	9.1	1.561	1.448	0.113	2.501	2.131	0.327	0.0739	0.0083
53	3.0	2.513	2.322	0.191	6.016	4.995	0.817	0.1347	0.0234
53	6.1	1.989	1.833	0.156	3.828	3.164	0.531	0.1683	0.0080
53	9.1	2.137	1.882	0.255	4.366	3.356	0.944	0.2023	0.0137
53	2.9	2.524	2.309	0.215	5.844	4.749	0.880	0.1793	0.0051
55	6.0	1.908	1.763	0.145	3.800	3.211	0.481	0.0831	0.0108

APPENDIX 6 - MOMENTUM AND ENERGY BALANCES

Appendix 6.1 - Momentum balance for Case A

Distance (ft)	Depth (ft)	$\int_A \bar{u}\,dA$ (cfs)	$\int_A \overline{u^2}\,dA$ (ft^4/s^2)	β	β QU (ft^4/s^2)	h (ft)	$gA_2(h_1 - h_2)$ (ft^4/s^2)	$\frac{F_\tau}{\rho}$ (ft^4/s^2)	Δh_M (ft)
0.0	0.986	4.284	5.361	1.69	5.361	1.2449			
							-1.158	0.051	-0.003
4.3	0.991	4.040	4.584	1.64	4.730	1.2511			
							-0.585	0.066	-0.002
10.2	0.997	4.040	4.222	1.52	4.356	1.2542			
							-0.364	0.078	0.001
17.3	1.007	4.068	3.681	1.33	3.747	1.2561			
							-0.255	0.052	-0.001
22.3	1.022	4.017	3.414	1.29	3.564	1.2574			

Appendix 6.2 - Energy balance for Case A

Distance (ft)	Depth (ft)	$\int_A \bar{u}\,dA$ (cfs)	$\int_A \overline{V^2 u}\,dA$ (ft^5/s^3)	α	$\alpha\frac{U^2}{2g}$ (ft)	h (ft)	H (ft)	h_f (ft)	Δh_E (ft)
0.0	0.986	4.284	7.476	3.18	0.0271	1.2449	1.2720		
								0.0003	-0.001
4.3	0.991	4.040	5.555	2.86	0.0220	1.2511	1.2731		
								0.0004	-0.001
10.2	0.997	4.040	4.854	2.54	0.0192	1.2542	1.2734		
								0.0004	0.002
17.3	1.007	4.068	3.764	1.99	0.0146	1.2561	1.2707		
								0.0003	-0.000
22.3	1.022	4.017	3.282	1.88	0.0132	1.2574	1.2706		

Appendix 6.3 - Momentum balance for Case B

Distance (ft)	Depth (ft)	$\int_A \bar{u}\,dA$ (cfs)	$\int_A \overline{u^2}\,dA$ (ft^4/s^2)	β	β QU (ft^4/s^2)	h (ft)	$gA_2(h_1 - h_2)$ (ft^4/s^2)	$\frac{F_\tau}{\rho}$ (ft^4/s^2)	Δh_M (ft)
0.0	0.853	1.418	0.764	1.79	0.764	1.1205			
							-0.092	0.008	-0.000
4.4	0.860	1.345	0.686	1.81	0.721	1.1211			
							-0.062	0.011	0.000
10.3	0.865	1.367	0.600	1.54	0.610	1.1215			
							-0.109	0.012	-0.000
17.4	0.871	1.353	0.523	1.39	0.543	1.1222			
							-0.129	0.008	-0.001
22.3	0.893	1.342	0.474	1.32	0.500	1.1230			

Appendix 6.4 - Energy balance for Case B

Distance (ft)	Depth (ft)	$\int_A \bar{u}\,dA$ (cfs)	$\int_A \overline{V^2 u}\,dA$ (ft^5/s^3)	α	$\alpha\frac{U^2}{2g}$ (ft)	h (ft)	H (ft)	h_f (ft)	Δh_E (ft)
0.0	0.853	1.418	0.445	3.48	0.0049	1.1205	1.1254		
								0.0001	-0.000
4.4	0.860	1.345	0.353	3.31	0.0043	1.1211	1.1254		
								0.0001	0.001
10.3	0.865	1.367	0.285	2.59	0.0033	1.1215	1.1248		
								0.0001	-0.000
17.4	0.871	1.353	0.228	2.17	0.0027	1.1222	1.1249		
								0.0001	-0.000
22.3	0.893	1.342	0.192	2.01	0.0023	1.1230	1.1253		

Appendix 6.5 - Momentum balance for Case C

Distance (ft)	Depth (ft)	$\int_A \bar{u}\,dA$ (cfs)	$\int_A \overline{u^2}\,dA$ (ft^4/s^2)	β	β QU (ft^4/s^2)	h (ft)	$gA_2(h_1 - h_2)$ (ft^4/s^2)	$\frac{F_\tau}{\rho}$ (ft^4/s^2)	Δh_M (ft)
0.0	0.899	6.403	9.224	1.14	9.224	1.1603			
							-0.593	0.158	-0.008
4.4	0.906	6.278	8.503	1.11	9.736	1.1639			
							-0.050	0.220	-0.000
10.2	0.912	6.368	8.537	1.09	9.500	1.1642			
							0.135	0.263	0.000
17.4	0.917	6.458	8.642	1.08	9.352	1.1634			
							-0.310	0.173	-0.002
22.2	0.934	6.369	8.210	1.08	9.136	1.1652			

Appendix 6.6 - Energy balance for Case C

Distance (ft)	Depth (ft)	$\int_A \bar{u}\,dA$ (cfs)	$\int_A \overline{V^2 u}\,dA$ (ft^5/s^3)	α	$\alpha\frac{U^2}{2g}$ (ft)	h (ft)	H (ft)	h_f (ft)	Δh_E (ft)
0.0	0.899	6.403	14.218	1.40	0.0345	1.1603	1.1948		
								0.0010	-0.005
4.4	0.906	6.278	12.170	1.30	0.0345	1.1639	1.1984		
								0.0013	0.000
10.2	0.912	6.368	11.975	1.24	0.0325	1.1642	1.1967		
								0.0016	0.000
17.4	0.917	6.458	12.047	1.22	0.0313	1.1634	1.1947		
								0.0010	-0.001
22.2	0.934	6.369	11.050	1.23	0.0300	1.1652	1.1952		

Appendix 6.7 - Momentum balance for Case D

Distance (ft)	Depth (ft)	$\int_A \bar{u}\,dA$ (cfs)	$\int_A \overline{u^2}\,dA$ (ft^4/s^2)	β	β QU (ft^4/s^2)	h (ft)	$gA_2(h_1 - h_2)$ (ft^4/s^2)	$\frac{F_\tau}{\rho}$ (ft^4/s^2)	Δh_M (ft)
7.4	0.993	3.962	4.075	1.52	4.448	1.2537			
							-0.244	0.058	-0.000
12.5	0.992	4.033	4.008	1.44	4.223	1.2550			
							-0.446	0.144	0.000
25.5	1.015	4.195	3.719	1.27	3.622	1.2573			
							0.000	0.127	-0.000
37.2	1.007	4.138	3.509	1.22	3.512	1.2573			
							-0.039	0.128	-0.000
48.9	1.011	4.094	3.317	1.19	3.392	1.2575			
							-0.261	0.123	-0.001
60.6	1.039	4.121	3.133	1.15	3.161	1.2588			

Appendix 6.8 - Energy balance for Case D

Distance (ft)	Depth (ft)	$\int_A \bar{u}\,dA$ (cfs)	$\int_A \overline{V^2 u}\,dA$ (ft^5/s^3)	α	$\alpha\frac{U^2}{2g}$ (ft)	h (ft)	H (ft)	h_f (ft)	Δh_E (ft)
7.4	0.993	3.962	4.428	2.43	0.0189	1.2537	1.2726		
								0.0003	-0.000
12.5	0.992	4.033	4.291	2.22	0.0174	1.2550	1.2724		
								0.0008	0.001
25.5	1.015	4.195	3.664	1.80	0.0132	1.2573	1.2705		
								0.0007	0.000
37.2	1.007	4.138	3.270	1.64	0.0123	1.2573	1.2696		
48.9	1.011	4.094	2.924	1.53	0.0113	1.2575	1.2688	0.0007	0.000
60.6	1.039	4.121	2.562	1.42	0.0097	1.2588	1.2685	0.0006	-0.000

Appendix 6.9 - Momentum balance for Case F

Distance (ft)	Depth (ft)	$\int_A \bar{u}\,dA$ (cfs)	$\int_A \overline{u^2}\,dA$ (ft^4/s^2)	β	β QU (ft^4/s^2)	h (ft)	$gA_2(h_1 - h_2)$ (ft^4/s^2)	$\frac{F_\tau}{\rho}$ (ft^4/s^2)	Δh_M (ft)
2.5	0.776	2.765	3.995	1.99	4.304	1.1920			
							-0.6095	0.0642	0.000
8.1	0.776	2.546	2.887	1.70	3.670	1.1970			
							-0.7260	0.0646	-0.001
13.6	0.773	2.618	2.534	1.40	3.045	1.2030			
							-0.6237	0.0632	-0.002
19.2	0.787	2.791	2.430	1.22	2.570	1.2080			

Appendix 6.10 - Energy balance for Case F

Distance (ft)	Depth (ft)	$\int_A \bar{u}\,dA$ (cfs)	$\int_A \overline{V^2 u}\,dA$ (ft^5/s^3)	α	$\alpha\frac{U^2}{2g}$ (ft)	h (ft)	H (ft)	h_f (ft)	Δh_E (ft)
2.5	0.776	2.765	5.588	3.83	0.0338	1.1920	1.2258		
								0.0005	-0.001
8.1	0.776	2.546	3.740	3.28	0.0290	1.1970	1.2260		
								0.0005	0.003
13.6	0.773	2.618	2.718	2.17	0.0194	1.2030	1.2224		
								0.0005	0.000
19.2	0.787	2.791	2.336	1.63	0.0137	1.2080	1.2217		

APPENDIX 7 - DATA FOR DIVERSION CULVERTS

Appendix 7.1 - Results for diversion culverts with three barrels, unsubmerged flow

Upstream discharge Q_u (cfs)	Diversion Q_w (cfs)	Upstream head on weir h_u (ft)	Down-stream head on weir h_d (ft)	Down-stream Froude number F_d	Down-stream weir Froude number Fw_d	Ratio of critical depth to depth at culvert outlet η_c/η_4	Loss coeffi cient from 0 to 2 K_E
1.6	0.560	0.324	0.330	0.113	0.143	1	0.642
1.6	0.438	0.277	0.283	0.128	0.171	1	0.751
1.6	0.303	0.215	0.221	0.149	0.218	1	0.804
1.6	0.173	0.148	0.154	0.174	0.294	1	1.050
3.2	0.574	0.336	0.342	0.178	0.223	1	0.876
3.2	0.459	0.291	0.297	0.194	0.255	1	1.006
3.2	0.320	0.229	0.235	0.218	0.312	1	1.213
3.2	0.185	0.162	0.168	0.249	0.406	1	1.823
6.6	0.482	0.317	0.323	0.278	0.356	1	1.943
6.6	0.376	0.274	0.280	0.299	0.401	1	2.449
6.6	0.273	0.230	0.236	0.323	0.461	1	3.360
6.6	0.185	0.185	0.191	0.350	0.542	1	4.758
9.1	0.412	0.306	0.312	0.338	0.437	1	3.476
9.1	0.355	0.282	0.288	0.351	0.467	1	4.023
9.1	0.257	0.241	0.247	0.376	0.528	1	5.597
9.1	0.180	0.207	0.213	0.398	0.592	1	7.950

Appendix 7.2 - Results for diversion culverts with three barrels, submerged flow

Upstream discharge Q_u (cfs)	Diversion Q_w (cfs)	Upstream head on weir h_u (ft)	Down-stream head on weir h_d (ft)	Down-stream Froude number F_d	Down-stream weir Froude number Fw_d	Ratio of critical depth to depth at culvert outlet η_c/η_4	Loss coeffi cient from 0 to 2 K_E
1.6	0.584	0.341	0.347	0.109	0.135	0.887	0.816
1.6	0.187	0.187	0.193	0.162	0.251	0.583	1.838
3.2	0.546	0.333	0.339	0.179	0.225	0.983	1.080
3.2	0.188	0.192	0.198	0.236	0.360	0.645	3.145
6.5	0.457	0.317	0.323	0.277	0.355	0.946	2.257
6.6	0.190	0.212	0.218	0.334	0.492	0.703	6.273
9.1	0.408	0.315	0.321	0.334	0.427	0.923	3.734
9.2	0.188	0.224	0.230	0.388	0.560	0.760	8.731

Appendix 7.3 - Results for diversion culverts with two barrels, unsubmerged flow

Upstream discharge Q_u (cfs)	Diversion Q_w (cfs)	Upstream head on weir h_u (ft)	Down-stream head on weir h_d (ft)	Down-stream Froude number F_d	Down-stream weir Froude number Fw_d	Ratio of critical depth to depth at culvert outlet η_c/η_4	Loss coeffi cient from 0 to 2 K_E
1.6	0.381	0.334	0.337	0.121	0.153	1	0.672
1.6	0.273	0.267	0.270	0.139	0.190	1	0.722
1.6	0.194	0.214	0.217	0.156	0.230	1	0.850
3.2	0.372	0.329	0.332	0.186	0.236	1	0.776
3.2	0.261	0.263	0.266	0.209	0.287	1	0.997
3.2	0.190	0.217	0.220	0.228	0.335	1	1.300
6.6	0.314	0.317	0.320	0.283	0.363	1	1.894
6.6	0.169	0.229	0.232	0.326	0.470	1	3.503
9.1	0.284	0.312	0.315	0.337	0.435	1	3.065
9.1	0.178	0.252	0.255	0.371	0.516	1	5.044

Appendix 7.4 - Results for diversion culverts with two barrels, submerged flow

Upstream discharge Q_u (cfs)	Diversion Q_w (cfs)	Upstream head on weir h_u (ft)	Down-stream head on weir h_d (ft)	Down-stream Froude number F_d	Down-stream weir Froude number Fw_d	Ratio of critical depth to depth at culvert outlet η_c/η_4	Loss coeffi cient from 0 to 2 K_E
1.6	0.202	0.296	0.299	0.137	0.180	0.473	0.662
3.2	0.178	0.284	0.287	0.205	0.274	0.454	1.109
6.6	0.182	0.298	0.301	0.294	0.386	0.461	2.692
9.1	0.198	0.312	0.315	0.338	0.437	0.482	3.764